Fluorinated Boronic Acid-Appended Pyridinium Salts and ^{19}F NMR Spectroscopy –

A valuable and highly discriminative Sensing Tool for Diols, Inorganic Anions and Hydrogen Peroxide under physiological Conditions

Dissertation

zur Erlangung des akademischen Grades doctor rerum naturalium

(Dr. rer. nat.)

vorgelegt dem Rat der Chemisch-Geowissenschaftlichen Fakultät der Friedrich-Schiller-Universität Jena

von Diplom Chemiker Jörg Harald Axthelm

geboren am 13.10.1986 in Rudolstadt.

Gutachter:

1. PD Dr. Alexander Schiller

2. Prof. Dr. Winfried Plass

Tag der Verteidigung: 13.07.2020

“We already have – thanks to technology, development, skills, the efficiency of our work – enough resources to satisfy all human needs. But we don’t have enough resources, and we are unlikely ever to have, to satisfy human greed.”

Zygmunt Bauman

TABLE OF CONTENTS

LIST OF ABBREVIATIONS

AIDA	Allosteric Indicator Displacement Assay
AMP, ADP, ATP	Adenosine (Mono-, Di-, Tri-) Phosphate
ARS	Alizarin Red S
BBpy	Boronic Acid-appended Benzylpyridine
BBV	Boronic Acid-appended Benzylviologen (strictly spoken the 4,4'-linked derivative)
BINOL	1,1'-binaphthalene-2,2'-diol moiety
CCl_3F	Trichlorofluoromethane
CCl_4	Tetrachloromethane
CD	Cyclodextrin
D_2O	Deuterium Oxide
DCM	Dichloromethane
DMF	Dimethylformamide
DMSO-d_6	Deuterated Dimethylsulfoxide
EA	Elemental Analysis
F-BBpy	Fluorinated Boronic Acid-appended Benzylpyridine
F-BBV	Fluorinated Boronic Acid-appended Benzylviologen
FID	Free Induction Decay
GOx	Glucose Oxidase (Enzyme)
GTIN	Global Trade Item Number
HEPES	(4-(2-hydroxyethyl)-1-piperazineethanesulfonic acid)
HIV	Human Immunodeficiency Virus
HPTS	8-hydroxypyrene-1,3,6-trisulfonic acid
ICT	Internal Charge Transfer
IDA	Indicator Displacement Assay
IMP	Material Implication (Gate)
IR	Infrared Spectroscopy
LOD	Limit of Detection
LOQ	Limit of Quantification
MeOD	Deuterated Methanol
MeOH	Methanol
MRI	Magnetic Resonance Imaging

MS	Mass Spectrometry
NAD^+/NADH	Coenzyme Nicotinamide Adenine Dinucleotide (oxidized/reduced)
NMR	Nuclear Magnetic Resonance
PBA	Phenylboronic Acid
PET	Photo-induced Electron Transfer
QR	Quick Response (Code)
ROS	Reactive Oxygen Species
S/N	Signal to Noise Ratio
SHA	Salicylhydroxamic Acid
SPhos	2-Dicyclohexylphosphino-2′,6′-dimethoxybiphenyl
SPO	Sucrose Phosphorylase (Enzyme)
TICT	Twisted Internal Charge Transfer
TLC	Thin-Layer Chromatography

LIST OF SYMBOLS AND UNITS

$\overrightarrow{B_0}$	Magnetic Flux Density Vector
γ_N	Gyromagnetic Ratio
E'	Excited State
E''	Ground State
E_{pot}	Potential Energy
$\vec{M}$	Magnetization Vector
N_x	Population Number
$\vec{P}$	Nuclear Spin Vector
m_l	Magnetic Quantum Number
$\vec{\mu}$	Dipole Moment Vector
$[CD_0]$	Initial Concentration of Chemodosimeter
[G]	Concentration of free Guest (Analyte)
$[H_0]$	Initial Concentration of Host (Receptor)
[HG]	Concentration of Host-Guest (Receptor-Analyte) Complex
[P]	Concentration of Degradation Product
$\Delta\delta_X$	Chemical Shift Change of specific Nucleus x
ΔE	Energy Difference
°	Degree (Angle)
°C	Grad Celsius
Å	Angström
F	Mole Fraction
h	Planck Constant
ħ	Reduced Planck Constant
Hz	Hertz
I	Nuclear Quantum Number
J	NMR Coupling Constant
K_b	Binding Constant
k_B	Boltzmann Constant
K_m	Michaelis-Menten Constant
M	Mole per Liter

Mg	Milligram
MHz	Megahertz
mM	Millimole per Liter
mMol	Millimole
ms	Milliseconds
nM	Nanomole per Liter
o-, *m*-, *p*-	*ortho*-, *meta*-, *para*-positioned Substituent
pH	Negative logarithmic Proton Concentration
pK_a	Logarithmic Acid Dissociation Constant
ppm	Parts per Million
R.F.U.	Relative Fluorescence Units
RT	Room Temperature
S_D	Standard Deviation
T	Temperature
U	Enzyme Activity
v_{max}	Maximum Reaction Rate
δ_X	Chemical Shift of specific Nucleus x
χ	Pauling Electronegativity

LIST OF FIGURES

LIST OF TABLES

1 INTRODUCTION

For a long time, scientists are interested in mimicking the perfected mechanisms of Mother Nature. Prominent examples are the seemingly simple key and lock principles, which play an essential role with respect to the sensory skills of taste, smell and reproduction of many creatures. Especially, the analytical chemist is looking for new concepts, which allow the recognition of target molecules that play an important role in verification procedures and the understanding of complex chemical processes in disciplines such as medicine, biology, agriculture, environmental and social sciences (Figure 1). These key molecules give an indication of e.g. the health status in terms of certain diseases or the quality of products such as drinking water, food or articles of daily use. The selective and unambiguous identification in presence of similar compounds with a certain robustness to the experimental conditions, and if needed, the quantification in the significant analyte concentration range are further requirements that need to be fulfilled by a synthetic receptor molecule (a so-called chemosensor).[1]

A potential analyte with an extensive relevance to cellular processes is the naturally abundant D-glucose. By far, this monosaccharide (an aldohexose) plays an outstanding role as a basic building block of life. Glucose is the most important source of energy in cells (mainly released by polysaccharide-containing food sources such as starch and is intracellular stored as glycogen) and is furthermore a carbon source for the buildup of secondary products of most living organisms. Glucose determines the blood sugar level in the human body which should stay in a certain range for a healthy person.[2] Metabolic disorders responsible for an altered blood sugar level can lead to e.g. renal glycosuria, cystic fibrosis and types of cancer. In fact, the modern humanity suffers from a tremendous increase of health issues induced by diabetes. This global issue is certainly caused by the insanitary lifestyle of the Western civilization.

Consequently, a reliable chemosensor, which can provide the selective detection and quantification of glucose, preferably in a real-time manner and without the need of invasive interventions of uncomfortable blood withdrawal, is highly desired by medicinal facilities as

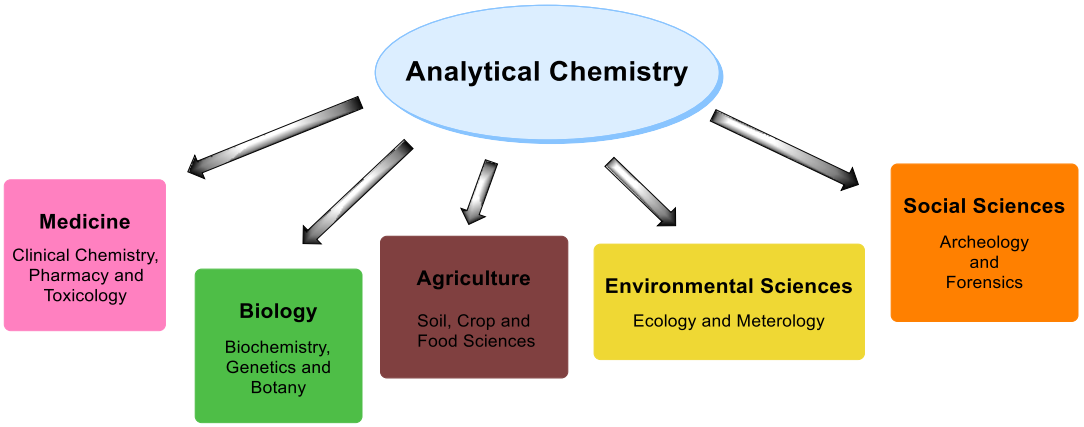

Figure 1: Significance of the analytical chemistry to the most important fields of the modern life sciences and social sciences.

well as affected patients. Up to date, mainly enzyme-based methods (blood or urine dipstick kits) are used in the diagnostic analysis and provide high selectivity for D-glucose.[3] Aside from glucose also other diol-related bioanalytes with a medicinal relevance play an important role for the identification of diseases. For example, the catecholamines dopamine and epinephrine can provide an indication for Alzheimer disease and specific cancer types such as neuroblastoma and pheochromocytoma. The detection of atypical amount of specific catecholamine derivatives in human urine provide an indication of the named cancer types.[4-6]

A further field of application for a potential chemosensor can be seen in the monitoring of environmental parameters such as the detection and discrimination of inorganic anions in aqueous systems. Inorganic anions play a fundamental role in chemical and biological processes as well and determine in a considerable way the quality of the aquatic ecosystem and of course the continuity of the latter. Thus, the probing and monitoring of problematic anions released by especially industrial processes, traffic, agriculture and mining is of critical interest. Examples of anions that endanger the global water systems include highly poisonous cyanide released by gold mining facilities as well as nitrate and phosphate, which both play an important role regarding eutrophication of the aquatic ecosystem.[7-8]

Consequently, reliable, highly selective and robust sensing systems are desired to solve the briefly discussed cases and numberless other analytical problems. The large pool of modern analytical techniques of the instrumental analytical chemistry such as NMR-, fluorescence-, UV-vis-, IR-spectroscopy and electrochemical techniques, to name only the most prominent examples, enable the scanning of a wide range of information of a potential molecular sensor. This said, each analytical problem should be addressable by a tailored chemosensor, which is

working under the required conditions. At its best, the concatenated property change of the receptor/sensor molecule induced by the interaction to a specific analyte should allow the unambiguous identification with respect to it's qualitative as well as quantitative property. Another important feature, which should be fulfilled by the sensing technique is the robustness in terms of interfering contaminants and influencing conditions to prevent false interpretation.

Since the 1990ies, prominent chemosensors equipped with one or more boronic acid functions were developed. In fact, the boronic acid moiety seems to be "the" superior receptor for 1,2- and 1,3-diol-containing analytes. Thus, an enormous collection of fluorescence-based assays for diols comprising chemosensors with one or more boronic acids and directly attached or external fluorescent probes have been postulated.[9-10] On the other hand the fast development of the NMR/MRI technique especially with respect to the ^{19}F nucleus with its intrinsic sensitivity has attracted high attention in the last decades.

With respect to the strong analytical property of boronic acids and ^{19}F NMR, the present thesis will focus on the potential of fluorinated boronic acid-appended (bi)pyridinium salts assisted by ^{19}F NMR spectroscopy as a novel qualitative and quantitative sensing tool for the screening of diol-containing analytes, inorganic anions and hydrogen peroxide under physiological conditions.

2 MOTIVATION AND RESEARCH GOAL

As previously mentioned, the identification and discrimination of carbohydrates and inorganic anions is of fundamental importance in many disciplines such as the elucidation of biochemical processes and the medicinal examination. Especially, sensing techniques are required that enable the selective detection and unambiguous discrimination of the analyte under given experimental conditions without false interpretation. In the past, mainly boronic acid based fluorescent assays have been extensively investigated and used for diol screening experiments but a detailed investigation using fluorinated boronic acid appended receptors assisted by ^{19}F NMR spectroscopy as a versatile diol and anion sensing tool has not been conducted till now.

In fact, fluorine NMR exhibits a few significant advantages compared to fluorescent-based assays such as the direct property response of the attached ^{19}F probe to structural changes, the concatenated highly characteristic spectroscopic output signal and the pH robustness. In comparison, the indirect fluorescence response is only one-dimensional, severely lack of discrimination power and predominantly is affected by pH changes, which might influence the reporting fluorescence dye.

Boronic acid-appended (bi)pyridinium salts were originally used in fluorescent diol assays and are a suitable class of highly water-soluble diol receptors. Their good access in synthesis via simple precursors (phenylboronic acids and pyridinium-based linkers) enable numerous structural modifications for the generation of in part diol-selective receptors. Due to their crystalline character and good water solubility, they can be easily handled with respect to sample preparation and storage. Nevertheless, without a molecular reporter such as an attached or supramolecular interacting fluorescent dye the binding event to diols is not applicable in a suitable manner. An alternative approach can be achieved by the attachment of a small fluorine atom as a molecular probe. Most importantly, such a sensitive ^{19}F nucleus is a 100% abundant

reporter which lack of a disturbing background signal in the NMR spectrum and has a slightly positive effect on the complexation ability of the boronic acid. Numberless commercially fluorinated boronic acid precursors are available and enable the development of a robust and reliable receptor/sensor molecule as presented in this thesis.

Thus, fluorinated and highly water-soluble boronic acid (bi)pyridinium salts assisted by ^{19}F NMR spectroscopy seem to be an alternative and elegant strategy compared to fluorescent diol assays. Furthermore, the presented sensing system fulfills a wide range of discriminatory sensing tasks for diols, inorganic anions, mixtures of them and hydrogen peroxide as another interesting analytical class under 100% aqueous and physiological conditions.

In summary, the following research objects were addressed:

- Development of a suitable path for the synthesis of a set of fluorinated (bis)boronic acid-appended receptors for versatile ^{19}F NMR sensing applications
- Elucidation of the best performing benzylpyridinium receptor/sensor with associated crucial molecular features in terms of the ^{19}F NMR diol sensing power, reproducibility, ease in synthesis, water solubility and pH robustness
- Unambiguous detection and discrimination of diol-containing analytes as well as binary and ternary diol mixtures using highly characteristic ^{19}F fingerprints via the best performing receptor/sensor
- Analysis of the recorded spectroscopic ^{19}F NMR data and determination of apparent receptor-diol affinities for the interpretation of receptor-diol interactions and possible receptor-diol binding modes under aqueous conditions
- Application of the sensing system for the monitoring of an exemplary enzyme-catalyzed reaction via target metabolites and the determination of enzymatic kinetic data
- Studies of possible bidentate receptors and receptor arrays for the generation of receptor-analyte bar codes as a modern and easy way for diol identification and enhanced discrimination
- Qualitative, quantitative and selective sensing of the highly demanding anions cyanide, fluoride and phosphate
- Enhanced applicability in a new chemodosimetric approach for the detection of the reactive oxidative species hydrogen peroxide
- Utilization of the ^{19}F NMR approach in a potential medicinal diabetes pretest for the detection and quantification of D-glucose in an exemplary urine sample

3 THEORETICAL BACKGROUND

BORONIC ACID CHEMISTRY

For the first time, Edward Frankland reported the preparation and isolation of ethylboronic acid in 1860.[11] As relatives to boric acid which contains three hydroxyl groups, boronic acids are composed of two hydroxyl groups and one alkyl or aryl moiety and belong to the class of organoboranes due to a direct carbon-boron bond (see Figure 2a). Typically, boronic acids exhibit high melting points, are mostly air-stable and willingly form anhydrides such as stable cyclic dimers and trimers by abstracting molecular water.

The synthetic access can occur via several methods such as the reaction of lithium or magnesium (Grignard) organometallics with borate esters and subsequent hydrolysis to the appropriate boronic acid. In detail, phenylboronic acid (PBA), a basic chemical, can be obtained from phenylmagnesium bromide and trimethyl borate, which in the first step form dimethyl-phenylborate and finally the desired product upon treatment with water (Figure 2b). A further common way is the reaction of arylsilanes with boron tribromide followed by acidic hydrolysis. Plenty other approaches are described in the literature and commercially available boronic acids

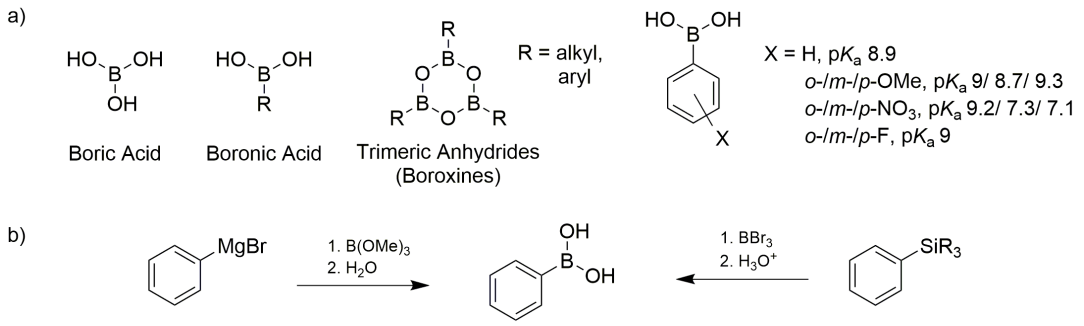

Figure 2: a) Molecular structures of sp^2 hybridized and trigonal planar boric acid, boronic acid, trimeric anhydride and selected pK_a values of phenylboronic acid (PBA) derivatives. b) Two possible pathways for the synthesis of PBA using organo-Grignard and arylsilane precursors.

cover a large range of molecular classes and applications (see chapter 3.2). Boronic acids are not belonging to the group of Brønsted acids as they are no proton donors (no direct deprotonation at the hydroxyl groups). However, their acidic behavior under aqueous conditions originates from the vacant p orbital of boron (sp^2 hybridized and trigonal planar) resulting in an electrophile center which readily accepts an electron pair from nucleophiles (Lewis bases). Dissolved in water boronic acids weakly tend to form the corresponding anionic boronates (sp^3 hybridized and tetrahedral boron) aby the abstraction of one proton (Figure 3). As a result, boronic acids are weak Lewis acids with moderate pK_a values and their strength of acidity is mainly determined by mesomeric or inductive effects of attached substituents such as methoxy, nitro or fluorine. Selected pK_a values of phenylboronic acids and derivatives are illustrated by Figure 2a and are ranging from 7.1 (4-nitrophenlyboronic acid) to 9.3 (PBA). Further possible interactions of boronic acids such as hydrogen bonding, boroxine formation, anion coordination and esterification under dehydrating conditions are represented by Figure 3. Another important feature of boronic acids is their behavior in forming reversible and covalent complexes with diol-containing compounds such as saccharides, sugar alcohols, amines and carboxylates. Under aqueous conditions and pH values around the pK_a of appropriate boronic

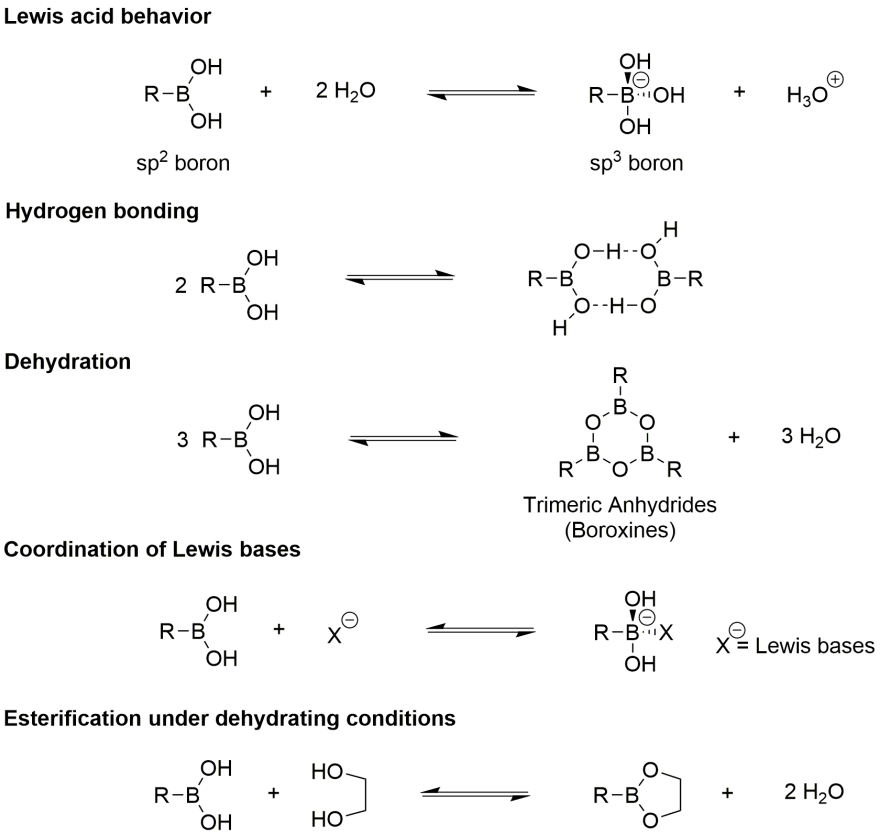

Figure 3: Overview of the manifold interactions of the boronic acid function to nucleophiles and diols.

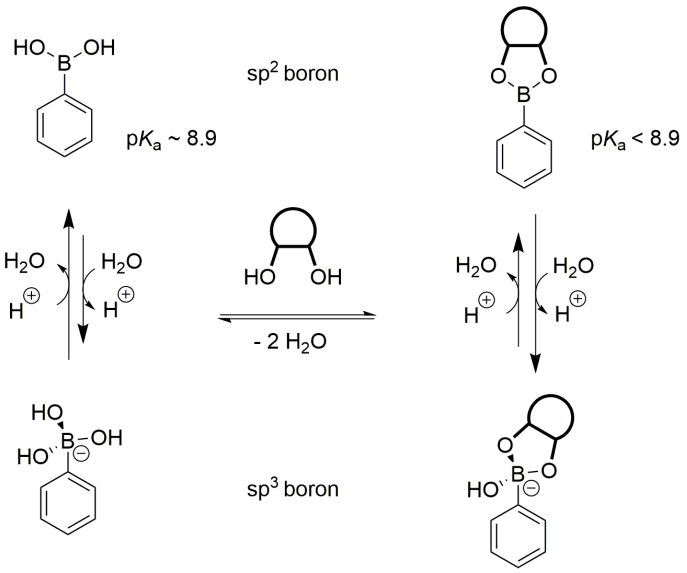

Figure 4: Equilibrium involving phenylboronic acid (PBA), the corresponding boronate, boronic acid diol ester and the corresponding boronate ester in presence of vicinal 1,2-diol under neutral aqueous conditions.

acid, 1,2- and 1,3-diol lead mainly to five- or six-membered boronate esters by the condensation of two equivalents of water (Figure 4). Lowered pK_a values (increased Lewis acidity) of appropriate boronic acid esters (e.g. phenylboronic-fructose ester with a pK_a of 4.6) compared to the original boronic acid (sp^2 hybridized) can be observed due to the esters increased bond angle strain (trigonal planar boron) and is dependent upon the nature of the involved boronic acid, the diol acidity and solvent.[12] As a matter of fact, tetrahedral boronate complexes (sp^3 hybridized boron) are favorably formed under physiological conditions. Associated is the release of bond angle strain (120° versus 109°) whereas in practice the apparent pH of the medium, respectively the pK_a of the boronic acid, the boronate and the diol are influencing parameters of the equilibrium and thus the quantity of the formed boronate species.[12-13] For example, vicinal diols (e.g. catechol with a pK_a of 9.3) are more acidic and show higher affinities than simple alcohols (pK_a in the range of 16) due to possible hydrogen bond stabilization via neighboring hydroxyl groups and inductive effects of the neighboring oxygen. Furthermore, the structural feature of the interacting vicinal diols is mainly determined by the constitutional position, steric configuration and molecular environment (solvent) of the hydroxyl groups.

Early studies of Lorand and Edwards[14] in 1959 used the pH depression method for the determination of apparent boronic acid diol binding constants K_b and recent investigations

Table 1: Selected binding constants K_b [M^{-1}] of phenylboronic acid (PBA) in presence of prominent diols determined via the ARS assay.

Alizarin Red S.	catechol	D-fructose	D-glucose	D-galactose
1300	830	160	4.6	15
D-mannose	**D-mannitol**	**D-ribose**	**D-lactose**	**sucrose**
13	120	24	1.6	0.7

mainly based on fluorescent assays revealed notably interaction of catechol followed by moderate affinities of mainly reducing sugars such as fructose, galactose, mannose and glucose. Minor or no binding affinities were found for non-reducing sugars and smaller alkyl alcohols such as sucrose, glycerol and 1,3-propanediol, respectively. Selected binding constants K_b of PBA and prominent diols elucidated by the ARS fluorescence assays are given by Table 1.

SIGNIFICANCE OF BORONIC ACIDS FOR MODERN CHEMISTRY

The unique behavior of boronic acid compounds is the determining factor for their wide application range in modern chemistry.[15] As mentioned before, the electrophilic character (weak Lewis acidity) of trigonal planar boron (sp^2 hybridized) can be inverted in presence of suitable nucleophiles (Lewis bases) associated by the formation of anionic and tetrahedral boron compounds (sp^3 hybridized) which become now nucleophilic. In general, both species, trigonal and tetrahedral boron present in many boron-element combinations such as B-X (X = H, C, O, N, F, Cl, etc.) are stable, fortunately retain significant reactivity and can be tailored in terms of their structural and electronic behavior for desired reaction routes and applications (Figure 5).

In the past decades, the development of boron-based chemistry lead to several new reactions which uses boron derivatives as building blocks and intermediates for the synthetic organic chemistry[16-18] such as asymmetric (enantioselective)[19-20] and multicomponent[21-23] as well as metal-catalyzed reactions.[24-25] The latter process is better known under the term Suzuki-Miyaura reaction (Nobel Prize 2010)[26] and enables the controlled and selective carbon-carbon bond formation of e.g. alkyl, alkenyl and biphenyl using alky-, alkenyl-, or aryl boronic acids in presence of alky- or aryl halogenides and catalytic amount of an activated palladium(0) specie (Figure 6a). Accompanied with this cross-coupling reaction behavior are advantages such as mild reaction conditions, water stability, high yields, tolerance of a broad range of functional groups and the nontoxic and environmentally friendly behavior.

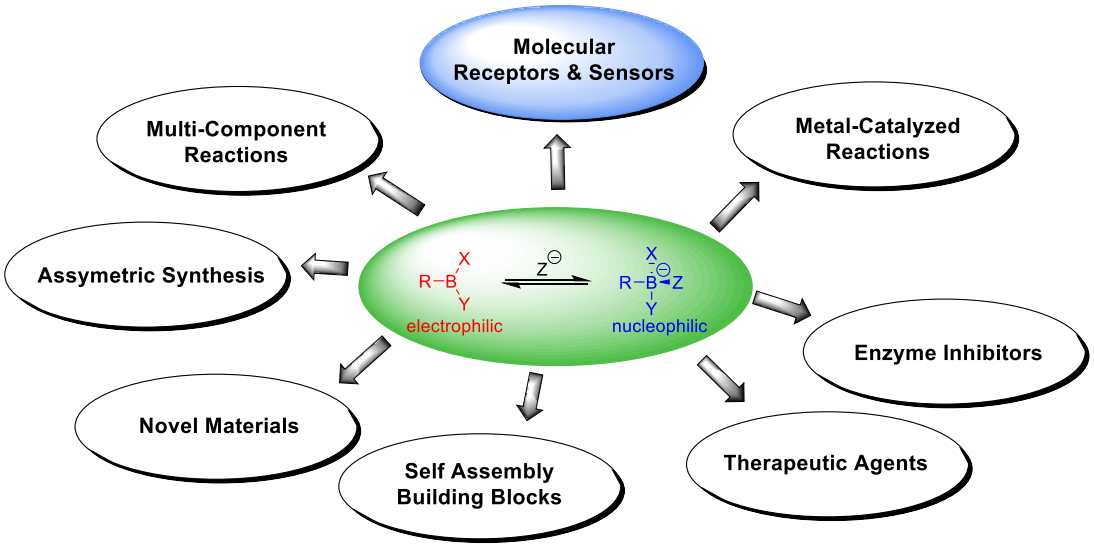

Figure 5: Versatile applications of organoboron compounds in modern chemistry enabled by the unique chemical behavior of the trigonal (electrophilic) and tetrahedral (nucleophilic) boron species (center equation). The field of molecular receptors/sensors is highlighted due to the in general remarkable relevance in diol sensing and in the sensing concept described within the present thesis.

With this valuable synthetic tool in hand, complex bioactive molecules exhibiting biological and medicinal applications can be easily synthesized and used as pharmaceutical and therapeutically agents for clinical use. [27-30] A prominent commercial pharmaceutical product is Velcade®,[31] which contains bortezomib, an α-aminoboronic acid-based protease inhibitor[32] as the active component for the treatment of multiple myeloma – a disease of bone marrow (Figure 6b). Another commercial pharmaceutical product is Kerydin®. The active component and fungicide tavaborole (a fluorinated benzoxaborole which is equal to compound **9**),[33] exhibit a high effectivity against onychomycosis which affects the nail and nail bed (Figure 6b).

Promising achievements have been gained with respect of human immunodeficiency virus (HIV) infection[34] which primarily occurs during heterosexual intercourse whereas the HIV virions from seminal fluid diffuse through the vaginal mucosa. The concept shown in Figure 6c represents an interesting approach for preventing HIV infection using copolymers of 2-hydroxypropylmethacrylamide either carrying phenylboronic acid (PBA) or salicylhydroxamic acid (SHA) moieties.[35] Application of the viscoelastic gel before intercourse (vaginal pH of 4-5) result in partial boronate esterification with the SHA groups and consequently in low cross-linking of the copolymers. By increasing the pH (>5.5, after insemination via basic semen) favored boronate esterification can be observed resulting in a highly covalently crosslinked elastomer. This effective HIV barrier prevents the HIV virions from reaching the vaginal

mucosa. Furthermore, ingeniously designed materials with novel electronic, optical or mechanical properties such as self-assembly building blocks[9] macrocycles,[22, 36-37] molecular capsules[38-39] and also polymeric structures[40-43] can be built up from multi-functional small molecules using boroxines or boronic acids. A highlight with respect to the present thesis is the field of molecular sensing and recognition via boronic acid-appended receptor compounds and will be intensively discussed within the following chapters.

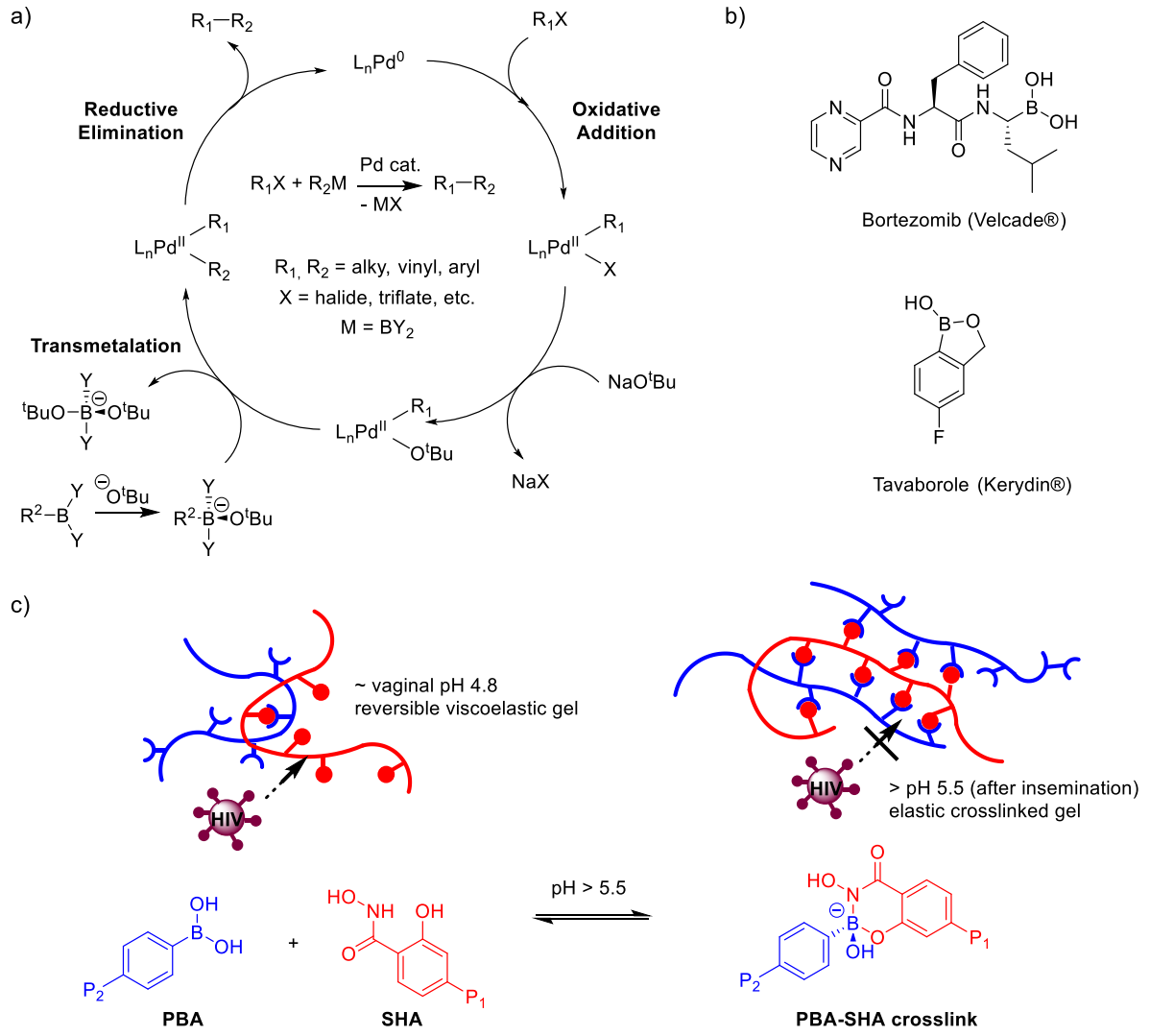

Figure 6: a) Mechanism of the Suzuki-Miyaura C-C coupling reaction mediated by the oxidative addition, transmetalation and reductive elimination step. b) Selected commercial pharmaceutical components for therapeutic applications such as the active component bortezomib in Velcade® and tavaborole in Kerydin®. c) A hydrogel-based concept for preventing HIV infection during heterosexual intercourse. After semination the cross-linked PBA-SHA gel is formed via pH increase and is no longer permeable for HIV virions.

BORONIC ACID-BASED RECEPTORS AND SENSORS FOR DIOLS

Beside lipids, proteins and nucleic acid, carbohydrates are one of the most abundant and of course essential biomolecules. Due to their regulative function in biological and medicinal processes, these analytes have gained a great deal of interest. As stated earlier, boronic acid-based compounds provide high potential to be used as receptors and sensors for the detection of carbohydrates as they can reversible and covalently bind to cis-1,2- or 1,3-diol-containing saccharides under aqueous conditions and even in the physiological range (see chapter 3.1 and Figure 4). Despite, approaches which use other techniques than boron-diol interaction are also known.[44]

Since the early 1990ies[14] tremendous efforts were carried out concerning boronic acid-based receptors with the goal of finding "the" sensing method which enables the selective and unambiguous detection of a specific carbohydrate. The volatile rise in the development of sensing techniques assisted by boronic acid-containing receptors/sensors is exemplary shown in Figure 7. Especially the wealth of carbohydrates caused by their complex equilibrium in water (free keto- or aldehyde, furanose and pyranose forms as well as α-/β-anomers of them) and their in part small structurally/sterically differences with respect to the carbon stereocenters (enantiomers and epimers) complicate the selective sensing approach of boronic acid-based chemosensors.

Until today, an explicit selectivity for any carbohydrate could not be successfully achieved and thus the selective detection stays a challenging task although the concept of the

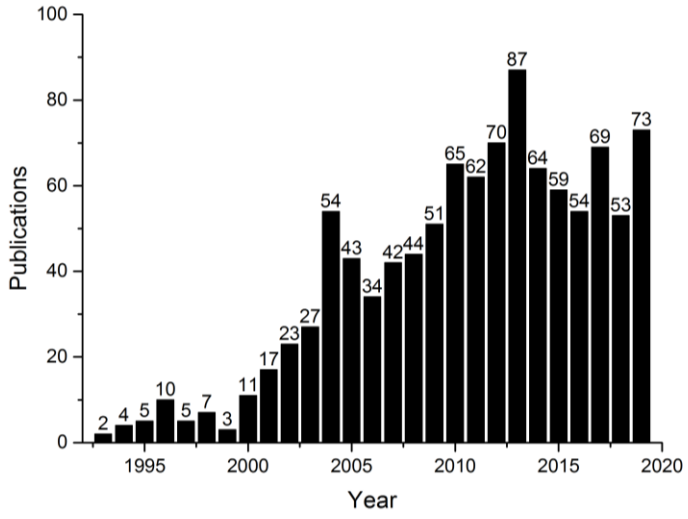

Figure 7: Sensing techniques based on boronic acid-containing receptors/sensors illustrated as publications per year containing the term "boronic acid sensor" via SciFinder® search (10/2019).

simple key and lock is evident and known for a long time within the natural world. Omnipresent examples are the mammalian senses of taste and smell which encourages the modern synthetic chemist and analyst to create artificial and highly selective receptors capable of mimicking natural receptors.[45-46] Therefore, the issue of insufficient analyte selectivity can be compensated via a rational design for the creation of synthetic receptors with a good deal of predictability and selectivity.

A simplified example of a possible molecular scaffold for the recognition of a target analyte is shown in Figure 8a. In presence of the specific analyte molecule, which should selectively bind at the binding site of the receptor, the chemical behavior of the receptor and the reporter moiety is altered. The binding event is simultaneously converted to an output signal at the reporter unit that is e.g. arbitrarily switched from the original status "OFF" to "ON" (or inversed from "ON" to "OFF" depending on the chemical/physical property of the reporter before and after analyte interaction). Consequently, the overall process of analyte binding converts the receptor with a covalently bound reporter moiety into an analyte sensitive sensor. The concatenated physical property changes such as the change in fluorescence emission can be measured. Effectively spoken, these two processes of selective binding and signal modulation are bridging the gap between the events of analyte binding/property change (molecular level) back to the recordable signal change which is finally observable by the analyst (macroscopic level).

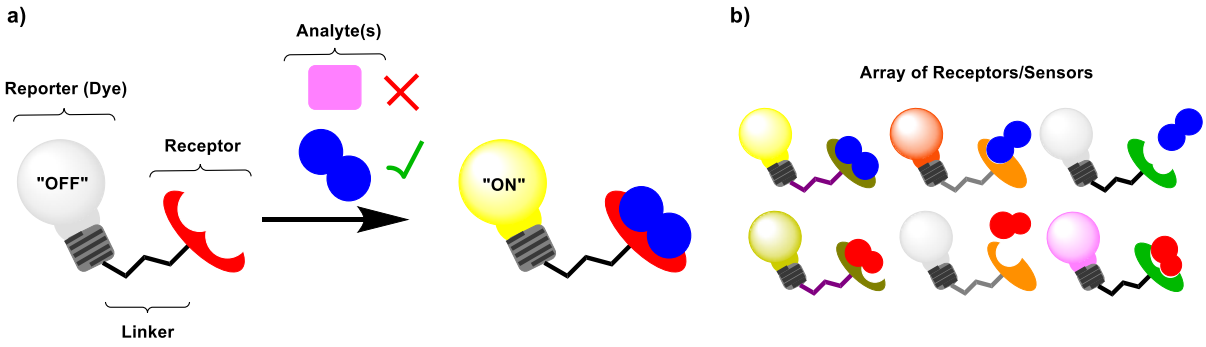

Figure 8: a) Simplified scheme of an artificial and selective molecular receptor/sensor scaffold containing the receptor moiety with a specific binding site to a target analyte, a molecular linker and reporter unit. In case of positive binding the chemical behavior of the receptor and the chemical/physical behavior of the reporter mediated by the linker (if necessary) is altered. The reporter output signal of both states (no and positive binding) can be measured by e.g. a change in absorbance or fluorescence emission. b) Simplified scheme of the response of a sensor array containing three receptors in presence of two different analytes creating increased discrimination power due to different receptor-analyte interaction and associated property changes.

Another clever approach that avoids the need of strong analyte selectivity uses a pool of structurally and chemically diverse receptors/sensors. This concept is better known under the term of array sensing. A significant increase of the discrimination power of similar analytes such as monosaccharides can be achieved due to the extended information given by the specific signal of each receptor/sensor upon analyte binding (Figure 8b).[47] The combination of a sensor array with chemometric techniques such as principle component analysis (PCA) or hierarchicalcluster theory (HCA), to name only two examples, represents a powerful and extended tool for complex sensing tasks.[46, 48-49]

Sensing techniques for carbohydrates using boronic acids[50-51] primarily use optical[52] or electrochemical[53-55] property changes upon diol binding. By far, fluorescence spectroscopy,[56] a very useful tool for the investigation of cells and tissues using biochemical contrast agents[57-58] in combination with boronic acid-based receptor molecules have attracted the most attention and numberless sensing systems for carbohydrates have been developed and intensively studied.[9, 50, 59-61] In the following the author is giving a brief overview of selected and pioneering concepts of fluorescent boronic acid-based sensing systems for carbohydrate recognition which paved the way for many related sensing systems.

The first report in 1980 of a fluorescent signal modulation induced by a molecular recognition event via calcium fluorescent indicators[62] was the starting point for the development of numerous boronic acid-containing fluorescent systems until today. Seminal work on fluorescence-based diol sensors was accomplished by Yoon and Czarnik who used the fluorescent behavior of anthracene by attaching a boronic acid function for the synthesis of 2-anthrylboronic acid **19** (Figure 9). At the same time Russel registered a patent which describes fluorescent derivatives of the basic structure **20** for diol sensing.[63] The "ON"-"OFF" chemo-

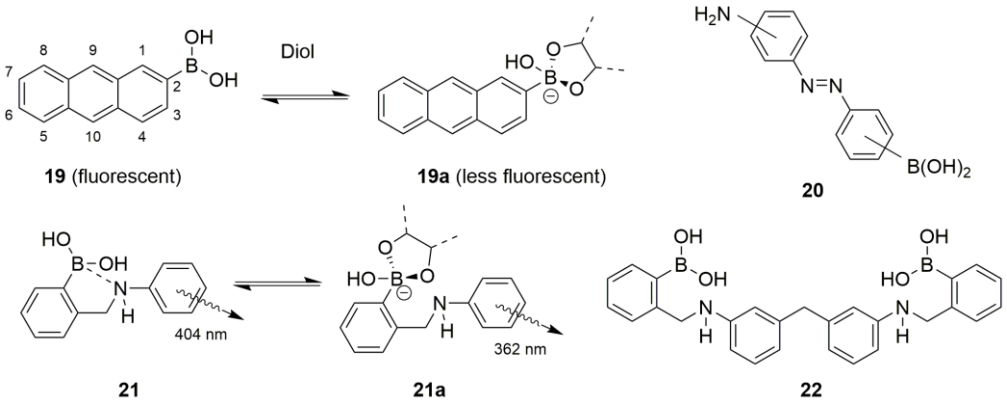

Figure 9: Early (19 and 20) examples of fluorescent ICT boronic acid-based receptors/sensors for saccharide sensing tasks and the first example (22) of a bidentate receptor for increased D-glucose selectivity.

sensor **19** uses the mechanism of excite-state internal charge transfer (ICT)[64-65] for signal modulation and is fluorescent in absence of diol but experiences a decrease in fluorescence emission in case of diol binding to the boronic acid moiety. The accompanied hybridization change upon diol binding from a sp^2 (**19**) to a sp^3 boron center (**19a**) is assumed to be the driving force on the ICT. In addition, further investigations concerning a anthrylboronic acid with boronic acid in position nine (not shown) revealed only minor changes in the fluorescence emission which might be the result of steric hindrance of the neighboring hydrogen atoms.[66]

Another sensory approach was achieved with the aniline derivative **21**.[67] In presence of D-fructose a shift in the fluorescence emission spectra from 362 to 404 nm with respect to the original spectra was observed. The mechanisms which influence the aniline fluorophore are assumed to be based on twisted internal charge transfer (TICT) for the unbound boronic acid and local exited states (LE) for the bound boronate-diol complex and could be further supported by derivatives of **21** with boronic acid in *meta* and *para* position.[68] A stabilization of the excited state of **21** is enabled by a nitrogen lone pair coordination to boron (in aprotic systems) and is released by the formation of the corresponding anionic boronate with respect to either diol ester (**21a**) or increased pH. Especially, the latter aspect can be an issue by using ICT systems under practical conditions. The previous concept was enhanced by the synthesis of the bidentate and symmetric compound **22.** Two suitable attached boronic acid groups enable increased selectivity of D-glucose due to an assumed chelation effect.[69] Consequently, the selectivity for glucose compared to D-fructose (K_{gluc}/K_{fruc}) could be increased from 0.1 to 2.5 with respect to receptor **21**, respectively. Further ICT sensors were developed by Lacowicz and coworkers.[70]

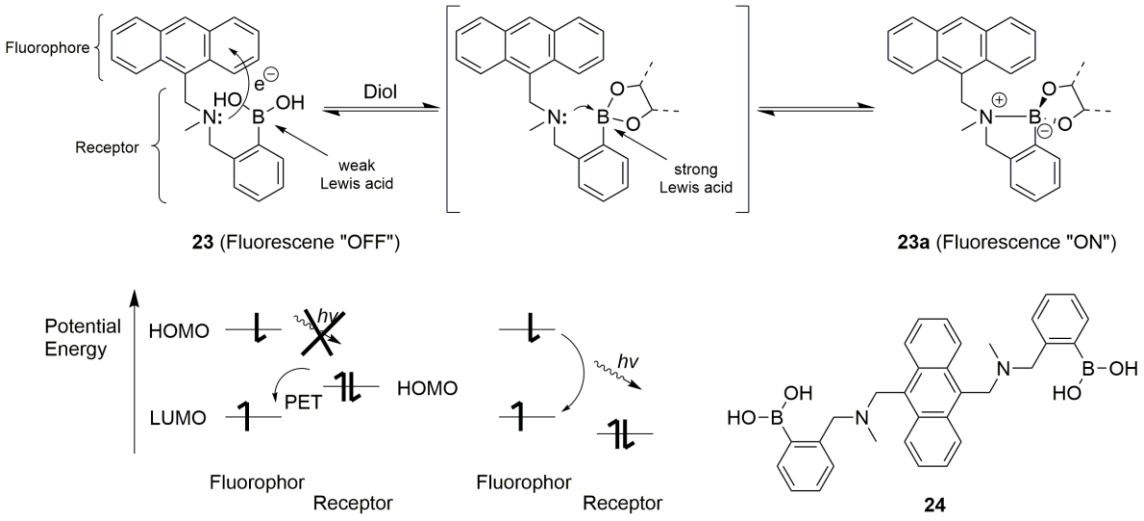

Figure 10: First example of a fluorescent "OFF" - "ON" PET boronic acid sensor for diol sensing. The mechanism of PET for the modulation of the fluorescence signal is illustrated as well.

Another class of most fluorescent sensor approaches is based on the mechanism of photoinduced electron transfer (PET).[71-73] Simply spoken, the receptor moiety transfers an electron from the HOMO to the LUMO of the excited fluorophore which disables the fluorescence emission. In the case of positive diol binding to the receptor the fluorescence emission is restored due to the altered redox potential of the receptor and the electron transfer is no longer energetically favored (Figure 10, bottom). Remarkable of PET-based sensors is the improved robustness against pH changes, which is suppressed by the structural character of the tertiary Lewis basic amines and the proximate Lewis acid *o*-methylphenylboronic acid. The monodentate receptor **23** illustrated by Figure 10 is the first mentioned PET sensor for saccharide detection that was introduced by James and Shinkai. For example, fluorescence is "OFF" in absence (**23**) and "ON" (**23a**) in presence of suitable saccharide.[74] Sensor **24** represents an advancement of **23** and exhibit also the ability to selectively (increased selectivity from 0.6 to 1.4 with respect to receptor **23** and **24**, respectively) chelate a glucose molecule due to a suitable binding pocket generated by the preferred position and distance of the two attached boronic acid binding sites and the resulting bidentate character of **24**.[75] The order of saccharide selectivity for **24** was found to be glucose > allose > fructose > galactose > ethylene glycol.

Due to the complex equilibrium of saccharides (open chain, pyranose, furanose forms and α-, β-anomers, respectively) and their resulting high number of plausible hydroxy groups which can bind to boronic acid receptors one is interested in the exact binding modes to synthesize highly selective receptor scaffolds. Investigations of Norrild et.al. who examined the ^{1}H NMR shifts and ^{13}C NMR coupling constants concerning the binding modes of **24** to D-glucose revealed favored binding via the 1,2- and 4,6-hydroxy groups of α-D-glucopyranose (Figure 11, compound **24a**) in anhydrous deuterated methanol and an increasing amount of a 1,2,3- and

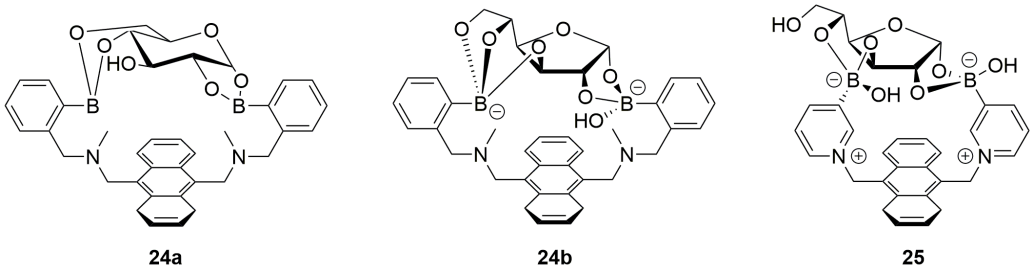

Figure 11: Binding modes of receptor 24 to D-glucose are assumed to be formed via the 1,2- and 4,6- hydroxy groups of α-D-glucopyranose in MeOD (24a) and increasingly via the 1,2,3- and 5,6-hydroxy groups of α-D-glucofuranose when water is present. After 8 days 24b is the predominant species. In D_2O the bipyridinium analogon is exclusively binding to the 1,2- and 3,5-hydroxy groups of α-D-glucofuranose resulting in 25.

5,6-bound complex of **24** to α-D-glucofuranose (Figure 11, compound **24b**) when equilibrated for a longer time.[76] In presence of water the complete equilibration to **24b** could be observed after a little while. A similar observation was found by the esterification of the 1,2- and 3,5-hydroxy groups of α-D-glucofuranose with a bipyridinium receptor resulting the complex **25** (Figure 11) which proofs the concept of a suitable saccharide binding pocket provided by tailored receptor design.[77]

With regards of diol receptors containing simple binding pockets also other clever approaches have been developed which use molecular tweezers or self-assembly inclusion complexes with cyclodextrins (CD). The bis-boronic acid PET sensor **26** is an example of a molecular tweezer which experiences a fluorescence change at 377 nm upon increasing concentration of D-glucose, -galactose, -mannose and -fructose.[78] Interestingly, the second emission band at 470 nm shows a different behavior for each of the saccharides. Increasing concentration of D-glucose and -mannose induces a decrease in the intensity, for D-fructose no change can be observed while D-galactose is quenching this band at low concentration followed by increasing intensity at higher D-galactose concentration. D-glucose, -galactose and -mannose are assumed to form a cyclic 1:1 complex with **26** and a concatenated spatial separation of the two pyrene fluorophores that lead to the quenching of the intramolecular excimer emission at 470 nm.

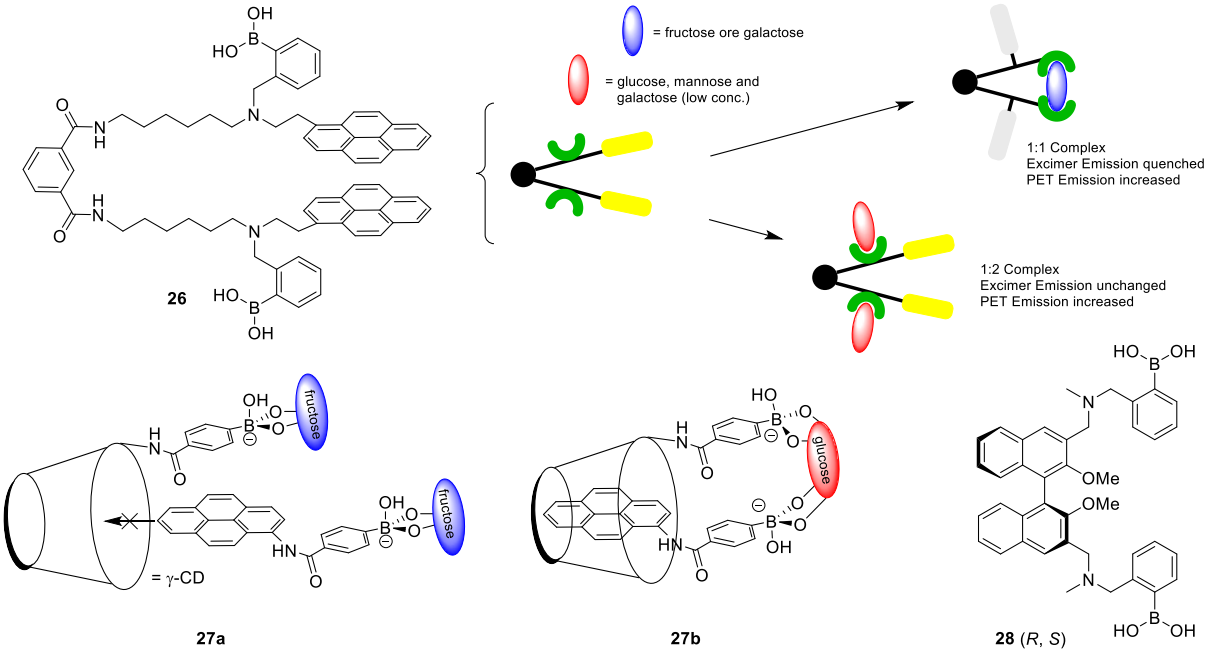

Figure 12: Molecular self-assembly sensors including boronic acid-based tweezer 26 and the D-glucose selective γ-cyclodextrin inclusion system for monosaccharide detection with increased molecular selectivity. The chiral BINOL-based sensor 28 is the first example for the discrimination of chiral monosaccharides.

Furthermore, D-galactose is assumed to form a 1:2 complex at higher concentrations while D-fructose only forms a 1:2 complex at all time. The sensing/folding behavior of **26** is exemplary shown in Figure 12. Increased selectivity to D-glucose, which is by the way the sugar of highest interest due to its medicinal significance, could be achieved with a combinatorial approach of a fluorescence sensor and γ-cylcodextrin.[79] When D-fructose, -galactose or -mannose is added the non-inclusion and weak fluorescent complex **27a** (1:1 boronic acid fructose complex) is formed. In presence of D-glucose the pyrene moiety is exclusively enclosed by the CD cavity due to the favored spatial arrangement of a 2:1 boronic acid-glucose complex (**27b**) and increased fluorescence emission can be observed.

Clever sensor design enabled also the discrimination of chiral monosaccharides and hydroxy-carboxylic acid such as the D- and L-enantiomers of e.g. glucose, fructose and tartaric acid.[80-82] Exemplary, compound **28** (pure enantiomers of it, respectively), a 1,1'-binaphthalene-2,2'-diol (BINOL)-based receptor was used to differentiate the D-/L-enantiomers of glucose, fructose, mannose and galactose. The sugars form a 1:1 complex with **28** inducing an increase in fluorescence intensity which is specific for each receptor (*R*, *S*)-diol (D-/L-) combination, respectively. Furthermore, the highest complex stability constants were found for the enantiomer sets of **28** (*R*) or **28** (*S*) in presence of D- or L-monosaccharide, respectively.

Beyond the concept of molecular scaffolds composed of a covalently bound receptor and reporter moiety (so-called integrated molecular sensors) the development of competitive approaches plays a major role within the field of carbohydrate sensing. In general, these systems which can be categorized under the term Indicator Displacement Assays (IDA)[83] use a receptor molecule and a separated reporter molecule which associate via a reversible and covalent (primary concept) or supramolecular (recent concepts) interaction. In presence of a target analyte that positively binds at the same binding site of the receptor species, both components (receptor and reporter) dissociate. The concatenated physical property such as absorbance or fluorescence of the reporter is altered and can be recorded. Consequently, the qualitative and quantitative monitoring of diols is enabled. A simplified illustration of the IDA concept is exemplary shown in Figure 13 (top).

Wang and co-workers used the catechol dye Alizarin Red S (ARS) and phenylboronic acid (PBA) as the reporter and receptor components, respectively, for the generation of a two-component system (Figure 13, bottom).[84] ARS alone is non-fluorescent but increased fluorescence intensity at 565 nm can be observed when PBA is present due to the formation of the ARS-PBA complex **29**. When a carbohydrate such as D-fructose is added ARS is displaced

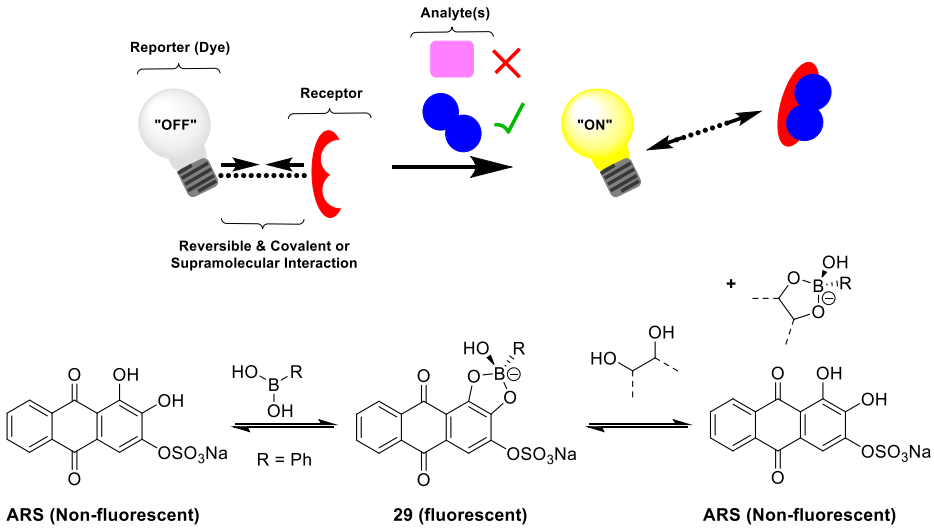

Figure 13: Simplified scheme of an indicator displacement assay (IDA) that uses a receptor and a reporter molecule which are associated via a reversible covalent or a supramolecular interaction. By addition of suitable analyte, the reporter is cleaved from the receptor molecule and experiences a change of its physical property inducing a change in e.g. absorbance or fluorescence emission.

resulting in free non-fluorescent ARS, the corresponding PBA-fructose ester and a decrease in fluorescence emission. The monitoring of the latter using the ARS approach was furthermore intensively used for the determination of binding constants of diols and various boronic acids (chapter 3.1).[12] Similar systems using catechol derivatives as the reporter were also developed by Anslyn et.al.[85-87]

Beside IDA approach, which uses reversible and covalent interactions between the reporter and receptor molecule intensive studies based on supramolecular interactions were carried by the Singaram work group.[88-91] Their first developed sensing system uses the fluorescent dye trisodium 8-hydroxypyrene-1,3,6-trisulfonate (HPTS) as the reporter and 4,4'-*N*,*N*'-bis(benzyl-2-boronic acid)-bipyridinium dibromide (*o*-BBV illustrated by the basic structure **30**) as the receptor/quencher molecule (Figure 14).[91] In general, the dye and quencher form a weakly fluorescent supramolecular indicator-receptor complex due to their oppositely induced charge attraction as illustrated in Figure 14 (top).[90, 92] When a carbohydrate is present the receptor willingly forms a receptor-diol complex (a formal neutral zwitterionic specie) which leads to the dissociation of the original indicator-receptor complex. This concatenated charge neutralization process leads to an increase in fluorescence emission of the dissociated dye and the quantity as well as binding affinities of diol can be determined via the resulting fluorescence modulation. Strong selectivity for D-glucose of the otherwise non-selective fluorescent approach was found with 3,3'-*o*-BBV (**31**).[89]

The original concept was significantly extended by investigating other reporters/ dyes such as MTPS or TSPP,[93] fluorescent quantum dots (FQD)[94] and structurally as well as charge modified receptors. These BBV's exhibit different bipyridine linkers and altered positions of the attached boronic acid functions (**30**)[89, 95-96], bis-viologen-based (**32**)[97] and bis-ethylpyridinium bipyridinium structures (**33**)[93] as represented by Figure 14 (bottom). Other interesting methods using the approach comprise e.g. a fluorescent array of sensors for saccharides[98] and a fluorescent enzyme assay[99]. A highlight with respect to a clinical application for online-monitoring of the blood sugar level was successfully achieved by imbedding the polymerizable diol receptor/precursor **34** and polymerizable HPTS dye into a poly(2-hydroxyethyl methacrylate) hydrogel.[100]

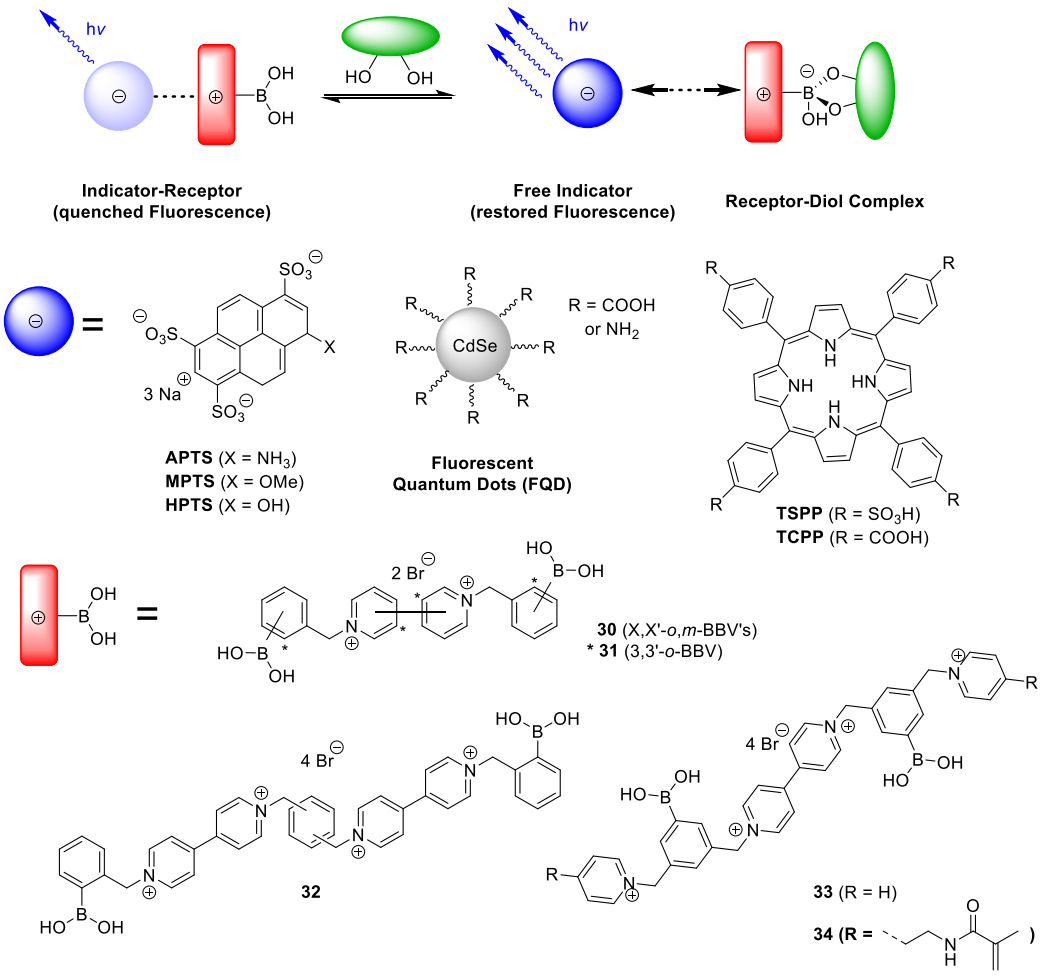

Figure 14: Top, simplified sensing principle of the AIDA concept and corresponding components. The dye and receptor form a weak fluorescent indicator-receptor complex induced by complementary charge attraction. When a diol is added the supramolecular interaction dissociates because of the formation of a neutral zwitterionic boronate-diol ester. Consequently, increased fluorescence can be observed and enable diol sensing. Bottom, exemplary fluorescent dyes, fluorescent quantum dots and versatile viologen-based receptor scaffolds which have been used in several sensing studies by the Singaram workgroup.[88-91]

The previously approach following the concept of an Indicator Displacement Assay (IDA) was further developed by our workgroup using the term Allosteric Indicator Displacement Assay (AIDA).[101-103] Strictly speaking, the binding of the reporter/indicator and the analyte takes place at another (allosteric) site of the receptor/quencher. This comprises the electrostatic interaction of the indicator and receptor and on the other site the esterification of diol via the boronic acid functions.

Apart from diol sensing the AIDA concept was used in the field of molecular logic.[104-105] The material inputs of dye, quencher and saccharide follow the truth table of an Material Implication (IMP) gate, whereas fluorescence (output = 1) or diminished fluorescence (output = 0, using a threshold) of HPTS dye are the output signals (Figure 15).[106] The resulting truth table of the IMP gate using HPTS dye as the driving signal, BBV and D-fructose as the two input signals is represented in Figure 15. Suitable concatenation of the IMP and FALSE gate enable the generation of all 16 Boolean operations[107] such as the AND, OR or XOR gates. These logic operations are inalienable when one is thinking about modern digital life with plenty of computer systems around us. In a next step and by suitable concatenation of the described IMP function the construction of a 4-bit full adder could be achieved by the use of microtiter plates and a processing routine.[108]

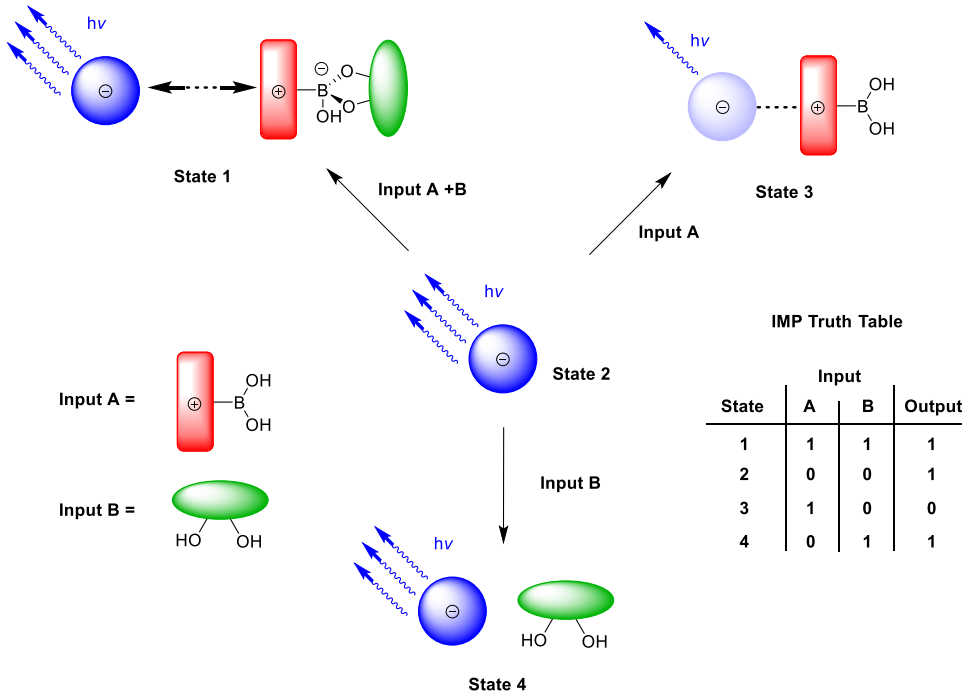

Figure 15: Realization of the IMP gate and the corresponding truth table using the AIDA concept. The HPTS dye is the driving signal, whereas BBV and/or D-fructose are the input signals. Fluorescence (output = 1) or diminished fluorescence (output = 0, using a threshold) generate the truth table of the IMP gate.

Furthermore, our group was successful in developing a combined material-logic approach for playing tic-tac-toe with a sugar-based molecular computer.[108]

Plenty other sensing techniques that follow similar approaches using single or competitive systems showing more or less selectivity for appropriate analyte can be found in the literature and go beyond the scope of this overview. Thus, the author refers to the many high-quality reviews available in literature.[9-10, 50, 60-61, 109-110]

With respect to the almost endless examples of fluorescent based receptor systems one should clearly keep in mind the negative aspects of the sensing technique such as the one-dimensional signal modulation of the fluorescent reporter, which provides no information in terms of the analyte's quality. Furthermore, most approaches show weak specificity to the analytes and the detection of a target analyte in mixtures with similar compounds is handicapped or merely possible by the use of receptor arrays. The often complex molecular scaffolds with complicated routes in synthesis, the need of special solvents which are commonly not physiological and the sensitivity to pH changes of the fluorescent unit are further drawbacks of these systems.

Encouraged not only by the named analytical drawbacks a new sensing concept based on one simple receptor molecule and the discriminative ^{19}F NMR spectroscopy was developed and will be described within the next chapters.

THE ^{19}F PROBE & ^{19}F NMR SPECTROSCOPY – A VALUABLE SENSING TOOL

Fluorine is a remarkable element and exhibits remarkable properties. The halogen's polar and steric effects have a distinct influence on the physical and chemical properties of organofluorine compounds at which it is attached to - even as a single substituent.[111] Fluoride minerals such as fluorite CaF_2 are the most abundant halogen sources in the crust of the earth (e.g. 270-740 ppm fluorine versus 10-180 ppm chloride in sedimentary rocks). In contrast, only 12 naturally organofluorine compounds such as fluoroacetate are known today.[112]

Under standard conditions elemental fluorine is a very toxic bimolecular gas and overall the most reactive element. Furthermore, this monotopic element (100% natural abundance of the stable ^{19}F isotope beside 17 other non-stable artificial radioisotopes) exhibits the strongest Pauling electronegativity of $\chi = 4.0$ which induces a less covalent and more electrostatic character to a C-F bond and a resulting larger molecular dipole.[113] Although the existence of such a polarized bond, fluorine provides no good donor ability due to tightly held lone electron pairs of the electronegative fluorine substituent. Usually, these lone pairs are weakly involved in resonance or hydrogen bonding.

Associated with the electron-withdrawing effect of fluorine in organofluorine compounds is the induced acidity change (in general decreased pK_a values compared to a non-fluorinated derivative) of adjacent functional groups such alcohols and carboxylic acids. This effect is highly dependent on the position and quantity of attached fluorine or fluorine-containing substituents with respect to the appropriate function. The size of the fluorine atom (1.47 Å) and the C-F bond length (1.35 Å) are intermediate between hydrogen (1.2 Å) and oxygen (1.52 Å) and the C-O bond (1.43 Å), respectively.[114] Thus, the substitution C-F for C-OH results in a virtually neutral property change. Attached at organofluorine compounds a single fluorine nucleus is the smallest substituent that can replace hydrogen and is not significantly affecting the steric property (conformational free energies) of e.g. cyclohexane derivatives.[115] Another associated property change by introducing fluorine(s) into a molecular scaffold of interest is the enhancement in the lipophilicity. This feature is highly desired for the design of fluorinated drugs that benefit from improved absorption and transport efficiency with regards to e.g. the gut or blood-brain barrier permeability.[116] Therefore, it is not surprising that the interest in fluorinated compounds continuously raises also in the fields of biological and medicinal chemistry and of course in drug discovery processes.[117-119]

Apart from the previously presented chemistry, fluorine can conveniently be used as an attached and alternative molecular reporter (a valuable molecular probe) to investigate the structural behavior of ^{19}F-labelled proteins or the metabolism of pharmaceutical compounds assisted by ^{19}F NMR and/or ^{19}F-MRI.[120-123] This concept which uses the properties of an attached ^{19}F probe for monitoring structural changes or binding events of fluorinated receptor compounds assisted by ^{19}F NMR spectroscopy will be discussed in the following chapters.

OUTSTANDING NMR PROPERTIES OF THE ^{19}F NUCLEUS

In terms of the available and manifold analytical tools involving spectrometric (e.g. optical and mass spectrometry), chromatographic (e.g. gas- and liquid chromatography), electrochemical (e.g. conductometry and potentiometry) and spectroscopic (e.g. infrared and UV/vis spectroscopy) and combined approaches, Nuclear Magnetic Resonance (NMR) spectroscopy is one, or even the most powerful technique. Especially the organic and biochemists are interested in clarifying complicated molecular structures are profiting considerably from NMR.[124-125]

Beside ^{1}H and ^{13}C, ^{19}F NMR spectroscopy is the most intensively studied method due to the increasing number of fluorine containing (bio) molecules and the specific spectroscopic properties that can be made accessible via an attached ^{19}F atom. Overall, 18 isotopes of fluorine are known, whereupon only the 100% natural abundant ^{19}F nucleus exhibits the highest stability. Further properties which highlight the nucleus with a nuclear spin of ½ as a suitable NMR probe are the coherent high sensitivity of 0.83 relative to ^{1}H, the resulting sharp NMR signals (no quadrupole moment present), the large chemical shift range of approximately 400 ppm for organofluorine compounds and well separated ^{19}F signals that usually lack of signal overlap. Important NMR parameters of the ^{19}F nuclei and for comparison other common NMR active nuclei are listed in Table 2. Especially the absent fluorine background signal of otherwise interfering media such as aqueous ^{1}H-containing systems (broad and overlapping signals induced by water or buffer media) and the NMR spectra which have usually first order character provide less complicated and easy interpretable spectroscopic information. Spin-spin coupling of the ^{19}F nucleus to neighboring ^{19}F nuclei as well as to proximate protons can be observed in a similar manner compared to ^{1}H NMR with long relaxation times. Long-range spin-spin coupling constants with a large magnitude can be observed in ^{13}C NMR spectra, which can provide information about the connectivity of the attached fluorine relative to the carbon scaffold. Furthermore, the reliable quantification of fluorinated compounds can be achieved comfortable via signal integration and if necessary by the use of an internal or external fluorine standard such as trifluoroacetic acid (TFA). Considering the broad set of ^{19}F NMR advantages, some disadvantages must be considered such as the high costs of the required NMR hardware and the maintenance compared to cost-saving analytical techniques such as UV/vis or fluorescence spectroscopy. Another drawback with respect to NMR sensitivity and coherent limit of detection (LOD) is the lower sensitivity (10^{-9} and 10^{-11} mol) compared to significantly more sensitive UV-vis (10^{-13} to 10^{-16} mol) and fluorescence spectroscopy (10^{-18} to 10^{-23} mol) as well as highly sensitive mass spectrometry (10^{-13} to 10^{-21} mol).[126]

Table 2: Characteristic NMR parameters of selected nuclei and the highlighted ^{19}F nucleus.[127]

Nucleus	Spin	Gyromagnetic Ratio [10^8 rad s^{-1} T^{-1}]	NMR Frequency [MHz] at 11.75 T	Natural Abundance [%]	Rel. Sensitivity	Shift Range [ppm]
^{1}H	1/2	2.675	500	99.98	1.00	~ 13
^{19}F	1/2	2.518	470.4	100	0.83	~ 400
^{31}P	1/2	1.084	200.2	100	0.07	~ 530
^{13}C	1/2	0.672	125.7	1.11	0.02	~ 250
^{11}B	3/2	0.858	160.4	80.42	0.17	~ 220

Usually, the broad chemical shift range for ^{19}F containing compounds is situated upfield to the commonly used and accepted trichlorofluoromethane (CCl_3F) reference (δ_F set to 0 ppm). The observed δ_F values reported in ppm are negative for most organofluorine compounds. Nevertheless, there are a few examples of structural situations for ^{19}F nuclei leading to positive shifts, for example acyl- and sulfinyl/sulfonyl fluorides (approx. δ_F +20 and +60 ppm). A qualitative overview of the observed ^{19}F shifts for carbon-bound F, CF_2 and CF_3 substituents is represented in Figure 16, left.[128] Considering the position of a recorded fluorine signal with a more positive chemical shift value relative to CCl_3F is situated in the deep field, whereas a signal with a more negative δ_F value relative to CCl_3F lies in the high field (Figure 16, right).

Equation 1 describes the effective magnetic field strength B_{eff} located at the fluorine nucleus that differs from the imposed field B_0 determined by the shielding constant σ. This dimensionless shielding constant is composed of three terms (Equation 2). σ_{dia} is the diamagnetic term corresponding to the opposing magnetic field as a result of the imposed field upon the surrounding electronic cloud of the ^{19}F nucleus. Thus, a higher electronic density (+I/M effects) at ^{19}F leads to a higher shielding (to high field), whereas a lowered electron density (-I/M effects) induces a deshielding (to deep field). The paramagnetic term σ_{para} has its origin in the excitation of p-electrons caused by the external magnetic field and is opposite to σ_{dia}. σ_{i} derives from the effect of neighboring groups (steric influences), which also influence the electronical environment of the ^{19}F nucleus.

$$B_{\mathrm{eff}} = B_0 - \sigma B_0 \qquad \text{(Equ. 1)}$$

$$\sigma = \sigma_{\mathrm{dia}} + \sigma_{\mathrm{para}} + \sigma^i \qquad \text{(Equ. 2)}$$

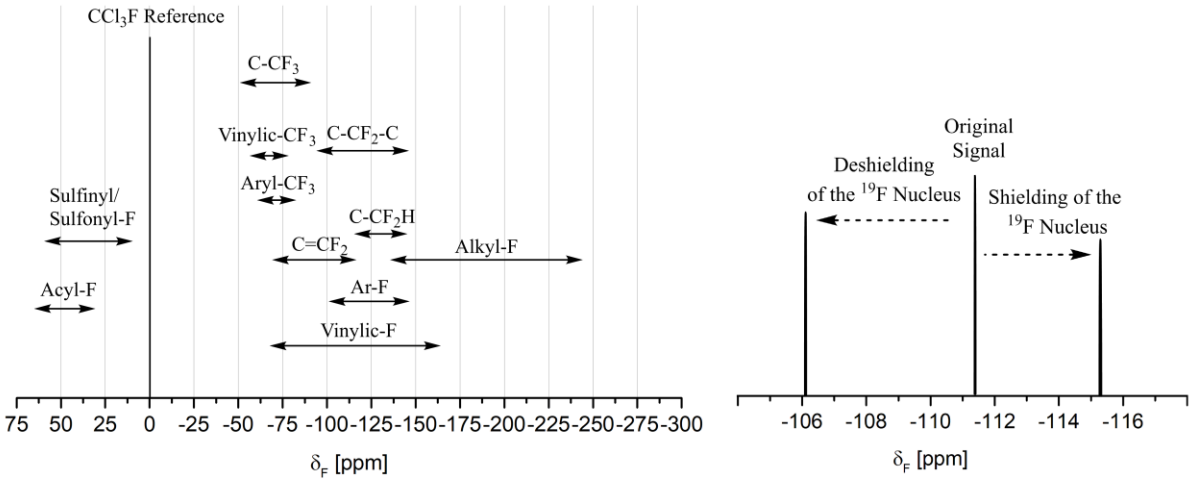

Figure 16: Left, qualitative ^{19}F NMR shift ranges of organofluorine compounds relative to the CCl_3F reference (δ_F = 0 ppm).[128] Right, deshielding and shielding of corresponding ^{19}F probes (approx. δ_F -106 and -115 ppm) in a hypothetical ^{19}F NMR spectrum relative to a reference signal (approx. δ_F -111 ppm) induced by inductive and mesomeric effects of the chemical and magnetic environment.

In addition, electronical changes beside these intramolecular effects can also be affected by intermolecular effects, such as the used solvents. Compared to proton spectra with exclusively s-orbitals present, σ_{para} can be neglected, whereas σ_{para} is dominant when having a look on the fluorine's relative shielding and the existence of p-orbitals. Consequently, the relative shielding behavior known of proton NMR does not fit for the prediction of hypothetical ^{19}F NMR shifts. For more details the author refers to the literature.[128-130]

BRIEF INTRODUCTION TO (^{19}F) NMR SPECTROSCOPY

Pioneering work and evidence of the Nuclear Magnet Resonance (NMR) phenomenon was achieved by Felix Bloch and Edward M. Purcell in 1946 (Nobel Prize in 1952).[131] The basic requirement is the existence of an atom which exhibits a nuclear spin $\vec{P}$ (Equation 3).[132-133] Associated with that spin is a permanent magnetic dipole moment $\vec{\mu}$. The total nuclear spin is results from the spins of the protons (atomic number) and neutrons of appropriate isotope. The mass number is determined by the sum of protons and neutrons. Thus the nuclear quantum number *I* is half-integral for an uneven mass number such as $^{19}_{9}$F or $^{1}_{1}$H (*I* = ½), integer for an even mass number and uneven atomic number such as $^{20}_{9}$F (*I* = 2), and zero for an even mass number and even atomic number such as $^{12}_{6}$C (*I* = 0, no resulting nuclear spin and not accessible to NMR spectroscopy).

$$\left|\vec{P}\right| = \hbar\sqrt{I\,(I+1)} \qquad \text{(Equ. 3)}$$

$$P_z = \hbar\, m_l \qquad \text{with} \qquad m_l = I, I-1, I-2, \ldots, -I \qquad \text{(Equ. 4)}$$

In contrast to optical spectroscopy where transitions occur between electronic states, the NMR technique is based on quantized nuclear spin states, which are degenerated in absence of an exterior magnetic field. A splitting of these degenerated states via an external magnetic field with the flux density $\overrightarrow{B_0}$ can be induced due to the interaction of the permanent magnetic dipole moments – better known under the term Zeeman effect (Nobel Price 1902).[134] Irradiation of high frequency (megahertz range) equal to the energy gap of the states will result in absorbance and emission of irradiation and simply spoken distinct spectral properties of the observed nucleus can be recorded.

Equation 4 describes the nuclear spin in z-direction (predominant field direction) with *I* and the magnetic quantum number (spin orientation) m_l resulting in $(2I+1)$ values for P_z. Consequently, the nuclear spin P_z component of e.g. a ^{1}H nucleus can have either a value of $+\frac{1}{2}\hbar$ (α-state) or $-\frac{1}{2}\hbar$ (β-state) and thus two possible orientations in an external magnetic field are possible. The vector $|P_z|$ is lying on a conus with an angle of $\arccos(\frac{\hbar}{2})/\sqrt{\frac{3}{4}}\,\hbar \approx 54.7°$ to the z-axis (Figure 17, right).

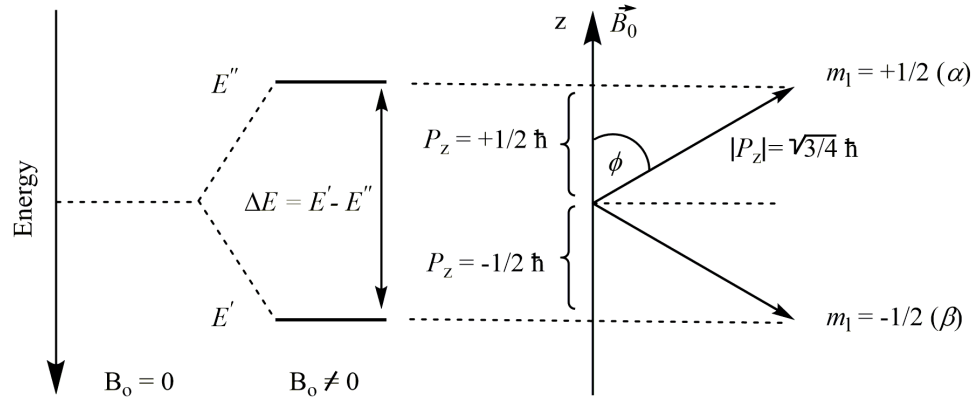

Figure 17: Left, energetic splitting of the ^{1}H nucleus in an external magnetic field with the flux density B_0. Right, orientation quantization of the angular momentum of a ½ spin nucleus (e.g. ^{1}H or ^{19}F) in an external magnetic field (z-direction) with the P_z components and vector $|P_z|$.

As mentioned earlier, the nuclear spin is associated with a magnetic dipole moment as illustrated by Equation 5. The incorporated gyromagnetic ratio γ_N (positive or negative values) can be experimentally determined and is a characteristic dimension with respect to the nucleus of interest. Values of γ_N which determine the detection sensitivity in an NMR experiment of common NMR active nucleus can be found in Table 2.

$$\left|\vec{\mu}_{\mathrm{mag,N}}\right| = \left|\gamma_N \vec{P}\right| = |\gamma_N|\, \hbar \sqrt{I\,(I+1)} \qquad \text{(Equ. 5)}$$

$$\text{in z-direction: } \vec{\mu}_{\mathrm{mag,N,z}} = \gamma_N \vec{P}_z = \gamma_N\, \hbar\, m_l \qquad \text{(Equ. 6)}$$

$$E_{\mathrm{pot}} = -\vec{\mu}_{\mathrm{mag,N}}\, \overrightarrow{B_0} \qquad \text{(Equ. 7)}$$

$$\text{in z-direction: } E_{\mathrm{pot}} = -\left|\vec{\mu}_{\mathrm{mag,N,z}}\right| \left|\overrightarrow{B_0}\right| \cos\phi = -\vec{\mu}_{\mathrm{mag,N,z}}\, B_0 \qquad \text{(Equ. 8)}$$

The orientations of the nuclear spin are no longer degenerated in an external magnetic field with the flux density $\overrightarrow{B_0} \neq 0$ and a splitting of the energy levels (e.g. $m_l = \pm\frac{1}{2}$ for ^{1}H or ^{19}F) can be observed (Figure 17, left). The potential energy E_{pot} is defined by Equation 7 and with the field of $\overrightarrow{B_0}$ in z-direction by Equation 8. The splitting of the energy levels is proportional to the flux density of the applied external field. Transformation using Equation 6 and 8 results in:

$$E_{\mathrm{pot}} = -\gamma_N\, \hbar\, m_l\, B_0 \qquad \text{(Equ. 9)}$$

Irradiation of a suitable angular frequency ω_0 can induce a transition between the energy levels and a "fold down" of the nuclear spins from α to β. Using $\Delta E = E' - E''$, the selection rule $m_l = \frac{1}{2}$ and Equation 9, the energy difference can be written as illustrated by Equation 10.

$$\Delta E = E' - E'' = -\gamma_N \hbar m_l B_0 = -\gamma_N \hbar B_0 \left(-\frac{1}{2} - \frac{1}{2}\right) = \gamma_N \hbar B_0 \qquad \text{(Equ. 10)}$$

In case of NMR resonance ($\Delta E = \hbar \omega_0$) the angular frequency which is also called Larmor frequency becomes $\omega_0 = \gamma_N B_0$. In general, NMR Resonance can be achieved in two ways: the first uses a variation of excitation frequency ω by keeping the field B_0 constant or by keeping ω constant and varying B_0. Modern NMR machines are equipped with superconducting magnet coils that provide magnetic fields up to 24 T (Tesla). For example, at this magnetic field and constant field flux density B_0, the resonance frequency (reference frequency) of ^{1}H is 1000 and 941 MHz at the same field for ^{19}F with the characteristic gyromagnetic ratios γ_N , respectively (different NMR nuclei experience different resonance frequencies ω_0 at the same magnetic field).

The intensity of an observable NMR signal is dependent on the existence of a transition dipole moment and the difference in population numbers of the excited state E' (β) and the ground state E'' (α) as given by the Boltzmann distribution (Equation 11):

$$\frac{N_\beta}{N_\alpha} = e^{\left(-\frac{\Delta E}{k_B T}\right)} \approx 1 - \frac{\Delta E}{k_B T} = 1 - 10^{-5} \qquad \text{(Equ. 11)}$$

$$\text{with } \nu = \frac{\omega}{2\pi} \; ; \; \hbar = \frac{h}{2\pi} ; \Delta E = \hbar \omega_0 = h \cdot 100 \text{ MHz}$$

$$\vec{M} = \frac{\sum_i \vec{\mu}_{\text{mag,N(i)}}}{V} \qquad \text{(Equ. 12)}$$

The NMR signal is proportional to the difference of the population numbers of the α and β states which is marginal as stated above and the transitions are easy saturable and strong magnetic fields are needed. Furthermore, an effective release of energy such as thermic energy to neighboring molecules (spin-lattice relaxation T_1) is necessary to get a suitable NMR signal. In practice, macroscopic NMR samples exhibit more than one single nuclear spin and the total detectable magnetization $\vec{M}$ corresponds to the vector sum of the magnetic dipole moments of the nuclei per volume unit (Equation 12 and Figure 18a).

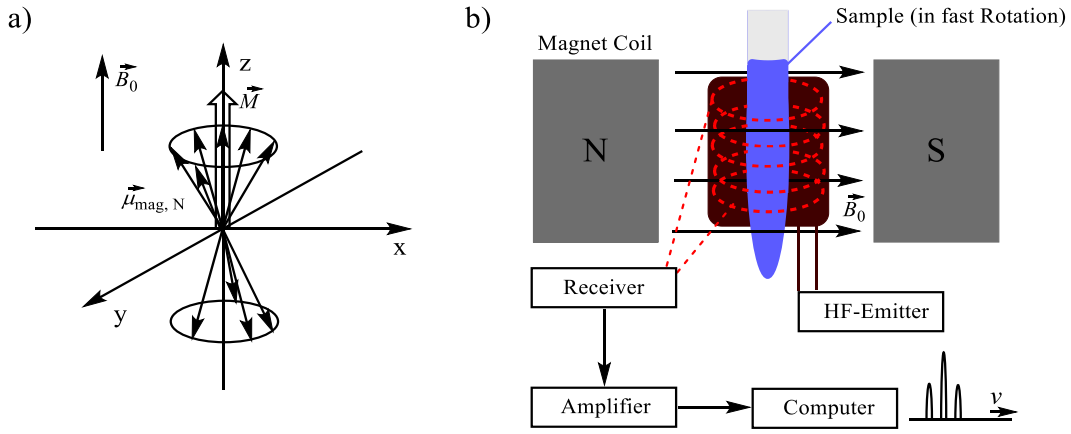

Figure 18: a) Resulting macroscopic magnetization vector $\vec{M}$ of a NMR sample containing N nuclei (with predominant $m_I = \pm\frac{1}{2}$ (α) orientation in z-direction) in a magnetic field with $\vec{B_0} \neq 0$ (z-direction). b) Schematic and very simplified setup of a NMR machine with separated emitter and receiver coils for the elucidation of structural features of condensed matter.

The setup of a NMR machine with an inserted NMR glass tube is exemplary illustrated by Figure 18b. A superconducting magnet coil (helium and nitrogen cooled at ~ 2.2 K) generates a strong magnetic field with a high and constant field homogeneity and the flux density $\vec{B_0}$ in z-direction. A NMR glass tube (in fast rotation to minimize field inhomogeneity) containing the condensed matter with the nuclei of interest is inserted in this field and the nuclear magnetic moments precess around the z-axis with their characteristic Larmor frequency ω_0.

In a continuous wave (CW) experiment the high frequency emitter coil induces a weak electromagnetic field $\vec{B_0}$ with the frequency ν in x-direction. NMR resonance is obtained when the frequency ν meets the requirement $\omega_0 = 2\pi\,\nu$ (with $\Delta E = \hbar\,\omega_0$) and the nuclear spins become excited and relax in a stationary state. The macroscopic magnetization vector $\vec{M}$ (exhibits components in x- and y-direction) rotates around the z-axle and the resulting transverse magnetization is detected by the receiver coil and then converted to an alternating voltage signal (Figure 18a).

In a CW-experiment the electromagnetic $\vec{B_0}$ field is irradiated continuously and varied whereas modern NMR technique uses experiments with short pulses and a strong $\vec{B_0}$ field. The latter method is better known under the term Fourier Transformation (FT) NMR and the short high frequency pulse applied induces a broad frequency spectrum that covers the whole range of resonance frequencies and thus all nuclei become excited simultaneously. After the high frequency pulse, the magnetization vector rotates by the influence of $\vec{B_0}$ around the z-axle (with

components in x- and y-direction as well) whereby each sort of nuclear spin exhibits their characteristic Larmor frequency ω_0. The receiver coil detects a time-dependent signal (Free Induction Decay – FID) which is then converted via Fourier Transformation (computer hard- and software) to the final NMR spectrum. Typically, a NMR spectrum is represented as the signal intensity versus the chemical shift δ (a relative and dimensionless value which is specified by Equation 13). The resulting chemical shift δ (in ppm) of a specific NMR nucleus is independent from the applied magnetic field strength and is furthermore relative to a specific reference signal such as tetramethylsilane and trichlorofluoromethane used in ^{1}H and ^{19}F NMR experiments, respectively. After excitation the spin system relaxes to the ground state by releasing the energy to the surrounding lattice and a new pulse can be applied. Repetition of the excitation and relaxation processes (number of scans) provide NMR signals with good signal-noise ratios (S/N) in a relatively short time (depending on the set scan number).

$$\delta = \frac{\nu_{Sample} - \nu_{Reference}}{\nu_{Spectrometer}} \qquad \text{(Equ. 13)}$$

Beside the earlier mentioned spin-lattice (T_1 or longitudinal) relaxation which describes the return of the excited nuclear spins to the thermic ground state by releasing thermal energy, two other relaxation processes, the transversal relaxation (T_2) and the time constant T^*_2 are limiting factors of the NMR performance. On the other hand, the relaxation times provide unique information of the molecular dynamic. The relaxation time T_1 becomes relevant if no complete relaxation between two NMR experiments is awaited. Consequently, every further NMR experiment experiences less magnetization and signal intensity.

The T_2 relaxation time describes the dephasing of the transversal magnetization caused by entropic effects. Here no energy is released because the spins stay excited and the transversal magnetization moves from a vector initially to a fan and lastly to a circular area whereas no NMR signal can be induced in the receiver coil (Figure 18a). In case of additional field inhomogeneity in the sample the accelerated T^*_2 can be observed instead. Both, the T_2 and T^*_2 relaxation times restrict the life time of the NMR signal directly after excitation. T_1 (determines how fast NMR experiments can be consecutively conducted) T_2 relaxation is highly dependent on the density and viscosity of the NMR sample which lead to broad and overlapping signals found e.g. for polymers. In general, the relative length of the time constants is $T_2^* \leq T_2 \leq 2\,T_1$ and in low-viscosity samples $T_2 = T_1$. Changing relaxation times in different tissue are the basis for the image contrast modulation of the valuable diagnostic tool of Magnetic Resonance Imaging (MRI).

STATE OF THE ART – RESEARCH BASED ON ^{19}F NMR/MRI SPECTROSCOPY

A selection of the latest and in the opinion of the author most interesting research results based on ^{19}F NMR/MRI spectroscopy will be presented within this chapter. In this connection, the focus was mainly laid on ^{19}F NMR analyte sensing concepts. Furthermore, the original work of fluorinated phenylboronic acids for diol sensing which can be seen as a very simple concept compared to the work presented within this thesis will be presented.

The rapid enhancement of the NMR technique and the progress in the synthesis of organofluorine compounds combined with the excellent properties paved the way for studying biological events, metabolic routes, the monitoring of enzymatic mechanisms, analyte sensing up to drug screening and the medical imaging in cellular tissue via ^{19}F NMR/MRI.[122, 135-141] Noteworthy is the considerably increasing number of research based on the image-guided MRI technique for medicinal and pharmaceutical applications.[142-149] For clarification, Figure 19 illustrates the increasing meaning of ^{19}F NMR (^{19}F MRI) based work. The trend of growth (shown as publications per year) is corresponding to the development of the NMR technique starting in the 1960'ies and the volatile and broad availability of NMR machines in the early 1990'ies.

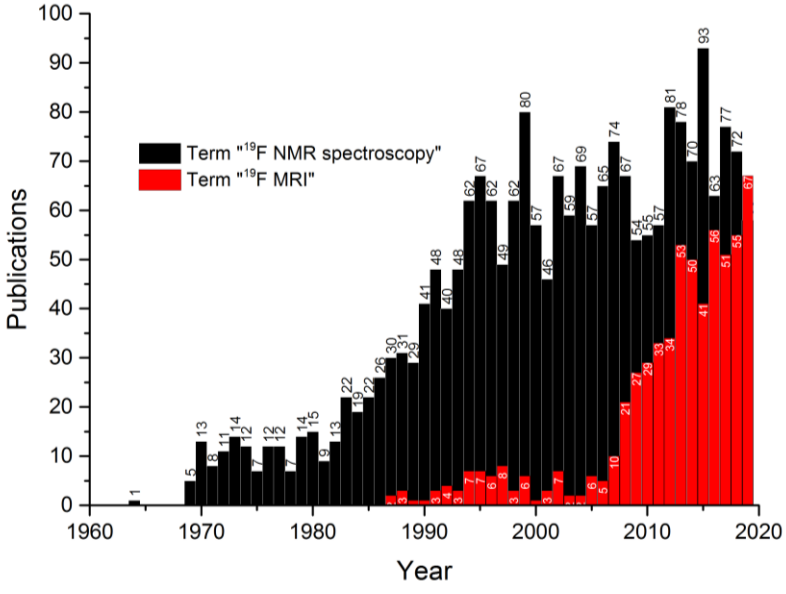

Figure 19: Development of ^{19}F NMR (^{19}F MRI) based work starting in the early 1960'ies and the volatile rise in the early 1990'ies illustrated by publications per year containing the term "^{19}F NMR" and "^{19}F MRI" via SciFinder® search (12/2017), respectively.

Current research based on simple fluorinated receptor scaffolds for analyte detection and discrimination using attached fluorine nuclei and ^{19}F NMR spectroscopy is mainly developed by the workgroups of Swager[150-153] and Smith[154-155].

The original receptor, a mono fluorinated tungsten calix[4]arene imido complex (**35**) of the Swager group was used for the detection and differentiation of neutral organic compounds such as carboxylic esters, amides, ketones and alcohols in a size-selective manner

Figure 20).[153] The added analytes are in a competitive equilibrium with the solvent molecules ($CDCl_3$) that can be incorporated in the calixarene binding pocket of **35** (a molecular container). In general, the characteristic ^{19}F pattern of **35** at δ_F −112.1 ppm becomes characteristically shifted (max 0.8 ppm) to positive ppm values depending on the analyte present and enable the differentiation of most tested analytes in the millimolar range whereas the analysis of mixtures is problematic. This original concept was further developed for the ^{19}F fingerprinting of neutral organic analytes using modified calixarene derivatives as an array of receptors (**36a-d**) and the resulting multidimensional data or by the use of non-equivalent ^{19}F probes (**37a**).[152] It was furthermore found that the proximity of the ^{19}F probes(s) to the incorporated analyte is a crucial feature for analyte discrimination of analytes with similar molecular structure and analyte identification in mixtures.

A similar approach was used for the identification of anions, biomolecules and mixtures of them using amide-based palladium pincer[156] complexes (**38a-f**).[150] The work group was furthermore successful in quantifying caffeine in coffee and aspartame, taurine, acesulfame K, niacinamid

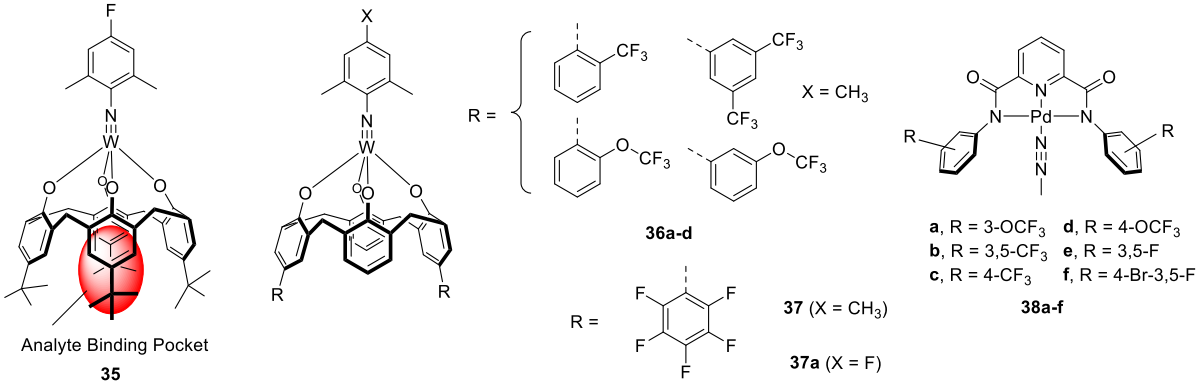

Figure 20: Fluorinated receptor compounds developed by the Swager group for sensing neutral organic analytes and anions via the attached fluorine probe(s) and ^{19}F NMR.[150-153] Structural modifications enabled the array-assisted analyte sensing with calixarene receptors (36a-d) as well as analyte sensing with attached non-equivalent ^{19}F probes (37a). 38f successfully enabled the identification of caffeine, aspartame, taurine, acesulfame K and niacinamid in commercially available drinks such as coffee, teas and energy drinks.

in other commercial drinks such as teas and energy drinks with the Pd-complex **38f** assisted by ^{19}F NMR spectroscopy. Chiral amines could also be discriminated using similar and chiral pincer complexes.[151]

Smith and coworkers also traced the concept of fluorinated metal complexes for sensing tasks. In a first approach they used a fluorine-labelled zinc(II)-dipicolylamine coordination complex (**39**) for the screening of various phosphate anions such as dihydrogen phosphate, pyrophosphate and adenosine phosphates (AMP, ADP and ATP) as well as binary mixtures of them via the ^{19}F NMR technique (Figure 21).[155] The formed receptor-anion complexes (**39a**) produced a maximal observable shift change $\Delta\delta_F$ of −3.7 ppm in presence of pyrophosphate (δ_F 17.8 ppm) with respect to the signal of the original receptor **39** at δ_F 21.5 ppm (with respect to a KBF_4 NMR reference signal). Other analytes show similar small shift changes and the components of a binary mixture containing ADP and pyrophosphate can be identified due to their characteristic shifts whereas other mixtures were found to be hardly clarified even at resonance frequencies of 564 MHz. In addition, the enzymatic hydrolysis of ATP could be conveniently monitored by **39** and ^{19}F NMR spectroscopy.

An interesting follow-up study using the zinc(II)-bis(dipicolylamine) receptor **40** with an attached paramagnetic relaxation agent (R) and the fluorinated phosphate indicator **41** was developed for the detection of phosphorylated analytes (Figure 21). The associated IDA sensing principle is realized by a switched-on ^{19}F NMR signal when a suitable anionic species is replacing the ^{19}F indicator (original short, and after the release long T_1 and T_2 relaxation times).

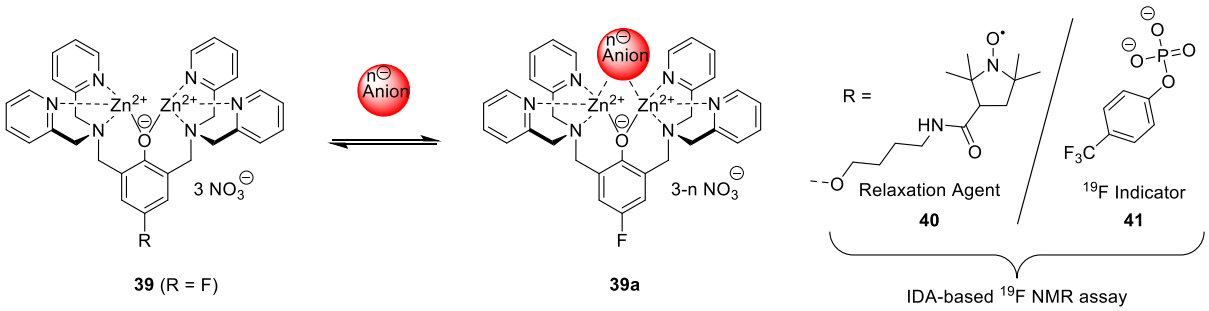

Figure 21: The fluorine-labelled zinc(II)-dipicolylamine coordination complex 39 developed by Smith *et.al.* enables the sensing of anions via ^{19}F NMR. Reversible association of bidentate anions such as phosphates can be visualized by the formation of the receptor-anion complex (39a) associated by a characteristic ^{19}F NMR shift change with respect to unbound 39.[155] An IDA-based ^{19}F assay was constructed using receptor 40 with an attached relaxation agent and the ^{19}F indicator 41. The latter is replaced by suitable anionic analyte inducing increased T_1 and T_2 relaxation times with upcoming ^{19}F NMR signal of the indicator.[154]

The field of medicinal/biological imaging techniques assisted by ^{1}H and relatively new by ^{19}F MRI is experiencing a dramatic rise due to their advantageous properties which enable the early monitoring of various disorders, diseases, the development of (non-invasive) diagnostic tools and targeted therapies.[136, 143] With regards to clinical application the MRI technique is working without radioactive nuclides or ionizing radiations which could cause collateral damage to the patient. While the anatomical resolution of ^{1}H MRI is an advantage the relative insensitivity is a drawback and thus tailored contrast agents (not directly visualizable) which can enhance the image contrast (^{1}H signal of surrounding water) of the imaged tissue are needed to overcome this issue. Beside the improvement in MRI performance accomplished by contrast agents they exhibit also significant disadvantages such as the still problematic contrast modulation associated with high background signals of water, long experimental acquisition times, their high demand in concentration for a good contrast and of course their inherent toxicity. An alternative strategy to overcome the contrast agent approach in ^{1}H MRI can be achieved by the additional use of ^{19}F MRI (see also chapter 3.6. for NMR properties of the ^{19}F nucleus) in a combined approach which adds a second "colored" layer of independent information to the anatomical tissue of interest.[145, 157-159]

In the following, three recent examples of ^{19}F MRI contrast agents with promising features for future medicinal application will be presented. The suPERFluorinatEdContrasT Agent (PERFECTA) **35** published by Tirotta *et al.* was obtained by a simple one-step reaction using pentaerythritol and perfluoro-tert-butanol (Figure 22, top).[146] Compound **35** bears 36 equivalent ^{19}F probes which in consequence produce one sharp signal at δ_F −73.48 ppm in the ^{19}F NMR spectrum and a strong MRI response. The polar core of **35** is completely hindered by the outer fluorinated and lipophilic shell but was successfully emulsified in water (monodisperse droplets of 140-220 nm measured via dynamic light scattering) and exhibits a good cellular compatibility up to a concentration of 9.92 mM for **35**. In a first *in vivo* ^{19}F MRI experiment **35-**labelled (4.96 mM) dendric cells were subcutaneously injected to rats and could be visualized by ^{19}F MRI as well as ^{1}H-^{19}F superimposed MR images after an incubation of 48 h.

Another approach developed by Jiang and coworkers uses dendritic molecules with an extraordinary high level of attached pseudo-symmetrical fluorines as illustrated by compound **36** (540 equivalent ^{19}F nuclei) to overcome the insensitivity of ^{19}F MRI with respect to the *in vivo* concentration of most (fluorine-labelled) drugs (Figure 22, top).[142] Interestingly, the fluorinated dendrimer **36** obtained by Williamson ether synthesis of the showed building blocks

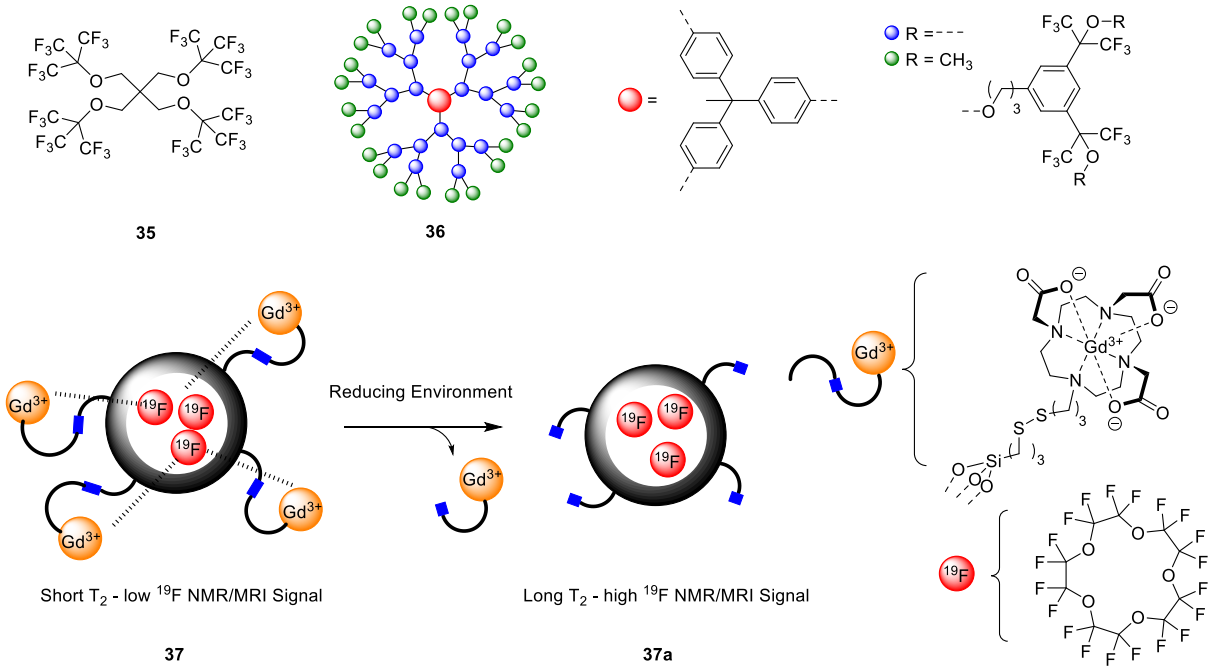

Figure 22: Top, Examples of recently published high fluorinated ^{19}F MRI contrast agents containing PERFECTA (35) with 36 equivalent ^{19}F nuclei and fluorinated dendrimer (36) with 540 equivalent ^{19}F nuclei used in ^{19}F MRI experiments.[146, 142] Bottom, perfluorocarbon-encapsulated and shell-modified nanoparticles (37) developed by Nakamura *et al.* which experience a T_2 time modulation with an increase of the ^{19}F NMR/MRI signaling for the resulting nanoparticle (37a) in presence of reducing conditions (S-S bond cleavage) such as found in abnormal redox reactions caused by liver damage or HIV.[144]

produce one single ^{19}F NMR shift at δ_F −73.94 ppm which is representative for all 540 fluorines of the different spherical layers and furthermore allows quantification tasks. With respect to the MRI sensitivity the T_1 and T_2 relaxation times usually decrease with increasing size and weight of the dendrimer and were found to be quite short for **36**. This observation can be attributed to the high mobility of the fluorines resulting in an enhancement of the ^{19}F MRI signal with a minimal detectable concentration of only 18.6 µM. Thus, the concept of highly fluorinated dendrimers with pseudo-symmetrical ^{19}F probes and suitable binding pockets for drugs (generation of unimolecular micelles in a next step) assisted by ^{19}F MRI possess a high potential for future *in vivo* ^{19}F MRI-guided drug therapy.

For the first time Nakamura *et al.* developed a clever ^{19}F MRI concept by the use of perfluorocarbon (PCF) encapsulated silica nanoparticles which experience a modulation in the ^{19}F NMR/MRI signaling by a paramagnetic relaxation enhancement effect (PRE).[144] The silica nanoparticle **37** (an OFF-type MRI probe) is comprised of perfluoro[15]crown-5-ethers as the ^{19}F MRI probes situated in the core and a silica shell which is modified with Gd^{3+}

diethylenetriamine pentaacetate complexes that are anchored via disulfide bridges (Figure 22, bottom). The PRE-effect which can be observed between a paramagnetic center (here the Gd^{3+} complex) and the observable NMR/MRI nuclei in the core induces a reduced T_2 relaxation time (40 ms) with a resulting broad ^{19}F NMR signal at δ_F −16.3 ppm and quenched MRI signals. In presence of a reducing environment such as found in abnormal redox reactions caused by liver damage or HIV the attached Gd^{3+} complexes are cleaved from the nanoparticle due to the breakup of the disulfide bridges as illustrated by the nanoparticle **37a**. Consequently, the PRE-effect is disabled and an increase in the T_2 relaxation time (420 ms) with an associated sharpening of the ^{19}F NMR signal at δ_F −16.3 ppm of the encapsulated ^{19}F probes as well as a switched-On MRI signal can be recorded. The approach is first example of an activatable ^{19}F MRI nanoparticle probe which exhibit a high stability, high MRI sensitivity and biocompatibility for future *in vivo* applications.

BORONIC ACID-BASED DIOL SENSING ASSISTED BY ^{19}F NMR SPECTROSCOPY

Compared to the previously presented work only a very few examples of boronic acid-based receptors which use attached ^{19}F probe(s) assisted by ^{19}F NMR/MRI for analyte sensing tasks have been published including our workgroup although the combination of these sensory features is accompanied by some notable benefits compared to common optical assays (see chapter 3.3). Since the first investigations by London and Gabel[160-161] and following studies by James,[162] Micouin[163] and Schiller[164-167] this relatively new field of analyte sensing assisted by ^{19}F NMR spectroscopy has attracted considerable improvements concerning the molecular and chemical nature of the receptors as well as the performed sensing experiments (Figure 23).

In 1994 Gabel postulated 4-fluorobenzeneboronic acid (FBA, **38**) and 3-chloro-4-fluorobenzeneboronic acid (CFBA, **39**) as useful ^{19}F NMR probes for studying the interactions and the intrinsic hybridization change of boron in presence of selected biologically relevant bioanalytes such as glucose, fructose-1,6-diphosphate, ribose-5-phosphate, sorbitol, L-DOPA, lactate, salicylic acid and NAD (Figure 23).[161] In detail, the shift changes in the ^{19}F NMR spectrum (400 MHz) of **38** were monitored as a function of the pH and the pK_a values were determined to be 8.7 and 7.9 for **38** and **39**, respectively, which is proposed to the associated hybridization change of boron. Besides, a hydroxyl ion exchange manner was assumed to the significant signal broadening in the range of pH 8 to 10 and the presence of phosphate buffer. The latter was found as a catalyst for the hydroxyl group exchange at boron. The performed analyte sensing experiments at pH 7.2 provide strong shifted ^{19}F NMR signals (up to $\Delta\delta_F$ −7.62 ppm for **38**-fructose-6-phosphate) of the formed FBA-diol complexes beside the original ^{19}F

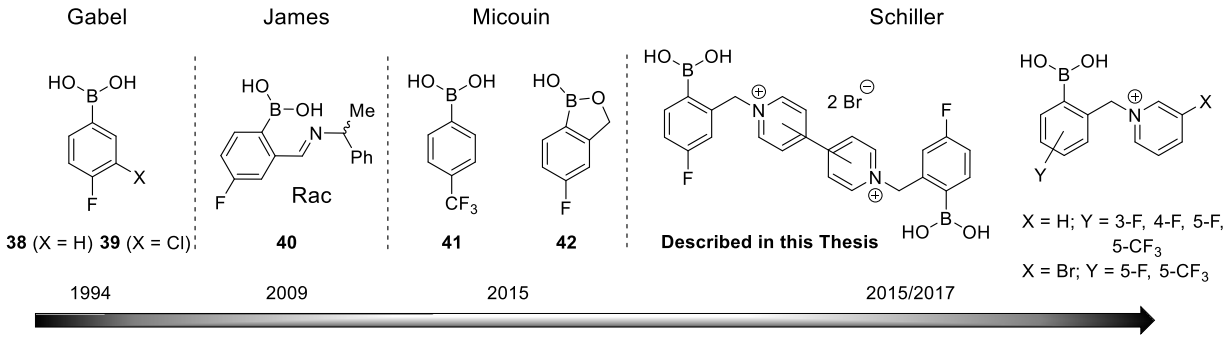

Figure 23: Development of boronic acid receptor scaffolds with attached fluorine probes used for diol sensing tasks assisted by ^{19}F NMR spectroscopy with workgroups and year of publication.[161, 102, 162, 163-167]

shift of **38** (1.5 mM, δ_F arbitrary set to 0 ppm). Both observed signals can be attributed to the slow chemical exchange characteristics of the free boronic acid and the formed boronate-esters (with a diol concentration of usually 20 mM). Although **38** shows a moderate affinity to all tested analytes the similarities of the recorded spectra with respect to the recorded single ^{19}F shifts allow no substantial analyte discrimination. A very first ^{19}F fingerprint-like pattern indicating the presence of three fluorine species could only be observed at higher pH values for of the formed **38**-α-D-glucose complexes.

A clever approach for the determination of the enantiopurity of several alkyl- and aryldiols was developed by the workgroup of James.[162] A racemate of the mono-fluorinated boronic acid receptor **40** with an attached chiral auxiliary amine assisted by ^1H and ^{19}F NMR spectroscopy was developed as an inexpensive chiral derivatization protocol. Derivatization of the resulting diastereomeric imino-boronate esters (50:50 mixtures) was achieved by the reaction of one equivalent appropriate chiral diol, (*rac*)-α-methylbenzylamine (chiral auxiliary) and 4-fluoro-2-formyl-phenylboronic acid in $CDCl_3$, respectively. A pair of well separated NMR signals of the formed diastereomeric imino-boronate species could be observed in the ^1H and the ^{19}F NMR spectra for two non-equivalent protons of the imine group and the attached fluorine probes ($\Delta\delta_F$ 0.03 – 0.3 ppm of both diastereomeric species), respectively. The concept was furthermore proofed by derivatization of methyl-(2*S*,3*R*)-dihydroxy-3-phenyl-propionoate (enantiomeric excess - ee of 80, 90 and 98%) with enantiopure (*R)*-α-methylbenzylamine and 2-formyl-4-fluorophenyl boronic acid resulting in the corresponding ester complexes (2*S*,3*R*, *α-R*)-**40** and (2*R*,3*S*, *α-R*)-**40**. Spectra analysis of the ^1H and ^{19}F NMR data (integral ratios) revealed the prior adjusted ee values of methyl-(2*S*,3*R*)-dihydroxy-3-phenyl-propionoate.

In 2015, quite recently before our first publication, Micouin described a method for monitoring boronic acid-diol interaction in aqueous media using fluorinated boronic acid probes and ^{19}F NMR spectroscopy.[163] The authors chose for the most part commercially available fluorinated boronic acid probes such as FBA **38**, (4-(trifluoromethyl)phenyl)boronic acid **41** and 5-fluoro-1,3-dihydro-1-hydroxy-2,1-benzoxaborole **42** for the qualitative ^{19}F NMR sensing of *cis*-diols in the millimolar range. Buffer media (Borax/HCl or Borax/NaOH) with relatively high pH values of 8.5 up to 10 were necessary to get a detectable single fluorine shift for the model *cis*-diol l,5-diaminocyclopentane-1,2-diol (DACP) in the case of the probes **38** and slightly more acidic **41** (Figure 24). Thus, the sensing concept was further followed up by the receptor **42** which moved the applicable pH to 7.5 and enabled the qualitative sensing of DACP, adenosine,

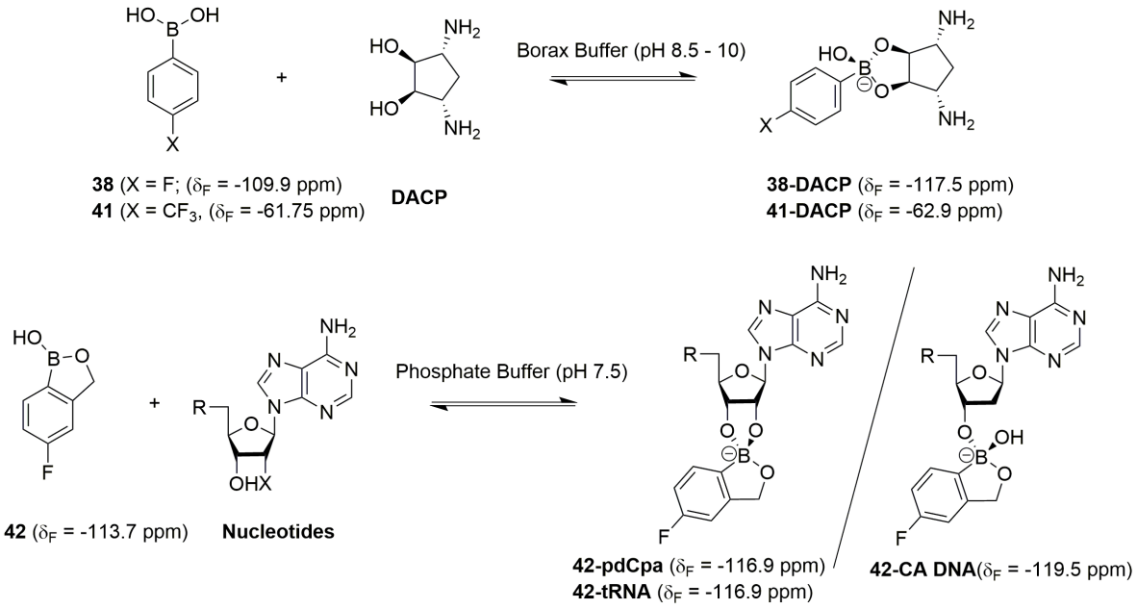

Figure 24: Proposed equilibrium and molecular structures of commercial available fluorinated boronic acid receptors for monitoring the boronic acid-diol interactions of l,5-diaminocyclopentane-1,2-diol (DACP) and oligonucleotides by Micouin with the recorded ^{19}F shifts in brackets.[163]

a hybrid dinucleotide pdCpa, CA DNA dinucleotide, tRNA as well as mixtures of CA DNA and DACP with a new appearing single fluorine shift for each formed **42**-analyte complex, respectively. The signal intensities of **42** titrated by the tested diols were found to be dependent on the amount of each analyte and would also enable quantitative sensing tasks. Nevertheless, the approach shows a very poor discriminatory power with respect to the probed diol-containing analytes due to the very similar ^{19}F shifts at around δ_F –117 ppm of the formed boronic acid–cis-diol complexes without the appearance of characteristic receptor-diol ^{19}F NMR fingerprints.

Based on the described pioneering work and the promising sensory features of attached ^{19}F probes for monitoring binding events that take place at boron we put a considerable effort on the investigation on a new class of highly sensitive receptors/sensor based on fluorinated boronic acid-appended bipyridinium salts assisted by ^{19}F NMR spectroscopy. The obtained research highlights include the differentiation of diol-containing analytes via qualitative and quantitative receptor-diol ^{19}F NMR fingerprints, the enhancement of the discrimination power using two-dimensional QR-like ^{19}F barcodes, the differentiation of inorganic anions as well as the monitoring of hydrogen peroxide with a chemodosimetric approach.[164-167] All these topics will be discussed in the following chapters of this thesis and illustrate the unique sensing potential of highly sensitive ^{19}F-labelled receptors and ^{19}F NMR spectroscopy in general.

4 RESULTS AND DISCUSSION

A SIMPLE ONE-COMPONENT ^{19}F NMR CHEMOSENSOR

In general, the presented work is focused on molecular scaffolds featuring a chemosensor moiety that contains the following attached chemical properties: (i) a benzylboronic acid-based binding site which is the receptor for analyte molecules, (ii) one or more ^{19}F atoms attached at the benzylboronic acid moiety that act as the molecular probe, (iii) an inherent arene system which provides the communication channel between the binding site and the ^{19}F probe, and (iv) a positively charged pyridinium-based backbone which enables the ionic character and enhances the solubility of the receptor under aqueous conditions.

In detail, each of the chemical components play a crucial role and work together as a robust and reliable sensing system (exemplary represented in Figure 25 by receptor **1**) for many applications such as the screening of diols and anions. In case of positive analyte interaction to

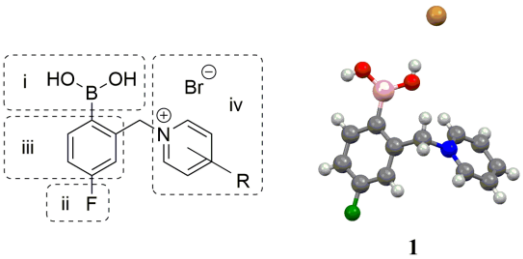

Figure 25: General molecular structure of fluorinated boronic acid-appended chemosensors exemplary represented by receptor 1 (R = H). Sensor components include an attached boronic acid binding site (i), a ^{19}F nucleus as the sensor probe (ii), an inherent arene system as the communication channel (iii), and a pyridinium-based backbone which provides the solubility of the receptor under physiological conditions (iv). The X-ray structure of receptor 1 represents the spatial arrangement of all components of the chemosensor.

the boronic acid function (e.g. in presence of a nucleophilic diol or anion) the ^{19}F probe experiences a change in its electronic environment mediated over the conjugated arene system.

Consequently, this property change (a specific NMR resonance change) of the fluorine nucleus can be monitored via ^{19}F NMR spectroscopy and allow qualitative as well as quantitative sensing tasks. With these properties in hand, structural sensor modifications have been performed to get a detailed knowledge about the resulting sensing behavior and to improve the sensory features with regards to water solubility, easy synthesis, ^{19}F NMR analyte discrimination power of analytes and robustness to experimental conditions and sample preparation processes.

Structural modifications of the sensor scaffolds resulted in monodentate receptors with attached pyridine and bromopyridine-based linkers as well as intramolecular boroxazole-based esters. The alteration of the ^{19}F probe's position (*ortho*, *meta* and *para*) relative to the boronic acid function and the substitution by a trifluoromethyl group was followed up to get a detailed knowledge about crucial sensor features and their influence on the sensing potential for especially diol-containing analytes. Furthermore, bidentate compounds have been synthesized including receptors with a linker backbone containing bipyridines, ethylene-bridged pyridines or azopyridines with the goal of the generation of ^{19}F NMR spectra which provide more information about the receptor-analyte interaction. In theory, photo switchable receptor scaffolds were also considered. High attention was laid on the enhancement of the discrimination power for diols. Thus, the single receptor concept was further developed by using a sensory array of fluorinated receptors.

An overview of all chemosensors which were synthesized and partially described in this thesis are presented in Figure 26. Overall the main focus was laid on the structurally simple but superior chemosensor **1** which exhibits outstanding chemically and sensory properties and enabled manifold ^{19}F NMR sensing experiments.

SYNTHESIS, CHARACTERIZATION AND PROPERTIES

In general, the synthesis of all described receptor compounds was performed via a two-step route (Figure 26). Commercial (fluorinated) methylphenylboronic acids or benzyl bromides, if directly available, were purchased to avoid extensive and dangerous fluorination procedures. In the first step, simple photo-bromination using elemental bromine, instead of bromination via *N*-bromosuccinimide found in the literature, was conducted to achieve the desired benzyl bromides. Thus, the appropriate precursor was suspended in tetrachloromethane and dried bromine dissolved in cooled tetrachloromethane was added drop by drop while the reaction vessel was irradiated by a halogen lamp. The purification of the bromination products (mostly mixture of boroxines and stepwise halogenated byproducts) was achieved by multiple recrystallization steps and washing with appropriate solvent. If not commercially available, linker compounds such as (bi)pyridines and azopyridine were separately synthesized using Suzuki-like or azo coupling reactions. In the final step, appropriate (bi)pyridine linker was *N*-alkylated with benzyl bromide in DMF. Usually after the precipitation of the crude product with acetone and diethylether the further purification processes were performed using cold actone and diethylether. More detailed parameters as well as all acquired analytical data for each interstage or final compound is provided in the experimental section.

Briefly, the analytical data which has been collected from receptor **1** will be discussed because this compound was selected due to the inherent properties as the main workhorse used in this thesis. Furthermore, **1** is the structural relative to the other described receptors of this work. Analytical data which has been acquired for the structural receptor elucidation include NMR spectra (^{1}H, ^{13}C and ^{19}F), HRMS (ESI), IR, elemental analysis, X-ray crystallography and melting points. UV/vis spectra and pH studies have also been determined and will be discussed in chapter 7.5, respectively.

Initially, the actual spectroscopic data of the ^{1}H NMR spectrum of receptor **1** containing the number of proton signals, shift splitting, and relative integrals fit well to the desired molecular structure (Figure 27 with structural assignment of the NMR signals of **1**). Highly characteristic is the singlet at δ_H 5.8 ppm that belongs to the protons of the methylene bridge. Hydroxyl protons of the boronic acid function are absent due to proton-deuterium exchange caused by the solvent D_2O.

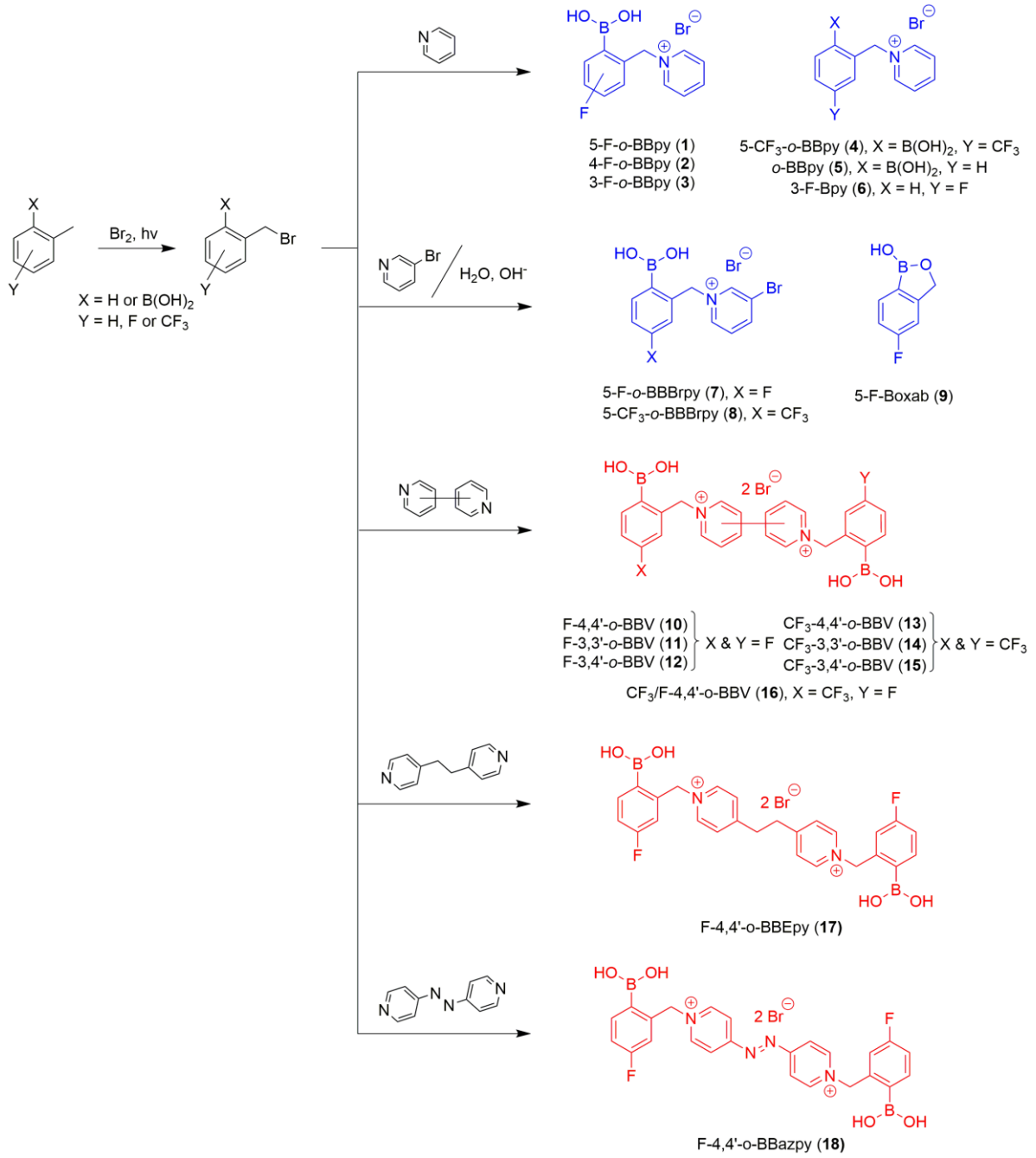

Figure 26: Overview of all precursors, receptors and control compounds (4-6) synthesized and characterized in the present thesis. In the first step commercial (fluorinated) methylphenyl (boronic acid) precursors have been photo-brominated to yield the appropriate benzyl bromide. Next, (bi)pyridine or commercial pyridine linkers (if necessary, prior synthesized) were *N*-alkylated with benzyl bromide to yield the desired (bi)pyridinium salt. Thus, the collection of compounds 1-18 contains monodentate (blue) and bidentate (red) sensors/receptors with symmetric (4,4' and 3,3') and asymmetric (3,4') scaffolds. Symmetric alteration includes also the use of two different probes on compound 16 owing a single fluorine and one trifluoromethyl function and in theory photo-switchable compound 18. Receptor 1 was used as the main workhorse in almost all sensing applications because of the inherent and superior chemical properties and concatenated sensing features.

Beside residue water and minor acetone signals (from purification) no impurities are present and proof the purity of the compound with respect to proton sources. The recorded and simple ^{19}F data provide similar results (Figure 28). As illustrated, receptor **1** is generating one sharp and intense fluorine signal at δ_F –110.75 ppm without any other appearing resonances. Consequently, the obtained high purity with no observable fluorine contaminants beside the signal of the ^{19}F probe highlight **1** for subsequent sensing experiments while false signals derived from potential contaminants and side products can be excluded. The collection of NMR data is completed by the ^{13}C spectrum indicating nine sets of carbon signals with observable spin-spin coupling to the ^{19}F nucleus of receptor **1**. The NMR signal of the ^{13}C at δ_C 163.82 ppm which is directly concatenated to the ^{19}F nucleus lead to a typical coupling constant of ^1J = 249 Hz (see chapter 7.5).

The infrared (IR) spectral data of **1** show the typical vibration bands for ν(OH) and ν(=C-H) at ~3360 and 3080 cm^{-1}, respectively (Figure 30). Characteristic IR fingerprints can be attributed to the ν(C-F) vibration in the region of ~1000-1400 cm^{-1}.

High resolution electrospray mass spectrometry (ESI MS) data of **1** was also collected and resulted in one main/mole peak at m/z, 246.1037 which corresponds to the formed boronic acid monomethyl ester (due to used MeOH solvent) of the pyridinium radical cation (see Figure 31). The calculated isotopic pattern for this mole peak perfectly fits to recorded mass data of **1** (inset Figure 31). Recorded and less intensive peaks at lower m/z values correspond to the free boronic acid pyridinium cation (m/z, ~223) and the corresponding dimethyl boronic acid ester (m/z, ~260).

The collection of spectroscopic data of receptor **1** was completed by X-ray crystallography and gave strong evidence for the success of synthesis (Figure 25). A suitable triclinic and colorless crystal was successfully crystalized out of a saturated solution of **1** dissolved in warm deuterium oxide. For advanced molecular properties of **1** such as bond lengths and angles the author refers to the experimental section. Molecular structures of the compounds **2**, **4** and **10** (see experimental section) have also been elucidated and the structural parameters and can be found in the experimental section as well.

Overall, spectroscopic data and corresponding spectra of all synthesized precursors and receptor compounds represented in Figure 26 can be found in the experimental section.

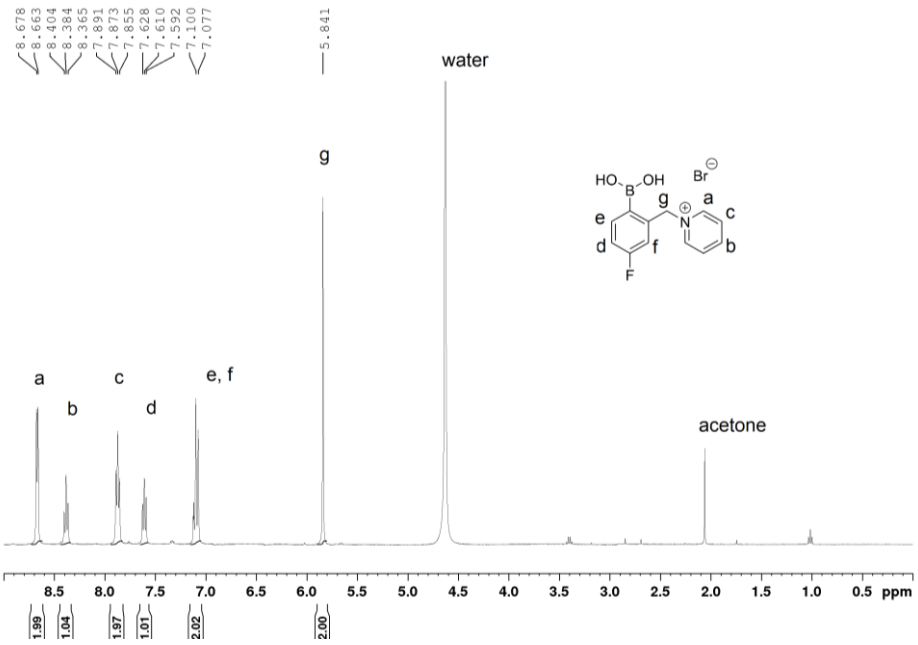

Figure 27: Exemplary ^{1}H {^{13}C} NMR (D_2O, 400 MHz) spectrum of 5-F-*o*-BBpy (1) with well separated proton resonances and the characteristic methylene bridge signal at δ_H 5.8 ppm indicating the success of the synthesis and high purity of the receptor with respect to the proton signals.

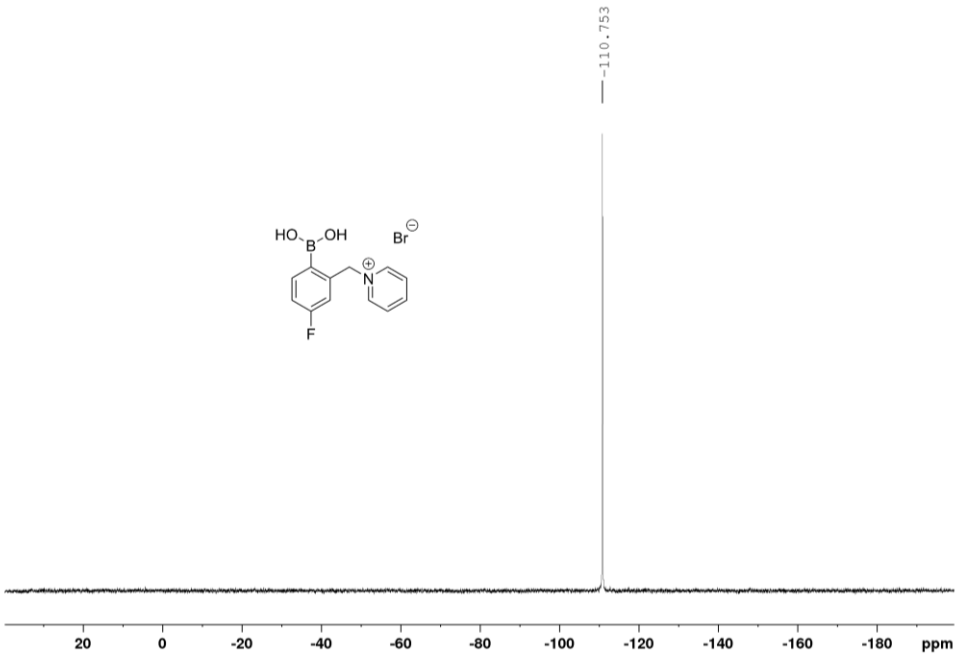

Figure 28: Exemplary ^{19}F {^{1}H} NMR (D_2O, 200 MHz) spectrum of receptor 5-F-*o*-BBpy (1) indicating one single fluorine resonance at δ_F –110.75 ppm of the single ^{19}F probe which proofs the absence of disturbing fluorine containing impurities and side products that could influence the interpretation of subsequent ^{19}F NMR sensing experiments.

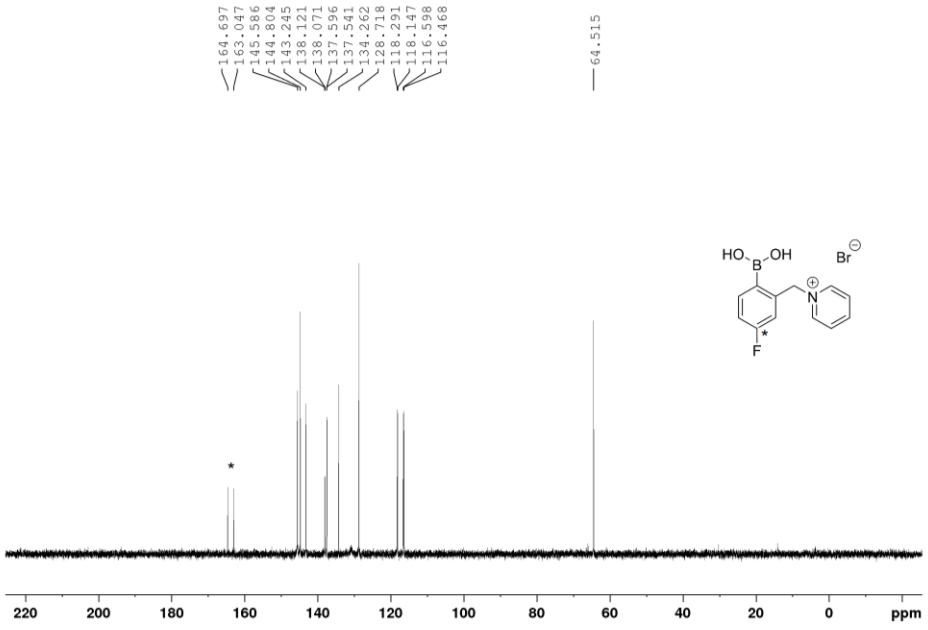

Figure 29: Exemplary ^{13}C {^{1}H} NMR (D_2O, 200 MHz) spectrum of receptor 5-F-*o*-BBpy (1) with a strong observable ^{13}C-^{19}F spin-spin coupling of the direct neighboring nuclei at δ_C 163.82 ppm and the resulting high coupling constant of 249 Hz.

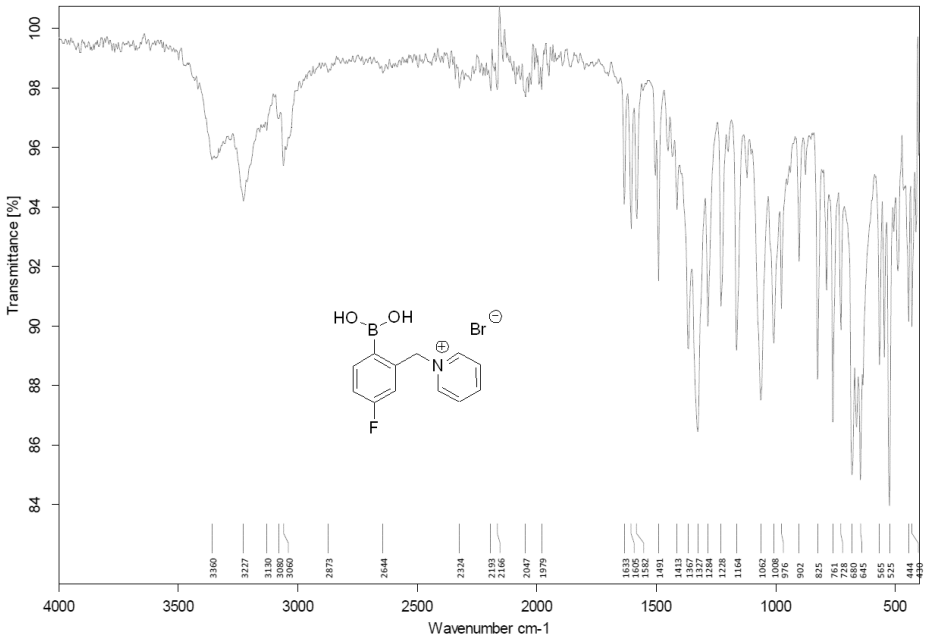

Figure 30: Exemplary FT-IR (ATR) transmission spectrum of receptor 5-F-*o*-BBpy (1) showing characteristic vibrational bands such as ν(OH), ν(=C-H) and ν(C-F) at ~3360 and ~3080 and ~1000-1400 cm^{-1}, respectively.

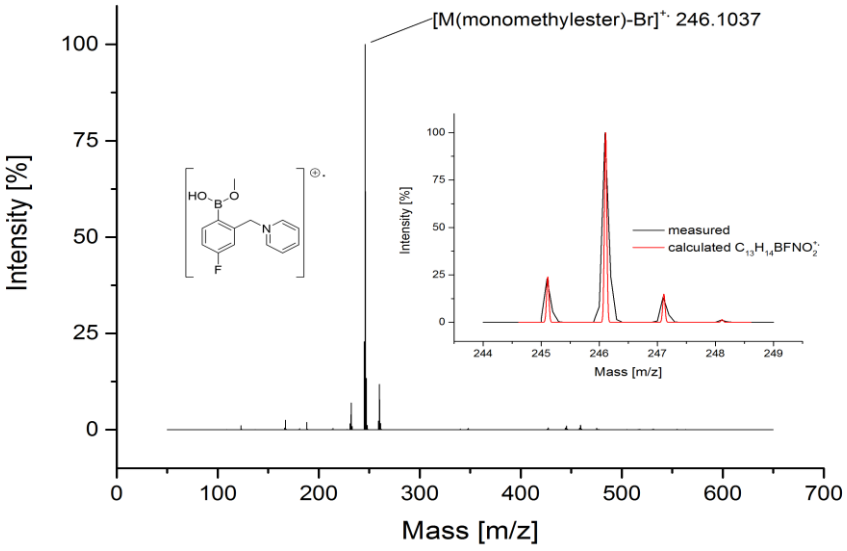

Figure 31: Exemplary high-resolution electrospray ionization mass (HRMS ESI) data of the monomethylester of receptor 5-F-*o*-BBpy (1). The measured and calculated isotopic pattern of the base (mole) peak are in very good agreement (inset). Less intense signals can be attributed to the free boronic acid pyridinium cation and the corresponding dimethylester with m/z values at 223 and 260 m/z, respectively.

DIOL SENSING PRINCIPLE USING THE SENSITIVE ^{19}F PROBE

As briefly mentioned before, all herein described chemosensors contain a molecular moiety with one benzylboronic acid function and one or more attached ^{19}F nucleus. The boronic acid is the receptor binding site to suitable analytes and the fluorine(s) act as a molecular probe. In solution and under neutral aqueous conditions, the boronic acid moiety experiences a complex equilibrium. This free boronic acid (trigonal planar sp^2 boron) with a Lewis acidic character willingly abstracts a hydroxide ion from the water medium resulting the corresponding boronate form (tetrahedral sp^3 boron, Figure 32, left). Under physiological conditions (~ pH 7.4) and in presence of suitable OH groups of e.g. a cis-1,2- or cis-1,3-diol, the boronic acid is transferred to the appropriate boronic acid-diol ester. In general, the equilibrium is considerably shifted to the boronate-diol ester which is attributed to the release of angle strain (120° versus 109.5° for the trigonal and tetrahedral boron, respectively) and the electronic saturation of the vacant p-orbital by a nucleophile hydroxide ion (Figure 32, right).

In general, this boronic acid-diol binding event with the concatenated boron rehybridization can be monitored via a suitable molecular reporter such as a highly sensitive ^{19}F NMR probe. The latter experiences a change in the electronic/magnetic environment of the aromatic system (even over five bonds with respect to receptor **1**) induced by the binding event at boron. On the NMR time scale, the equilibrium between the free boronic acid and the corresponding ester is slow and pushed to the boronate-diol species. Consequently, ^{19}F NMR signals of unbound receptor and the formed receptor-diol complexes can be observed in the NMR spectrum and demonstrate the high sensitivity and selectivity of the fluorine probe on the binding event at boron and the molecular character of the specific analyte. Especially well preorganized diol derivatives and reducing saccharides such as catechol and D-fructose are highly favored for boron-diol interaction and can be easily monitored by the fluorine probe assisted by ^{19}F NMR spectroscopy. Usually, no disturbing fluorine background signals are present.

For demonstrative purpose a buffered aqueous solution (100 mM HEPES buffer, 10% D_2O, pH 7.4) of receptor **1** (10 mM) produces one single red highlighted shift at δ_F –111.75 ppm with respect to $CFCl_3$ reference (δ_F 0 ppm) as illustrated by the ^{19}F NMR spectrum in Figure 32 (left). This characteristic ^{19}F signal with a distinct line broadening represents the equilibrium of the free boronic acid binding site and its corresponding boronate species. An exemplary mixture of **1** (10 mM) and the aldohexose D-glucose (100 mM) produce several new appearing and blue

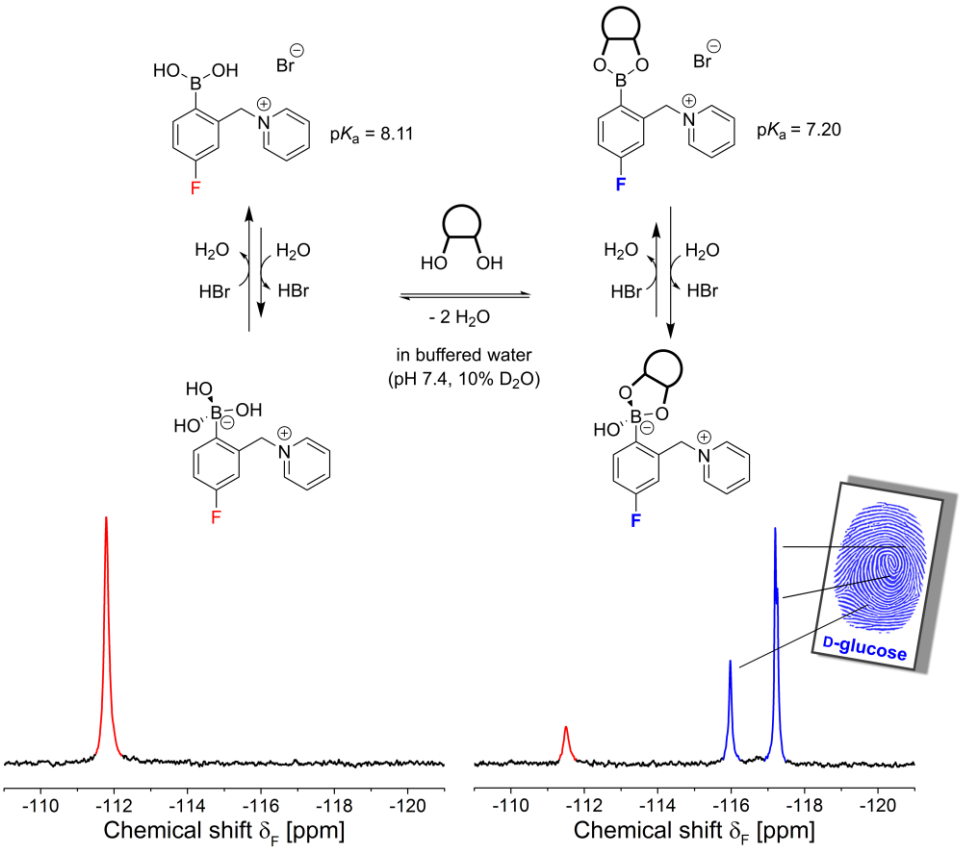

Figure 32: Top, equilibrium of the fluorinated boronic acid receptor 1 under aqueous conditions and in presence of suitable diol such as D-glucose. Bottom, resulting ^{19}F {^{1}H} NMR spectra containing the recorded signal of unbound receptor 1 (red) at δ_F –111.75 ppm and the unique ^{19}F NMR fingerprint of the formed receptor-1-glucose complexes (blue) at δ_F –115.97, –117.21 and –117.26 ppm. Experimentally determined pK_a values of 1 and the boronic acid ester of 1 and D-glucose are also given. Conditions: receptor 1 (10 mM), D-glucose (100 mM) in HEPES buffer solution (100 mM, pH 7.4, 10% D_2O) measured at 188 MHz and 256 scans at 25°C.

highlighted ^{19}F peaks at δ_F –115.97, –117.21 and –117.26 ppm which indicate the formation of at least three different boronate-diol species in solution. Due to the boron hybridization change from sp^2 to sp^3 upon esterification the new signals are significantly upfield shifted relative to the signal of unbound **1** (Figure 32, right). The observable spectroscopic information resulting from the ^{19}F shifts and shift intensities provide a highly characteristic ^{19}F NMR fingerprint that is unique for each receptor-diol combination. A minor extend of unbound receptor **1** is still visible indicated by the shift at δ_F –111.50 ppm (still highlighted in red). This residue signal can be furthermore seen as a qualitative indicator of the apparent binding affinity under equal sensing conditions. A detectable signal indicates free receptor **1** and unbound D-glucose under given conditions.

Compared to common sensing approaches using e.g. the modulation of the fluorescence emission the resulting ^{19}F pattern obtained by receptor **1** are not sensitive to pH variation in a certain range. Exemplary, this behavior is shown in Figure 33 whereby D-glucose was exemplary screened via **1** at pH values of 6.6 up to 8.2. Starting from physiological pH of 7.4 the typical ^{19}F fingerprint of **1** in presence of D-glucose was recorded. At more acidic conditions (< 7.4) the ^{19}F pattern of the receptor-diol complexes start to disappear until no binding of **1** to D-glucose occurred. Consequently, the pH of the sensing medium for diol sensing application using **1** should be not set considerably below the pK_a of the expected boronic acid-diol complex (see chapter 3.1). At more basic pH the signal of unbound **1** becomes significantly upfield shifted and the intensities of resulting fluorine signals increase which indicate a strong shift of the equilibrium to the more favored boronate complexes with an associated increased degree of diol complexation (boronate ester in Figure 32).

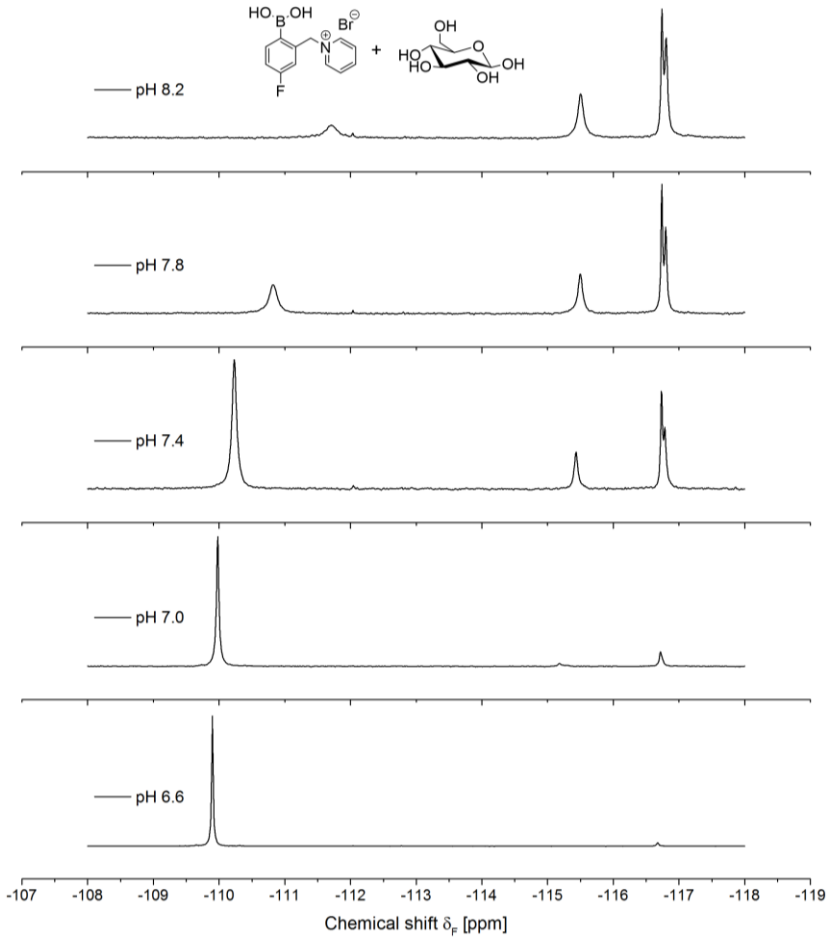

Figure 33: Robustness of the recorded ^{19}F NMR shifts of the formed receptor-1-glucose complexes at different pH values. Only a change of the signal intensity (corresponding binding affinity due to pH influence) can be observed whereas the signal shifts do not alter. Conditions: 1 (10 mM) and D-glucose (50 mM) in HEPES buffer solution (100 mM, pH as noted above, 10% D_2O, 188 MHz, 256 scans).

Quantitative values of the equilibrium constant of D-glucose complexation via **1** at the tested pH were determined using signal integration and are listed in Table 3. Thus, more basic conditions are helpful to increase the diol complexation behavior of **1** but might be problematic for experiments which require physiological conditions such as for many bio samples. However, the chemical shift positions of the receptor-diol complex are not affected and characteristic ^{19}F NMR fingerprints remain.

Overall, the presented sensing concept is an elegant method to qualitatively fingerprint diol containing analytes in a relatively broad pH range which include physiological pH via the attached and sensitive ^{19}F probe and ^{19}F NMR spectroscopy. The associated intensity modulation of the receptor-diol shifts (and concatenated shift integral change) upon changing diol portions enable quantitative sensing tasks and the determination of binding receptor binding affinities to certain diol. Furthermore, the unique ^{19}F fingerprints of each receptor-diol combination can be used for the identification of diols in mixtures or other complicates matrices. These mentioned and further sensing tasks will be addressed in the following chapters.

Table 3: Equilibrium constants *K* of receptor 1 in presence of D-glucose at different pH values determined via appropriate shift integrals and law of mass action at 24°C. Moderate diol complexation was determined starting at physiological pH 7.4 and above which push the equilibrium to the boronate ester.

pH	*K* [M^{-1}]
6.6	0
7.0	4
7.4	16
7.8	58
8.2	123

CRUCIAL FEATURES OF THE FLUORINATED BORONIC ACID RECEPTOR

The easy access to commercial fluorinated phenylboronic acid precursors and the use of versatile pyridine-based linker compounds original used in the Singaram-Wessling-type fluorescent assay[91] enable the synthesis of manifold receptors/sensors with an almost infinite number of possible structural modifications. Thus, the receptor-analyte selectivity e.g. in terms of diol binding via a suitable receptor pocket and multiple binding sites, which might allow multidentate binding, can be influenced. Another aspect that must be considered is the positioning and the concatenated magnetic property of the attached fluorine(s). Thus, a good communication channel (a conjugated system) to the binding site is required for the ^{19}F nucleus to function as a sensitive molecular probe. This feature significantly influences the sensing success and the spectroscopic signal generation of the fluorine probe in highly characteristic ^{19}F NMR receptor-analyte pattern. Minor changes, e.g. a simple constitutional change of the ^{19}F nucleus from *para* to *meta* relative to the receptor binding site can lead to a drastic response change or can even be completely interrupted. Another important feature is the applicable pH range of the chemosensor which is mainly influenced by the pK_a of the boronic acid and influencing substituents of the latter.

With these considerations in mind, investigative studies have been realized to get a detailed knowledge about crucial sensing features based on the simple pyridinium compounds **1**-**6** which can be also transferred to similar scaffolds such as bidentate scaffolds. Figure 34 represents all structural modifications which could be successfully realized using commercial available fluorinated precursors.[166] Receptor variations include the linkage of fluorine in *para*, *meta* and *ortho* position (compounds **1**, **2** and **3**, respectively) relatively to the boronic acid function and the introduction of a trifluoromethyl group (compound **4**) in *para* position. For advanced investigations concerning the influence of the substituents on the pK_a and the response/influence of the fluorine probe in the corresponding NMR spectra, the control compounds **5** (fluorine free analog to **1**) and **6** (non-boronic acid analog to **1**), respectively, were synthesized as well.

Initially, the ^{19}F NMR sensing behavior of the mono-fluorinated isomeric receptors 5-F-*o*-BBpy (**1**), 4-F-*o*-BBpy (**2**) and 3-F-*o*-BBpy (**3**) was investigated to get a knowledge on how esterification with diol affected their resulting chemical shifts with respect to the direction, complexity and shift intensity. The results in Figure 35 show, that the ^{19}F shift is strongly de-

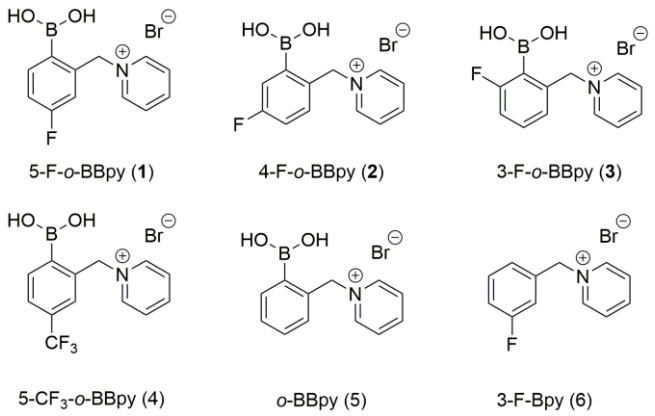

Figure 34: Overview of monodentate fluorinated receptors 1-4 and the model compounds 5 and 6 for the investigation of crucial molecular features required for diol sensing application via ^{19}F NMR spectroscopy.

pendent on the position of the fluorine atom at the benzyl moiety. In detail, the fluorine signals of the pure receptors are located at δ_F –111.75 (**1**), –113.74 (**2**) and –104.84/–112.48 ppm (**3**) with fluorine in *para, meta* and *ortho* position to boron, respectively (Figure 35a). Although only one single signal was expected for each unbound receptor, only **3** shows a minor peak (δ_F –112.48 ppm) beside the strongly downfield shifted main peak (δ_F –104.84 ppm). Addition of the three selected and exemplary diols D-glucose, D-fructose and catechol, lead to strongly upfield shifted ($\Delta\delta_F$ up to 5 ppm, Figure 35b-d) ^{19}F signals for receptor **1**. Receptor **3** provide downfield shifted ($\Delta\delta_F$ up to –2 ppm) whereas **2** showed minor upfield shifted ($\Delta\delta_F$ up to 0.6 ppm) fluorine signals. This trend supports the enhanced ability of *para*- and *ortho*-positioned fluorine probes, compared to the *meta* derivative, to strongly respond to changes of boron $sp^2 \rightarrow sp^3$ rehybridization upon diol binding via the conjugated system. The reversed direction in shifting of the *ortho* isomer **3** can be explained by the probe's proximity directly to the boron binding site associated with possible B-O-H--F- hydrogen bonding.

Overall, the number of new appearing receptor-diol signals is identical for all three receptor isomers and appropriate diol. This observation verifies that each ^{19}F probe (*para*-, *meta*- and *ortho*-) recognizes the same number of formed receptor-analyte complexes. ^{19}F NMR spectra of the mono-fluorinated receptors and appropriate diol such as D-glucose, D-fructose, and catechol are shown in Figure 35b-d. Going beyond, the spectroscopic information gained by the receptors **1-3** can be processed as an array-like sensor ensemble with a significantly enhanced diol discrimination power as presented in chapter 4.7 where a set of bipyridinium-based receptors has been used to generate QR-like barcodes for enhanced diol discrimination. The whole ^{19}F NMR collection of all screened diols using **1-3** can be found in the appendix. The trifluoromethyl probe 5-CF_3-*o*-BBpy (**4**) (enhanced fluorine content with respect to **1**) was

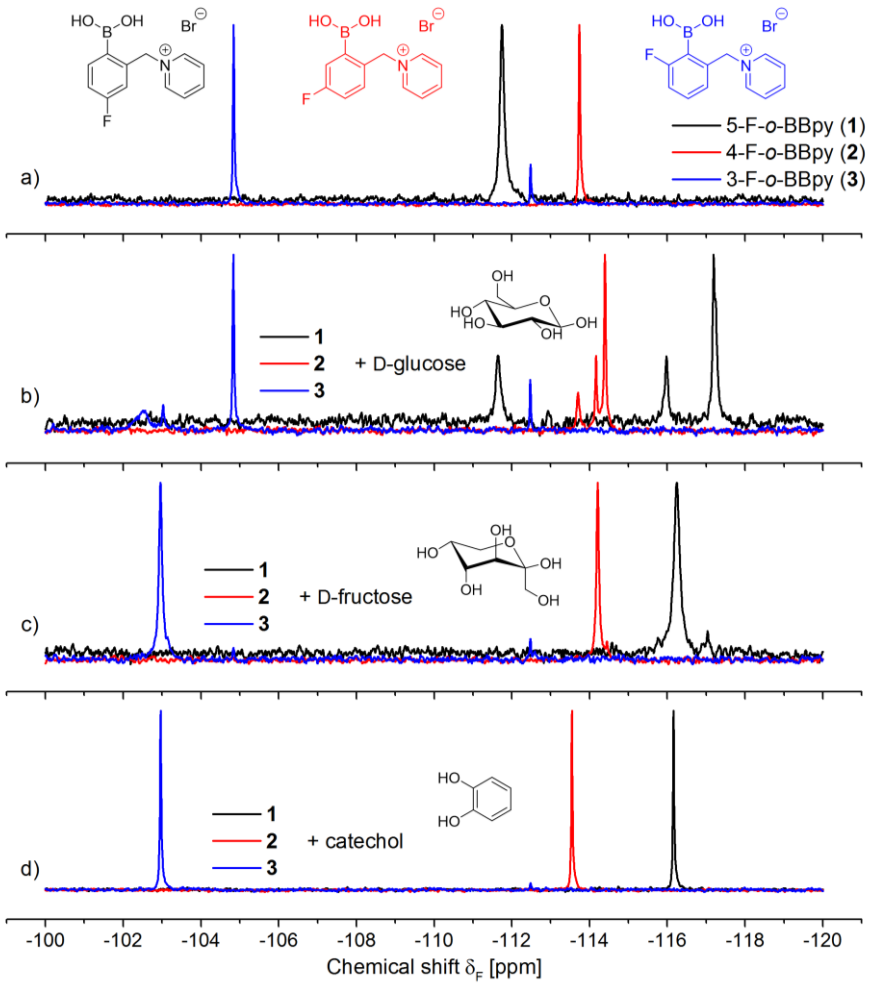

Figure 35: Influence of the ^{19}F probe position on the ^{19}F NMR diol sensing behavior (signal response and shift trend) of the receptors 1-3 and in presence of selected diols. Conditions: receptor (10 mM) and appropriate diol (40 mM) in HEPES buffer solution (100 mM, pH 7.4, 10% D_2O) at 188 MHz, 256 scans).

primarily introduced to increase the sensitivity of the sensing approach. As expected the signal to noise ratio (S/N) of the trifluoromethyl receptor **4** could be significantly improved compared to the mono-fluorinated receptor **1** with an approximately ten-fold increase in signal intensity. Figure 36 shows the tremendous difference in the resulting chemical shifts at δ_F –62.23 and –110.46 ppm for **4** and **1**, respectively, as well as the determined S/N values (514 versus 82) measured in water (10% D_2O). However, no significant shift changes in the ^{19}F NMR spectra of unbound **4** (Figure 37a) compared to **4** with catechol (Figure 37b) and D-fructose c) could be recorded. Only a minor downfield shift of the unbound receptor at δ_F –62.66 to –62.43 ppm could be observed in the case of D-glucose (see appendix).

With these finding in hand, unfortunately compound **4** provided only very poor ^{19}F NMR sensing potential due to the lack of characteristic receptor-**4**-diol ^{19}F fingerprints. This behavior might be explained by the absent conjugation between the boronic acid group and the

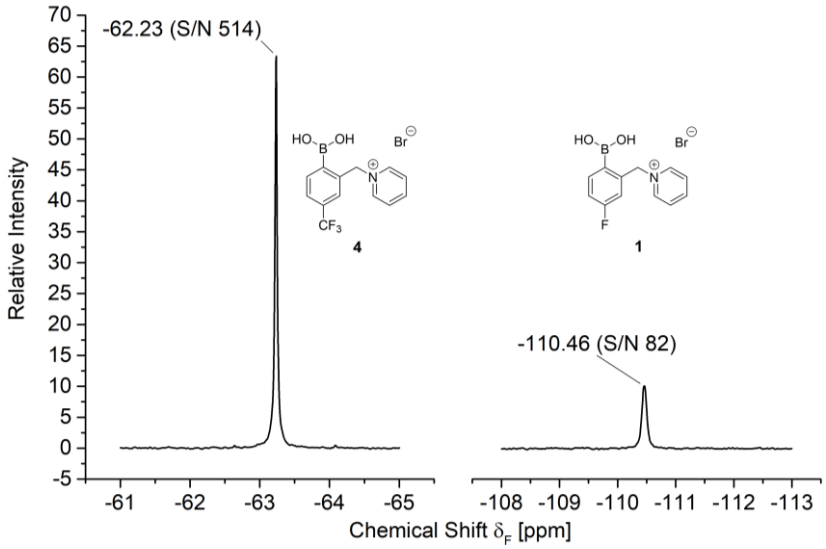

Figure 36: Resulting ^{19}F {^1H} NMR spectra of the trifluoromethyl receptor 4 and the mono-fluorinated receptor 1 which show the influence of the fluorine content on the observable signal to noise ratio (S/N) of the appropriate ^{19}F shifts measured under identical experimental conditions. Conditions: receptor 4 and 1 (10 mM each) in water (10% D_2O) at 188 MHz and 256 scans.

fluorine probes of the trifluoromethyl moiety. Thus, the attached fluorine probe(s) of a fluorinated boronic acid receptor need a suitable communication channel (conjugated electron system) to the arene boronic acid binding site. In the pool of the presented pyridinium salts this crucial requirement is only fulfilled by the fluorinated receptors **1-3** whereas the derivatives **4-6** lack of this feature.

To exclude the ^{19}F probe's response to other property changes than the esterification taking place at boron the negative control 3-F-Bpy (**6**) was introduced as a model-like compound. In detail, the ^{19}F NMR spectrum of the non-boronic acid compound **6** (Figure 37a) produce no new signals beside the original peak at δ_F –112.46 ppm in presence of catechol or D-fructose (Figure 37b and c, respectively). Furthermore, the signals of **6** are very sharp without distinct line-broadening which in general arise from the inherent boronic acid/boronate equilibrium of the receptor. This negative control experiment gave evidence that the boronic acid is another crucial property for a working diol chemosensor and that only a directly to the arene attached ^{19}F probe can recognize possible diol interaction taking place at the boronic acid binding site.

Beside the receptors behavior concerning their ^{19}F sensing ability in presence of diol, the influence of the structural modifications to the acid-base property of the attached boronic acid was investigated. Inductive and mesomeric effects of the fluorine substituents with their strong electron withdrawing property can alter the pK_a value of the boronic acid function (weak

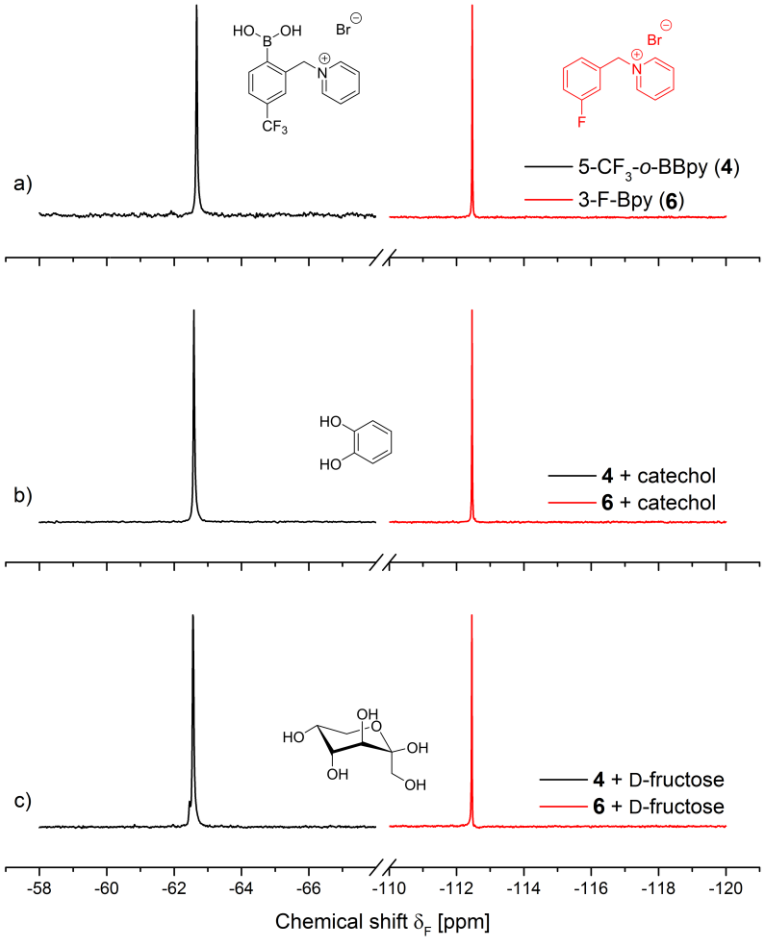

Figure 37: ^{19}F {^{1}H} NMR spectra of the trifluoromethyl receptor 4 and the negative control 5 and in presence of catechol and D-fructose, respectively. The CF_3-functionalized receptor 4 is almost insensitive for binding events due to interrupted conjugation whereas the ^{19}F probe of 5 experiences no change in its electronic environment due to the absent boronic acid function. Conditions: receptor 4 and 5 (100 mM each) in HEPES buffer solution (100 mM, pH 7.4, 10% D_2O) at 188 MHz and 256 scans.

Lewis acid) which therefore determines the applicable pH range of the receptor/sensing concept. Approximately, a pK_a value of the receptor-diol ester of interest at around 7 and little below are desired to achieve a considerably diol esterification in the physiological pH range.

In detail, potentiometric pH titration experiments were conducted to demonstrate the influence of the fluorine probe(s) upon the acidity of unbound receptor and selected boronic acid esters (Figure 38). Stock solutions of appropriate receptor (8 mM) in acidified deionized water were titrated with 50 µL aliquots of base solution (100 mM NaOH and 150 mM NaCl in deionized water) and the pH was recorded at the point of equilibration. The weak-acid strong-base titration curves were then plotted, fitted and the apparent pK_a values was extracted. From the pool of tested compounds, the non-fluorinated receptor **5** exhibits the highest pK_a value (8.50). Decreased pK_a values were observed for all fluorinated receptors: **3** (8.39) > **1** (8.11) >

2 (7.46) > **4** (7.14). Overall, the acidity raised with increasing fluorine content **5** < (**1, 2, 3)** < **4**. The electron-withdrawing effect of fluorine facilitates strongest acidity in case of the trifluoromethyl receptor **4** (pK_a drop of 1.36 compared to **5**). With respect to the fluorine positioning upon the increasing acidity of unbound receptor the order is **3** < **1** < **2**. The high pK_a of **3** seems to have its origin in possible fluorine-hydrogen interactions. Lowered pK_a values were found for **1** in presence of D-glucose, D-fructose and D-mannitol with pK_a values of 7.2, 5.4 and 5.97, respectively, with respect to unbound **1**. This is a result of the earlier mentioned and preferred OH^- abstraction due to a lowered angle strain of the formed boronate-diol ester compared to the boronic acid-diol ester (120° versus 109.5°). Overall, these pK_a values (below pH 7.4) of the boronic acid-diol esters of **1** furthermore indicate quantifiable amounts of the appropriate complexes in sensing experiments performed under physiological conditions.

Thus, the fluorinated receptor **1** was selected as the best performing receptor due to the outstanding properties and provides excellent diol sensing properties which are associated by strong upfield shifted signals in the ^{19}F NMR spectra, good signal-to-noise ratios (S/N) and well separated signals of the unbound and bound receptor-**1**-diol species. The latter feature could not be achieved with the receptors **2**-**4**. Furthermore **1** and especially the appropriate diol esters of

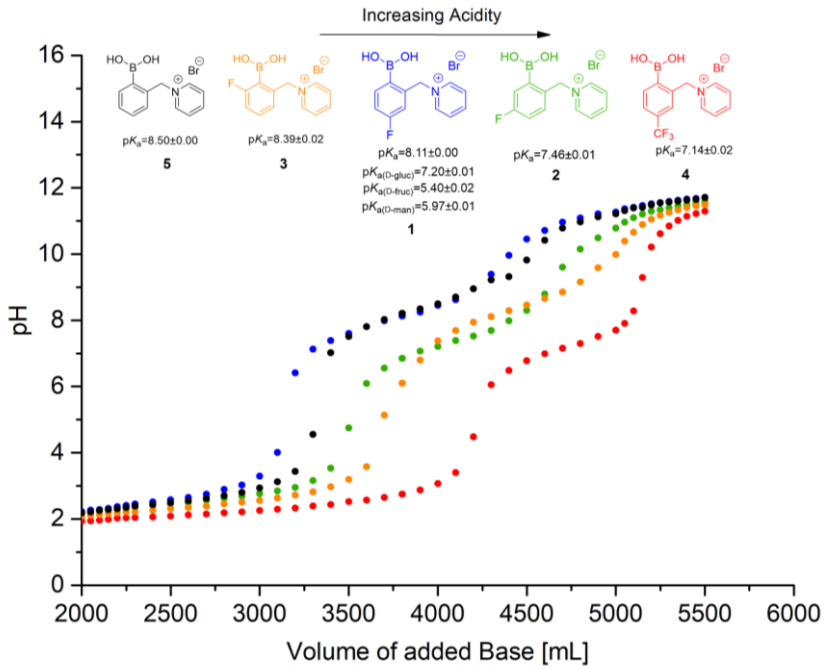

Figure 38: Weak-acid strong-base pH titration profiles of the fluorinated boronic acid-appended pyridinium receptors 1-4, 6 and appropriate boronic acid-diol esters of receptor 1 upon addition of base solution (100 mM NaOH, 150 mM NaCl) recorded at 22-23 °C. The pK_a values were extracted from the halfway point of each pH profile via polynomial data fitting.

1 exhibit suitable pK_a values which enable sensing application in the physiological pH range of ~ 7.4. The strong photo-stability under experimental conditions compared to the photo-labile bipyridinium-based receptors and the easy access in synthesis are further important aspects which underline the strong potential of chemosensor **1**.

QUALITATIVE & QUANTITATIVE SENSING OF DIOLS AND RELATED ANALYTES

The great diversity of diols and saccharides with numberless constitutional and sterical isomers, their in part different chemical behavior and inherent character in many biochemical processes require highly selective sensing concepts for the recognition of the specific analyte as well as for quantification tasks. The prior described reversible interaction of boronic acids with a structurally suitable diol and the formation of appropriate boronate-diol esters is the mechanism of all boronic acid-based diol receptors and has found broad applicability in especially combined fluorescence sensing approaches as described in chapter 3.3. Nevertheless, new sensing concepts such as the presented approach using fluorinated boronic acid receptors assisted by ^{19}F NMR spectroscopy can provide noticeable benefits in individual diol sensing experiments.

In general, the ^{19}F NMR technique provides detailed information of the qualitative and quantitative diol property and especially in samples comprising complicated matrices and/or mixtures of diol due to the characteristic NMR data of formed receptor-diol complexes and the absent ^{19}F background. The following chapters will present these scenarios using fluorinated receptors such as the monodentate compound **1** as well as more complicated and bidentate receptors. Qualitative receptor-diol information for discriminative tasks were obtained by simple but highly characteristic ^{19}F NMR spectra as well as by processing this data via an array-like setup. Quantitative tasks, the sensing of diol mixtures, investigation of diol binding modes, receptor-diol affinities and the comparison of the ^{19}F NMR sensing system to a common fluorescence assay are presented as well.

(BIO)ANALYTE SCREENING USING UNIQUE ^{19}F NMR FINGERPRINTS

With respect to the performed investigations (chapter 4.4), 5-F-*o*-BBpy (**1**) was chosen as the best performing sensor compound due to the ease in synthesis, water-solubility, photo-stability and of course the inherent ^{19}F NMR sensing potential. At first receptor **1** was chosen for the screening of a large pool of biological relevant analytes such as saccharides, catechols, carbolic acids and nucleotides to check (i) crucial analyte properties for positive binding, (ii) the correlation of analyte structural motifs upon the receptors affinity and resulting ^{19}F pattern, and (iii) the discrimination power to analytes with similar structural features. The main sensing focus was laid on monosaccharides (aldoses and ketoses), glyceraldehyde, dihydroxy acetone, hexoses (e.g. fructose, glucose, and galactose), and phosphorylated or *N*-acetylated sugars. The pool of overall 59 tested analytes also included disaccharides, carboxylic acids, simple alcohols, polyols, catechols, amines, nucleotides and one nucleoside to get a detailed understanding of crucial structural moieties of the analytes for positive binding. Meanwhile these experiments a large ^{19}F NMR spectroscopic database for analyte discrimination purposes was established. A selection of the analyte collection screened by receptor **1**, their structures and resulting ^{19}F spectra are represented by Figure 39.

In practice, ^{19}F NMR sensing experiments using receptor **1** (10 mM) and an excess of appropriate analyte (100 mM) were performed in aqueous HEPES buffer solution (100 mM, pH 7.4, 10% D_2O) at 188 MHz and 256 scans to achieve sufficient receptor saturation. The resulting spectra are categorized in a systematically manner according to the screened analyte classes. The results of selected ^{19}F NMR spectra represented by Figure 39a-l will be discussed in the following.

Starting with blank receptor **1**, the spectrum shows the already known single ^{19}F NMR shift (Figure 39a). In presence of D-fructose (Figure 39b), one main signal at δ_F −116.23 and a minor signal at δ_F −117.04 ppm can be found with a complete loss of the unbound signal of **1** which is completely different to the discussed fingerprint of the aldohexose D-glucose (c). This spectroscopic information clearly allows the discrimination of both constitutional isomeric monosaccharides. As expected, the complementary enantiomers L-fructose (b) and L-glucose (c) produce the identical spectra and allow no discrimination because of the achiral property of receptor **1**. With the loss of one accessible OH group in D-fructose-6-phosphate (b) compared to D-fructose, the spectrum signals are reduced to one sharp peak at δ_F −117.17 ppm.

In case of D-glucose-6-phosphate (d), the spectrum was reduced to two signals at δ_F –116.53 and –117.12 ppm versus the three original signals of D-glucose. No new shifts could be recorded in presence of D-glucose-1-phosphate (d), probably because of disabled isomerization possibility of the acetal to the open ring form. Next, the three aldohexoses D-galactose, D-talose and D-mannose are represented by Figure 39e. These diastereomers can be clearly distinguished with one ^{19}F signal at δ_F –116.07 ppm (D-galactose) and two signals at δ_F –117.00/–117.18 (D-talose) and δ_F –117.70/–117.34 ppm (D-mannose).

D-Mannose, which is the epimer (inversed configuration at C-2) of D-glucose, can be clearly distinguished. The same observation was found in the group of the pentoaldoses D-ribose, -xylose and -lyxose (Figure 39f) which again highlight the discrimination power of the system even by minor differences in the absolute configuration in one or more stereo centers. Strong affinity could be observed for the diagnostic marker D/L-lactic acid (g) with a strong signal at δ_F –116.04 ppm and *N*-acetylneuraminic acid at δ_F –115.72 ppm. D-mannitol, D-sorbitol and D-dulcitol (h), which can be seen as simplified open-ring polyols of monosaccharides, show overall a strong affinity to **1**. They produce one broad peak at δ_F –116.19, –115.95 and –116.17 ppm, respectively. The group of disaccharides D-maltose, D-cellobiose, and sucrose (i), resulted in weak ^{19}F NMR signals at δ_F –117.01 and –117.20 ppm, respectively, which indicate very weak or no binding to **1**. Sucrose as a non-reducing sugar showed no interaction. In the case of the nucleotides (j), only adenosine monophosphate (AMP) produced one sharp high affinity shift at δ_F –116.99 ppm compared to ADP and ATP. However, adenosine shows a very similar spectrum compared to AMP with a fluorine signal at δ_F –116.96 ppm. Presumably, a higher grade of phosphorous residues is in competition with the cis-1,2 OH groups of the adenosine backbone.

Strong preference of **1** to catechol, dopamine and salicylhydroxamic acid with one single shift each was found which also enables the discrimination of these analytes (Figure 39k). Interestingly is the result within the group of small aliphatic alcohols containing one, two or three OH or amino groups, whereas only 3-aminopropanol results in a strong interaction at δ_F –117.72 ppm. Thus, a chelating effect involving the hydroxyl and amino group with respect to boron can be assumed (Figure 39l). Further ^{19}F NMR spectra of receptor **1** in presence of other screened analytes can be found in the appendix.

To sum up, a large collection of bioanalytes was screened with the optimally performing and structurally simplest fluorinated receptor **1** assisted by ^{19}F NMR spectroscopy. Most of the diols

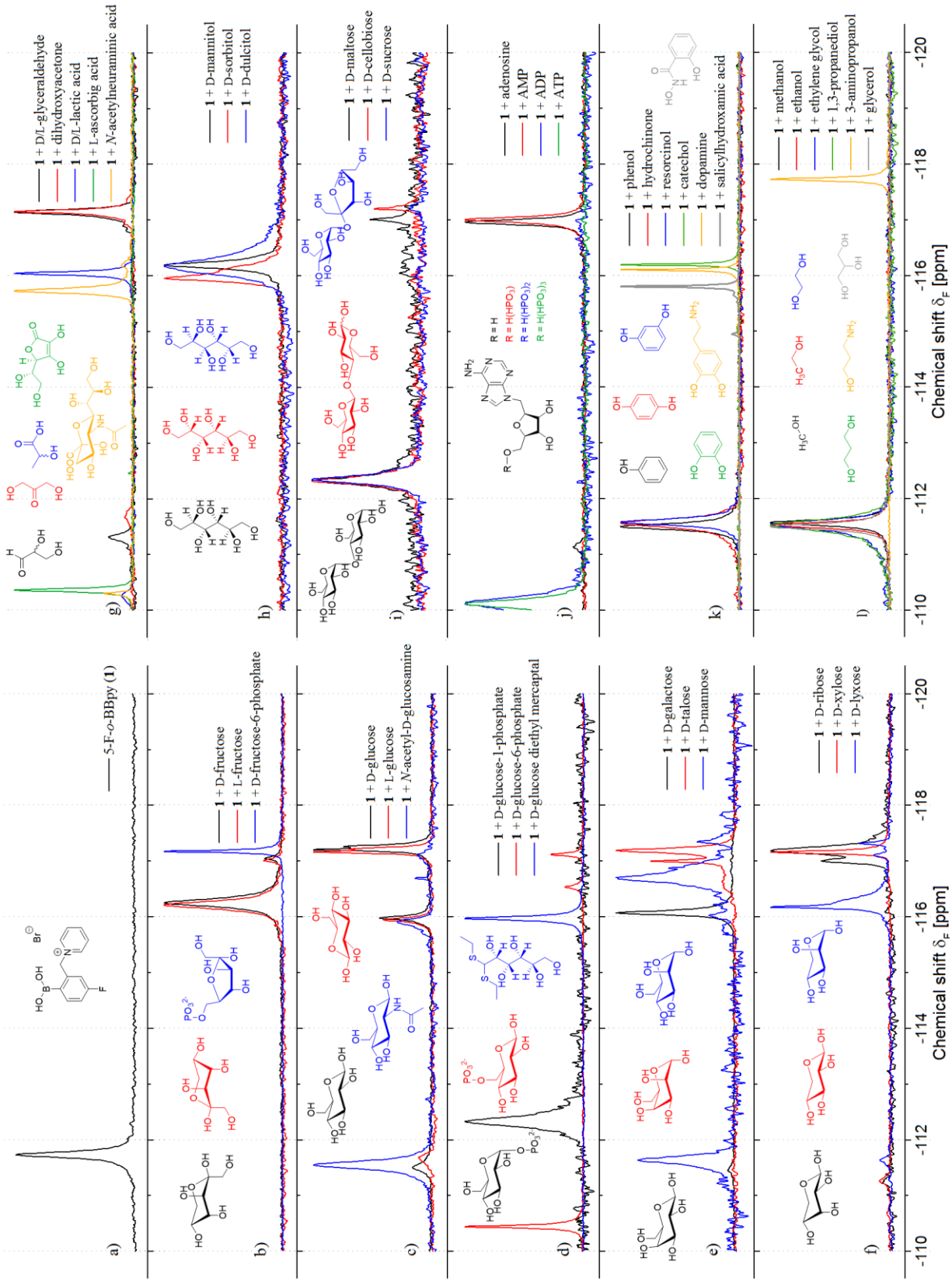

Figure 39: Collection of selected ^{19}F NMR spectra of the fluorinated and structurally simple receptor 1 and in presence of (di)ol-containing analytes with highly characteristic and discriminative ^{19}F fingerprints. Conditions: receptor 1 (10 mM) and appropriate analyte measured in aqueous HEPES buffer solution (100 mM, pH 7.4, 10% D_2O) at 188 MHz, 256 scans and 25°C.

positively bind to the sensor and the resulting receptor-**1**-analyte complexes exhibited unique ^{19}F NMR fingerprints originated by distinct ^{19}F shifts and intensities. Thus, the approach allowed easy diol discrimination by constitutional and sterical diversity such as e.g. found for D-glucose and D-fructose (constitutional isomers) and D-ribose and D-xylose (epimers with respect to each other), respectively. Furthermore, the recorded spectroscopic information was used in the next step for the elucidation of possible binding modes of the diols to receptor **1** and quantitative sensing tasks in various sensing setups. Selected spectroscopic results of the other receptors which cannot be discussed in detail can be found in the appendix.

TUNED DISCRIMINATION POWER VIA A RECEPTOR ARRAY & BAR CODES

The previously described diol sensing experiments showed highly characteristic ^{19}F fingerprints for the monodentate receptor approach. Nevertheless, in a few cases the resulting fluorine pattern of similar analytes can interfere in the spectroscopic information. This circumstance could lead to false interpretation and consequently to misleading analyte identification.

To overcome this circumstance an array of bidentate receptor compounds was introduced to check their cross-reactive sensing potential and to increase the ^{19}F NMR information output with respect of analyte probing. In detail, the well performing benzyl moiety of **1** was linked to 4,4'-, 3,3'- and 3,4'-bipyridine linkers, respectively. By following this concept, the isomeric compounds **10-12** were achieved (Figure 26). All three bidentate receptors are identical concerning the receptor/sensor moiety but differ in their linker units which result in symmetric (4,4'- and 3,3'-) and asymmetric scaffolds (3,4'-). Consequently, the minor sterical change at the linker induces also a NMR property change of the attached ^{19}F probes. In pure DMSO-d_6 one single ^{19}F signal for the symmetrical receptor **10** and **11** (δ_F −110.45 and −110.42 ppm, respectively) and two ^{19}F signals for the unsymmetrical **12** (δ_F −110.49 and −110.54 ppm) were recorded (see experimental section).

With the structurally enhanced property of the bidentate receptors in hand the qualitative sensing of selected diols was expected to be significantly improved. Furthermore, the magnetically diversity of the attached ^{19}F NMR probes of each receptor should produce enhanced spectroscopic pattern in a combined array of the receptors **10-12**. Thus, three unique NMR spectra of the receptors **10-12** and appropriate diol, respectively, were expected to significantly increase the discrimination power compared to the single and monodentate receptor **1** sensing approach (chapter 4.6).

Beyond that, the obtained ^{19}F shifts of the array were further processed to QR-like (quick response) and two-dimensional bar codes which represent a suitable visualization of the generated ^{19}F NMR data as well as the easy readout of the code with a bar code scanner. Moreover, this concept avoids complicated chemometric techniques. A similar approach based on a self-generated bar code was shown by Bode *et.al.* who used a ^{13}C-labelled self-contained boronic acid sensor array.[168] QR codes first introduced in 1994 by *Denso Wave* play an important role for the storage of product information, item identification/tracking and can be easily scanned via a barcode scanner or a smartphone camera in almost all directions of view.

Overall, this approach enables the comfortable inventory of items and manifold applications of the modern digital life.[169]

In practice, reversible boronic acid−diol interactions were probed in buffered aqueous solution (50 mM phosphate buffer, 10% D_2O, pH 7.4) at room temperature. Receptors **10**−**12** (single receptor solutions, 4 mM each) generated unique fluorine NMR patterns in the presence of selected bioanalytes (40 mM for good receptor saturation).

The processing of the obtained spectroscopic data based on the array of the fluorinated receptors **10-12** in presence of D-glucose to a unique QR-like barcode is exemplary shown in Figure 40. At first, the ^{19}F NMR spectrum of each sample containing appropriate receptor and D-glucose was recorded and chemical shifts and intensities were extracted and then processed as described in the following. The final QR-like bar code is composed of colored squares (the color corresponds to the appropriate spectroscopic data of each receptor) which are positioned

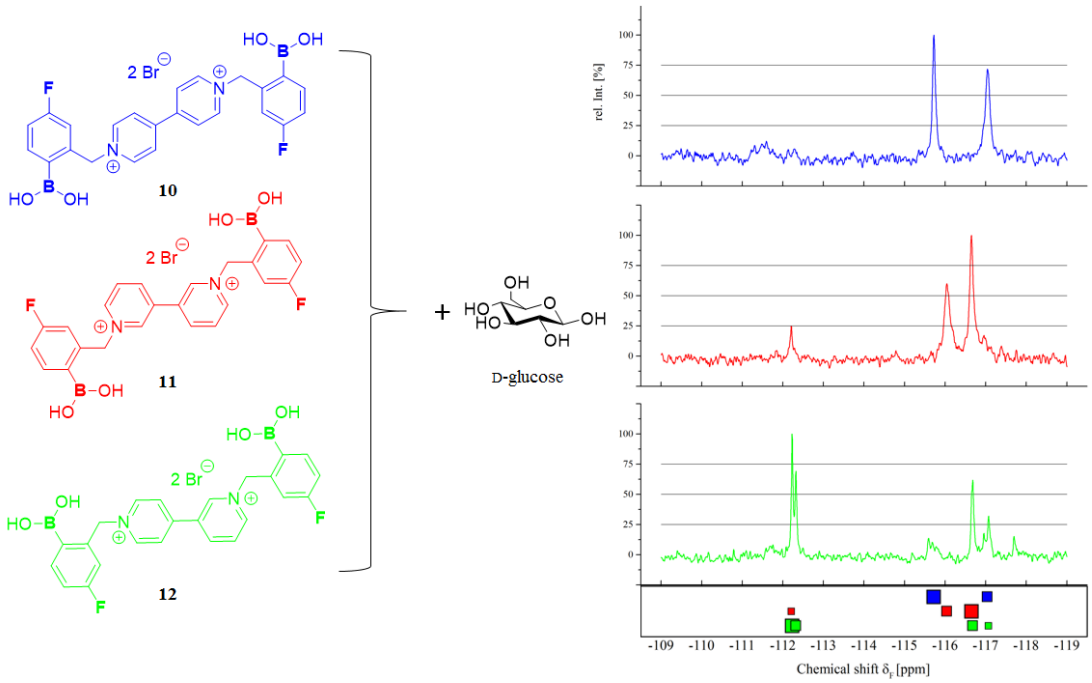

Figure 40: Exemplary bar code generation by processing the ^{19}F NMR data of the array of receptors 10-12 for enhanced diol discrimination via naked eye or a bar code scanner. The information of the resulting bar code was extracted from the original spectrum of appropriate receptor 10-12 in presence of D-glucose, respectively. The distinct position of each colored square is corresponding to the chemical shift and the square size is determined by the shift intensity (three arbitrary set thresholds at 25, 50 and 75%) of the corresponding ^{19}F signal and represented in three square size increments. Conditions: receptor 10-12 (4 mM), D-glucose (40 mM) in aqueous phosphate buffer solution (50 mM, 10% D_2O, pH 7.4) at 188 MHz, 256 scans and 25°C.

corresponding to the specific chemical shift of each recorded ^{19}F signal. The size of each square is corresponding to the shift intensity of the based ^{19}F signal. Arbitrarily, three thresholds at 25, 50 and 75% of relative NMR signal intensity (cutoff below 25%) determine the square size in three increments, respectively. The unique square pattern of each spectrum originates from the ^{19}F NMR shifts of unbound and complexed receptor, respectively. Further variance is given by the different sizes of the colored squares. Consequently, each analyte exhibits a distinctive bar code pattern which considerably profits from the enhanced spectroscopic information provided from each of the used receptors. To demonstrate the enhanced discrimination power of the array-based sensing concept compared to the single receptor sensing approach, nine diol-containing analytes were selected and screened by the array. The collected ^{19}F NMR data was processed to the specific analyte bar codes. Figure 41 illustrates the original ^{19}F NMR spectrum of receptor **10** in presence of appropriate diol, whereas the processed bar code generated by the combined spectroscopic information of the receptor array is presented underneath each spectrum, respectively.

Briefly, the ^{19}F NMR spectra obtained by solutions of the array and diols will be discussed below. Starting with the array of **10**-**12** in absence of diol, the representative blue spectrum of unbound **10** illustrates one sharp signal at δ_F −111.76 ppm with one corresponding blue square. Receptor **11** (3,3'-linked) produce one intensive red square at δ_F −112.21 ppm and the asymmetric receptor **12** (3,3'-linked) is represented by the two green squares at δ_F −112.24 and -112.33 ppm. The ^{19}F spectra of **10** in presence of catechol and the neurotransmitter dopamine provide a very similar shift with **10** at δ_F −116.05 and −115.93 ppm, respectively, accompanied is the complete disappearance of the signal of unbound **10** which indicates the complete formation of high affinity 1:1 boronate esters (Figure 41, b and c). The blue spectra of the single receptor **10** in presence of catechol and dopamine does not allow confident analyte discrimination but the resulting bar code of the array enhances the discrimination power due to the diverse bar codes of both analytes. This observation becomes more obvious by comparing the similar spectra of **10** in a mixture with dopamine and D-fructose whereas the discrimination of these diols tremendously profits from the diverse bar codes (Figure 41, c and d). Next, D-fructose, a strong binding monosaccharide, produces one sharp receptor-**10**-fructose peak at δ_F −116.10 ppm and a completely diverse bar code of the array compared to the constitutional isomer D-glucose (Figure 41d and e, respectively) with two shifts at δ_F −115.72 and −117.04 ppm. A similar discriminative result was found for the isomeric phosphorylated sugars D-glucose-1-phosphate (Figure 41f) and D-glucose-6-phosphate (Figure 41g). Obviously, the 1-

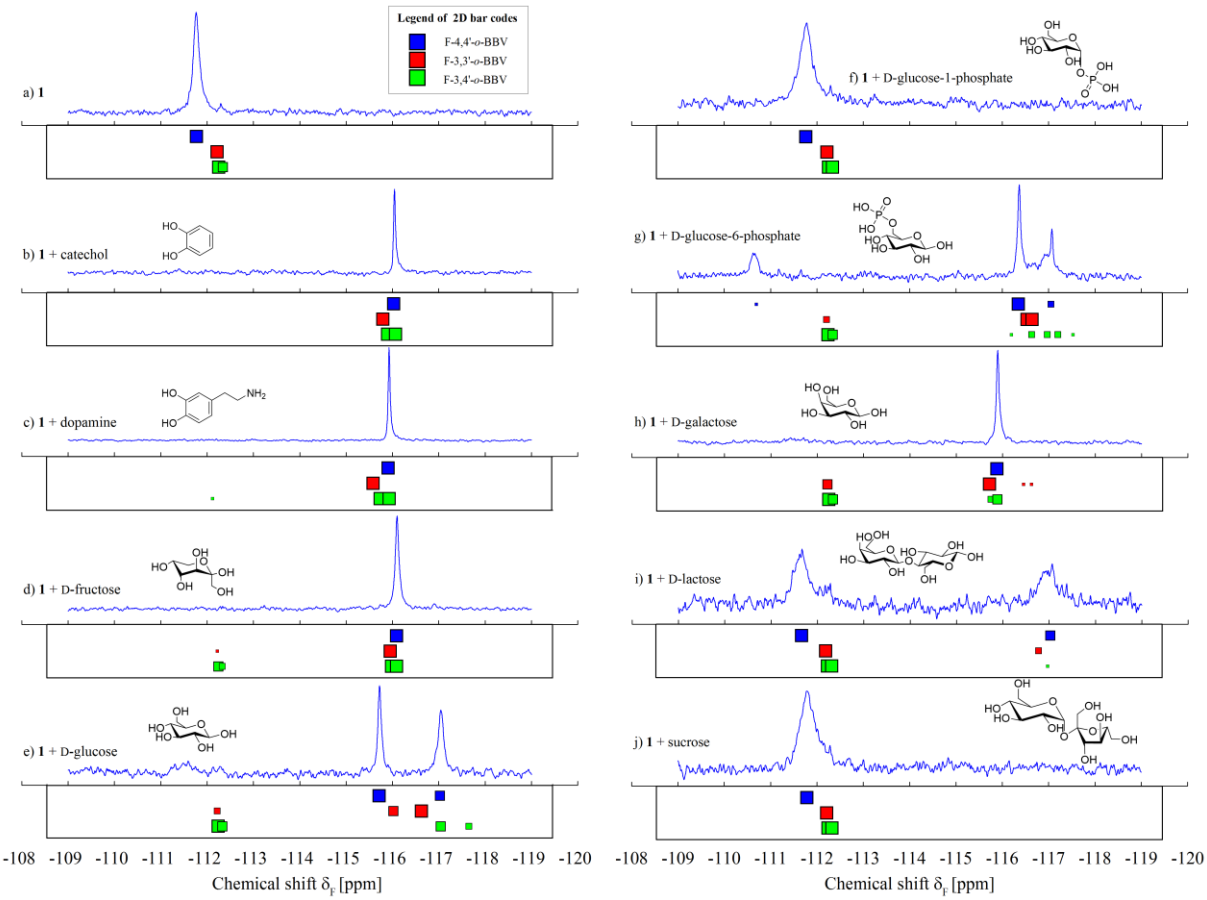

Figure 41: Exemplary ^{19}F NMR spectra (in blue) of unbound 10 and in presence of diol represent the single receptor approach whereas the generated QR-like bar codes (underneath each spectrum) of the array of the receptors 10-12 provide enhanced discriminatory property. Conditions: 10-12 (4 mM each), diol (40 mM) measured in phosphate buffer (50 mM, 10% D_2O, pH 7.4,) at 188 MHz, 256 scans and 25°C.

phosphate is not binding at all due to the relative similar bar code of the unbound array, whereas the 6-phosphate derivative produce the most unique code pattern. Thus, the screened derivatives of glucose can be easily discriminated via the presented array of fluorinated receptors. D-galactose which is another isomer of D-fructose (constitutional) and D-glucose (epimer) produces one sharp shift at δ_F −115.90 ppm in the spectrum of **10** and another highly discriminative bar code (Figure 41h). The two screened disaccharides D-lactose and sucrose show weak or no interaction with the receptor array and consequently produce a bar code which is similar to the code of the unbound array.

Another concept for storing the spectroscopic information in an easy to readout code can be achieved by the generation of a standardized bar code. The Global Trade Item Number (GTIN)[170] decodes the non-interchangeable product identification of commercial articles and is attached to the packaging of items. Most commonly, a 13-digit bar code (GTIN-13) is used and composed of a starting digit and two blocks (left and right) of digits with each containing six

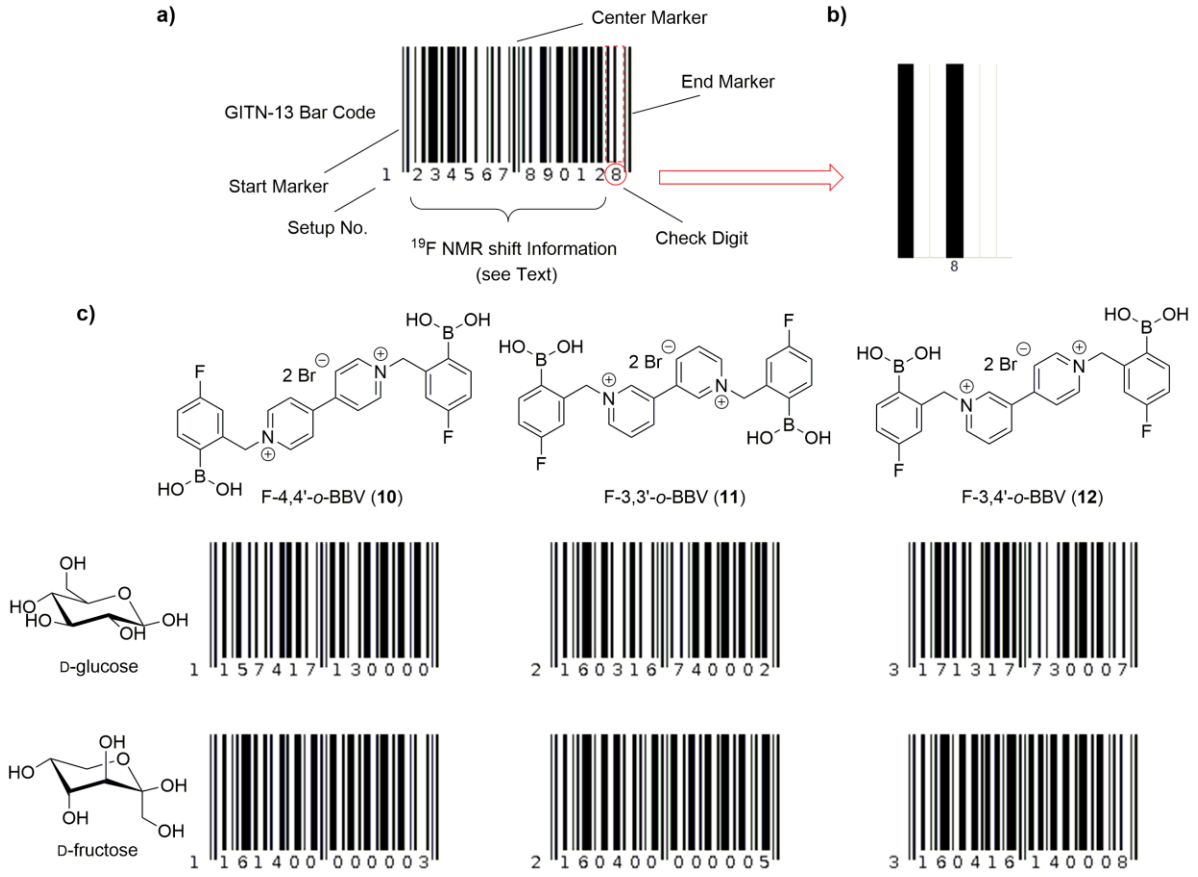

Figure 42: a) Exemplary composition of the information (12+1 digits) used for bar code generation based on the GTIN-13 bar code layout. b) Exemplary bar code encoding of the last digit (check digit) represented by a seven-segment bar code above each digit. c) Unique bar codes of the fluorinated BBV's in presence of D-glucose and D-fructose that could be easily read out via a commercial bar code scanner.

digits (Figure 42a). Furthermore, the bar code is composed of one start marker, end marker, center marker, respectively, and the internal routine for the bar code generation, which enables bar code scanning in almost every angle and direction. The starting digit determines the internal routine of the bar code generation of all other digits (and vice versa) whereas the last digit is the check digit that provides the self-checking property of the bar code. All digits except the first one (indirectly decoded in the pattern of the other twelve digits) are separately decoded in the seven-segment pattern above each the appropriate digit (Figure 42b). All segments of the overall digits represent the unique bar code pattern of a specific item. The numerical information of a commercial item can be stored in all digits except the check digit and contains in general from left to right the country code (three digits), the manufacturer code (variable length), the product code (variable length) and the check digit (last digit). A usual bar code scanner allows the read out of the stored article. Thus, the concept enables the comfortable inventory and handling of items at any time.

As a first attempt, the characteristic spectroscopic ^{19}F NMR data of the receptors **10-12** was processed and transferred into standardized GTIN-13 bar codes. The assigned digits were arbitrary assigned from the left to the right as follows: The first digit was assigned to the used sensing setup (setup no.) holding the value 1, 2 or 3 with respect to fluorinated boronic acid receptor **10**, **11** or **12**, respectively. Hence, a unique bar code pattern is guaranteed due to the routine determining property of the first digit. Instead of the receptor also setup parameters such as the used NMR machine, frequency etc. are thinkable.

Next, the following eleven digits (except the check digit) were continuously assigned by the resulting new appearing chemical shifts and the corresponding shift intensity as processed in the QR bar code approach above. Thus, the GTIN-13 bar code of receptor **10** and D-glucose (Figure 42c) starts with 1 (setup no.= 1 = receptor **10**) followed by the digits 1, 5, 7 and 4 which correspond to the new appearing ^{19}F signal at δ_F −115.72 ppm (signal intensity = 4). The prefix and first digit position (-1) were not used and the position after the decimal point was rounded to one digit. All other available digits of the GTIN-13 bar code were filled in the same manner, whereby 0's correspond to no available ^{19}F data. Consequently, the resulting digital code for **10** and D-glucose (two new shifts, δ_F −115.72 ppm, intensity 4 and δ_F −117.12 ppm, intensity 3) was generated to "1 1 5 7 4 1 7 1 3 0 0 0 and 0" (check digit). Another example of receptor **12** in presence of D-fructose resulted in "3 1 6 0 4 1 6 1 4 0 0 0 8" which corresponds to setup no. 3 (first digit) and the shifts at δ_F −116.00 ppm (intensity 4), δ_F −116.11 ppm (intensity 4) and the check digit 8 at the end.

All generated GTIN-13 bar codes of the receptors **10-12** in presence of D-glucose and D- are illustrated in Figure 42c. Due to the distinct ^{19}F shifts, the associated shift intensities and the different sensing setups every receptor-diol combination provides a unique digital code and thus a non-interchangeable GTIN-13 bar code. Accordingly, the selected diols and in theory also other analytes can be distinctively discriminated and unmistakably identified via the standardized bar codes and inventoried using a bar code scanner.

Overall, the approach using an array of the three fluorinated boronic acid-appended bipyridinium salts **10-12** assisted by ^{19}F NMR spectroscopy is a convenient method for creating highly characteristic and discriminative two-dimensional or GTIN-13 bar codes which can be generated by clever processing of the recorded ^{19}F NMR data. Isomeric and similar analytes with minor structural difference at the backbone can be differentiated via intuitively or systematically readable bar codes. Beside the discriminative feature of the bar codes it is also possible to get a qualitative insight of the binding affinity of the specific analyte to the array.

No or weak interfering analytes produce ^{19}F NMR signals and bar codes that are similar to the signals and bar codes of the unbound receptors (Figure 41a). In contrast, strong interaction of the receptors to the diols lead to the disappearance in this range with new appearing and characteristic bar code pattern in the range of δ_F −116 to 118 ppm.

The presented approach using a QR-like bar code for the code generation is only one very simple possibility with respect to the used NMR data. Nevertheless, the use of a standardized bar code format such as the GTIN-13 code and the clever processing of the spectroscopic data generated by the receptor-diol interaction is assumed to be a promising approach for automated analyte (diol) identification and discrimination. This concept is especially thinkable in combination with modern software solutions which could generate and archive distinct analyte (diol) bar codes. Such an approach would lead to a very comfortable archiving system for the unambiguous analyte identification and discrimination. The addition of further spectroscopic parameters such as the line width, S/N or changing/adding the thresholds or cutoff would add further discriminative property to the bar codes with a resulting tremendously increase in discrimination power. Quantitative parameters such as integral values are also thinkable to be included into the bar code.

SCREENING OF BINARY AND TERNARY DIOL MIXTURES

The previously sections showed unique ^{19}F NMR fingerprints of appropriate receptor in presence of interacting diol. Beyond that, the qualitative sensing approach of single diol screening experiments can be extended by the screening of diol mixtures. Thus, one can expect the identification/ discrimination of each diol component in a binary or ternary mixture as long as the characteristic ^{19}F NMR shifts are not overlapping and moderate affinity of all components of the mixture to the fluorinated receptor is given.

A primary example with regards of diol discrimination which is challenging especially for all fluorescent approaches is the sensing of the constitutional isomers D-fructose and –glucose in a mixture. As shown before both monosaccharides produce a completely diverse ^{19}F NMR pattern with **1** and can be easily distinguished in samples containing the pure components. Therefore, the screening of a binary mixture of the isomers via receptor **1** assisted by ^{19}F NMR is also expected to show the characteristic and distinguishable fingerprints of both diols, respectively.

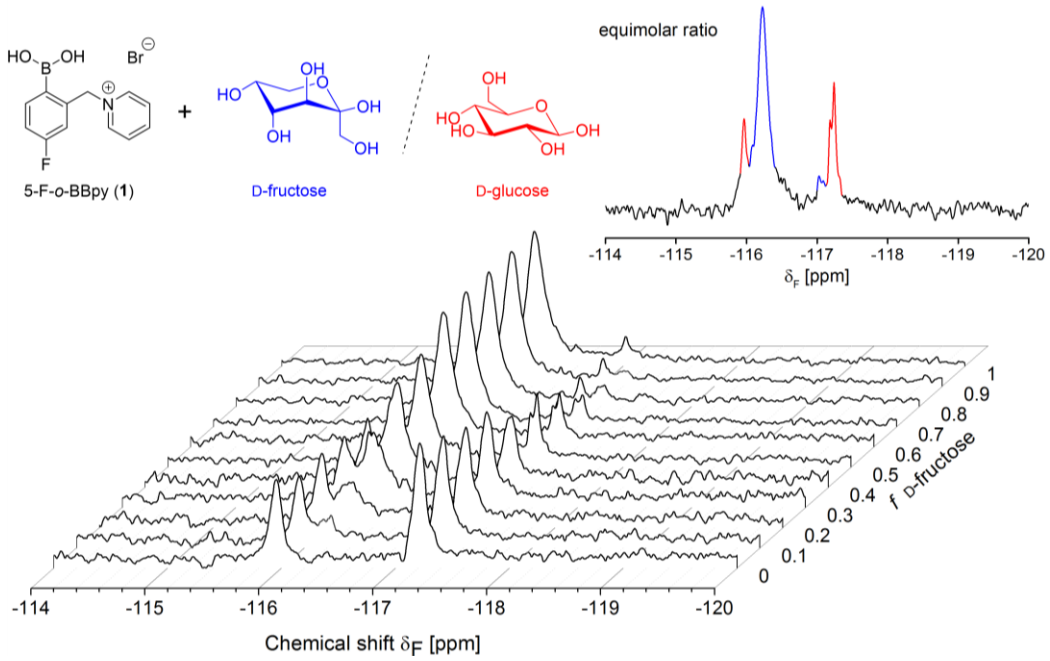

Figure 43: ^{19}F sensing of diol mixtures containing D-fructose and -glucose via receptor 1. The fluorine spectra of 1 in the presence of changing molar fraction of D-fructose illustrate the sensing potential concerning diol mixtures. D-glucose can still be identified in a mixture with D-fructose by a ratio of 1:9 respectively. Conditions: 1 (10 mM), D-fructose and -glucose (f = 0−1, 0−10 mM) in HEPES buffer (100 mM, pH 7.4, 10% D_2O).

As an initial experiment, receptor **1** (10 mM) was applied for diol sensing of a diol mixture containing D-fructose and -glucose (10 mM total saccharide concentration) with changing mole fraction *f* (0-10 mM, respectively) in aqueous HEPES buffer solution (100 mM, pH 7.4, 10% D_2O). For each molar fraction the corresponding ^{19}F NMR spectrum was recorded as represented by Figure 43. The inset clearly shows the already known ^{19}F shifts of D-fructose (blue) and –glucose (red) at equimolar ratio, respectively. Due to the highly characteristic shifts and minor signal overlap, D-glucose could be positively identified along with D-fructose up to a 9-fold excess of the latter (1 vs. 9 mM), even though a higher affinity of D-fructose compared to D-glucose was found (K_b 1620 vs 132 M^{-1}, see also chapter 4.9). Vice versa, D-fructose could be at minimum positively identified beside D-glucose at $f = 0.1$.

With these obtained results in hand, the ^{19}F approach has a considerable advantage when compared to common fluorescent probes which are not able in identifying analyte components in a mixture or disturbing matrices. As a matter of fact, fluorescent approaches suffer from discrimination of single diol samples and even more of diol mixtures due to nonselective signal modulation of the fluorescence emission which is furthermore sensitive to interfering compounds, the solvent or pH.

A further screening experiment of a binary mixture is represented by Figure 44. Clearly, mixtures of D-glucose and D-/L-lactic acid, d), as well as D-glucose and dopamine, c) show the characteristic fluorine pattern of the single components, respectively. A mixture of lactic acid and dopamine, b), lack of analyte discrimination because of the overlapping manner of both single ^{19}F NMR shifts at around δ_F −115.7 ppm (see also Figure 39). A ternary sensing experiment containing D-glucose, dopamine and D-/L-lactic acid is shown in Figure 44a. Beside the characteristic shifts of D-glucose the ^{19}F NMR spectrum again lack of the identification/discrimination of dopamine and lactic acid due to signal overlapping.

In terms of the performed binary and ternary sensing experiments the presented approach is a robust and valuable method and can conveniently be used for the identification and discrimination of diols in mixtures as long as high affinity of desired analytes among interfering compounds and no signal overlap of distinct fluorine shifts is given. Especially, important medicinal markers such as D-glucose, dopamine and lactic acid that are necessary for disease diagnosis can be identified via receptor **1** assisted by ^{19}F NMR spectroscopy.

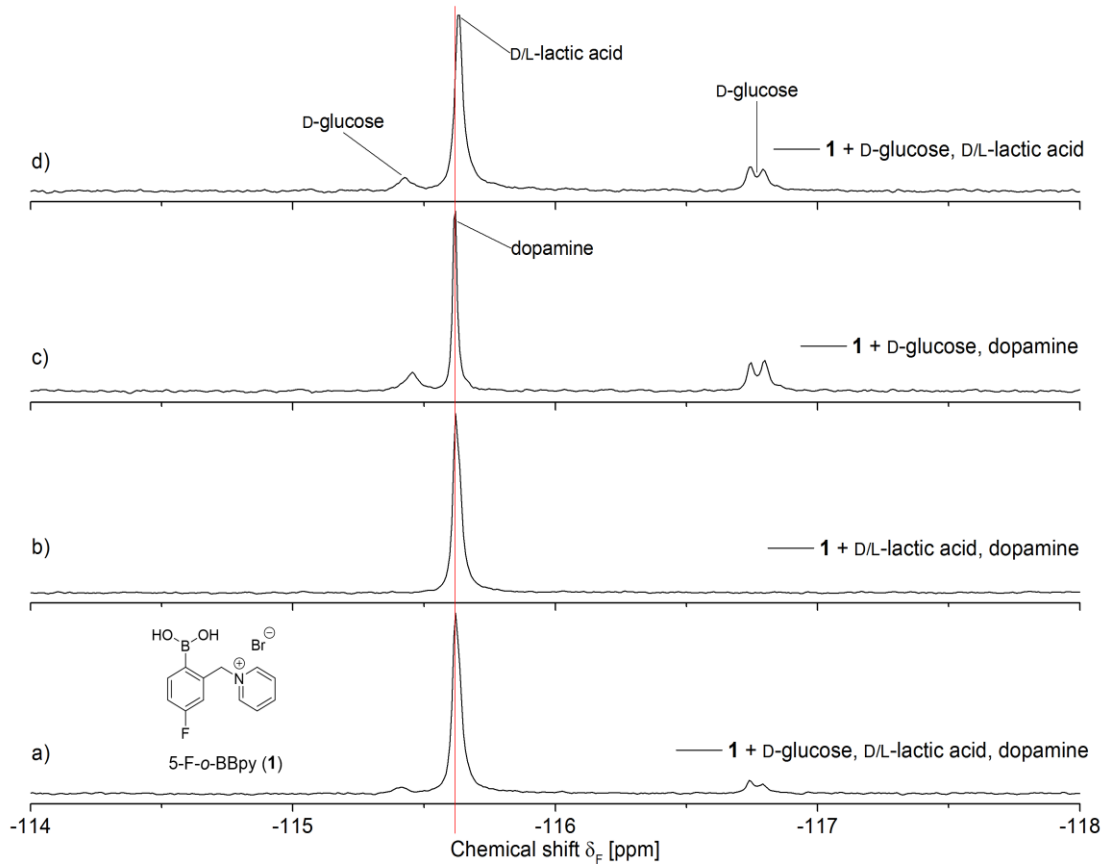

Figure 44: ^{19}F {^{1}H} NMR spectra of receptor 1 in binary and ternary mixtures of the medicinal relevant analytes D-glucose, D/L-lactic acid and dopamine for the competitive diol identification. D-glucose and D/L-lactic acid as well as D-glucose and dopamine, respectively, can be clearly distinguished in a binary mixture via their characteristic ^{19}F NMR shifts. Mixtures containing and D/L- lactic acid and dopamine lack of discrimination of both analytes due to overlapping signals. Conditions: receptor 1 (10 mM), D-glucose (5 mM), D/L-lactic acid (5 mM) and dopamine (1 mM) measured in HEPES buffer (100 mM, pH 7.4, 10% D_2O) at 188 MHz, 256 scans and 25°C.

Beside the presented qualitative approach of analyte discrimination in mixtures one could also expect quantitative determination of the analyte of interest as long as the other components of the mixture are silent (show no affinity to the receptor) or are kept constant with respect to the concentration (see chapter 4.14 for anion sensing in a ternary mixture).

APPARENT DIOL BINDING AFFINITIES AND DIOL QUANTIFICATION

Binding constants describe the affinity of receptor compounds to a specific analyte which stand in an equilibrium with each other under given conditions such as solvent, pH and temperature. Commonly, the binding constant can be determined using a fixed concentration of receptor that is titrated with increasing amount of analyte. Meanwhile, the correlated physical property change such as the fluorescence intensity, absorbance or chemical shift is recorded. At full conversion (at receptor saturation) no further significant property change can be observed, and the equilibrium corresponds to the pure receptor-analyte complex. The binding isotherm of the receptor-analyte interaction can be obtained by plotting the physical property change versus the analyte concentration. Subsequently, the fitting of the data with a suitable equation, which explains a 1:1 or 1:2 binding model lead to the apparent binding constant K_b.

In this chapter the binding constants were determined to get an understanding of apparent binding affinities of the presented fluorinated boronic acid receptors to selected diols. Thus, the fluorinated receptors **1** and **10** were chosen as representatives of monodentate and bidentate receptor scaffolds for diol esterification, respectively.

In detail, binding constants K_b of **1** to a analyte collection containing D-fructose, D-glucose, D-glucose-6-phosphate, D-galactose, D-mannitol, D-sorbitol, *N*-acetylneuraminic acid and catechol were determined by using the quantitative sensing feature of ^{19}F NMR spectroscopy. For each series of measurement, samples containing a solution of **1** (10 mM) titrated with appropriate diol (0-100 mM) were prepared in aqueous HEPES buffer solution (100 mM, pH 7.4, 10% D_2O) and consecutively recorded via ^{19}F NMR spectroscopy at 188 MHz, 256 scans and 24 °C. For comparison, K_b values of the bidentate receptor **10** to D-fructose, D-glucose and catechol have also been determined. Titration experiments have been conducted as described above using final concentrations of 2 mM of **10** (due to limited solubility) and increasing concentrations of diol (0-10 mM) which have been performed at 188 MHz and 1024 scans (for better signal resolution due to reduced total fluorine content).

The FID of each spectrum was processed with the data processing guide (automatic mode) of the Bruker Top Spin 3.2 software containing Fourier Transformation, phase and baseline correction. With the knowledge of the specific fluorine concentration in each sample (e.g. total fluorine concentration of 10 mM for samples of receptor **1**) and good ^{19}F signal separation (first order spectra) the absolute concentrations of unbound receptor and receptor-analyte complex were determined via simple signal integration. Relative shift integral changes

of the upcoming signals were determined with respect to the integrals of unbound receptor. With the known concentration of unbound receptor and the calculated concentration of the formed receptor-diol complexes in hand, the free analyte concentration was calculated. Exemplary, the recorded ^{19}F NMR titration spectra of **1** in presence of D-mannitol are represented by Figure 45 with decreasing signal of unbound receptor **1** and increasing characteristic signal of the formed single receptor-**1**-mannitol complex.

The binding isotherms of **1** were obtained by plotting the data as [HG]/[H_0] vs. [G], whereas [HG] is the concentration of the receptor-diol complex (sum of all appearing receptor-diol signals), H_0 the initial concentration of receptor **1** (10 mM) and [G] is the concentration of unbound diol. Subsequently, fitting of the curves was performed using the binding model of Equation 14. The latter is achieved by the combination and rearrangement of the mass balance of the 1:1 equilibrium (Equation 13) and the relation of the initial concentration H_0. All obtained binding isotherms and the described data fitting of receptor **1** and appropriate diol are illustrated in Figure 46. Overall, the good quality of data fitting (R^2) supports the existence of the expected 1:1 binding behavior of the monodentate receptor **1**. As expected and known from literature, the boronic acid receptor **1** exhibits superior affinity to catechol indicated by K_b = 3980 M^{-1}

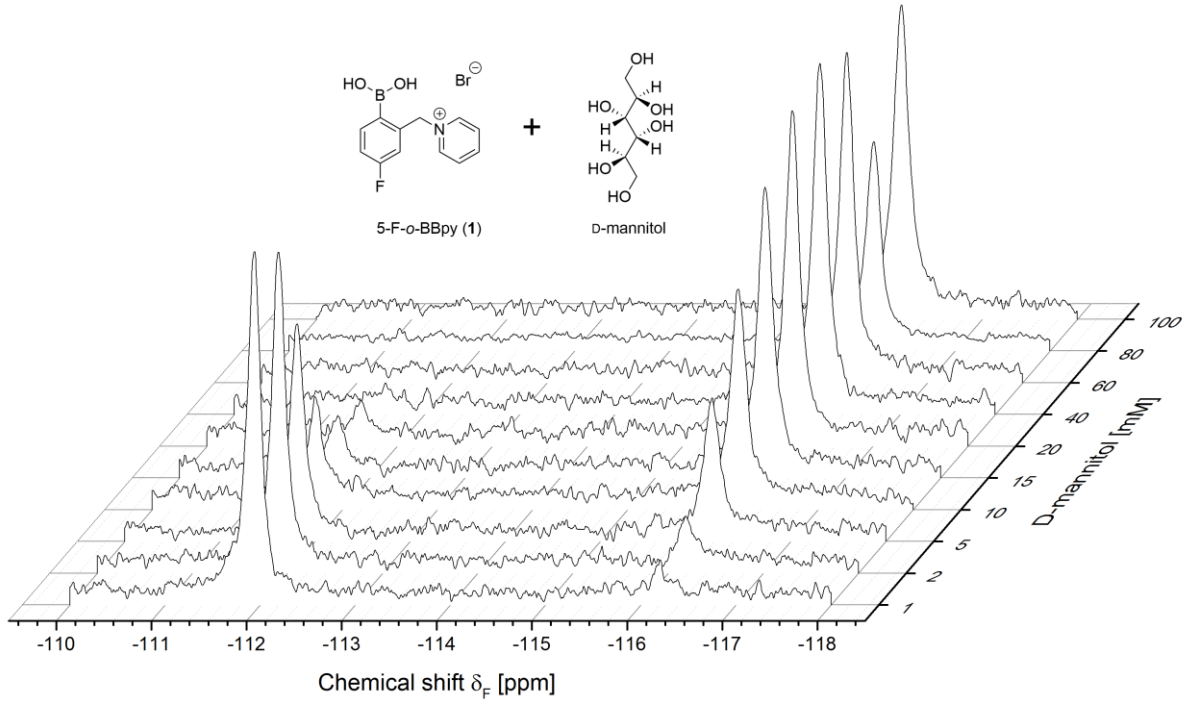

Figure 45: Exemplary titration behavior for K_b determination of receptor 1 in presence of increasing amount of D-mannitol visualized by appropriate ^{19}F {^1H} NMR spectra. Conditions: Receptor 1 (10 mM) and D-mannitol (0-100 mM) measured in aqueous HEPES buffer solution (100 mM, pH 7.4, 10% D_2O) at 188 MHz, 256 scans and 24°C.

$$\text{1:1 equilibrium:} \qquad H + G \underset{\rightleftarrows}{K_b} HG \quad \text{with} \quad K_b = \frac{[HG]}{[H] \cdot [G]} \qquad \text{(Equ. 13)}$$

$$\frac{[HG]}{[H_0]} = \frac{K_b \cdot [G]}{1+(K_b \cdot [G])} \qquad \text{with} \qquad [H_0] = [H] + [HG] \qquad \text{(Equ. 14)}$$

and the following trend: D-fructose > D-sorbitol > D-mannitol >> D-galactose > D-glucose > (D-glucose-6-phosphate) > *N*-acetylneuraminic acid. Thus, the ideal synperiplanar cis-1,2 hydroxyl groups of catechol provide a highly preferred binding access for receptor **1** which is indicated by the instantly quantitative conversion of the ^{19}F signal of unbound **1** to the receptor-1-catechol complex at each point of the titration. The result of the titration via D-glucose-6-phosphate must be treated with caution due to assumed interfering and competitive reaction of the phosphate moiety which is visible by decreasing values of $[HG]/[H_0]$ and strong shifting of the ^{19}F shift of the unbound receptor **1** (not shown). The binding constant of **1** with catechol

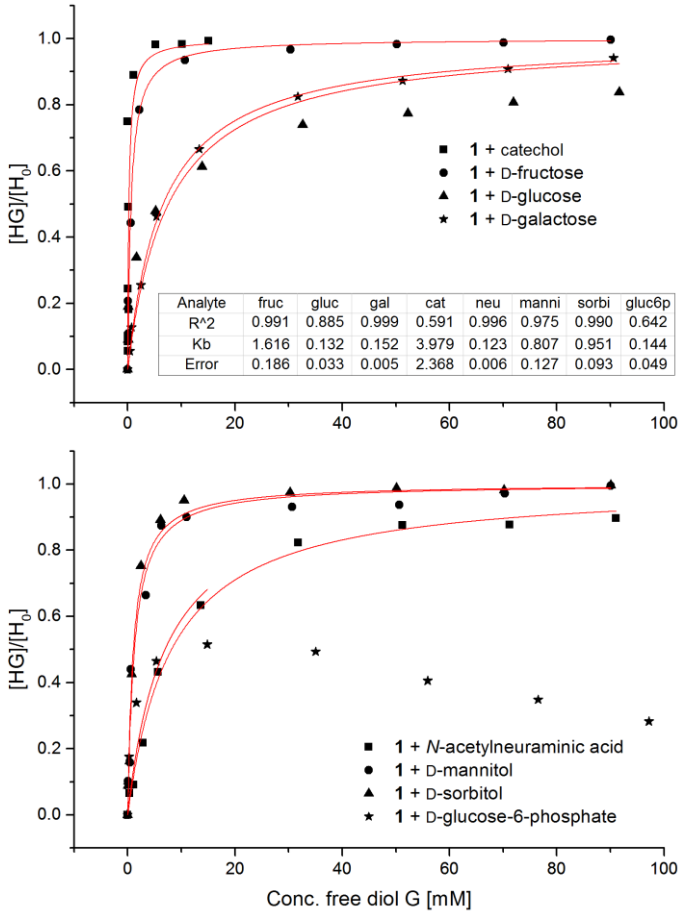

Figure 46: Binding isotherms of monodentate receptor 1 titrated with selected diols and plotted as $[HG]/[H_0]$ versus free diol [G]. The plotted data was fitted with the 1:1 binding model for binding constant K_b determination. Conditions: receptor 1 (10 mM), appropriate diol (0-100 mM) measured in aqueous HEPES buffer solution (100 mM, pH 7.4, 10% D_2O) at 188 MHz, 256 scans and 24°C.

was too high to be accurately determined and the K_b contains a defective value. All calculated K_b values are summarized in Table 4.

For comparison, the binding constants of the bidentate receptor **10** in presence of D-fructose, D-glucose and catechol have also been determined. For this purpose, the law of mass action for a 1:2 binding equilibrium (assumed 1:2 to binding) described by Equation 15 was modified with Equation 14 and rearrangement resulted in the fit model of Equation 16. The resulting binding isotherms were generated by plotting $[HG_2]/[H_0]$ vs. [G] and subsequently fitted as shown in Figure 47. For comparison, the 1:1 binding model was also applied on the plotted data. The resulting R^2 values of the 1:2 model imply a slight preference compared to the 1:1 binding model. Thus, the binding behavior of the bi-functionalized receptor **10** can be better described by the 1:2 binding model of Equation 16. The order of analyte affinity is identical to the monodentate receptor **1** with catechol > D-fructose > D-glucose, whereby the calculated values are smaller which give no hint for possible bidentate binding of especially the monosaccharides.

Beside titration experiments for binding constant determination monitored via ^{19}F NMR spectroscopy, the quantitative detection of diol is also a suitable task with respect of an applicable diol sensing tool. For this purpose, a quantitative calibration curve is required. In practice, this calibration was obtained from the increasing amount of the formed receptor-diol

1:2 equilibrium: $$H + G \underset{\rightleftarrows}{K_1} HG; \qquad HG + G \underset{\rightleftarrows}{K_2} HG_2 \quad \text{with } K_2 = \frac{[HG_2]}{[HG]\cdot[G]} \qquad \text{(Equ. 15)}$$

$$\frac{[HG]}{[H_0]} = \frac{K_1 \cdot K_2 \cdot [G]}{1 + K_1 \cdot [G]} \qquad \text{(Equ. 16)}$$

Table 4: Apparent binding constants K_b [M^{-1}] of monodentate receptor 1 (1:1 binding model) and bidentate receptor 10[a] (1:2 and 1:1 binding model for comparison given in brackets) determined via the ^{19}F NMR sensing approach. Measured in aqueous HEPES buffer solution (100 mM pH 7.4, 10% D_2O) at 188 MHz, 256 and 1024 scans for 1 and 10, respectively, and 24°C.

Catechol	D-fructose	D-glucose	D-glucose-6-phosphate
3979±2368	1616±186	132±33	144±49
964±16[a] (1271±259)	694±10 [a] (893±145)	519±2 [a] (521±22)	-
D-galactose	**D-mannitol**	**D-sorbitol**	***N*-acetylneuraminic acid**
151±4	807±127	951±93	123±6

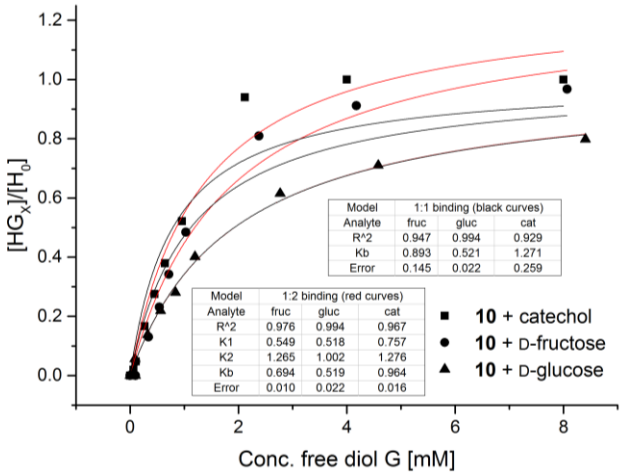

Figure 47: Binding isotherms of bidentate receptor 10 titrated with D-fructose, -glucose and catechol, respectively, and plotted as $[HG_x]/[H_0]$ versus free diol [G] and data fitting with the 1:2 and 1:1 binding model for binding constant K_b determination. Conditions: receptor 10 (2 mM), appropriate diol (0-10 mM) measured in aqueous HEPES buffer solution (100 mM, pH 7.4, 10% D_2O) at 188 MHz, 1024 scans and 24°C.

$$\frac{[HG]}{[H_0]} = m\,x + n \qquad \text{(Equ. 17)}$$

complex (relative integral) versus the added diol concentration. The plotted data of exemplary selected receptor **1** and the monosaccharides D-fructose, D-glucose and D-galactose, respectively, shown as $[HG]/[H_0]$ versus the diol concentration is given by Figure 48. All three data sets provide a good linear dependency of the recepot-**1**-diol complex evolvement in the measured range of 0-10 mM of appropriate diol. The calibration line (Equation 17) obtained by data fitting can now be used in a consecutively step for the quantitative deteermination of the unknown diol concentration.

Overall, the apparent binding constants K_b could be conveniently determined using the ^{19}F NMR approach and suitable data fitting using the 1:1 and 1:2 binding model of receptor **1** and **10**, respectively. The order of the obtained affinities corresponds to values found in literature. Nevertheless, one must mention that the calculated K_b values do not reflect the real binding behavior of the receptors and can be regarded as a general affinity estimation. One main reason, which has to be considered, is the procession of NMR integrals of the formed receptor-diol complexes that cover numerous binding species and naturally exhibit different affinities each receptor-diol species. Furthermore, it could be exemplary shown that the observed physical data change (integrals) of the fluorinated receptor **1** upon diol titration can be used for the generation of calibration curves. Due to the linear behavior of the integral evolvement with respect to increasing amount of diol the approach can be used for the quantitative determination of the diol in real samples.

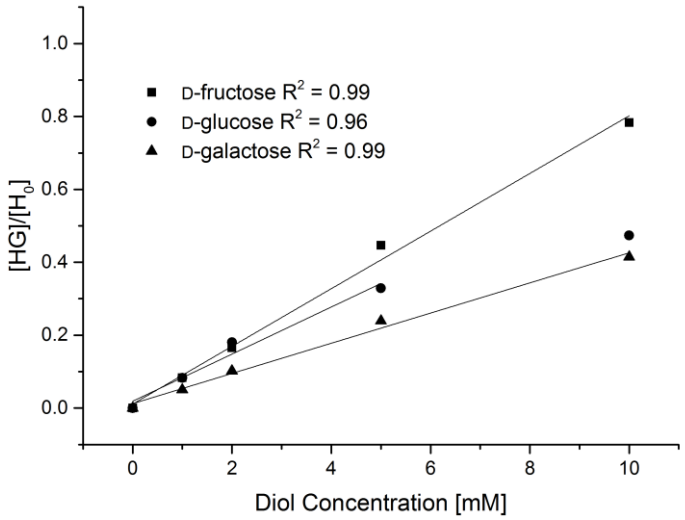

Figure 48: Exemplary data plot of complex formation upon increasing amount of D-fructose, D-glucose and D-galactose plotted as [HG]/[H_0] versus the diol concentration [G]. The fitting of the data shows the linear portion for quantitative diol sensing tasks, respectively. Conditions: receptor 1 (10 mM) and D-fructose, D-glucose and D-galactose (0-10 mM) measured in aqueous HEPES buffer solution (100 mM, pH 7.4, 10% D_2O) at 188 MHz, 256 scans and 24 °C.

INVESTIGATION ON RECEPTOR BINDING MODES TO CARBOHYDRATES

The distinct ^{19}F NMR fingerprints of diol containing analytes generated by the fluorinated boronic acid receptors assisted by ^{19}F NMR spectroscopy enable a reliable way for the discrimination of diol containing analytes including numerous similar derivatives of them. Beyond that, the distinct ^{19}F NMR shifts can also be used for the investigation of possible binding modes of appropriate diol to the boronic acid binding site of the receptor molecule and to get a knowledge about preferred receptor-diol affinities. Indeed, the latter are determined by the structural character of the analyte.

Another aspect is the ongoing dispute of several workgroups in the field of boronic acid-based diol sensing with contrary opinions in how monosaccharides are binding to boron.[76, 171-173] The presented ^{19}F NMR diol sensing concept has the advantage of less complicated spectroscopic information (first order spectra, signals with minor or no signal overlapping) compared to e.g. ^{1}H or ^{13}C NMR. that are accompanied by more complicated spectra, spin-spin coupling or overlapping signals induced by the solvent or other molecular species. A drawback of the ^{19}F technique concerning the elucidation of binding modes is the indirect sensing character. The attached fluorine probe is located in a larger spatial distance compared to other NMR sensitive nuclei. Thus, a directly to place of action (the binding site) positioned nuclei such as ^{1}H, ^{13}C or ^{11}B might be more suitable for studying the binding modes of appropriate diol to the receptor site.

As described earlier in chapter 4.6, the multitude of screened analyte classes and their corresponding ^{19}F NMR spectra (see Figure 39) produced by receptor **1** and ^{19}F NMR showed primarily positive and strong interaction in presence of reducing sugars, sugar alcohols and well preorganized diols. For the elucidation of possible binding modes these recorded ^{19}F NMR spectra and available binding affinities (chapter 4.9) were analyzed to get a qualitative insight in how monosaccharide isomers are supposed to bind to boron under aqueous conditions. Analyte classes which have been involved in this study include catechols, monosaccharides (trioses, pentoses and hexoses, available naturally and synthetically origin) and derivatives of the latter such as phosphates and corresponding sugar alcohols (simply spoken reduced analogs with respect to the keto/aldo open chain form of monosaccharides). Furthermore, model-like cyclopentanediol and cyclohexanediol compounds with stereochemical diverse configurated OH groups have been screened to get a knowledge about the influence of the orientation of the

hydroxyl groups for esterification. Figure 49 presents the ^{19}F NMR spectra of **1** and in presence of the analytes of interest for the consideration of possible binding modes.

The investigation started with catechol which is a structurally well preorganized diol and provides the strongest observed affinity of all tested diols to receptor **1** (K_b = 3979 M^{-1}). The aromatic diol exhibits two 1,2-OH groups in plane which are supposed to form exclusively a five-membered boronate catechol ester (lowest found pK_a for the formed boronic acid catechol ester compared to other esters, see chapter 4.9 and proposed structure in Figure 50a). Other isomers of catechol in solution are not possible (no isomerization of catechol). This binding behavior was also seen for the other monodentate receptors **2** and **3,** which produce only one single and sharp signal in their ^{19}F NMR spectra (Figure 35). This observation strongly indicates that each ^{19}F probe of the receptors **1**-**3** reports one single receptor-diol complex in solution, respectively. The same result was also seen for **1** in presence of dopamine, a structurally closely related catecholamine, albeit the structural aminoethyl backbone induced a minor shift change compared to catechol (structure in Figure 50a).

In contrast, monosaccharides display a complex equilibrium in water and produce a much more complex fluorine pattern. Under aqueous conditions monosaccharides display the isomers α-/β-pyranose, α-/β-furanose (chain forms and their anomers, respectively) and aldehyde/ketone and hydrates, respectively (open chain forms, respectively) which can lead to numerous possible binding modes to a boronic acid receptor. As mentioned earlier, cis-1,2 and cis-1,3 hydroxyl groups of the monosaccharide isomers provide suitable binding sites to boron.

As a first approach a set of cyclic and model-like diol analytes with respect to the pyranose and furanose isomers of monosaccharides including cis/trans-1,3-cyclopentanediol, cis-1,2-cyclopentanediol, trans-1,2-cyclopentanediol, cis/trans-1,3-cyclohexanediol, cis-1,2-cyclohexanediol and trans-1,2-cyclohexanediol was screened to investigate the binding behavior and influence of the OH orientation to receptor **1**. As shown in Figure 49a moderate binding to only cis-1,2-cyclopentanediol could be recorded with one new appearing and broad ^{19}F shift at δ_F –114.69 ppm beside the signal of unbound **1**. In theory, cis-1,2-cyclopentanediol is a furanose-like analogue with neglected interaction to the hypothetical saccharide backbone and provides 1,2-OH groups with the same cis orientation. Thus, special preference of the boronic acid function of **1** in forming five-membered cyclic esters with the cis-1,2 OH groups of furanose isomers, which provide a suitable attack side to the receptor, can be assumed (see proposed structure in Figure 50b).

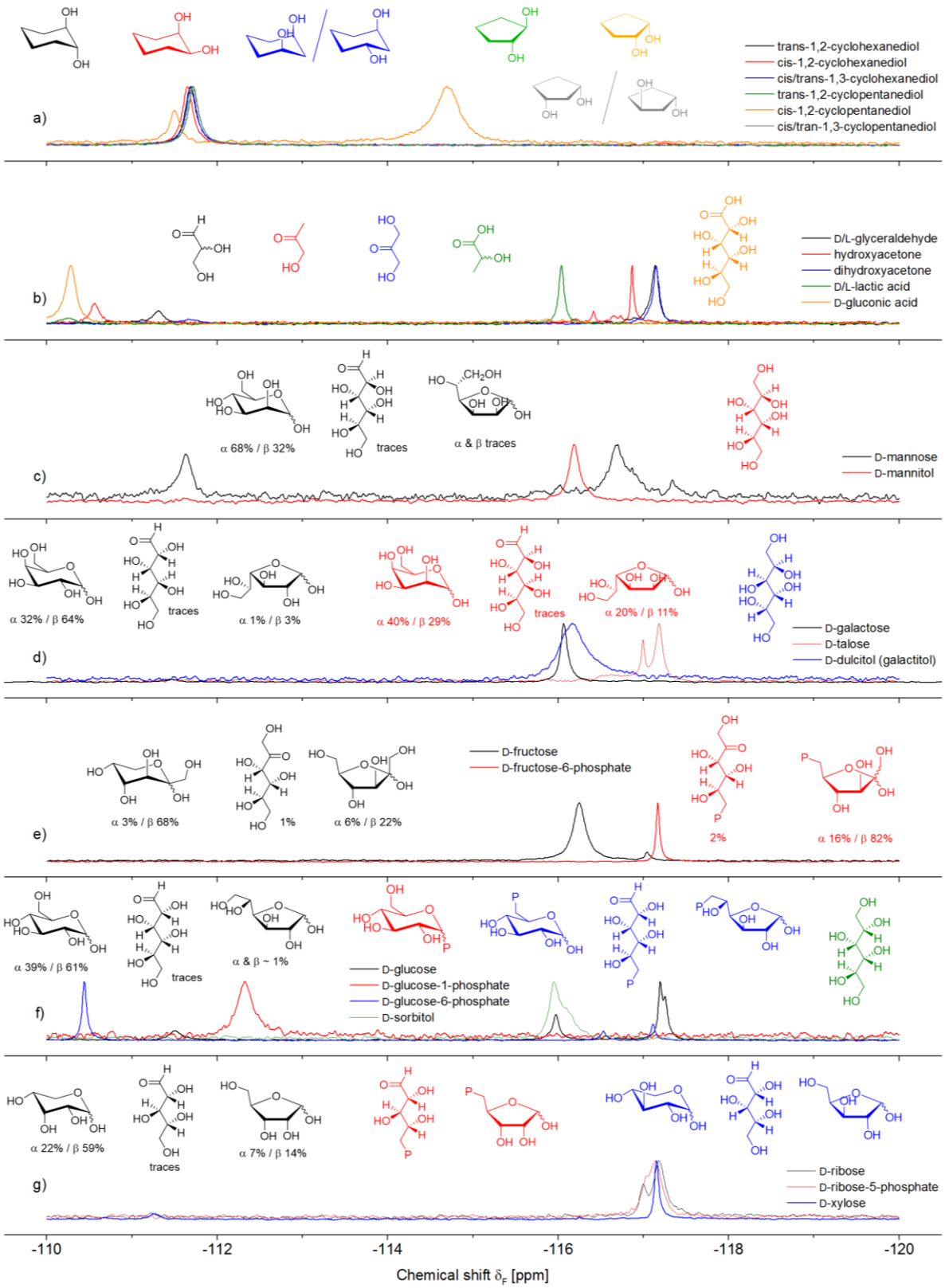

Figure 49: ^{19}F NMR spectra collection of receptor 1 in presence of selected diol derivatives for the elucidation of possible boronic acid-diol binding modes. Possible analyte structures (except the aldo- and ketohydrates of the open-chain isomers). The corresponding isomeric composition under aqueous conditions are shown as well.[174-176] Conditions: receptor 1 (10 mM), diol (100 mM) measured in aqueous HEPES buffer solution (100 mM 10% D_2O, pH 7.4) at 188 MHz, 256 scans and 24°C.

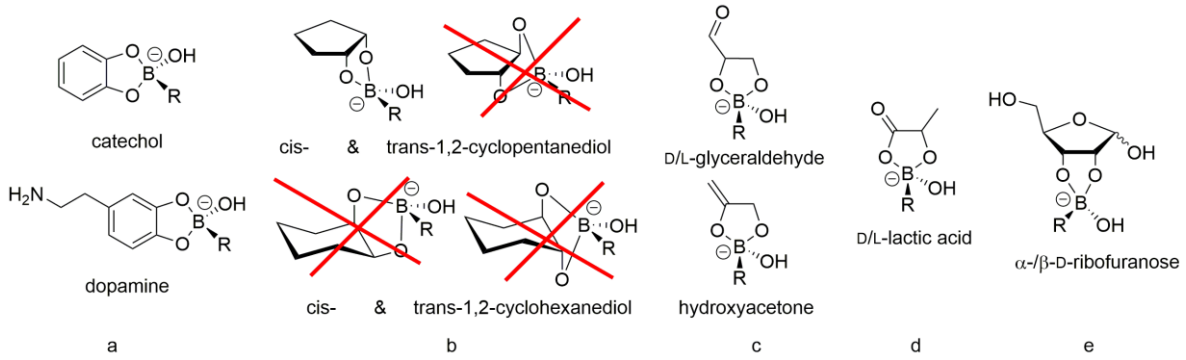

Figure 50: Proposed molecular structures (binding modes) of resulting boronate-diols esters of receptor 1 and selected diol-containing analytes under physiological conditions derived from ^{19}F NMR data and possible considerations with respect to the molecular properties.

Next, the binding behavior of **1** to some simple sugars and hydroxycarboxylic acids was tested as shown in Figure 49b. The simplest possible monosaccharide, D/L-glyceraldehyde and **1**, produce one sharp shift at δ_F –117.14 ppm that is probably associated with the binding of boron to the accessible 1,2 OH groups (see Figure 50c for a proposed molecular structure). Interestingly, the constitutional isomer dihydroxyacetone provides the identical ^{19}F NMR signal although only two isolated 1,3-hydroxy groups are available for esterification. A different but also moderate binding was observed for hydroxyacetone with a main signal at δ_F –116.86 ppm which implies that boron is interacting presumably with a hydroxyl group formed in a keto-enol reaction albeit weak driving force of the latter (see Figure 50c for a proposed molecular structure). This may also be the case for dihydroxyacetone. D/L-lactic acid an exemplary small carboxylic acid shows a strong affinity to **1** with one fluorine shift at δ_F –116.04 ppm. Here, the proposed binding takes places via the free and the carboxylic OH group (proposed structure in Figure 50d). The chain extended D-gluconic acid is producing a very weak signal in the same range although plenty other hydroxyl functions are accessible.

In solution, monosaccharides such as the aldo/keto pentoses and hexoses, respectively, are in a more complex equilibrium due to their manifold possible isomers (exemplary equilibrium of e.g. D-fructose and D-fructose-6-phosphate in Figure 51). From the spectroscopic way of view the obtained affinities (qualitative in the appropriate spectra and the apparent binding constant, see section 4.2.4) of **1** to the tested monosaccharides dramatically differ as well as the resulting ^{19}F fingerprints. D-mannose, an example of an aldohexose (**Figure 49c**) which mainly exists in the pyranose form shows moderate affinity with a few new upcoming signals at around δ_F –117 ppm. Interestingly, the reduced and open ring analog D-mannitol exhibits a much stronger affinity producing only one sharp ^{19}F NMR signal at δ_F –116.19 ppm. With regards to the open

chain form of D-mannitol no other isomers are possible, thus proposed boronate diol ester formation is achieved via the ecliptic cis-1,2 OH groups (synperiplanar by chain rotation and a torsion angle between 0° and ± 30° of the hydroxyl groups).

Improved affinity was found for **1** in presence of D-galactose and D-talose with one shift at δ_F –116.06 ppm and two characteristic shifts at δ_F –117.00 and –117.19 ppm, respectively. Probably, the existence of a moderate portion of the furanose isomer of both compounds is responsible for a good boron-diol interaction at the cis-1,2 OH groups (Figure 49d). Interestingly, the fluorine pattern of D-talose (epimer of D-galactose) is completely different due to the single inversed configuration at C-2. Receptor **1** and the reduced analog with respect to the open ring isomer of D-galactose, D-dulcitol, produce one broad ^{19}F NMR signal at δ_F –116.18 ppm which again indicate preferred affinity to the open chain form (available synperiplanar hydroxyl groups). For a more detailed investigation concerning preferred binding of the open chain form and furanose forms of monosaccharides to boron further spectra were investigated. Figure 49e illustrates the ^{19}F NMR data of receptor **1** in presence of D-fructose and the corresponding 6-phosphate derivative with strong observed receptor saturation for both analytes. Presumably, D-fructose shows a strong affinity (δ_F –116.24 and –117.04 ppm) caused by the high furanose isomer content in solution (pair of synperiplanar OH's in the β-anomer,

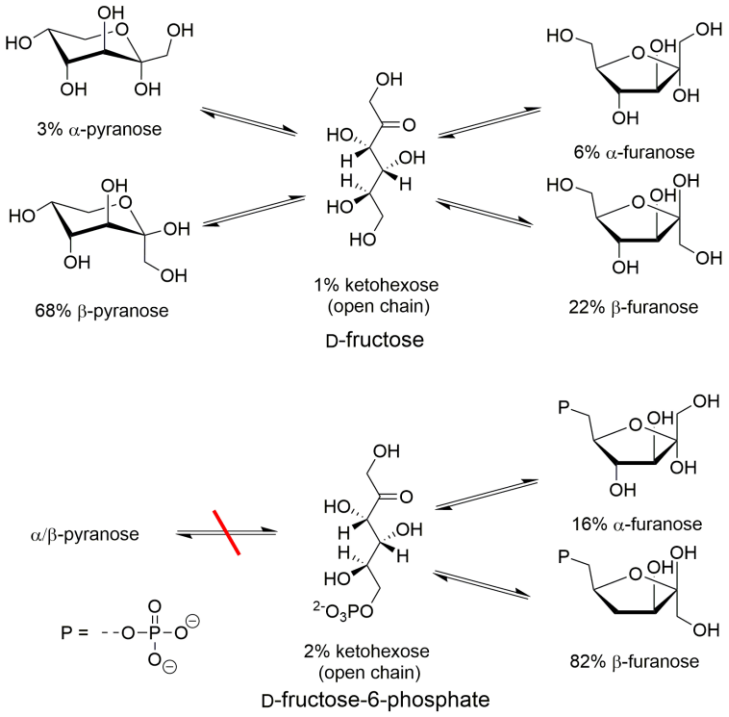

Figure 51: Exemplary equilibrium of the ketohexose D-fructose and the 6-phosphate analog under aqueous conditions with isomeric compositions.[174-176] Possible isomers are the ketohexose open chain form (ketohydrate not shown) and the hemiacetals including the α-/β-pyranose and α-/β-furanose. D-fructose-6-phosphate exists only in the open chain and the α-/β-furanose form due to the phosphate function at C-6.

see also Figure 51). D-fructose-6-phosphate with one remaining and sharp signal at δ_F –117.16 ppm does not allow any pyranose isomers beside the open ring and furanose forms (same pair of cis-1,2 OH's in the β-anomer, see again Figure 51).

The derivatives of D-glucose in Figure 49f lead to the same conclusion. Strictly spoken, D-glucose has a notable portion of both furanose anomers under aqueous condition and provides a good affinity to receptor **1**. D-glucose-1-phosphate is not interacting although four hydroxyl groups of the pyranose species are accessible for boron-diol interaction (possible binding competition to phosphate must be considered, see chapter 4.14). Furthermore, the blocked anomeric carbon atom of D-glucose-1-phosphate avoids the isomerization to the open chain and furanose forms. Weak affinity of **1** was found in presence of D-glucose-6-phosphate, which exists in all possible furanose and pyranose isomers. Strong interaction of **1** to the open-chain sugar alcohol D-sorbitol could be observed. This reduced derivative with respect to the open chain form of D-glucose and D–fructose produces a broad signal at δ_F –115.94 ppm with **1**. This shift overlaps with the signal of receptor **1** and D-glucose and is in the same range as the shift of D-fructose.

The exemplary ^{19}F NMR spectra of the screened aldopentoses in Figure 49g provide further explanation for the open chain and furanose isomers to be suitable binding partners to boron. D-ribose (high content of the furanose isomers) and the corresponding 5-phosphate provide very similar spectra with two shifts at around δ_F –117 and –117.19 ppm. In solution, D-ribose-5-phosphate does not allow any pyranose species and consequently the absent pyranoses do not play any role for binding to receptor **1**. Furthermore, the two at the α-/β-furanose isomers attached cis-1,2 hydroxyl groups are present at both pentose derivatives which should enable boron interaction. The situation changes for chemosensor **1** in presence of D-xylose (inversed configuration at C-3 and epimer of D-ribose) whereat the resulting ^{19}F NMR spectrum is reduced to one single signal at δ_F –117.15 ppm. This observation implies that the remaining ^{19}F shift is corresponding to the assumed binding mode of the cis-1,2 OH groups at C-1 and C-2 of the α-pyranose forms of both diols, respectively (proposed structure in Figure 50e). Hence, a good evidence is given that at least one possible binding mode involves the cis-1,2 hydroxyl groups at C-1 and C-2, and C-2 and C-3 at the α-anomer of D-ribose and D-ribose-6-phosphate, respectively, and the C-1 and C-2 of D-xylose.

With the spectroscopic information recorded via ^{19}F NMR and previously discussed considerations in hand proposed binding modes of the fluorinated receptor **1** to the investigated diols can be qualitatively summarized:

- Moderate boronate-diol binding in presence of simple aldoses, ketoses and hydroxycarboxylic acids such as glyceraldehyde, dihydroxyacetone and lactic acid via synperiplanar 1,2-OH groups
- Evidence for preferred binding modes to the open-chain form of reducing sugars and sugar alcohols due to similar observed affinities and similar ^{19}F NMR shifts in the range of δ_F –116 ppm with receptor **1** for both diol classes
- Indication for no or negligible interaction to the pyranose anomers (no sterical accessible and suitable cis-1,2 or -1,3 OH groups) observed for pyranose-blocked derivatives
- Strong evidence for boron binding to cis-1,2 hydroxyl groups of suitable furanose anomers (especially pentoaldoses) with resulting ^{19}F signals in the range of δ_F –117 ppm

In conclusion, the findings of receptor **1** assisted by sensitive ^{19}F NMR and considerations based on the molecular structure of appropriate diol provide qualitative information with respect to the effective boronate-diol binding modes under physiological conditions. Strong evidence was found for reducing monosaccharides such as D-fructose, D-glucose, D-ribose and similar derivatives to provide boron interaction mainly via the open ring form and/or the α-/β-furanose anomers. Especially suitable cis-1,2 hydroxyl groups with an torsion angle of 0 to 30° (synperiplanar) appearing at the open-chain and furanose isomers seem to be clearly preferred for boron-diol binding. Another evidence for no or very minor interaction of **1** to possible pyranose species is given by the spectroscopic results of the screened analytes and related derivatives. Thus, D-glucose-1-phosphate is only existent in the pyranose anomer and indicates no interaction with **1** whereas D-ribose-5-phosphate is showing strong complex formation although no pyranose anomers are possible. The spectra of receptor **1** and all sugar alcohols (exist only in the open-chain form) produce one single shift in the range of δ_F –116 ppm which is similar to the shifts of D-fructose, D-glucose and D-galactose. This observation indicates possible boron interaction to the open ring forms of monosaccharides as well. Further support for this hypothesis is given by the determined binding constants of D-sorbitol and D-mannitol. Both K_b values are similar compared to e.g. D-fructose (chapter 4.9 and Table 4). Nevertheless, it must be noted that the presented results are in contrast to the assumptions found in the

literature which attribute boron interaction to monosaccharides mainly via hydroxy groups of the β-pyranose and the α-furanose form with negligible affinity to the remaining isomers. As a matter of fact, a change of the monosaccharide tautomeric composition in presence of a boronic acid receptor, which obviously prefers the affinity to the open-ring and/or furanoses of suitable diol, cannot be excluded and needs more detailed investigation. Thus, a combined sensing approach using the described and other sensing techniques for the screening of structurally modified monosaccharides and sugar alcohols should elucidate the real binding modes of appropriate monosaccharide isomers in solution.

ANALYTICAL PERFORMANCE AND LIMITATIONS OF THE ^{19}F NMR SENSING APPROACH

The previous chapters portrayed the versatile sensing possibilities of the approach for diols and mixtures of them. With the NMR sensitive ^{19}F probe(s) attached to the boronic acid receptors and ^{19}F NMR spectroscopy in hand highly characteristic receptor-analyte information were recorded. Compared to common diol sensing approaches such as boronic acid-based fluorescence assays the presented concept is associated with notable advantages and of course some disadvantages which will be briefly discussed in this chapter. Furthermore, important analytical parameters such as the robustness, precision, reproducibility, selectivity, stability, sensitivity, the limit of detection and quantification must be considered. These parameters give evidence for the applicability of the presented approach under given conditions.

From the qualitative point of view the obtained ^{19}F NMR spectra of e.g. receptor **1** and D-fructose provide new appearing and unique fingerprint-like signal information that are characterized by the specific NMR shift and signal intensity corresponding to the formed boronate-diol complexes in solution. Interestingly, the chemical shifts are robust to pH changes in a certain range and do not noticeably vary even by changing analyte concentration. Figure 52a illustrates clearly the reproducibility of the ^{19}F NMR fingerprint of the formed receptor-**1**-D-fructose complexes with resulting shifts at δ_F –116.26 and –117.05 ppm (calculated shift error of 0.0018 and 0.0049 ppm, respectively) with changing D-fructose concentration under the same experimental conditions. The observable integrals of the ^{19}F signals show a strong linear dependency upon increasing concentration of diol (Figure 48 and chapter 4.9) and furthermore provide the quantitative diol sensing feature of the approach.

In contrast, the exemplary and related Singaram-Wessling-type fluorescent (chapter 3.3) responds in a one-dimensional manner to the interacting diol whereas only the relative fluorescence emission of the fluorescence dye is modulated depending on the receptor's affinity to the diol and the present diol concentration. Figure 52b represents this fluorescence-based sensing behavior using receptor **10** and the fluorescence dye HPTS. In absence of D-fructose the fluorescence of the dye is quenched by the receptor/quencher **10** whereas only an increase in fluorescence with increasing amount of D-fructose at the emission maximum of 512 nm can be observed. The fluorescence emission itself provides no information about the quality of the specific diol such as obtained by the unique ^{19}F NMR fingerprint and is furthermore dramatically sensitive to pH changes. The qualitative sensing character of the presented system

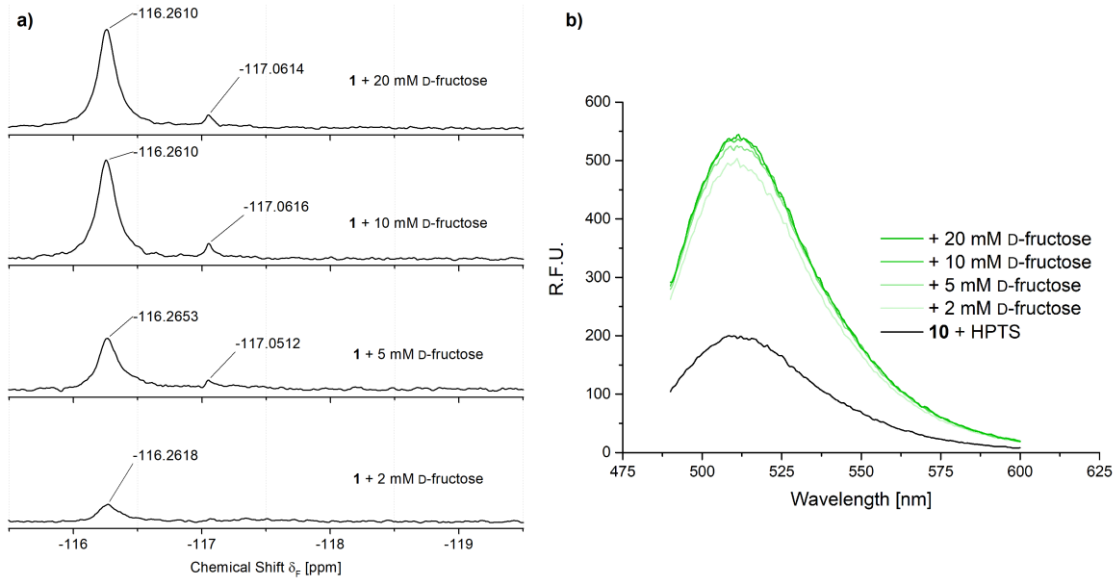

Figure 52: Comparison of the signal response and discrimination power of the presented ^{19}F NMR approach and an exemplary fluorescence assay for diol sensing. a), the new appearing and unique ^{19}F NMR shifts of the formed receptor-1-D-fructose complexes show a strong reproducibility and precision in their chemical shift. Conditions: receptor 1 (10 mM) and D-fructose (2-20 mM) measured in HEPES buffer solution (100 mM, pH 7.4, 10% D_2O) at 188 MHz, 256 scans and 24 °C. b), the one-dimensional fluorescence response (512 nm) arising from the formed receptor-10-D-fructose complexes and the released HPTS dye correlates to the amount of D-fructose whereas no qualitative diol information are accessible. Conditions: receptor 10 (120 µM), HPTS (4 µM) and D-fructose (2-20 mM) measured in HEPES buffer solution (50 mM, pH 7.4) at 24 °C.

becomes more obvious with respect to diol mixtures. A binary mixture containing D-fructose and D-glucose can clearly be discriminated via the characteristic ^{19}F NMR shifts of the formed receptor-**1**-diol complexes (Figure 43). Compared to these findings the exemplary emission spectra of the fluorescence assay illustrated by Figure 53 provide no qualitative information about the diol composition of a binary diol mixture. Thus, a discriminatory task can only be fulfilled by a sensory array associated with complicated and time-consuming chemometric techniques.

The analyte selectivity of the system to selected diols was investigated in several experiments such as the sensing of a diol mixture containing D-fructose and D-glucose, the monitoring of formed D-fructose in an enzymatic reaction and the sensing of D-glucose in complex urine sample. In general, the selectivity of **1** to diols quantifiable via apparent binding constants (Table 4) is in the order catechol >> fructose > sorbitol = mannitol > galactose = glucose. But, due to complex chemistry of single diol as well as diol mixtures taking place at the boron binding site of receptor **1** no absolute analyte selectivity can be predicted in diol mixtures. This observation becomes obvious by the significant higher affinity of **1** to D-fructose

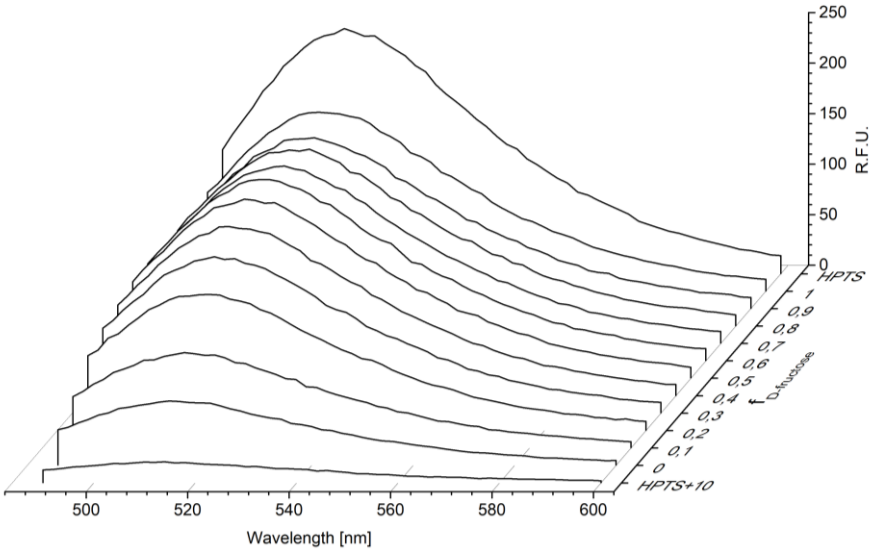

Figure 53: Exemplary and non-selective fluorescence response of the Singaram-Wessling-type assay using HPTS dye and receptor/quencher 10 for sensing of a binary diol mixture. The one-dimensional modulation of the fluorescence emission (512 nm) induced by changing fraction of D-fructose and D-glucose provides no information about the quality of the diols. Conditions: receptor 10 (120 µM), HPTS (4 µM), D-fructose (0-5 mM) and D-fructose (5-0 mM) measured in HEPES buffer solution (50 mM, pH 7.4) at 24°C.

(1616 M^{-1}) compared to D-glucose (132 M^{-1}) whereas a mixture of both diols still shows a detectable ^{19}F fingerprint of D-glucose even in a ten-fold excess of D-fructose (Figure 43). In the case of non-interfering environments such as a complex urine matrix or D-glucose-1-phosphate in an enzyme reaction high selectivity of **1** to D-glucose and D-fructose, respectively, was observed with no interfering signal at all. Thus, the selectivity of the ^{19}F NMR sensing system to a specific diol is dependent on the content of potentially interfering diols/contaminants, the preferred isomers of diol in solution and needs to be specifically established for every sensory problem.

As mentioned earlier (chapter 3.6) the signal intensity of an NMR-based sensing concept is mainly dependent on the applied magnetic field strength (NMR signal is proportional to the difference of the population numbers of the spin states) of the NMR machine, furthermore to the natural abundance of the nucleus (100% for ^{19}F) and the amount of equivalent ^{19}F probes at the receptor molecule. Other hard- and software parameters (probe head, scan numbers etc.) of the NMR setup are contributing aspects for the realization of good signal to noise ratios (S/N) and low values for the limit of detection (LOD) and quantification (LOQ). Consequently, the dependency of the applied magnetic field strength and the number of scans on the S/N were studied and are illustrated by Figure 54.

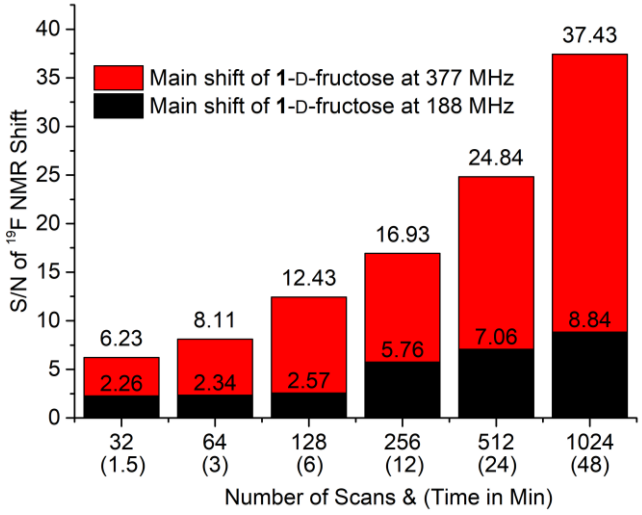

Figure 54: Dependency of the used NMR setup on the S/N of the resulting ^{19}F shifts of the formed receptor 1-D-fructose complexes (main signal at δ_F –116 ppm). Samples were recorded on two different NMR machines (188 and 377 MHz) and at different scan numbers. Conditions: receptor 1 (10 mM) and D-fructose (1 mM) measured in HEPES buffer solution (100 mM, pH 7.4, 10% D_2O) at 25°C.

In detail, ^{19}F NMR spectra of a NMR sample containing receptor **1** (10 mM) and D-fructose (1 mM) were recorded at two different NMR machines with a field strength of 188 and 377 MHz, respectively. The resulting S/N of the main signal at δ_F –116.26 ppm of the formed receptor **1**-D-fructose was calculated from each spectrum. Clearly visible is the tremendous signal intensity increase when the magnetic field strength is doubled from 188 (AVANCE I 200 MHz) to 377 MHz (AVANCE III 400 MHz) resulting in an average three-fold higher S/N value. The influence of the increase in the scan number upon the S/N was found to be minor for the measurements at 188 MHz whereas a strong improvement of ^{19}F NMR signals intensities was achieved with the new setup at 377 MHz. A suitable S/N value of a characteristic receptor-diol signal should be around 2 and 5 to allow a decision if the diol is present (LOD - yes/no decision) and for safe diol quantification (LOD), respectively. Due to the unique property of each ^{19}F NMR spectrum the specific thresholds for the LOD and LOQ must be determined individually via the signal of interest and the noise area.

The thresholds for the limit of detection and quantification were determined for the following setup: receptor **1** (10 mM) in presence of D-fructose (1 mM), D-glucose (1 mM) and catechol (100 and 400 µM),respectively, measured in HEPES buffer solution (100 mM, pH 7.4, 10% D_2O) at a magnetic field strength of 188 MHz and 256 scans (Figure 55 LOD and LOQ shown as threshold, respectively). The Individual values for the LOD and LOQ of each spectrum were

calculated using Equation 18 and were found to be in the lower millimolar range for D-fructose and D-glucose (LOD ≪ 1 mM both, LOQ ≤ 1 and ≪1 mM, respectively) and in the micromolar range for catechol (LOD ≤ 100 µM, LOQ ≤ 400 µM) with respect to the main ^{19}F NMR shift of appropriate receptor-**1**-diol complex. Especially, receptor-diol interactions which exist only in one single species associated with one small line width of the corresponding ^{19}F signal such as found for **1** and catechol profit from very low LOD and LOQ values. The detection limits of diols such as D-fructose and D-glucose are usually higher due to the more complex receptor-diol interactions with numerous possible boronate-diol species in solution and ^{19}F signal broadening behavior.

In summary, the presented one-component sensing approach comprising a fluorinated boronic acid receptor such as the simple and robust receptor **1** assisted by ^{19}F NMR spectroscopy

$$\text{Limit} = y_{blind} + x \cdot s_{blind}\text{; for LOD } (x = 3) \text{ and LOQ } (x = 9) \quad \text{(Equ. 18)}$$

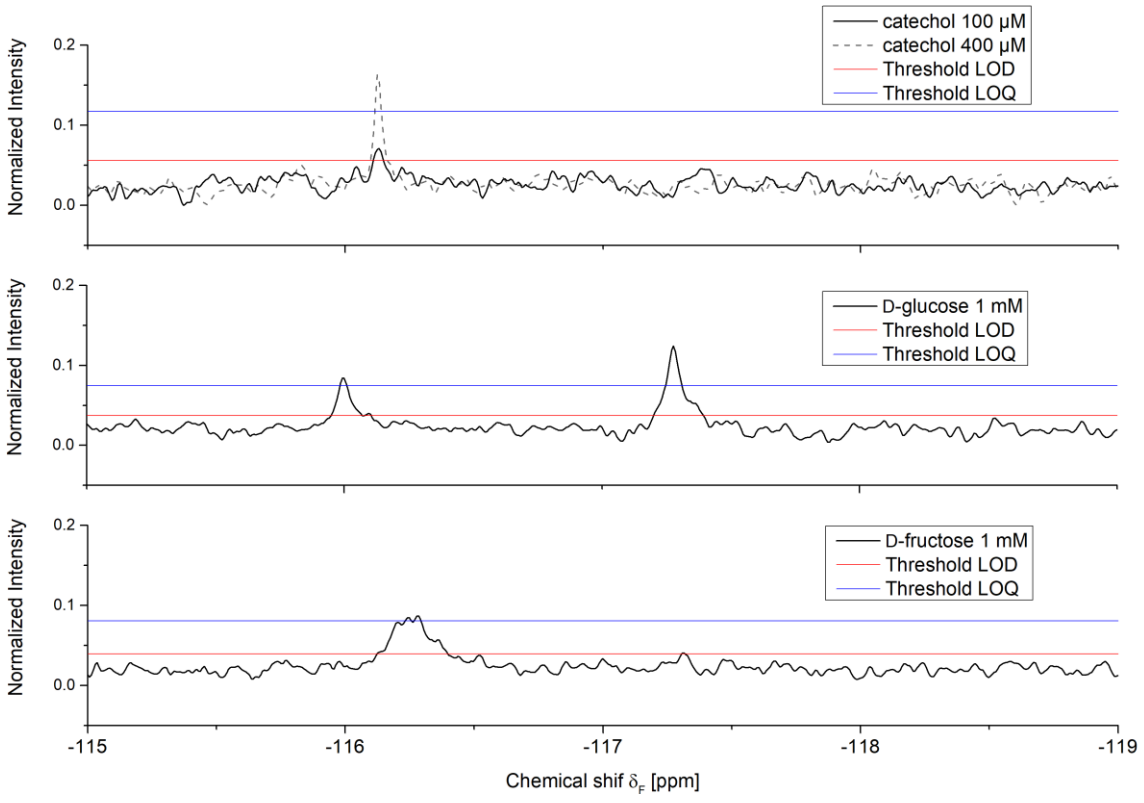

Figure 55: The limit of detection (LOD) and quantification (LOQ) of 1 illustrated as thresholds in the individual ^{19}F NMR spectra of 1 in presence of D-fructose, D-glucose and catechol, respectively. The selected sensing setups enable LOD values (analyte yes/no decision) and LOQ values (minimum quantification values) in the micromolar range for catechol and lower millimolar range for D-fructose and D-glucose. Conditions: receptor 1 (10 mM) and appropriate diol measured in aqueous HEPES buffer solution (100 mM, pH 7.4, 10% D_2O) at 188 MHz, 256 scans and 25°C.

provide distinct advantages with respect to the qualitative recognition of diol analytes. The highly characteristic and robust ^{19}F fingerprints enable the unambiguous identification of diol under physiological conditions and in a wide pH range without qualitative false interpretation. Resulting from the well separated ^{19}F shifts of distinct receptor-diol complexes and the absent fluorine background the present method could be successfully used for the qualitative component analysis of binary and ternary diol mixtures even for D-fructose and D-glucose mixtures in which one component is present in high excess. Strong affinities were observed for well preorganized diols whereas the approach is robust to contaminants and the buffer medium. Quantitative sensing tasks using the changing integrals of appropriate ^{19}F signals which correlate in a strict linear manner to the present analyte concentration could be performed in complex media and an enzyme catalyzed reaction such as well. The signal calibration can be realized via an external TFA reference or the use of the inherent and known total fluorine content of the used receptor. The intensities of the recorded fluorine signals and thus the associated S/N values are highly dependent on the applied magnetic field strength and the scan number. Thus, well-equipped and unfortunately expensive NMR setups are highly desired for the reduction of the LOD and LOQ.

An overview of important experimental and analytical parameters of the presented ^{19}F NMR sensing concept compared to the related Singaram-Wessling-type fluorescence assay with regards to general sensing aspects are summarized in Table 5.

Table 5: Important aspects of the presented method using fluorinated receptor 1 assisted by ^{19}F NMR spectroscopy compared to the related Singaram-Wessling-type fluorescence assay for diol sensing tasks.

	Presented ^{19}F NMR method	Singaram-Wessling-type fluorescence assay
Molecular setup	One-component (^{19}F receptor)	Two-component (dye + quencher)
Experimental setup	Expensive NMR spectrometer	Inexpensive fluorescence spectrometer
Experiment duration	Slow, minutes up to hours	Very fast, seconds up to minutes
Diol signal	Unique ^{19}F NMR fingerprint	One-dimensional fluorescence response only
Diol selectivity	Suitable for single diol in presence of non-interfering compounds/matrices	
Diol discrimination	Very strong, via ^{19}F fingerprints	Weak, array + chemometric techniques needed
Discrimination of diol mixtures	Strong, via ^{19}F fingerprints, even in excess of one component	Not applicable due to superimposed fluorescence response
Diol quantification	Strong, by using a suitable calibration	
Calibration reference	Internal (receptor itself) or external (TFA) standard	Fluorescence response relative to quenched system (Blank)
pH sensitivity	Robust to pH changes from ~ 7 and above	Strict pH regulation needed due to pH-sensitive fluorescence dye
Stability	Strong, no light sensitivity	Moderate, BBV quencher are highly light sensitive, dye can bleach out
Water solubility	Very high up to ~ 80 mM for **1**	Limited by quencher < 5 mM (BBV)
Background/interfering signals	No natural ^{19}F background	Usually no fluorescent background
Limit of detection	Millimolar to micromolar range dependent on NMR setup	Down to the nanomolar range

ENHANCED SENSING APPLICATIONS USING THE ^{19}F NMR TECHNIQUE

The previously presented approach using fluorinated boronic acid-appended receptors assisted by the sensitive ^{19}F NMR spectroscopy for qualitative and quantitative diol sensing in simple matrices can be further developed by enhanced sensing tasks. In general, reversible as well as irreversible reactions, which take place at the boronic acid functi on can be followed up as long as the attached fluorine(s) probe can experience the chemical/structural change of the receptor molecule. Thus, the detection and quantification of diol producing/consuming enzyme catalyzed reactions and simple Lewis acid-base adducts as known from anion-boron interactions are further interesting sensing applications.

MONITORING OF ENZYME CATALYZED REACTIONS

Enzyme catalyzed reactions play an essential and extensive role in numerous metabolic processes and enable an energy efficient way for the composition/decomposition of complex bio molecules such as amino acids, the hydrolysis of fat and proteins, and the saccharification of starch-containing fruits. Enzymes are categorized in six classes whereas especially enzyme oxidases and transferases catalyze many reactions which consume saccharide substrates.

A prominent example in modern glucose test kits is the enzyme glucose oxidase (GOx) which originates from several insects/fungi and furthermore serve as a protection agent. The latter feature can be explained when having a look on the general reaction equation in which the substrate β-D-glucose in presence of oxygen is oxidized at the C1-carbon atom to D-gluconic δ-lactone and hydrogen peroxide. The latter compound is a so called reactive oxidative species (ROS) and is harmful to bacteria. The formed H_2O_2 content is important for the quantitative detection of glucose in clinical blood or urine samples via a coupled electrochemical reaction.[177]

Beyond that, the conversion of saccharides to similar derivatives via enzyme catalysis can also be addressed by the presented approach using a fluorinated boronic acid-appended receptor assisted by ^{19}F NMR spectroscopy. Especially the high selectivity and discrimination power in terms of diol analytes, the signal robustness of the ^{19}F NMR shifts to pH changes and interfering contaminants of the system allow the detection of interacting diol species that are consumed/produced or transferred by a suitable enzyme. Consequently, enzyme reactions can

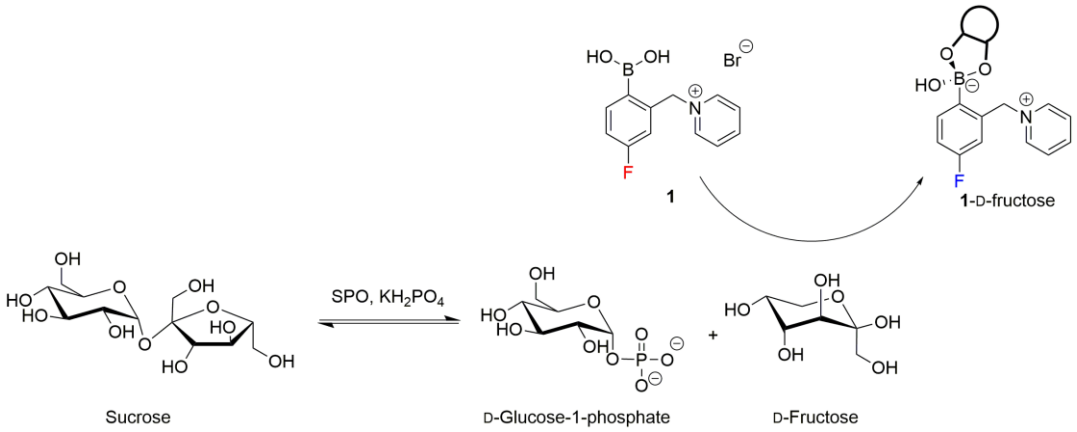

Figure 56: Reaction scheme of the glucosyltransferase sucrose phosphorylase (SPO) in presence of sucrose substrate and phosphate producing one equivalent D-fructose and D-glucose-1-phosphate. D-fructose can be selectively and quantitatively monitored beside all other components via receptor 1 assisted by ^{19}F NMR spectroscopy. Conditions: receptor 1 (10 mM), sucrose (5-40 mM), KH_2PO_4 (40 mM) and SPO (0.5 U) measured in aqueous HEPES buffer (100 mM, pH 7.4, 10% D_2O) at 188 MHz, 128 scans and 24 °C.

be indirectly monitored using the ^{19}F NMR technique to get information about the diol consumption/production, enzyme kinetics and activities.

To proof the potential of the ^{19}F NMR approach used as a sensing tool for enzyme catalyzed reactions, the enzyme sucrose phosphorylase (SPO) and the substrate sucrose were selected and screened with the established setup of receptor **1** assisted by ^{19}F NMR spectroscopy. Sucrose phosphorylase, a glucosyltransferase expressed from *Escherichia coli* transfers sucrose in presence of phosphate to one equivalent D-fructose and *α*-D-glucose-1-phosphate, respectively, as represented by Figure 56. As previously mentioned, D-fructose can be easily detected by receptor **1** whereas the starting substrate sucrose and the formed byproduct D-glucose-1-phosphate are showing no characteristic ^{19}F pattern with **1** (Chapter 4.6). Hence, the growth of D-fructose concentration can be conveniently followed up via the characteristic shifts of the formed receptor-**1**-D-fructose species.

In practice, samples for ^{19}F NMR assisted enzyme monitoring containing SPO (0.5 U), KH_2PO_4 (40 mM), sucrose (5-40 mM) and receptor **1** (10 mM) in HEPES buffer solution (100 mM, pH 7.4, 10% D_2O) were prepared and measured at 188 MHz, 128 scans (acquisition time of ~6 min) at 24°C. A coaxial NMR insert filled with an aqueous TFA (100 mM) solution was used as the fluorine reference signal. The spectroscopic data at t_0 was acquired by measuring the reaction mixture in absence of SPO enzyme. Figure 57 exemplary illustrates the normalized and time resolved (0-54 min) ^{19}F NMR spectra of the sensing setup in presence of 40 mM sucrose substrate and the new appearing and typical D-fructose main signal at δ_F –116.23 ppm. Unbound

1 and the TFA reference signal are represented by the shift at δ_F –110.88 and δ_F –75.91 ppm, respectively. The inset of Figure 57 shows the evolvement of formed receptor-**1**- D-fructose complex dependent upon the sucrose substrate concentration. Quantitative values of D-fructose production by the SPO enzyme were calculated using a previously recorded calibration curve (40 mM sucrose, 40 mM KH_2PO_4, 0-20 mM D-glucose-1-phosphate and 0-20 mM D-fructose in 100 mM HEPES buffer, pH 7.4, 10% D_2O, 188 MHz, 256 scans and 24°C) as illustrated by Figure 58. Fortunately, the receptor-**1**-D-fructose complex formation follows a strict linear dependency for increasing D-fructose concentrations in the range of 0-10 mM. This observation highlights the ^{19}F NMR method as a selective and quantitative sensing tool for D-fructose formation in an SPO enzyme catalyzed reaction. Furthermore, the quantification of D-fructose in a time-dependent manner was used to determine the activity of SPO under the described conditions. The initial rates of turnover for D-fructose in µMol/min of each monitored enzyme reaction with appropriate substrate concentration (5-40 mM) was calculated using the D-fructose calibration curve achieved from the data fitting illustrated by Figure 58. A Michaelis-Menten plot representing the initial rate of turnover versus the substrate concentration and a double reciprocal plot (Lineweaver-Burk) were used for the calculation of the enzyme activity. Both methods are illustrated by Figure 59 and provide a value of 0.18 µMol/min for the maximal reaction rate and a specific activity of 45 µMol/min/mg (U/mg) which is slightly under the enzyme activity given by the producer (57 U/mg). One reason might be the diminished activity due to storage of the enzyme stock solutions in the freezer, enzyme degradation, the lower reaction temperature used and possible enzyme inhibition induced by receptor 1.[178] The substrate concentration at the half maximal reaction rate K_m (Michaelis-Menten constant) which provides an indication for the affinity of the enzyme was calculated with an value of 5.9 mM. This value is in accordance with the K_m data of SPO enzymes found in the literature (K_m = 3-21.12 mM). All determined kinetic values and experimental conditions are furthermore listed in Table 6.

Overall, it could be shown that the presented fluorinated boronic acid-appended receptor **1** assisted by ^{19}F NMR spectroscopy is a suitable method for monitoring the devolution of an exemplary enzyme reaction by the selective detection and quantification of the D-fructose byproduct. An established calibration curve of the increasing D-fructose under identical experimental conditions enabled the determination of the rates of turnover and consequently important kinetic values such as the Michaelis-Menten constant and the enzyme activity in an SPO catalyzed enzyme setup. The obtained spectroscopic data exhibit a poor time-resolution

(~ 6 min) which represents only the average values of the formed saccharide each 128 scans. Other enzyme assays use e.g. the coenzyme NAD^+/NADH with an associated change in UV/vis absorption or fluorescent reporter molecules that provide a snapshots-like response of the current reaction process.[103, 179-180] Consequently, the kinetic data obtained by the ^{19}F NMR are defective and the accuracy of the results have to be treated with caution. The applied magnetic field strength and the selected scan numbers are a compromise of moderate S/N values and relatively short acquisition times for the follow up of the enzyme reaction.

Nevertheless, it could be shown for the first time that a fluorinated boronic acid receptor assisted by ^{19}F NMR spectroscopy can be used for the monitoring of an enzyme-catalyzed reaction via the selective detection and quantification of an enzyme originated diol byproduct.

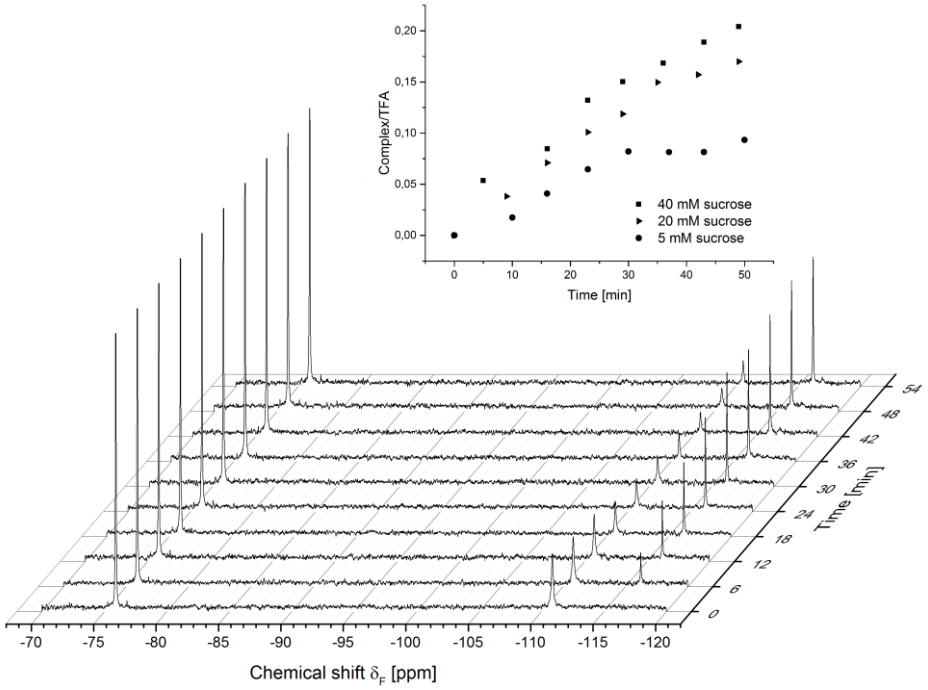

Figure 57: Selective monitoring of upcoming ^{19}F NMR receptor-1-D-fructose signals in an exemplary enzyme catalyzed reaction using the enzyme sucrose phosphorylase, KH_2PO_4 and sucrose substrate. Characteristic signals of D-fructose complex (δ_F -116.23 ppm), unbound 1 (δ_F -110.88 ppm) and TFA reference signal (δ_F -75.91 ppm) can be clearly distinguished. Inset: dependency of complex formation upon the used substrate concentration. Conditions: receptor 1 (10 mM), sucrose substrate (5-40 mM), KH_2PO_4 (40 mM) and SPO (0.5 U) measured in aqueous HEPES buffer (100 mM, pH 7.4, 10% D_2O) at 188 MHz, 128 scans and 24 °C.

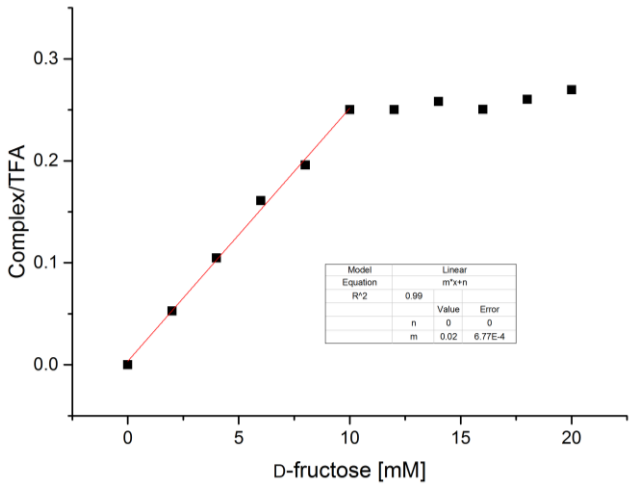

Figure 58: Calibration curve for the quantitative detection of D-fructose (initial rates of turnover) produced in a hypothetical enzyme setup by the enzyme sucrose phosphorylase, sucrose substrate and KH_2PO. A strict linear correlation of the integral evolvement versus increasing D-fructose concentration was observed until saturation of receptor 1. Conditions: receptor 1 (10 mM), sucrose substrate (40 mM), KH_2PO_4 (40 mM), D-glucose-1-phosphate (0-20 mM) and D-fructose (0-20 mM) measured in aqueous HEPES buffer (100 mM, pH 7.4, 10% D_2O) at 188 MHz, 128 scans and 24 °C.

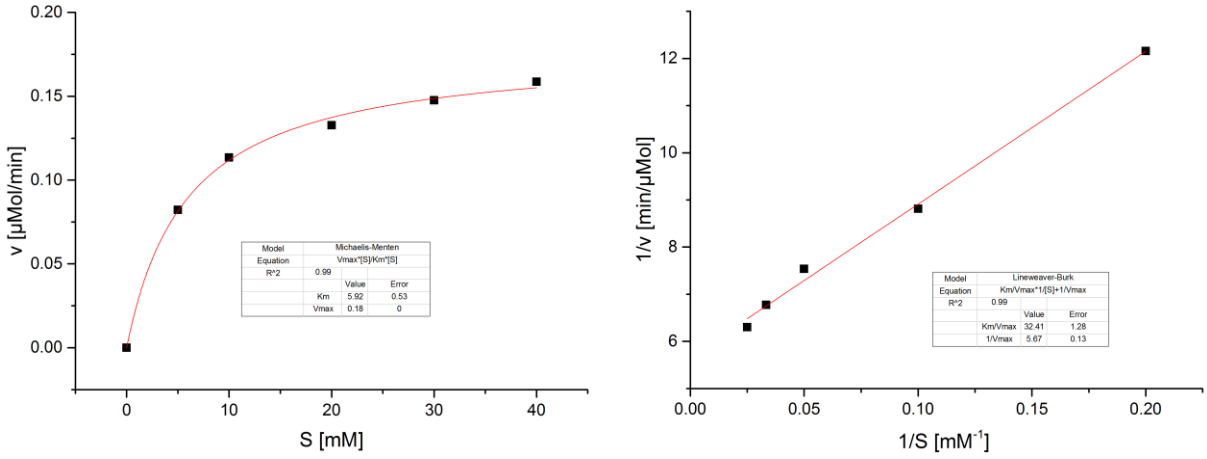

Figure 59: Left, Michaelis-Menten relationship showing the rate of turnover v versus the substrate concentration S in a saturation manner of the enzyme reaction. Right, the linear Lineweaver-Burk diagram illustrates the inversed rate of turnover 1/v versus the inversed substrate concentration 1/S. Apparent kinetic parameters were obtained by fitting with the appropriate equation such as the maximum turnover rate v_{max} (enzyme activity) and the Michaelis-Menten constant K_m which provides an indication for the enzyme affinity.

Table 6: Experimentally kinetic parameters of the enzyme sucrose phosphorylase (SPO) obtained from the described sensing approach using receptor 1 assisted by ^{19}F NMR spectroscopy. For comparison, the kinetic parameters and experimental conditions of selected work found in the literature are listed as well. [a]Specific activity of the enzyme at pH 7.6 and 25°C given by the producer.

Author	Specific Activity [U/mg]	K_M [mM]	Experimental Conditions
Present work	45; 57[a]	5.9±0.5	pH 7.4, 24°C, from *Leuconostoc ssp.*
Goedl *et. al.*[181]	48-190	5.7±0.3	pH 7.0, 30°C, from *Leuconostoc* mesenteroides
Aerts *et. al.*[182]	n.a.	18±2	pH 6.5, 53°C, from *Streptococcus mutans*
Vilozny *et. al.*[103]	n.a.	8.7±1.9	pH 7.4, 22°C, expressed in *E. coli*

QUALITATIVE & QUANTITATIVE SENSING OF INORGANIC ANIONS

Within the field of analyte sensing the unambiguous detection and discrimination of inorganic anions in aqueous systems is of high importance as they play a fundamental role in a crucial number of chemical and biological processes.[183] Furthermore, the probing and monitoring of environmental pollution produced and released especially by industrial processes, agriculture and mining is of critical interest. For example, gold mining facilities produce a massive amount of waste water which is contaminated with highly poisonous cyanide.[54] Aside, other anionic contaminants which endanger our water systems such as nitrate, fluoride and phosphates have to be taken into account.[7-8, 184-185] Phosphates play an important role regarding eutrophication of the aquatic ecosystem. Unfortunately, it is a great difficulty to achieve the specific detection and discrimination of these anions in pure aqueous medium due to similar solvation energies.[186] Consequently, reliable and highly selective chemosensors are desired which can detect the anion of interest even beside otherwise interfering compounds combined with high sensitivities and the in the practical analyte concentration range.

Due to boron's relatively weak Lewis acidic character the binding of hard anions such as cyanide and fluoride must be considered with regards of boronic acid-based receptors as a potential anion sensing tool.[187] Common sensing approaches use optical property changes such as UV/vis, fluorescence and phosphorescence. Nevertheless, other techniques, which respond to chemical property changes of the receptor molecule such as ^{19}F NMR spectroscopy, have evolved in the last years to be a valuable sensing tool. The high sensitivity of an attached ^{19}F probe at a boronic acid receptor allows the detection of certain anions as well. Hence, the slightly modified receptor 5-F-o-BBBpy (**7**) compared to the related receptor **1** was chosen for this sensing task. Receptor **7**, a boronic acid-appended bromopyridinium salt, exhibits the same properties and a slightly improved water solubility due to inductive effects of the attached bromine atom. As mentioned earlier **7** has an attached ^{19}F fluorine probe in *para* position to boron which provides superior sensing properties as also found for diol sensing via compound **1**. As also seen for diol complexation, inorganic anions interact with boron and induce a hybridization change of the latter from trigonal sp^2 to tetrahedral sp^3. Subsequently, this event can be recognized by the ^{19}F probe. The associated boronic acid-anion sensing principle assisted by ^{19}F NMR spectroscopy is shown in Figure 60. Under physiological conditions and in absence of anion the probe of unbound **7** produce one signal at δ_F –111.88 ppm which represents the boronic acid-boronate equilibrium (red spectrum on the left side, Figure 60). In presence of a

Lewis basic anion such as cyanide, the original signal of **7** becomes considerably shifted to δ_F –113.54 ppm (blue spectrum on the right side). This shifting in the fluorine NMR spectrum is dependent upon (i) the anion species present with its associated affinity (basicity) and (ii) upon the underlying anion concentration (equilibrium). Compared to the observations of diol sensing via ^{19}F NMR, the resulting ^{19}F NMR shifts reflect the equilibria taking place in solution (Figure 60, top) and are fast on the NMR timescale. Consequently, the observable ^{19}F shift is the averaged signal of the following species/interactions of **7** in solution: the free boronic acid, boronate, boron-anion adduct and ionic interaction between the pyridinium moiety and surrounding anion.

With the discussed receptor and sensing property in hand **7** was used to screen a pool of twelve common inorganic anions. This task was followd up to check the anion discrimination capacity by expected shift differences enabled by the high sensitivity of the attached ^{19}F probe.

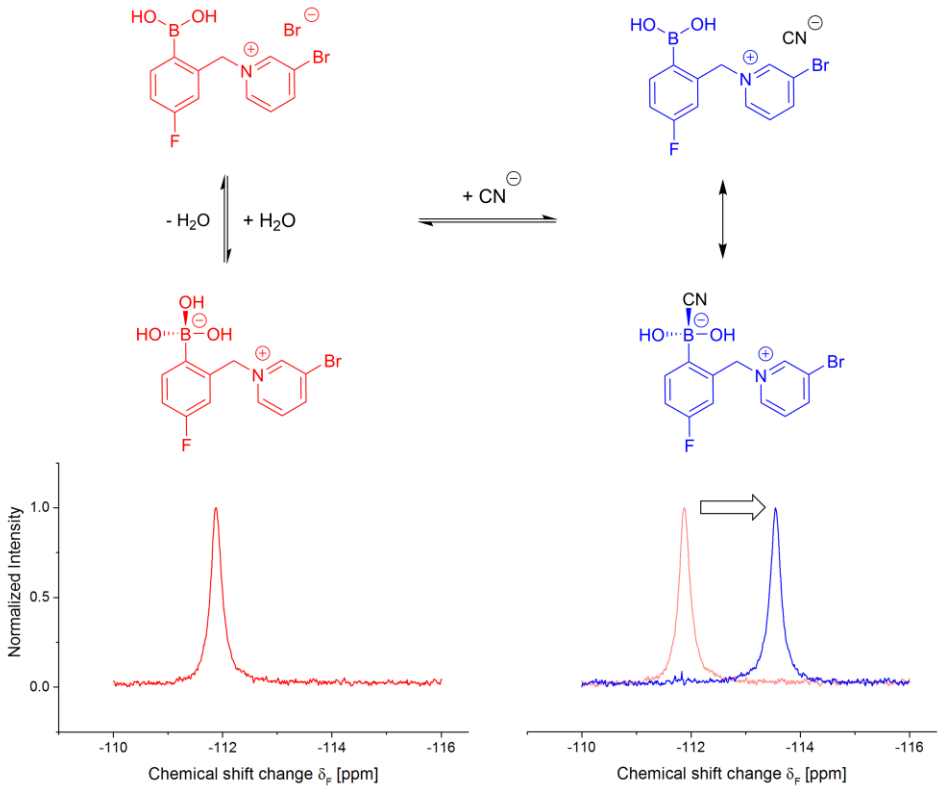

Figure 60: Exemplary equilibrium and corresponding ^{19}F NMR spectra of receptor 7 and in presence of the hard cyanide anion. The ^{19}F probe indicates a single shift at δF -111.88 ppm representing unbound 7 and the corresponding boronic acid-boronate equilibrium (red). In presence of positively interacting cyanide anion the ^{19}F signal is shifted to negative ppm value (blue). Conditions: receptor 7 (5 mM) and cyanide (25 mM) measured in HEPES buffer (100 mM, pH 7.4, 10% D_2O) at 377 MHz, 256 scans and 25°C.

In detail, single ^{19}F NMR anion screening experiments were performed using sensor **7** (5 mM) in presence of appropriate anion (25 mM). All NMR spectra were recorded in aqueous HEPES buffer solution (100 mM, pH 7.4, 10% D_2O) at 377 MHz, 256 scans and 25°C. The resulting shifts of the original spectra are illustrated by Figure 61a (unbound **7** and **7** in presence of cyanide, fluoride and phosphate only). A bar diagram of all screened anions was processed by using the shift change $\Delta\delta_F$ relative to unbound **7** (-111.88 ppm, intuitively set to 0 ppm) as shown in Figure 61b. Obviously, cyanide ($\Delta\delta_F$ –1.63 ppm), fluoride ($\Delta\delta_F$ –0.65 ppm) and phosphate ($\Delta\delta_F$ +0.90 ppm) produced the strongest ^{19}F shifting with respect to the signal of unbound **7**. Unfortunately, the remaining nine anions showed no significant shift changes (Figure 61b and appendix).

As a first result, cyanide, fluoride and phosphate can be exclusively identified and discriminated among all other screened anions due to the discriminative ^{19}F shifts, respectively. Certainly, detection and discrimination power of fluoride is widened by the characteristic ^{19}F shift of free fluoride at ~ δ_F -119.5 ppm. Quite unusually, only phosphate produce a strong fluorine shift at more positive ppm value with respect to unbound **7**. Probably this is a result of possible boron-hydrogen--phosphate interaction induced by the proton donor capacity (Brønsted acid) of the boronic acid group (proposed molecular structure of the receptor 7 phosphate adduct in Figure 61). This instance could be observed before also for receptor **1** and interacting phosphorylated diols and nucleosides which shift the original ^{19}F signal of unbound **1** to more negative ppm

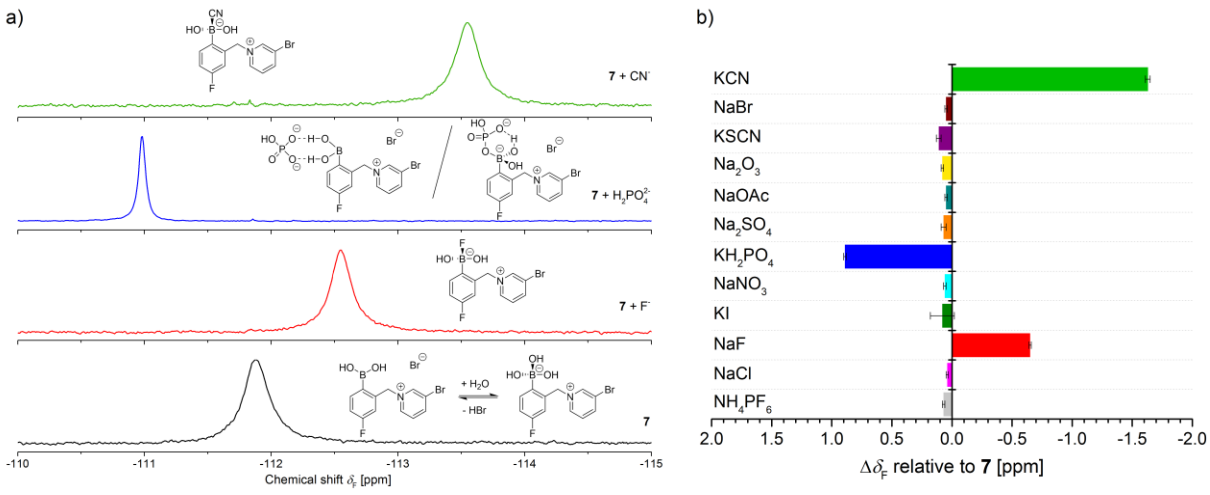

Figure 61: a) Recorded ^{19}F NMR spectra of receptor 7 and in presence of fluoride, phosphate and cyanide and proposed molecular structures. b) Bar diagram highlighting the discriminative ^{19}F shift change $\Delta\delta_F$ of complexed anion relative to unbound 7. Conditions: receptor 7 (5 mM) and appropriate anion (25 mM) recorded (n = 3) in HEPES buffer solution (100 mM, pH 7.4, 10% D_2O) at 377 MHz, 256 scans and 25°C.

values. On the contrary cyanide resulted in an outstanding shift with inverted direction which is due to its strong Lewis basic character forming the tetrahedral cyanide-boronate complex. Overall, the resulting pattern allow the discrimination of cyanide, fluoride and phosphate with respect to the nine other screened anions by simple ^{19}F shift changes using the fluorinated receptor **7** at the identical experimental conditions.

Next, Job plot experiments have been performed to elucidate the binding stoichiometry of **7** to the strong-shifting anions. ^{19}F NMR titration experiments were conducted using receptor **7** (2-20 mM) fluoride, phosphate and cyanide (18-0 mM), respectively, with fixed total concentrations of 20 mM of both components. Figure 62 illustrates the shift change recorded versus the mole fraction *f* of receptor **7**. A maximum shift change of the plotted data of all three tested anions versus the receptor at $f = 0.5$ clearly indicates a strict 1:1 binding behavior of all three analytes to the boronic acid function.

The confirmed 1:1 binding model for anion interaction of receptor **7** was used for the determination of apparent binding constants K_b of fluoride, phosphate and cyanide. For this purpose, receptor **7** (2 mM) was titrated with cyanide, fluoride and phosphate (0-200 mM), respectively. Titration isotherms were achieved by plotting the resulting chemical shift change $\Delta\delta_F$ versus the anion concentration. Subsequent data fitting using equation 19 for the 1:1 model offered the apparent K_b values (Figure 63a)[188]. The trend of affinity of **7** to the anions was found to be in the following order: phosphate (K_b = 73 M^{-1}) >> fluoride (K_b = 14 M^{-1}) > cyanide (K_b

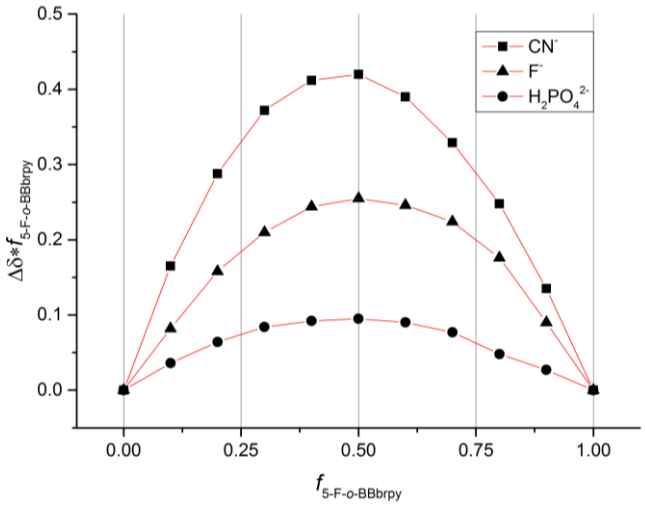

Figure 62: Job plot of receptor 7 (2-20 mM) in presence of cyanide, fluoride and phosphate anion (0-18 mM each) plotted as the shift change versus mole fraction. Conditions: HEPES buffer (100 mM, pH 7.4, 10% D_2O, 377 MHz and 256 scans).

$$\Delta\delta_F = \frac{\Delta_{max} \cdot K_b \cdot [Anion]}{1 + K_b \cdot [Anion]} \quad \text{(Equ. 19)}$$

= 7 M^{-1}) which is in contrary to the strength in ^{19}F shifting of appropriate anion but in agreement with respect to expectations given by the HASAB concept. The boronic acid moiety is a hard acid, fluoride and phosphate are hard bases, whereas the ambident cyanide can be attributed as a soft base. Consequently, higher binding constants are expected for the adducts of **7** in presence of either phosphate and fluoride compared to a weaker adduct of **7** and cyanide. The significant higher K_b value of phosphate can be explained by the inherent higher solvation energy and presumably a possible chelating effect as shown in Figure 61a. Overall, a significant preference of phosphate, fluoride and cyanide over the residue anions could be observed and highlight the presented approach as a discriminative anion sensing tool.

The limit of detection (LOD) and the limit of quantification (LOQ) was determined which specifies the sensing performance of the presented system under given conditions. The following parameters for the LOD and LOQ have were calculated at 377 MHz, 256 scans and by processing the recorded chemical shift changes: LOD/LOQ ≤ 2.6/≤ 26; ≤ 19/19 and ≤ 19/≤ 19 ppm for cyanide, fluoride and phosphate, respectively.

Due to the distinct ^{19}F shift changes of receptor **7** and its exclusive selectivity to cyanide, fluoride and phosphate, quantitative anion experiments were performed as well. For this reason, cyanide and phosphate were chosen as anions of interest (fluoride can already be quantified via ^{19}F NMR spectroscopy without the need of a fluorinated receptor). Experimental conditions were set to quantitatively follow up cyanide or phosphate (0-10 mM, each) in selected mixtures of chloride, bromide, iodide and nitrate (fixed concentration of 25 mM, each), respectively, using **7** (5 mM) assisted by ^{19}F NMR. As expected and seen before from qualitative sensing (Figure 61b), both, cyanide and phosphate can be selectively quantified in presence of the named anions without any interference. The chemical shift change versus the effective concentration of appropriate anion was plotted and fitted. The obtained data follow a strict linear dependency (R^2 = 0.99, both experiments) for the selected points. Thus, quantitative sensing tasks of cyanide and phosphate can be conveniently performed also in presence of otherwise interfering anions. This said, the approach becomes imprecise in mixtures of varying concentration of either cyanide, fluoride or phosphate, whereupon the observed ^{19}F shift is composed of the appropriate portion of each receptor-anion adduct in solution. Thus, no reliable discrimination and consequently no quantification can be achieved under these conditions.

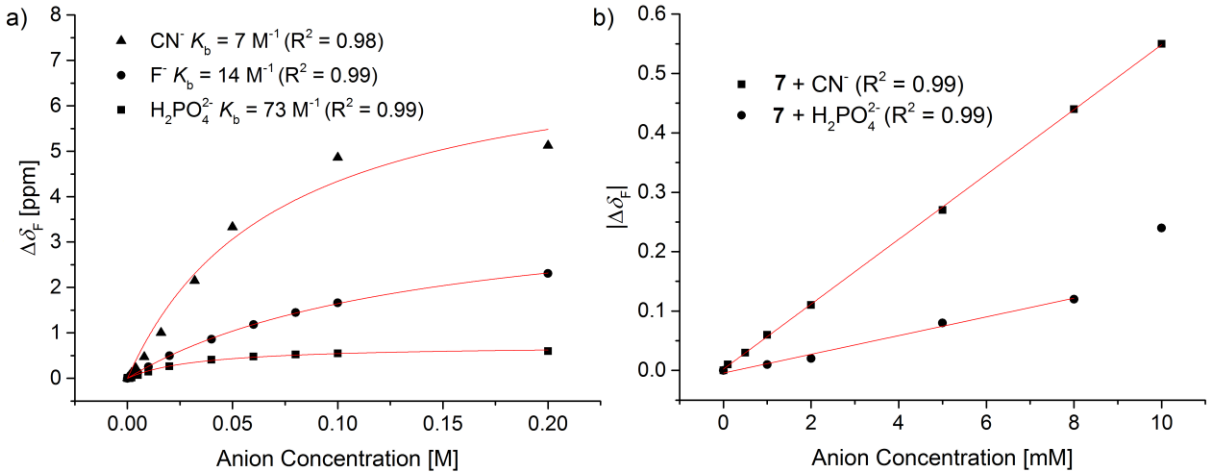

Figure 63: a) Binding isotherms of receptor 7 (2 mM) and is presence of cyanide, fluoride and phosphate (0-200 mM), respectively, for binding constant determination. b) Linear portions of the calibration curves of receptor 7 (10 mM) in presence of cyanide and phosphate (0-10 mM each), respectively, in mixture with chloride, bromide, iodide and nitrate (25 mM each). Conditions: Measured in HEPES buffer (100 mM, pH 7.4, 10% D_2O) at 377 MHz, 256 scans and 25°C.

In summary, the concept of diol sensing by using fluorinated boronic acid appended (bi)pyridinium salts assisted by ^{19}F NMR spectroscopy was transferred to the high demanding field of anion recognition and discrimination. The chemosensor **7** fulfils the requirements of a water-soluble anion receptor that uses the attached boronic acid function for anion binding and the attached ^{19}F probe for the recognition of this binding event. Therefore, anion identification and discrimination can be achieved by using this simple one-component system assisted by ^{19}F NMR spectroscopy producing an anion-dependent ^{19}F shift change relative to the original shift of the unbound **7**. Twelve common inorganic anions were screened under physiological conditions and exclusively cyanide, fluoride and phosphate provided superior selectivity to receptor **7**. Job-Plot experiments indicated a strict 1:1 receptor-anion stoichiometry for these three analytes. Furthermore, binding constants as well as LOD/LOQ values have been determined and titration experiments allowed the quantification of cyanide or phosphate beside four otherwise interfering anions.

Overall, the presented method exhibits high potential for sensing cyanide, fluoride and phosphate in terms of the environmental monitoring of wastewaters or in a physiological medium. In future, ongoing advances in NMR technique will widen the field including tailored fluorine-decorated boronic acid receptors in many sensing areas with increasing analyte sensitivity and discrimination power. For sure, medicinal, environmental and life science will profit from this versatile approach which directly responds to analyte recognition without false interpretation caused by interfering background signal.

POTENTIAL REAL-LIFE APPLICATIONS

The previous chapters highlighted the manifold possible sensing applications of fluorinated boronic acid-appended (bi)pyridinium receptors assisted by ^{19}F NMR spectroscopy. The unique and discriminatory sensing power of the presented system for diols and anions especially in complicated matrices such as diol mixtures or enzyme-catalyzed reactions and the robustness against moderate pH changes should also open up sensing tasks for real life samples.

Hence, two possible scenarios, the glucose sensing in human urine and the screening of hydrogen peroxide samples were chosen to check the diol sensing capacity and a new chemodosimetric approach, respectively, in potential real-life applications.

GLUCOSE SENSING IN HUMAN URINE SAMPLES

Diabetes mellitus the most popular and widespread disease of the modern world with over 415 million people being affected is a group of metabolic disorders leading to high blood sugar level in the human body.[2, 189] One can distinguish between three main types of diabetes. Type 1 leads to a deficit of insulin due to a failure of the pancreas in producing insulin (destruction of the beta cells of the pancreatic islets). Type 2 has its origin in an insulin resistance and cells do not respond properly to insulin and later an insulin deficit can be developed. One of the third main forms is gestational diabetes which affects pregnant women without any previous indication. People who are diseased by diabetes have in common that they suffer from symptoms such as frequent urination, increased thirst and increased hunger arising from the heightened glucose concentration in blood. To some extend serious complications can be the consequence when diabetes is left untreated such as diabetic ketoacidosis, cardiovascular disease, stroke, damage to eyes or even death. Current diagnostic methods for glucose blood tests mainly rely on invasive and uncomfortable testing procedures, but also noninvasive techniques which determine glucose in urine samples via dip sticks or even new approaches using smart tatoos are known.[3, 190-191] In principal, the main part of available glucose test kits use an enzymatic oxidation (GOx) of the glucose to gluconic acid with a coupled redox reaction that allows the quantification of the original glucose via the associated hydrogen peroxide production.[177, 192] Latest approaches based on medicinal contact lenses determine the glucose level by analyzing the patient's tear fluid.[193-194]

Again, chemosensor **1** assisted by ^{19}F NMR was chosen due to the inherent sensing power and robustness in complex media for the screening of urine samples spiked with D-glucose. This task was followed up for the approach's potential as a diagnostic tool for the preexamination of urine concerning diabetes mellitus. As a matter of fact, the D-glucose concentration in the urine of a healthy sober person ranges between 0 and 0.8 mM, while that of a diseased person can be significantly higher and is known under the term glycosuria. The glucose concentration in urine correlates to the blood sugar level (healthy sober person between 3 and 6 mM). Consequently, a pretest which determines the glucose concentration of a collected urine sample can provide information of the patient's glucose balance.

To simulate a diagnostic real-life sample for the selective detection of glucose, a complex synthetic urine matrix was spiked with known amounts of D-glucose. Like genuine human urine, synthetic urine is containing many possible interfering compounds, mainly urea, potassium chloride, creatine and other inorganic salts and amino acids which are problematic for common sensing systems with respect to direct glucose detection.[195]

In practice, synthetic urine, Surine™, was stabilized with HEPES buffer (70% synthetic urine, 30 mM HEPES buffer, pH ~7.4, 3% D_2O) and used as the diagnostic medium. Samples containing receptor **1** (10 mM) and increasing amount of D-glucose (0-5 mM) were prepared and consecutively the ^{19}F NMR spectra were recorded as shown in the waterfall diagram of Figure 64. As already seen for single diol samples, two characteristic main shifts of the receptor-**1**-glucose complex could be observed with slightly altered values at δ_F –115.92 and –117.18 ppm (matrix effects) besides the residual signal of unbound **1** at δ_F –111.63 ppm starting by the addition of 600µM of D-glucose. Consequently, the approach enables the selective detection of D-glucose in synthetic urine.

For quantitative sensing purposes the ^{19}F NMR signal response of the formed complex shows a linear correlation versus the effective D-glucose concentration. The plotted data of the insert in Figure 64 describe the linear correlation of integral evolvement upon increasing glucose amount for the internal (reference standard is the total integral area which corresponds to 10 mM fluorine) and as well as the external method (a coaxial insert containing a 100 mM TFA solution was used as reference standard). Both methods seem to be applicable for glucose quantification in synthetic urine samples containing major contaminants.

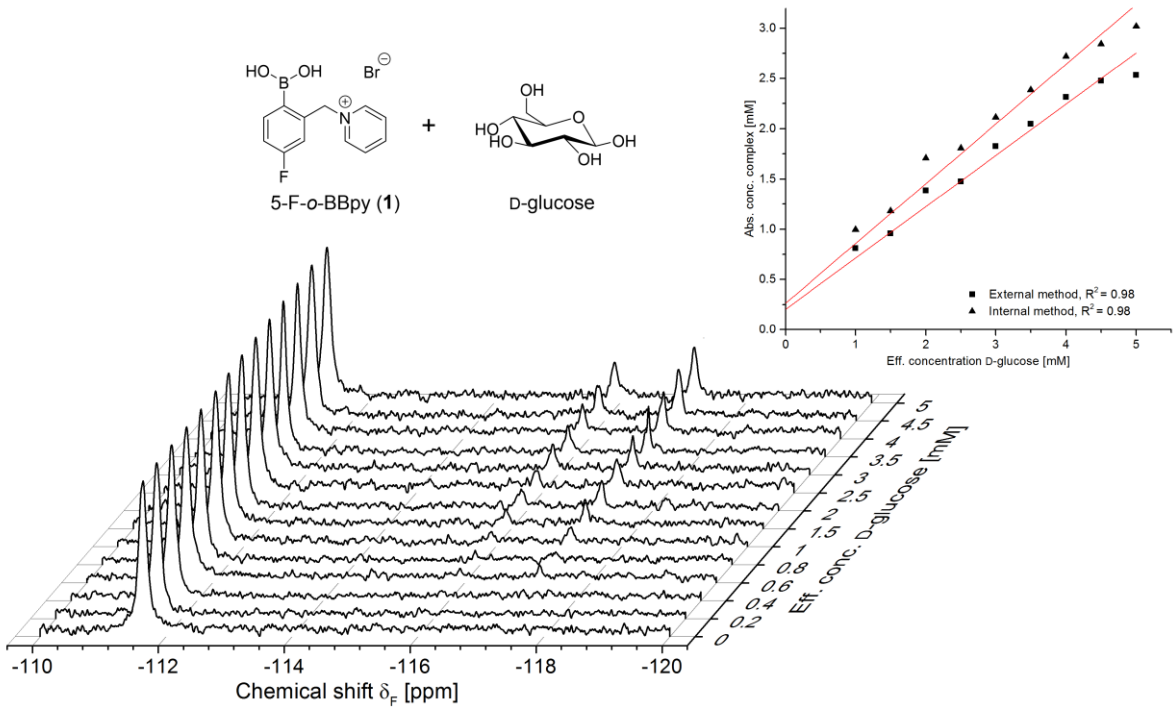

Figure 64: Screening of D-glucose in synthetic urine assisted by receptor 1 and ^{19}F NMR as an alternative diagnostic approach for the examination of diabetes. The spectra of 1 and increasing amount of D-glucose in synthetic urine show the selectivity of 1 for D-glucose in a complex matrix beside interfering contaminants. Conditions: receptor 1 (10 mM) and D-glucose (0−5 mM) measured in aqueous HEPES buffer (30 mM, pH 7.4, 3% D_2O) at 188 MHz, 256 scans and 25°C.

The limit of detection and quantification for D-glucose under given conditions was found to be < 0.6 and 0.6 mM, respectively (see appendix). These findings indicate that glucose can be conveniently determined and quantified in a urine sample within the required concentration range of 0 - 0.8 mM for a healthy patient and values above which would give a hint for diabetes. However, it must be considered that the experiments were conducted using merely a 188 MHz NMR spectrometer (256 scans, 12 min acquisition time per sample). Thus, the applicable detection limits of D-glucose in the used sensing setup can be adjustable to lower ranges by using stronger NMR field strength and longer acquisition times (see chapter 3.6). Nevertheless, the findings highlight the sensing method as potentially pretest for potential diabetes candidates in a medicinal application. Even though, the applicability in genuine human urine has to be investigated.

Overall, the selective screening of D-glucose in a synthetic urine medium could be successfully and the first time shown via the fluorinated receptor **1** assisted by ^{19}F NMR spectroscopy. The presented sensory setup allowed the selective and quantitative detection of D-glucose in the lower millimolar range beside otherwise interfering compounds. Thus, the

presented method can be seen as a potential tool for the noninvasive screening of human glucose levels in urine and a possible diabetes pretest.

The evolvement of the NMR technique, especially by small-sized benchtop machines with increasing field strength and sensitivity for the ^{19}F nucleus will be a supporting aspect on the way to a future test kit with high selectivity and sensitivity for D-glucose and presumable other important metabolites for medicinal diagnosis such as e.g. catecholamines.

A CHEMODOSIMETRIC APPROACH FOR HYDROGEN PEROXIDE

All previously described sensing experiments using the fluorinated boronic acid-appended receptors assisted by ^{19}F NMR spectroscopy are based on the same sensing principle that is the boronic acid function which is standing in an equilibrium with interacting nucleophilic diol or anion. Due to the high sensitivity of the attached fluorine probe, the induced electronic environment change, which is mainly concatenated with boron rehybridization and the structural character of the formed complexes, can be monitored via ^{19}F NMR spectroscopy. On the other side, an irreversible transformation of the sensor induced by interacting species should give a spectroscopic information change visible by ^{19}F NMR as well. A molecule which selectively detects the analyte of interest and is irreversible transformed by the latter is called a chemodosimeter.[196]

A potential scenario for such an irreversible transformation of a boronic acid-based receptor is the reaction with oxidative hydrogen peroxide.[197] H_2O_2 belongs to the group of reactive oxygen species (ROS) and is produced by oxidative metabolism reactions.[198-199] Furthermore, hydrogen peroxide plays an important role in other biological processes, e.g. signal transduction, inflammation and immune response.[199] Its oxidative character, especially of the highly reactive hydroxyl radical (directly formed via UV radiation) is associated with cellular aging, DNA damage and carcinogenesis.[200] Besides, H_2O_2 is the active component of many pharmaceutical and clinical products, which benefit from the oxidative and sterilizing behavior and is used for wound disinfection, hair bleaching and a minor degree for teeth whitening. Due to its broad application and large quantities released to the environment H_2O_2 identification and discrimination from other ROS and of course H_2O_2 quantification is of high interest. Available verification procedures for hydrogen peroxide include high-performance liquid chromatography (HPLC), liquid-phase fluorometry and chemiluminescence (CL) which in general need several steps for sample preparation and lack of direct detection of instable H_2O_2.[201] Another aspect that has to be considered is the limited stability of hydrogen peroxide solutions, which force the analyst to an urgent sample preparation and measurement.

Hence, the trifluoromethyl receptor **8** was tested for the sensing of hydrogen peroxide under aqueous conditions. Noteworthy, **8** did not show suitable sensing potential for reversible diol interaction due to the inherent low ^{19}F sensitivity upon diol binding (interrupted conjugation of the attached fluorine probes to boron) but exhibits improved sensitivity in terms of the increased fluorine content compared to e.g. the mono-fluorinated receptors **1** and **7**. The

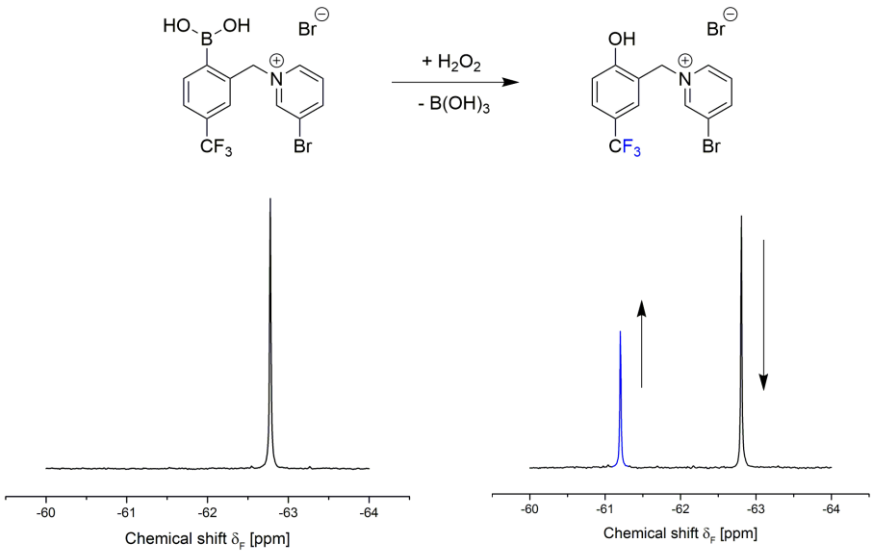

Figure 65: Chemodosimetric sensing approach of hydrogen peroxide using the trifluoromethyl-based receptor 8 assisted by ^{19}F NMR spectroscopy. One equivalent of 8 is transformed to the phenol degradation product by H_2O_2, respectively. The recorded ^{19}F NMR spectrum on the left represents unreacted 8 at δ_F –62.8 ppm (black shift) and on the right side the original decreased shift of 8 and the degradation product of 8 with a new appearing signal at δ_F –61.2 ppm (blue shift). Conditions: receptor 8 (3 mM) and H_2O_2 (1 mM) in aqueous HEPES buffer (50 mM, pH 7.0, 10% D_2O) at 377 MHz, 32 scans and 25°C.

indirect sensing of H_2O_2 via chemodosimeter **8** (3 mM) assisted by ^{19}F NMR spectroscopy is represented by Figure 65. Under aqueous conditions (50 mM HEPES buffer, pH 7.0, 10% D_2O) the attached and magnetical equivalent fluorine probes produce one sharp signal in the ^{19}F NMR spectrum at δ_F –62.8 ppm corresponding to the unreacted chemodosimeter **8** (Figure 65, left). By addition of hydrogen peroxide (1 mM) the spectroscopic information is extended by the appearance of one new shift of lower field strength at δ_F –61.2 ppm which corresponds to the reaction product of **8** (Figure 65, right). This phenol is formed by an oxidation of the original boronic acid function of the chemodosimeter upon insertion of H_2O_2 and release of boric acid. The phenol degradation product exhibits lowered electron density at the ^{19}F probes (deshielding). Because of their diverse chemical/magnetic character both ^{19}F signals of the original chemodosimeter **8** and the degradation product, respectively, are well separated. The qualitative detection of hydrogen peroxide is enabled via the distinct fluorine shifts. The transformation of **8** is irreversible and both species can be quantified by processing of the signal integrals. Furthermore, the approach showed good selectivity for H_2O_2 beside other screened ROS which showed no or only weak interaction to chemodosimeter **8** (appendix). The LOD and LOQ values which determine the detection limits of the chemodosimetric approach are clearly below the smallest tested value of 50 µM H_2O_2 as shown in Figure 66.

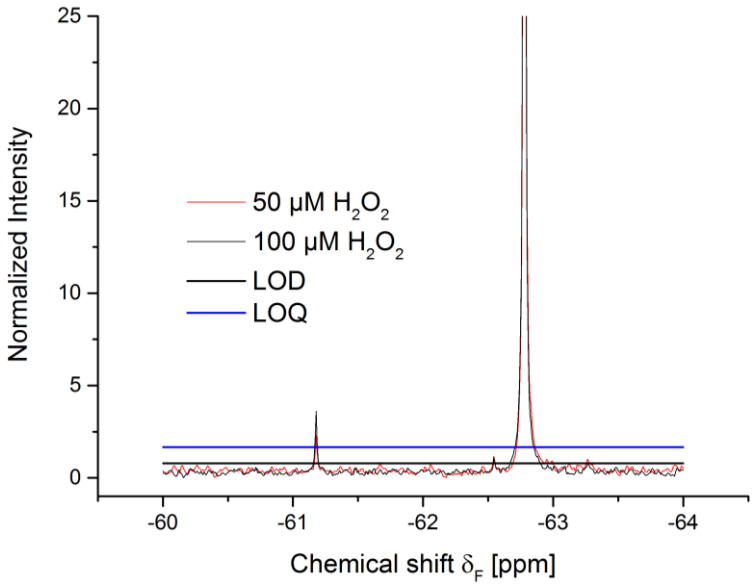

Figure 66: Exemplary ^{19}F NMR spectra of chemodosimeter 8 in presence of ROS hydrogen peroxide for the determination of the limit of detection and quantification. The resulting signal at δ_F –61.2 ppm which corresponds to the formed degradation product of 8 can be used for the detection and quantification of 50 µM and less hydrogen peroxide. Conditions: chemodosimeter 8 (3 mM), hydrogen peroxide (50 and 100 µM) measured in aqueous HEPES buffer (50 mM, pH 7.0, 10% D_2O) at 377 MHz, 32 scans and 25°C.

The quantitative sensing feature of the chemodosimeter **8** was checked by measuring the resulting ^{19}F NMR spectra of **8** (3 mM) and increasing amount of H_2O_2 (0-8 mM) in buffered water. The recorded ^{19}F NMR spectra provide increasing signal intensity of the formed degradation product at δ_F –61.2 ppm beside the ^{19}F shift at δ_F –62.8 ppm of unreacted chemodosimeter **8** (normalized intensities) which are illustrated by Figure 67. As stated before, the characteristic ^{19}F signals and changing integrals of the original chemodosimeter **8** and the formed product allow the quantitative determination of the H_2O_2 content. One equivalent of chemodosimeter **8** is converted to one equivalent of the phenol degradation product and one equivalent of H_2O_2. Consequently, the determination of the H_2O_2 content of an unknown sample can be conveniently performed by using a suitable calibration curve. The dependency of the phenol formation ([P]/[CD_0], [P] = phenol concentration, [CD_0] = initial chemodosimeter concentration) versus added amount of hydrogen peroxide (0-8 mM) follow a strict linear correlation (0-2 mM H_2O_2)in the appropriate ^{19}F NMR spectra until saturation of chemodosimeter **8** (3 mM) and can conveniently by processed for the H_2O_2 quantification (inset of Figure 67).

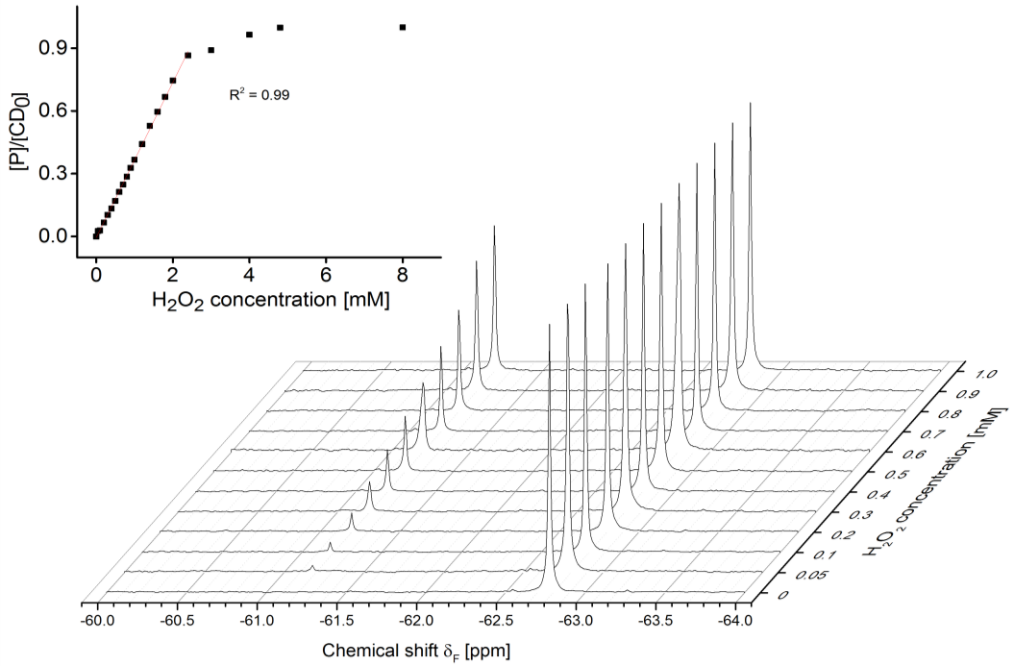

Figure 67: Quantitative sensing of the ROS hydrogen peroxide using the chemodosimeter 8 assisted by ^{19}F NMR spectroscopy. The NMR spectra illustrate the signal evolvement of the formed phenol degradation product of 8 at δ_F –61.2 ppm with increasing amount of H_2O_2. A strict linear correlation of the formed phenol species upon hydrogen peroxide addition up to the saturation of the chemodosimeter is illustrated by the inset. Conditions: chemodosimeter 8 (3 mM) and H_2O_2 (0-8 mM) measured in aqueous HEPES buffer (50 mM, pH 7.0, 10% D_2O) at 377 MHz, 32 scans and 25°C.

As a terminal screening experiment, three commercial available pharmaceutical/dental products were selected and the content of H_2O_2 was quantitatively determined with the described approach. In detail, two aqueous hydrogen peroxide solutions with known H_2O_2 content (3w% H_2O_2) and one teeth whitener gel with unknown H_2O_2 content were chosen and screened with chemodosimeter **8** (3 mM) assisted by ^{19}F NMR spectroscopy and the recorded calibration curve. NMR samples (triplicates) comprising of 20, 30 and 40 µL aliquots of the commercial products, respectively, were mixed with chemodosimeter **8** in aqueous HEPES buffer solution (50 mM, pH 7.0, 10% D_2O) and the ^{19}F spectra were recorded at 377 MHz, 32 scans and 25°C. For data processing, the overall fluorine content (equal to the initial concentration of **8**) of each sample was used as the reference and the absolute concentrations of unreacted chemodosimeter **8** and the formed degradation product of **8** were determined via ^{19}F NMR signal integration. The obtained data of all three commercial H_2O_2-containing samples, respectively, show a linear trend of the formed degradation product content versus increasing amount of aliquot used as represented by Figure 68. The recalculated H_2O_2 content of the commercial products with the labeled hydrogen peroxide concentration content (3w% H_2O_2) was determined as 2.51 and 2.28

w%, respectively. Thus, the determined concentrations are close to the hydrogen peroxide content given by the label even though they are slightly under the expected content of H_2O_2. This result might arise e.g. from possible H_2O_2 decomposition induced by the experimentally sample preparation, the sample storage, the product matrices and the manufacturing process. For the commercial teeth whitener, a content of 1.83 w% H_2O_2 was determined which might be a suitable concentration for teeth whitening agents. Furthermore, the findings of this complex matrix indicate a strong selectivity of chemodosimeter **8** to exclusively hydrogen peroxide without any interference to other ingredients. All values of the H_2O_2 concentration of the commercial samples determined by chemodosimeter **8** assisted by ^{19}F NMR and the H_2O_2 content given by the product label are listed in Table 7.

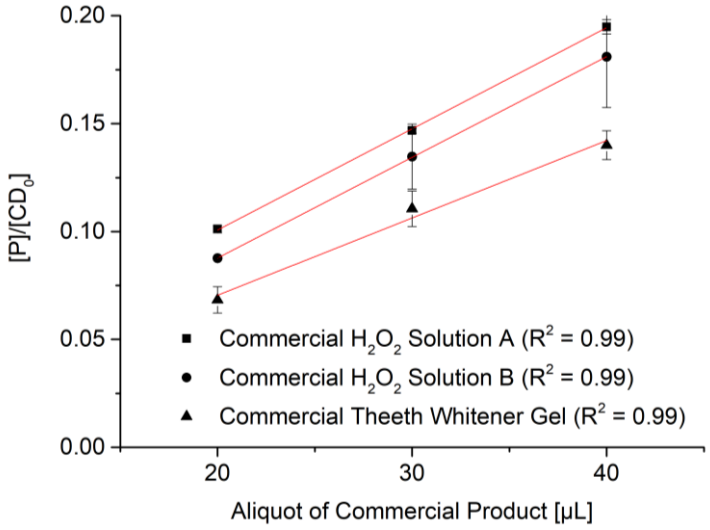

Figure 68: Quantitative hydrogen peroxide determination of commercial available H_2O_2-containing products via the presented chemodosimetric approach. The plotted data ([P]/[CD$_0$] versus the amount of aliquot of commercial product screened, respectively, show a strict linear correlation. Conditions: chemodosimeter 8 (3 mM), aliquots of commercial products measured in aqueous HEPES buffer (50 mM, pH 7.0, 10% D_2O) at 377 MHz, 32 scans and 25°C.

Table 7: Hydrogen peroxide content of commercial pharmaceutical/dental products determined via the presented chemodosimeter 8 assisted by ^{19}F NMR spectroscopy and as given by the label.

Sample	H_2O_2 conc. [w%]	
	Measured	As labeled
Commercial H_2O_2 Solution A	2.51 ± 0.07	3
Commercial H_2O_2 Solution B	2.28 ± 0.00	3
Commercial Teeth Whitener	1.83 ± 0.05	n.a.

To sum up, the ^{19}F NMR sensing principle used for the qualitative and quantitative detection of reversible boronic acid-diol/anion interaction can also be transferred to irreversible reactions involving the boronic acid function. Thus, the structural transformation of chemodosimeter **8** in presence of hydrogen peroxide can be easily monitored via the attached ^{19}F probes, which experiences a dramatic change in their electronic environment. Due to the increased fluorine content of **8** compared to other monofluorinated derivatives the sensitivity and achievable detection limits allow the detection of H_2O_2 in the lower micromolar area. The simple spectroscopic data follow a linear dependency versus the applied hydrogen peroxide concentration and enable easy quantification with subsequent calibration for given experimental conditions. Quantitative H_2O_2 values of two pharmaceutical samples which have been measured are in accordance with the labeled product H_2O_2 concentration. A high selectivity of the sensing approach could be observed for the ROS in a complicated mixture such as the screened teeth whitener. Therefore, the presented approach features a high potential for the selective, qualitative as well as quantitative detection of ROS hydrogen peroxide in complex bio samples. An increase in the applied NMR field strength would enable the detection even in the nanomolar range.

5 CONCLUSION AND OUTLOOK

More than ever and mainly induced by the rapid demographic and technological development associated with the mankind's self-imposed global problems, the unambiguous and reliable detection of target analytes not only within the field of the analytical chemistry is highly desired. Pressing tasks, which have to be fulfilled, are e.g. the monitoring of medicinal tracers for (newfound) diseases and contaminants, which are associated with the dramatically upcoming environmental pollution. Still and in the future, the approach using tailor-made molecular scaffolds (receptors) and the correlated sensory response (reporter) of new sensing systems are in the focus of worldwide research. In this connection, the task is to increase the selectivity and reliability with respect to analyte detection in a specific analytical setup.

In the manifold group of diol-containing analytes, especially saccharide and catecholamine derivatives are examples of important medicinal tracers that need to be identified and quantified for the identification of specific diseases and the monitoring of the course of disease. Serious is the worldwide progress with respect of diabetes indisposition and the associated demand of reliable glucose detection systems, which can provide the patient's blood sugar in a real-time manner. Furthermore, several types of cancer and the Alzheimer disease that are accompanied with upcoming catecholamine concentrations need reliable medicinal detection tools too. On the other side, the detection of hazardous substances, which endanger the environment and thus our health, is another important task that must be ensured. Contaminants such as fluoride, phosphate and highly toxic cyanide have moved in the focus of interest because of their considerably accumulation into the global water systems.

Fortunately, the boronic acid function and the inherent chemistry proved to be a suitable binding partner for the named target analytes and thus is a well-known receptor moiety in numerous tailored and mainly fluorescent-based sensing systems.

In the present thesis, a pool of novel fluorinated boronic acid-appended (bi)pyridinium receptors have been synthesized and characterized which in part exhibit strong ability for diol sensing tasks in combination with ^{19}F NMR spectroscopy under physiological conditions. The attached boronic acid function(s) of the one-component sensing concept provide a suitable binding (reaction) site for the screening of diols, inorganic anions and hydrogen peroxide, whereas the attached fluorine atom(s) assisted by ^{19}F NMR are highly sensitive probes for the recognition of these binding events. Connected in one molecule, the attached boronic acid function(s) and fluorine(s) offer complementary and additional advantages such as the good water solubility under physiological conditions, robustness of the signal response against pH change, the direct signaling of e.g. the boronic acid-diol binding event with overall no disturbing fluorine background signals and highly sensitive ^{19}F shifts.

The sensing mechanism relies on boron rehybridization and the structural and chemical character of the binding analyte assisted by non-invasive ^{19}F NMR spectroscopy. Structural modifications of the receptor compounds, such as varying the amount of attached fluorine probes, its relative position to boron and the introduction of model compounds were used for the elucidation of crucial sensing features for diol sensing via ^{19}F NMR spectroscopy.

The fluorinated boronic acid-appended benzyl pyridinium salt **1** with one attached fluorine in *para*-position with respect to boron was found to be the superior receptor scaffold for manifold applications because of the good communication property between the binding site and the fluorine reporter. Thus, unique and highly discriminative ^{19}F NMR fingerprints were obtained for a wide pool of analyte classes containing e.g. monosaccharides, phosphorylated and *N*-acetylated sugars, sugar alcohols, carboxylic acids, nucleotides, and (hydroxy)amines.

Differences in the recorded ^{19}F shifts were observed even by small structural diversity of the appropriate diols such as a change in one single stereocenter (epimers). Receptor **1** assisted by ^{19}F NMR spectroscopy and the unique ^{19}F pattern was furthermore successful in the identification and discrimination of the single components of a binary mixture containing the monosaccharide isomers D-glucose and D-fructose even in high excess of one of the named components. This scenario is still a challenging task in the field of diol receptors/sensors in which the unambiguous diol identification and discrimination is highly desired.

Unfortunately, the trifluoromethyl sensing probe of receptor **4** provided no suitable sensing property for diols and anions but could be utilized in a new chemodosimetric approach for the qualitative and quantitative sensing of the reactive oxygen species hydrogen peroxide.

Fluoride, phosphate and highly toxic cyanide anion could be identified via **1** out of a pool of nine other anions. In addition, the amount of cyanide and phosphate, respectively, was quantitatively monitored in mixtures beside four other anions.

The diol sensing concept was enhanced by the use of fluorinated boronic acid-appended bipyridinium-based receptors and by their increased discriminative ^{19}F NMR property induced by the alteration of the bipyridine linkers. Increased diol discrimination power produced by the receptor-diol interactions was achieved using an array of bipyridine receptors and the processing of the recorded ^{19}F NMR data to two-dimensional QR-like bar codes. Moreover, this new and helpful approach with respect to inventory of receptor-analyte databases avoids complicated and time-consuming chemometric techniques that are predominantly required in non-discriminative fluorescent systems.

Beside qualitative also quantitative sensing experiments of diols via the characteristic ^{19}F NMR signal information such as the chemical shift δ_F and signal integrals of receptor **1** were performed. Quantitative sensing tasks include the determination of apparent binding constants of selected diols and the quantification of diol samples. In addition, the reliable determination of glucose down to 0.6 mM in a glucose-spiked synthetic urine sample was successfully performed by using merely a 188 MHz spectrometer. This experiment is a nice example, which shows strong potential as a clinical diabetes pretest.

Good applicability of the sensing tool was found for the selective monitoring of released fructose formed by a complex enzymatic reaction, which provided furthermore kinetic parameters such as the Michaelis-Menten constant and the enzyme activity.

The qualitative analysis of ^{19}F NMR spectra of receptor **1** to selected monosaccharide derivatives, the inherent structural character and binding affinities of the latter provided strong evidence for the binding of monosaccharides to boron via the synperiplanar cis 1,2-hydroxyl groups of the open-ring and furanose forms. An indication for no or minor binding to the sterically unfavored hydroxyl groups of the pyranose isomers was discussed. Nevertheless, these findings stay in contrast to other findings in literature and still need intensive investigation.

Overall, the cooperation of fluorinated boronic acid receptors and ^{19}F NMR represent a suitable sensor system that allows the unambiguous diol identification and discrimination under physiological conditions without interfering background signals. The detection limits for diols

are situated in the lower millimolar range and are dependent on the binding affinity, the applied NMR field strength and the number of NMR scans.

With respect to the continuously improving quality and cost effectiveness of modern NMR spectrometers (growing number of benchtop NMR spectrometers) the presented sensing concept is presumably applicable to medical pretests and diagnostic situations. Furthermore, this simple concept can be arbitrarily widened to structurally tailor fluorinated receptors for the sensing of specific diol subclasses and medicinal relevant catecholamines which are highly important in disease diagnosis.

6 ZUSAMMEN-FASSUNG

Durch den schnellen technologischen als auch demografischen Wandel und die durch die Menschheit selbstauferlegten globalen Probleme ist die zuverlässige Detektion von Analytmolekülen auf dem Gebiet der Analytischern Chemie und der angrenzenden Wissenschaften heute von größter Bedeutung. Dringende Zielstellungen, die es zu lösen gilt, sind z.B. die Überwachung von medizinisch-relevanten Tracern und Verunreinigungen welche mit der dramatisch ansteigenden Verschmutzung der Umwelt einhergehen. Um die Zuverlässigkeit der Analytdetektion und –selektivität, besonders unter individuellen Bedingungen zu erhöhen, sind maßgeschneiderten Rezeptormoleküle in neuartigen Sensorsystemen heute und in Zukunft im Fokus der weltweiten Forschungsanstrengungen.

Besonders Saccharid- und Katecholaminderivate aus der Gruppe der Polyole sind Beispiele von bedeutenden medizinischen Analytmolekülen. Die Identifizierung und Quantifizierung dieser Analyte ermöglicht die Erkennung und das Monitoring von bestimmten Erkrankungen. Ernstzunehmend ist die weltweit zu beobachtende Zunahme von Diabeteserkrankungen, welche mit einer Störung des Glukosehaushalts einhergehen. Basierend darauf ist die steigende Nachfrage an zuverlässigen Glukosetests zu erklären, die wenn möglich, eine Echtzeit Verfolgung des Blutzuckerspiegels erlauben sollen.

Weitere bedeutende Erkrankungen stellen Alzheimer und verschiedenen Krebsarten dar. Diese führen zu erhöhten Katecholaminanreicherungen in spezifischen Körpersekreten die es mit einem verlässlichen diagnostischen Tool zu identifizieren gilt. Hierfür werden zuverlässige Werkzeuge zur medizinischen Erkennung benötigt. Desweiteren ist die Detektion von giftigen Substanzen, welche die Umwelt und unsere Gesundheit gefährden, von besonderer Bedeutung. Im Fokus des Interesses stehen besonders Targetmoleküle wie Fluorid, Phosphat und hochtoxisches Cyanid, welche sich beträchtliche in den globalen Wassersystemen anreichern.

Glücklicherweise stellt die Boronsäurefunktion einen geeigneten Bindungspartner für die genannten Analytklassen dar und dient in vielen maßgeschneiderten, meist fluoreszenz-basierenden Sensorsystemen, als nützlicher Rezeptor Baustein.

In der vorliegenden Arbeit wurde ein Pool von neuartigen fluorierten Boronsäurerezeptoren synthetisiert und charakterisiert. In Kombination mit der ^{19}F NMR-Spektroskopie zeigen diese größtenteils eine gute Eignung zur Detektion von Diol-Analyten unter physiologischen Bedingungen.

Die verknüpfte Boronsäurefunktion(en) dieses Einkomponenten-Sensorkonzepts stellt eine geeignete Bindungsstelle für das Screening von Diolen, anorganischen Anionen und Wasserstoffperoxid dar. Die angebundenen Fluor Atome fungieren unter Zuhilfenahme der ^{19}F-NMR als hoch sensitive Sonden, welche die Analytenanbindung erkennen. Verknüpft in einem Molekül besitzen die Boronsäurefunktion und Fluor komplementäre und für das Rezeptorgerüst positive chemische Eigenschaften. Hierbei sind die gute Wasserlöslichkeit des Rezeptors, die Robustheit des ^{19}F NMR Signals gegenüber pH Änderungen, die direkte Erkennung der Boronsäure-Diol Bindungsknüpfung, das Ausbleiben von störenden Fluorhintergrundsignalen und die hoch sensitiven und charakteristischen ^{19}F NMR Signal zu nennen.

Der Detektionsmechanismus basiert auf der Änderung der Hybridisierung des Bors welche mit dem strukturellen und chemischen Charakter des anbindenden Analyten verknüpft ist. Die Signalgebung wird dabei durch die nichtinvasive ^{19}F NMR Spektroskopie realisiert. Strukturelle Modifikationen an den Rezeptormolekülen wie die Variation des Fluorgehalts, der relativen Position von Fluor zu Bor und das Heranziehen von Vergleichsverbindungen wurden für die Aufklärung von notwendigen Kriterien in Bezug auf den Sensormechanismus untersucht.

Der fluorierte Benzylpyridinium Rezeptor **1** mit einer Fluor Sonde in *para*- Position zu Bor hat sich im Rahmen der Untersuchungen auf Grund seiner guten Kommunikationseigenschaften zwischen der Rezeptorseite und der Fluor Sonde als herausragendes Sensormolekül herausgestellt und wurde in vielen interessanten Experimenten eingesetzt. Dabei wurden für einen großen Pool von Analyten bestehend aus Monosacchariden, phosphorylierten und acetylierten Zuckern, Zuckeralkoholen, Carboxylsäuren, Nukleotiden und (Hydroxy)Aminen einzigartige und hoch diskriminative ^{19}F NMR Fingerprints erhalten. Signalunterschiede

bezüglich der aufgenommen Spektren konnten besonders bei kleinsten strukturellen Variationen des entsprechenden Diols wie z.B. in einem Stereozentrum (Epimere) beobachtet werden.

Mittels Rezeptor **1** und den resultierenden charakteristischen ^{19}F NMR Mustern konnte D-Glukose und D-Fruktose selbst bei einem großen Überschuss von einer der genannten Komponenten sicher nebeneinander detektiert werden. Dieses Analysenszenario ist nach wie vor eine herausfordernde und nachgefragte Aufgabenstellung im Bereich der Diol Rezeptoren Analytik.

Entgegen aller Erwartungen zeigte die Trifluormethyl Sonde von Rezeptor **4** keine Sensitivität für Diole und Anionen. Hingegen entpuppte sich jedoch die Verbindung **4** als nützliches Chemodosimeter für den qualitativen und quantitativen Nachweis der reaktiven Sauerstoff Spezies - Wasserstoffperoxid. Die Anionen Fluorid, Phosphat und hochtoxisches Cyanid konnten mithilfe von Rezeptor **1** und den erzeugten ^{19}F NMR Signalen von neun weiteren Anionen unterschieden werden. Der Gehalt von Cyanid und Phosphat konnte außerdem in Gemischen neben vier weiteren Anionen quantitativ bestimmt werden.

Das Diol-Sensing Konzept wurde durch fluorierte Bipyridin-Boronsäurerezeptoren und deren verbesserter diskriminatorischer ^{19}F NMR Eigenschaften weiterentwickelt. Eine gesteigerte Diol-Diskriminierung konnte durch die Rezeptor-Diol-Wechselwirkungen mittels eines Arrays von Bipyridin Rezeptoren erreicht werden. Die dabei generierten ^{19}F-NMR Signale wurden dazu in zweidimensionale, QR-ähnliche, Barcodes übersetzt. Mit entsprechender Hard- und Software wäre ein Inventarisierungssystem für verschiedenste Analytklassen denkbar. Dieser neuartige Ansatz vermeidet komplizierte und zeitaufwendige chemometrische Techniken. Letztere sind vorwiegend bei der Anwendung von fluoresenz-basierten Systemen, welche meist keine Unterscheidung von Diolen mittels ihrer eindimensionaler Signalmodulation zulassen, dringend erforderlich.

Unter Zuhilfenahme der chemische Verschiebung δ_F und der Signalintegration der resultierenden ^{19}F Signale von Rezeptor **1** konnten Diole nicht nur qualitativ, sondern auch quantitativ bestimmt werden. In diesem Rahmen wurden die Bindungskonstanten ausgewählter Rezeptor-Diol Verbindungen bestimmt. Darüber hinaus konnte der Glukosegehalt in einer synthetischen Urin Matrix welche mit Glukose versetzt wurde mittels eines 188 MHz Spektrometers bis zu einer minimalen Konzentration von 0,6 mmol/l detektiert werden. Eine

gute Eignung des Sensor Systems konnte bei der selektiven Detektion von Fruktose in einer weiteren komplexen Matrix beobachtet werden. Dabei wurde die Freisetzung von Fruktose aus einer enzymatischen Reaktion quantitativ verfolgt. Weiterhin konnten kinetische Parameter wie z.B. die Michaelis-Menten-Konstante und die Enzymaktivität bestimmt werden.

Qualitative Untersuchungen auf die vorliegenden Bindungsmodi zwischen Rezeptor und Diol wurden mittels der Analyse der aufgenommenen ^{19}F-NMR-Spektren von Rezeptor **1** und ausgewählten Monosaccharidderivaten durchgeführt. Dabei wurden der strukturelle Charakter des entsprechenden Diols, die resultierenden ^{19}F-NMR-Signale sowie die ermittelten Bindungsaffinitäten herangezogen. Die Ergebnisse deuten dabei auf die Bindung der Monosaccharide an das Borzentrum über die synperiplanaren cis-1,2-Hydroxylgruppen der offenkettigen und furanosen Isomere hin. Ein Hinweis für geringe oder keine Bindung an die sterisch nicht bevorzugten Hydroxylgruppen der pyranose Isomere wurde diskutiert. Diese Überlegungen stehen jedoch im Widerspruch zu anderen Publikationen und bedürfen noch weiterer tiefgreifender Untersuchungen.

Insgesamt stellt die Kooperation von fluorierten Boronsäurerezeptoren in Kombination mit der ^{19}F-NMR Spektroskopie ein sehr robustes Sensorystem dar. Die eindeutige Identifizierung und Unterscheidung von verwandten Analyten unter physiologischen Bedingungen konnten gezeigt werden. Die Nachweisgrenzen des Systems für Diole liegen im niedrigen millimolaren Bereich und sind typischerweise abhängig von der Bindungsaffinität, der verwendeten NMR Feldstärke und der Anzahl an NMR Scans. Durch die stetig fortschreitende Entwicklung der NMR Technik, besonders im Hinblick auf moderne Benchtop Geräte, könnte das vorgestellte Rezeptorsystem in medizinischen Vorscreenings und weiteren diagnostische Untersuchungen mit spezifischer Analytenselektivität eingesetzt werden. Durch die Herstellung von strukturell maßgeschneiderte Rezeptormolekülen kann dieses einfache aber starke Konzept beliebig erweitert werden. In Zukunft könnten hierdurch spezifische Diol-Unterklassen und medizinisch relevante Katecholamine detektiert werden um die Diagnostik von Erkrankungen weiter zu verbessern.

7 EXPERIMENTAL SECTION

SYNTHESIS

Unless not otherwise noted all reactions were performed using standard syringe techniques and carried out in oven-dried glassware under nitrogen atmosphere. The used chemicals were purchased and used as described. All NMR experiments were either performed on Bruker AVANCE I 200 MHz, AVANCE III 400 MHz or 600 MHz spectrometers using Bruker TOP Spin 3.2 software for acquisition and processing. Chemical shifts (in ppm) were reported relative to tetramethylsilane (TMS), whereas ^{19}F NMR shifts were reported with respect to trichlorofluoromethane (CCl_3F). All ^{19}F and ^{13}C NMR spectra were measured proton decoupled $\{^1H\}$. Mass spectra were obtained using electrospray ionization (ESI+) or electron impact mode (EI+) on a Finnigan MAT SSQ 710 or MAZ95XL machine, respectively. All FT-IR (ATR) spectra were recorded on a Bruker Optics Equinox 55-IR spectrometer. Elemental analysis was performed on a Vario EL III CHNS. Melting points were determined with a Stuart melting point apparatus SMP3.

General Procedure for Photo-Bromination of fluorinated Precursors

All chemicals were purchased and used as received if not otherwise described: all fluorinated starting compounds (Fluorochem), tetrachloromethane (VWR) was dried over P_4O_{10} and then distilled prior use. Bromine (Merck) was dried with concentrated H_2SO_4 prior use.

A two-necked round bottomed flask of suitable size (with an attached reflux condenser, bubble counter and a dropping funnel) was loaded with 1 equivalent (typically, 10 mmol) appropriate (fluoro)methylphenylboronic acid dissolved/suspended in 10 mL of tetrachloromethane and a stirring bar. This mixture was flushed with nitrogen under stirring for

15 minutes. In distance of 10 cm a 500-Watt halogen bulb was installed, then the mixture was irradiated and heated to reflux. For the brominating step 1.1 equivalent (typically, 11 mmol) of elemental bromine were dissolved in 5 mL cold tetrachloromethane and loaded into the funnel. The bromine solution was added drop by drop within 30 minutes to the flask so that the refluxing solvent stays almost colorless. After the completed addition of bromine, the reaction was stirred and refluxed for further 20 minutes with the bulb turned on. The solution was then allowed to cool to room temperature with the bulb turned off and was then concentrated to half of its original volume. After storage over night the crystals, which have formed, were collected, then washed with a small amount of cold CCl_4 and then recrystallized. Repetition of the latter steps eventually yield further fractions of product. After drying in high vacuum, the desired compound was stored under inert conditions at 5 °C in the dark.

2-bromomethyl-4-fluorophenylboronic acid (a)

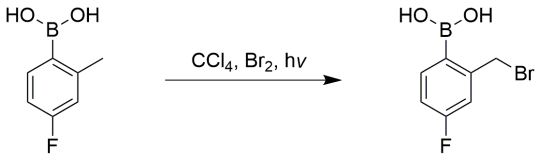

153.95 232.84

The title compound was isolated as colorless and needle like crystals: 1740 mg (64% yield).

^{1}H NMR (400 MHz, $CDCl_3$) δ 5.06 (s, 2H), 7.17 (m, 2H), 7.23 (dd, J = 9.5, 2.2 Hz, 1H) 8.36 (dd, J = 8.4, 6.5 Hz, 1H); **^{13}C{^{1}H} NMR** (100 MHz, $CDCl_3$) δ 32.35, 115.48 (d, J = 19.9 Hz), 118.09 (d, J = 21.13 Hz), 140.52 (d, J = 8.83 Hz), 148.45 (d, J = 8.08 Hz), 165.46 (d, J = 254.64 Hz); **^{19}F{^{1}H} NMR** (188 MHz, $CDCl_3$) δ -105.82; **IR** (ATR) $\tilde{\nu}$ 3366 (w), 3036 (w), 1597 (s), 1415 (m), 1332 (s), 1213 (s), 1160 (s), 689 (s), 526 (s); **Elemental analysis** calculated for $C_{21}H_{15}B_3Br_3FO_3$ (trimeric anhydride): C = 39.14%, H = 2.35%, B = 5.03%, Br = 37.19%, F = 8.84%, O = 7.45%, found: C = 38.80%, H = 2.40%.

2-bromomethyl-5-fluorophenylboronic acid (b)

153.95 232.84

The title compound was isolated as colorless crystals: 2270 mg (83% yield).
^{1}H NMR (400 MHz, $CDCl_3$) δ 5.05 (s, 2H), 7.23 (dt, 1H), 7.48 (m, 1H), 8.00 (dd, 1H). **^{13}C{^{1}H} NMR** (100 MHz, $CDCl_3$) δ 32.57, 120.03 (d, J = 21.3 Hz), 124.16 (d, J = 20.3 Hz), 133.04 (d, J = 8 Hz), 141.3 (d, J = 3.6 Hz), 162.3 (d, J = 249.9 Hz). **^{19}F{^{1}H} NMR** (188 MHz, $CDCl_3$) δ -113.20. **IR** (ATR) $\tilde{\nu}$ 3259(m), 1576(m), 1488(m), 1417(m), 1338(s), 1220(s), 1071(m), 830(m), 587(s). **MS** (EI+) m/z calculated for $C_7H_7BFO_2$ [M-Br]+: 153.1; found: 153.1.

2-bromomethyl-6-fluorophenylboronic acid (c)

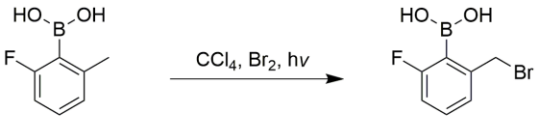

153.95 232.84

The title compound was isolated as colorless crystals: 110 mg (23% yield).

^{1}H NMR (400 MHz, acetone-d_6) δ 4.78 (s, 2H), 6.98 (t, J = 8.5 Hz, 2H), 7.24 (d, J = 7.6, 1H), 7.34 (m, 1H), 7.68 (s, 2H). **^{13}C{^{1}H} NMR** (100 MHz, acetone-d_6) δ 33.96 (d, J = 2.1 Hz), 115.32 (d, J = 25.33 Hz), 126.38 (d, J = 2.8 Hz), 131.52 (d, J = 8.8 Hz), 144.28 (d, J = 9.9 Hz), 165.93 (d, J = 240.13 Hz). **^{19}F{^{1}H} NMR** (188 MHz, $CDCl_3$) δ -106.28. **IR** (ATR) $\tilde{\nu}$ 3278(m), 1607(m), 1561(m), 1450(s), 1336(s), 1246(s), 1021(m), 795(s), 642(s). **MS** (EI+) m/z calculated for $C_7H_7BFO_2$ [M-Br]+: 153.1; found: 153.1.

2-bromomethyl-4-(trifluoromethyl)phenylboronic acid (d)

203.96 282.85

The title compound was isolated as colorless crystals: 2950 mg (89% yield).

^{1}H NMR (400 MHz, $CDCl_3$) δ 5.12 (s, 2H), 7.78 (m, 2H), 8.48 (m, 1H). **^{13}C{^{1}H} NMR** (100 MHz, $CDCl_3$) δ 32.19, 124.89, 127.37, 135.19, 138.32, 146.27. **^{19}F{^{1}H} NMR** (188 MHz,

$CDCl_3$) δ -61.65. **IR** (ATR) $\tilde{\nu}$ 3265(m), 1504(m), 1418(m), 1330(s), 1169(s), 1028(m), 764(m), 745(m), 474(m). **MS** (EI+) m/z calculated for $C_8H_7BF_3O_2$ [M-Br]+: 203.1; found: 203.1.

General Procedure for the Synthesis of 3,3‘-bipyridine and 3,4‘-bipyridine

The following chemicals were purchased and used as received: 3-bromopyridine 4-bromopyridine hydrochloride, 3-pyridineboronic acid, K_3PO_4, Pd_2dba_3 (Alfa Aesar), 2-dicyclohexylphosphino-2′,6′-dimethoxybiphenyl (SPhos) and dioxane (Sigma Aldrich). An aqueous stock solution of K_3PO_4 (1.27 mM) was prepared by dissolving 840 mg (3.84 mmol) K_3PO_4 in 3 mL of deionized water and the use of ultrasonic sound to facilitate the dissolution.

In general, a 25 mL Schlenk flask was loaded with 1.1 mmol 3-pyridineboronic acid or 4-bromopyridine hydrochloride, respectively, 9.2 mg (0.01 mmol) Pd_2dba_3, 9.9 mg (0.024 mmol) SPhos and a stir bar. The flask was then plugged with a septum and five-times evacuated and refilled with nitrogen. Via syringe 95 µL (1 mmol) 3-bromopyridine, 3 mL dioxane and 1.4 mL of the aqueous stock solution were added. The brownish suspension was then stirred and bubbled with nitrogen at room temperature for 15 minutes. Next, the Schlenk flask was sealed with a Teflon valve by the use of a positive nitrogen stream and heated in an oil bath at 100 °C for 18 hours under vigorous stirring. The color of the two-phase reaction mixture changed immediately to a clear orange upper phase and a clear colorless downer phase with a dark precipitate in both phases (catalyst and boronic acid derivatives). After cooling to room temperature, the reaction mixture was filtered through a thin pad of silica to remove the excess of the boronic acid and the catalyst (washing with ethyl acetate), then extracted with ethyl acetate, dried and concentrated under vacuum. The residue was then purified by flash column chromatography (CH_2Cl_2:MeOH 1:0 → 20:1 on silica) und residue solvent was removed in high vacuum.

3,3‘-bipyridine (e)

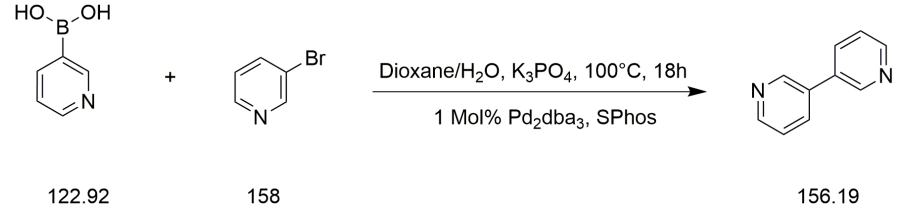

122.92 158 156.19

The title compound was isolated as an orange oil: 124 mg (79% yield).

^{1}H NMR (300 MHz, $CDCl_3$) δ 7.35 (d, J = 12.43 Hz, 1H), 7.35 (d, J = 2.43 Hz, 1H), 7.82 (d, J = 7.93 Hz, 1H), 8.59 (d, J = 3.75 Hz, 1H), 8.78 (d, J = 1.17 Hz, 1H); **^{13}C{^{1}H} NMR** (50 MHz, $CDCl_3$) δ 123.44, 133.13, 134.11, 147.80, 148.93; **IR** (ATR) $\tilde{\nu}$ 3395 (w), 3030 (w), 2930 (w), 2854 (w), 1709 (w), 1586 (m), 1425 (m), 714 (s), 528 (s); **TLC** (CH_2Cl_2:MeOH 10:1 on silica) R_f = 0.41 (external reference 4,4'-bipyridine, R_f = 0.41).

3,4'-bipyridine (f)

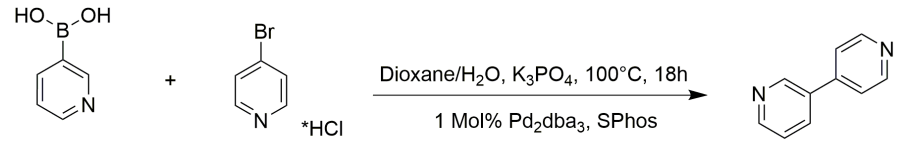

122.92 194.46 156.19

The title compound was isolated as an orange oil: 152 mg (97% yield).

^{1}H NMR (300 MHz, $CDCl_3$) δ 7.38 (dd, J = 7.5, 5.2 Hz, 1H), 7.46 (d, J = 6.1 Hz, 2H), 7.88 (d, J = 8 Hz, 1H), 8.67 (m, 3H,), 8.84 (d, J = 1.3 Hz, 1H; **^{13}C{^{1}H} NMR** (50 MHz, $CDCl_3$) δ 121.24, 123.50, 133.41, 134.04, 144.92, 147.70, 149.76, 150.02; **IR** (ATR) $\tilde{\nu}$ 3033 (w), 2961 (w), 1595 (m), 1423 (m), 1026 (m), 796 (s), 636 (s), 494 (s); **TLC** (CH_2Cl_2:MeOH 10:1 on silica) R_f = 0.41 (external reference 4,4'-bipyridine, R_f = 0.41).

Synthesis of 4,4′-azopyridine (g)

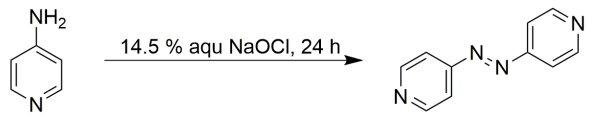

94.12 184.2

For the synthesis of 4,4′-azopyridine the following chemicals were purchased and used as described: diethyl ether, ethyl acetate (VWR), methanol (Roth) 4-aminopyridine (Alfa Aesar) and sodium hypochlorite solution (Sigma Aldrich) were used as received.

A 50 mL round-bottom flask cooled in an ice bath was loaded with 1g (10.6 mmol) 4-aminopyridine dissolved in cold deionized water. 30 mL of an aqueous sodium hypochlorite solution (14.5%) were added drop by drop within 30 minutes which turned the initial clear and colorless solution to a deep red suspension. The reaction mixture was stirred for 24 hours at

room temperature. The orange-red precipitate was isolated via centrifugation and the remaining solution was extracted with diethyl ether. After evaporation of residue solvent, the combined crude product was first recrystallized from methanol and then chromatographed via a silica-loaded column and ethyl acetate. After drying in high vacuum, the title compound was isolated as an orange crystalline solid: 362 mg (37% yield).

^{1}H NMR (400 MHz, $CDCl_3$) δ 7.72 (d, J = 2.96 Hz, 1H), 7.72 (d, J = 6.16 Hz, 1H), 8.86 (d, J = 3.08 Hz, 1H), 8.86 (d, J = 6.12 Hz, 1H); **^{13}C{^{1}H} NMR** (100 MHz, $CDCl_3$) δ 156.75, 151.59, 116.17.

General Procedure for the Synthesis of Pyridinium Bromides

For the synthesis of appropriate pyridinium bromides the following chemicals were purchased and used as described: acetone (Roth), diethyl ether (VWR), dimethylformamide (Roth) and pyridine (Alfa Aesar) were purified and dried prior use, 2-(bromomethyl)phenylboronic acid (Alfa Aesar) and 1-(bromomethyl)-3-fluorobenzene (Alfa Aesar) were used as received, 3-bromopyridine (Alfa Aesar) was dried before use, 2-bromomethyl-4-fluorophenylboronic acid, 2-bromomethyl-5-fluorophenylboronic acid, 2-bromomethyl-6-fluorophenylboronic acid and 2-bromomethyl-4-(trifluoromethyl)phenylboronic acid were synthesized as described before.

In general, a mini vial with an attached syringe screw cap was loaded with 0.64 mmol of appropriate phenylboronic acid, 0.51 mmol appropriate pyridine derivative, 1 mL dry DMF and a stirring bar. The colorless solution was then flushed with nitrogen via syringe for 15 minutes and was then heated and stirred at 70 °C for 24 hours. Usually, a visible color change to slightly yellow was observed. Consecutively, 20 mL acetone and 10 mL diethyl ether were added which induced precipitation of the crude product. After centrifugation, the appropriate product was washed three-times under vigorous stirring with 5 mL acetone. A final washing step was performed in 10 mL diethyl ether using ultrasonic sound. The appropriate pyridine bromide was obtained after centrifugation and drying under a stream of nitrogen.

1-(2-borono-5-fluorobenzyl)pyridin-1-ium bromide; 5-F-*o*-BBpy (1)

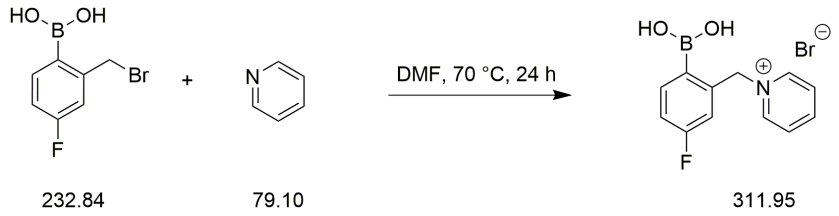

232.84 79.10 311.95

The title compound was isolated as a white hemicrystalline solid: 149 mg (93% yield). **^{1}H NMR** (400 MHz, D_2O) δ 5.84 (s, 2H), 7.10 (t, J = 8.54 Hz, 2H), 7.61 (t, J = 7.18 Hz 1H), 7.87 (t, J = 7.08 Hz, 2H), 8.38 (t, J = 7.8 Hz, 1H), 8.67 (d, J = 6.1, 2H). **^{13}C{^{1}H} NMR** (100 MHz, D_2O) δ 63.84, 116.13 (d, J = 19.8 Hz), 117.90 (d, J = 21.7 Hz), 128.04, 137.29 (d, J = 8.5 Hz), 138.70 (d, J = 7.7 Hz), 144.59, 146.2, 163.82 (d, J = 249 Hz). **^{19}F{^{1}H} NMR** (188 MHz, D_2O) δ -110.75. **IR** (ATR) $\tilde{\nu}$ 3360(m), 3227(m), 3080(m), 1605(m), 1491(s), 1327(s), 1062(s), 645(s), 525(s). **Elemental analysis** calculated for $C_{12}H_{12}BBrFNO_2$: C = 46.20%, H = 3.88%, B = 3.47%, Br = 25.62%, F = 6.09%, N = 4.49%, O = 10.26%, found: C = 46.18%, H = 4.23%, N = 5.27%. **MS** (ESI+) m/z calculated for $C_{13}H_{14}BFNO_2$ [M(monomethylester)-Br]+: 246.1; found: 246.1. **Melting point** 180.2-181.8 °C (decomposition).

1-(2-borono-4-fluorobenzyl)pyridin-1-ium bromide; 4-F-*o*-BBpy (2)

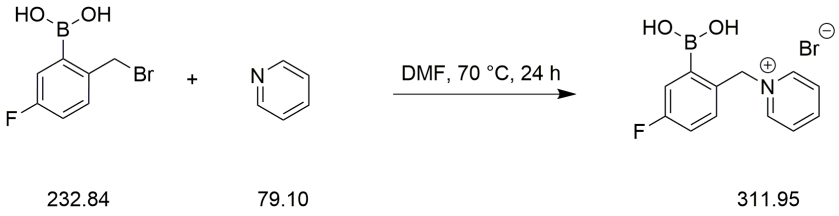

232.84 79.10 311.95

The title compound was isolated as a pale yellow odorless solid: 142 mg (71% yield).

^{1}H NMR (400 MHz, DMSO-d_6) δ 6.02 (s, 2H), 7.32 (dt, J = 2.92, 8.52 Hz 1H), 7.47 (q, J = 4.64 Hz 1H), 7.55 (q, J = 4.19 Hz, 1H), 8.13 (q, J = 4.79 Hz, 2H), 8.60 (m, 3H), 8.99 (d, J = 5.56 Hz, 2H). **^{13}C{^{1}H} NMR** (100 MHz, DMSO-d_6) δ 62.59, 117.17 (d, J = 21.45 Hz), 121.69 (d, J = 19.63 Hz), 128.02, 132.95 (d, J = 7.95 Hz), 133.62 (d, J = 2.90 Hz), 144.74, 145.75, 162.09 (d, J = 247.07 Hz). **^{19}F{^{1}H} NMR** (188 MHz, DMSO-d_6) δ -113.77. **IR** (ATR) $\tilde{\nu}$ 3160(w), 3045(w), 1489(m), 1413(m), 1329(s), 1213(m), 1063(m), 772(m), 684(s), 547(s). **Elemental analysis** calculated for $C_{12}H_{12}BBrFNO_2$: C = 46.2%, H = 3.88%, B = 3.47%, Br =

25.61%, F = 6.09%, N = 4.49%, O = 10.26%, found: C = 46.36%, H = 3.83%, N = 4.44%, Br = 24.26. **MS** (ESI+) m/z calculated for $C_{12}H_{12}BFNO_2$ [M-Br]+: 232.1; found: 232.1. **Melting point**: 173.9-177.7. °C (decomposition).

1-(2-borono-3-fluorobenzyl)pyridin-1-ium bromide; 3-F-*o*-BBpy (3)

232.84 79.10 311.95

The title compound was isolated as a pale green odorless solid: 138 mg total (69% yield).

^{1}H NMR (200 MHz, DMSO-d_6) δ 5.85 (s, 2H), 7.21 (q, J = 6.24, 2H), 7.46 (q, J = 7.38 Hz 1H), 8.17 (t, J = 7.08 Hz, 2H), 8.63 (t, J = 7.81 Hz, 1H), 8.79 (s, 2H), 8.99 (d, J = 5.54 Hz, 2H). **^{13}C{^{1}H} NMR** (100 MHz, DMSO-d_6) δ 63.76, 116.12 (d, J = 24.8 Hz), 125.84 (d, J = 2.6 Hz), 128.71, 131.7 (d, J = 8.7 Hz), 138.03 (d, J = 10.4 Hz), 145.49, 146.58, 164.71 (d, J = 239.8 Hz). **^{19}F{^{1}H} NMR** (188 MHz, DMSO-d_6) δ -104.06**. IR** (ATR) $\tilde{\nu}$ 3168(w), 3061(w), 1243(s), 978(m), 769(m), 697(s), 612(s), 517(s). **Elemental analysis** calculated for $C_{12}H_{12}BBrFNO_2$: C = 46.2%, H = 3.88%, B = 3.47%, Br = 25.61%, F = 6.09%, N = 4.49%, O = 10.26%, found: C = 46.23%, H = 3.86%, N = 4.53%, Br = 25.49%. **MS** (ESI+) m/z calculated for $C_{13}H_{14}BFNO_2$ [M(monomethylester)-Br]+: 246.1; found: 246.1. **Melting point**: 170.3-173.3 °C (decomposition).

1-(2-borono-5-(trifluoromethyl)benzyl)pyridin-1-ium bromide; 5-CF_3-*o*-BBpy (4)

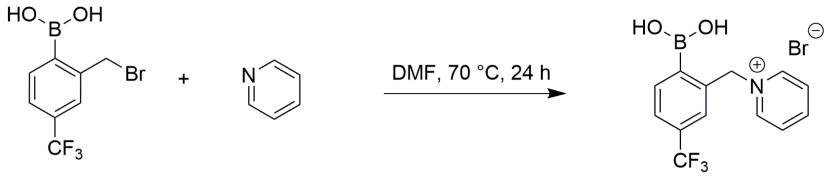

282.85 79.10 361.95

The title compound was isolated as a white and odorless solid: 146 mg total (63% yield).

^{1}H NMR (200 MHz, DMSO-d_6) δ 6.08 (s, 2H), 7.80 (m, 2H), 7.97 (d, J = 7.71 Hz 1H), 8.14 (t, J = 7.12, 2H), 8.61 (t, J = 7.17Hz, 1H), 8.72 (s, 2H), 9.01 (d, J = 5.72 Hz, 2H). **^{13}C{^{1}H} NMR**

(100 MHz, DMSO-d_6) δ 63.27, 123.01, 125.54 (d, J = 3.5 Hz), 125.71, 127.0 (d, J = 3.5 Hz), 128.59, 130.87 (d, J = 32.1 Hz), 137.71 (d, J = 214.8 Hz), 145.45, 146.43. **^{19}F{^{1}H} NMR** (188 MHz, DMSO-d_6) δ -61.77. **IR** (ATR) $\tilde{\nu}$ 3204(w), 3049(w), 1630(w), 1481(s), 1373(m), 1324(s), 1134(s), 1077(s), 1099(s), 681(s). **Elemental analysis** calculated for $C_{13}H_{12}BBrF_3NO_2$: C = 43.14%, H = 3.34%, B = 2.99%, Br = 22.08%, F = 15.75%, N = 3.87%, O = 8.84%, found: C = 43.17%, H = 3.33%, N = 3.75%, Br = 21.68%. **MS** (ESI+) m/z calculated for $C_{13}H_{12}BF_3NO_2$ [M-Br]+: 282.1; found: 282.1. **Melting point** 179.6-180.2 °C (decomposition).

1-(2-boronobenzyl)pyridin-1-ium bromide; *o*-BBpy (5)

213.98 79.10 293.02

The title compound was isolated as a white and odorless solid: 185 mg total (99% yield).

^{1}H NMR (400 MHz, D_2O) δ 5.89 (s, 2H), 7.48 (m, 3H), 7.65 (d, J = 3.42 Hz, 1H), 7.94 (t, J = 7.1 Hz, 2H), 8.45 (t, J = 7.1 Hz 1H), 8.73 (d, J = 5.6 Hz, 2H). **^{13}C{^{1}H} NMR** (100 MHz, D_2O) δ 64.55, 127.91, 129.35, 130.87, 130.98, 134.70, 135.82, 144.79, 145.81. **IR** (ATR) $\tilde{\nu}$ 3351(w), 3207(m), 3053(m), 1630(m), 1489(m), 1365(m), 1332(s), 1065(m), 1010(m), 781(s), 682(s), 647(s), 574(s). **Elemental analysis** calculated for $C_{12}H_{13}BBrNO_2$: C = 49.03%, H = 4.46%, B = 3.68%, Br = 27.18%, N = 4.77%, O = 10.89%, found: C = 49.17%, H = 4.46%, Br = 26.91%, N = 4.78%. **MS** (ESI+) m/z calculated for $C_{13}H_{15}BNO_2$ [M(monomethylester)-Br]+: 228.1; found: 228.1. **Melting point** 183.5-184.9 °C (decomposition).

1-(3-fluorobenzyl)pyridin-1-ium bromide; 3-F-Bpy (6)

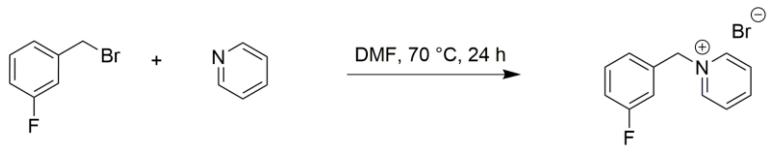

189.03 79.10 268.13

The title compound was isolated as a white and odorless solid: 129 mg total (75% yield).

^{1}H NMR (400 MHz, D_2O) δ 5.69 (s, 2H), 7.11 (m, 3H), 7.36 (m, 1H), 7.95 (t, J = 7.14Hz, 2H), 8.44 (m, 1H), 8.78 (d, J = 5.48Hz, 2H). **^{13}C{^{1}H} NMR** (100 MHz, D_2O) δ 63.82, 115.81 (d, J

= 22.75 Hz), 116.75 (d, *J* = 21.16 Hz), 124.86 (d, *J* = 2.97Hz), 128.43, 131.39 (d, *J* = 8.67 Hz), 134.81 (d, *J* = 7.78 Hz), 144.43, 146.19, 162.81 (d, *J* = 245.49 Hz). **^{19}F{^{1}H} NMR** (188 MHz, D_2O) *δ* -112.66. **IR** (ATR) *ṽ* 3002(w), 1630(m), 1587(m), 1484(m), 1252(m), 1154(m), 775(s), 742(s), 698(s), 681(s). **Elemental analysis** calculated for $C_{12}H_{11}BrFN$: C = 53.75%, H = 3.57%, B = 4.14%, Br = 29.80%, F = 7.09%, N = 5.22%, found: C = 54.33%, H = 4.16%, Br = 29.74%, N = 5.27%. **MS** (ESI+) m/z calculated for $C_{12}H_{11}FN$ [M-Br]+: 188.1; found: 188.1. **Melting point** 148.3-148.9 °C (decomposition).

1-(2-borono-5-fluorobenzyl)-3-bromopyridin-1-ium bromide; 5-F-*o*-BBBrpy (7)

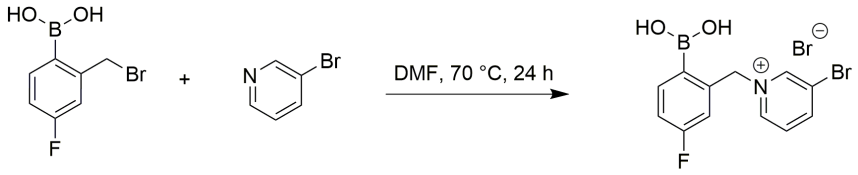

232.84 158 390.84

The title compound was isolated as a white and odorless solid: 218 mg total (87% yield).

^{1}H NMR (400 MHz, D_2O) *δ* 5.91 (s,1H), 7.18 (m, *J* = 2.19 Hz, 1H), 7.70 (d, *J* = 2.68 Hz, 1H), 7.70 (d, *J* = 15.45 Hz, 1H), 7.86 (d, *J* = 14.56 Hz, 1H), 7.86 (d, *J* = 2.12 Hz, 1H), 8.64 (d, *J* = 8.52 Hz, 1H), 8.77 (d, *J* = 6.20 Hz, 1 H), 8.98 (s,1H). **^{13}C{^{1}H} NMR** (100 MHz, D_2O) *δ* 64.15, 116.33 (d, *J* = 19.79 Hz), 118.14 (d, *J* = 21.97 Hz), 122.70, 128.46, 137.43 (d, *J* = 8.27 Hz), 138.06 (d, *J* = 7.37 Hz), 143.52, 145.73, 148.67, 163.79 (d, *J* = 249.32 Hz). **^{19}F{^{1}H} NMR** (188 MHz, D_2O) *δ* -110.19. **Elemental analysis** calculated for $C_{11}H_{12}BBr_2FNO_2$: C = 36.88%, H = 2.84%, B = 2.77%, Br = 40.89%, F = 4.86%, N = 3.58%, O = 8.19 found: C = 37.13%, H = 2.82%, Br = 40.89%, N = 3.67%.

1-(2-borono-5-(trifluoromethyl)benzyl)-3-bromopyridin-1-ium bromide; 5-CF_3-*o*-BBBrpy (8)

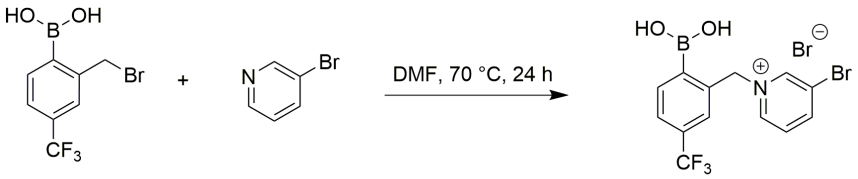

282.85 158 440.85

The title compound was isolated as a pale white and odorless solid: 130 mg total (46% yield).

^{1}H NMR (400 MHz, D_2O) δ 5.96 (s, 2H), 7.75 (d, J = 5.44 Hz, 2H), 7.82 (d, J = 8.16 Hz, 1H), 7.87 (t, J = 7.22 Hz, 1H), 8.66 (d, J = 8.32 Hz, 1H), 8.77 (d, J = 6.04 Hz, 1H), 9.00 (s, 1H). **^{13}C{^{1}H} NMR** (100 MHz, D_2O) δ 64.33, 122.83, 126.20 (d, J = 3.77 Hz), 127.56, 128,59, 135.45, 135.98, 143.56, 145.84, 148.85 **^{19}F{^{1}H} NMR** (377 MHz, D_2O) δ -62.88. **IR** (ATR) $\tilde{\nu}$ 3431(w), 3245(m), 1083(s). **Elemental analysis** calculated for $C_{13}H_{11}BBr_2F_3NO_2$: C = 35.42%, H = 2.52%, B = 2.45%, Br = 36.25%, F = 12.93%, N = 3.18%, O = 7.26% found: C = 35.23%, H = 2.34%, Br = 36.12%, N = 3.08%.

Synthesis of 5-fluorobenzo[*c*][1,2]oxaborol-1(3*H*)-ol; 5-F-*o*-Boxab (9)

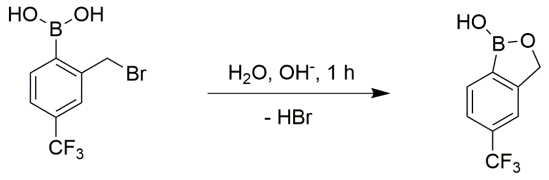

282.85 151.93

For the synthesis of 5-fluorobenzo[*c*][1,2]oxaborol-1(3*H*)-ol the following chemicals were purchased and used as described: 2-bromomethyl-4-fluoromethylphenylboronic acid was synthesized as described before.

A centrifuge vial was loaded with 100 mg (0.43 mmol) 2-bromomethyl-4-fluoromethylphenylboronic acid dissolved in 1.25 mL KOH solution (14%) and a stirring bar. The solution was stirred at room temperature for 1 hour. After cooling a pH of 2 was adjusted by adding hydrochloric acid (20%). The white precipitate which was formed was collected by centrifugation and washed with 2 mL of deionized water. The solid was again washed two times with deionized water and centrifuged. The title compound was isolated as a white odorless powder which was then dried overnight in high vacuum: 43.5 mg total (65% yield).

^{1}H NMR (400 MHz, DMSO-d_6) δ 4.96 (s, 2H), 7.15 (m, J = 3.37 Hz, 1H), 7.36 (q, J = 3.67 Hz, 1H), 7.75 (q, J = 4.65 Hz, 1H), 9.24 (s, 1H). **^{13}C{^{1}H} NMR** (100 MHz, DMSO-d_6) δ 69.58 (d, J = 3.09 Hz), 108.50 (d, J = 22.09 Hz), 114.52 (d, J = 21.80 Hz), 132.71 (d, J = 9.39 Hz), 156.82 (d, J = 8.87 Hz), 164.26 (d, J = 246.43 Hz). **^{19}F{^{1}H} NMR** (188 MHz, D_2O) δ -110.79.

General Procedure for the Synthesis of Bipyridinium Bromides

The following chemicals were purchased and used as received: 4,4'-bipyridine, 1,2-di(4-pyridyl)ethylene (Alfa Aesar), acetone (Roth) and diethyl ether (VWR). Dimethylformamide (Roth) was purified and dried prior use. 3,3'-bipyridine, 3,4'-bipyridine, 4,4′-azopyridine, 2-bromomethyl-4-fluorophenylboronic acid and 2-bromomethyl-4-(trifluoromethyl)phenylboronic acid were synthesized as described before.

In general, and not otherwise mentioned, a mini vial with an attached syringe screw cap was loaded with 1.1 mmol appropriate phenylboronic acid, 0.45 mmol bipyridine derivative, 4 mL dry DMF and a stirring bar. The initial and colorless solution was then flushed with nitrogen via syringe for 15 minutes and was then heated and stirred at 65 °C for 6 days and usually a visible color change from slightly to intensive yellow. Next, the reaction mixture was mixed with appropriate amount of acetone and diethyl ether so that precipitation of the crude product occurred. After centrifugation the overlaying phase was separated, then concentrated in vacuo and mixed with diethyl ether to obtain another fraction of the product. The combined solid fractions were then washed two times in 20 mL acetone under vigorous stirring at 30 °C. A final washing step was performed in 20 mL diethyl ether and the use of ultrasonic sound. The appropriate bipyridinium bromide was obtained after centrifugation and drying under a stream of nitrogen.

***N*,*N*'-4,4'-bis-(benzyl-5-fluoro-2-boronic acid)-bipyridinium dibromide; F-4,4'-*o*-BBV (10)**

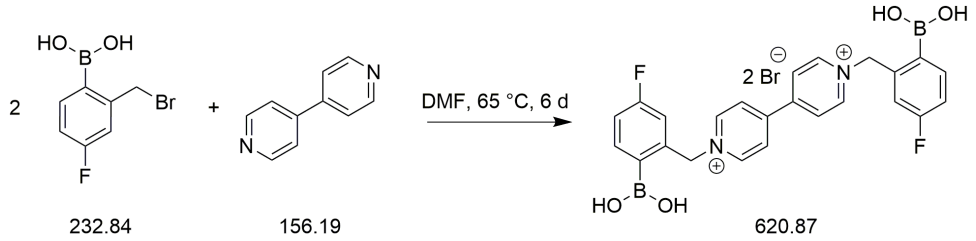

The title compound was isolated as a pale yellow and odorless solid: 278 mg total (99% yield).

^{1}H NMR (400 MHz, DMSO-d$_6$) δ 6.17 (s, 4H), 7.28 (m, 4H), 7.9 (dd, J = 8.2, 6.8 Hz 2H), 8.54 (s, 4H), 8.75 (d, J = 7.3 Hz, 4H), 9.35 (d, J = 7 Hz, 4H); **^{13}C{^{1}H} NMR** (100 MHz, DMSO-d$_6$) δ 62.81, 115.39 (d, J = 19.39 Hz), 116.72 (d, J = 21.39 Hz), 126.81, 138.20 (d, J = 8.07 Hz), 140.60 (d, J = 7.33 Hz), 145.88, 149.03, 163.32 (d, J = 247.81 Hz); **^{19}F {^{1}H} NMR** (188 MHz, DMSO-d$_6$) δ -110.45; **IR** (ATR) $\tilde{\nu}$ 3347 (w), 3029 (w), 1638 (m), 1349 (s), 1225 (m), 1027 (m),

844 (m), 753 (s), 540 (s); **Elemental analysis** calculated for $C_{24}H_{22}B_2Br_2F_2N_2O_4$: C = 46.35%, H = 3.57%, B = 3.48%, Br = 25.70%, F = 6.11%, N = 4.50%, O = 10.29%, found: C = 45.66%, H = 4.18%, N = 4.76%; **HRMS** ESI-TOF m/z calculated for $C_{24}H_{21}B_2F_2N_2O_4$ [M-H]+: 461.1670 found: 461.1638.

***N*,*N*'-3,3'-bis-(benzyl-5-fluoro-2-boronic acid)-bipyridinium dibromide; F-3,3'-*o*-BBV (11)**

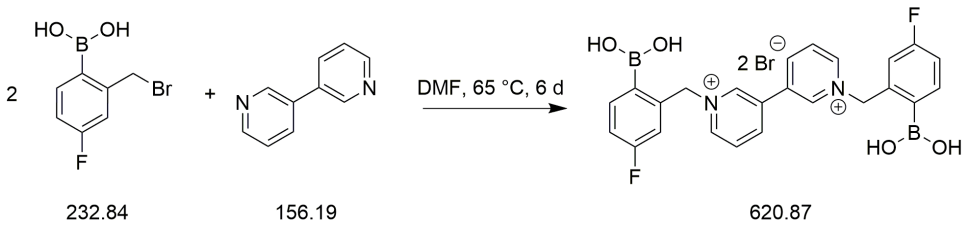

The title compound was isolated as a dirty white and odorless solid: 151 mg total (54% yield).

^{1}H NMR (400 MHz, DMSO-d_6) δ 6.15 (s, 4H), 7.16 (dd, J = 2.44, 10.24 Hz, 2H), 7.28 (dt, J = 2.46, 8.57 Hz, 4H), 7.89 (m, 2H), 8.35 (m, 2H), 8.59 (s, 4H), 9.05 (d, J = 8.32 Hz, 2H), 9.09 (d, J = 6.16 Hz, 2H); **^{13}C{^{1}H} NMR** (150 MHz, D_2O) δ 64.51, 116.53 (d, J = 19.62 Hz), 118.22 (d, J = 21.76 Hz), 128.72, 134.26, 137.57 (d, J = 8.27 Hz), 138.10 (d, J = 7.55 Hz), 143.24, 144.80, 145.59, 163.88 (d, J = 249.02 Hz); **^{19}F{^{1}H} NMR** (188 MHz, DMSO-d_6) δ -110.42; **IR** (ATR) $\tilde{\nu}$ 3268 (m), 3057 (m), 2945 (w), 1582 (m), 1330 (s), 1009 (s), 677 (s), 640 (s), 525 (s); **Elemental analysis** calculated for $C_{24}H_{22}B_2Br_2F_2N_2O4$: C = 46.35%, H = 3.57%, B = 3.48%, Br = 25.70%, F = 6.11%, N = 4.50%, O = 10.29%, found: C = 43.93%, H = 3.85%, N = 5.72%. **HRMS** ESI-TOF m/z calculated for $C_{24}H_{21}B_2F_2N_2O_4$ [M-H]+: 461.1670 found: 461.1667.

***N*,*N*'-3,4'-bis-(benzyl-5-fluoro-2-boronic acid)-bipyridinium dibromide; F-3,4'-*o*-BBV (12)**

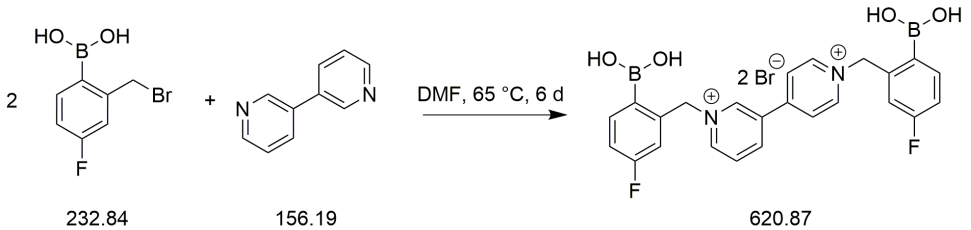

The title compound was isolated as a yellowish odorless solid: 229 mg total (82% yield).

^{1}H NMR (400 MHz, D_2O) δ 6.15 (s, 2H), 6.17 (s, 2H), 7.20 (m, 2H), 7.29 (m, 2H), 7.89 (q, J = 7.05 Hz, 2H), 8.36 (d, J = 1.76 Hz, 1H) 8.56 (s, 2H), 8.57 (s, 2H), 8.67 (d, J = 6.8 Hz, 2H), 9.14 (d, J = 6.16 Hz, 1H), 9.20 (d, J = 8.24 Hz, 1H), 9.32 (d, J = 6.80 Hz, 2H), 9.91 (s, 1H); **^{13}C{^{1}H} NMR** (100 MHz, DMSO-d_6) δ 62.68, 63.32, 115.22 (d, J = 8.47 Hz), 115.41 (d, J = 8.36 Hz), 116.45 (d, J = 7.92 Hz), 116.66 (d, J = 8.10 Hz), 126.13, 128.44, 131.13, 133.65, 138.07 (d, J = 8.19 Hz), 138.24 (d, J = 8.04 Hz), 140.68 (d, J = 7.45 Hz), 140.85 (d, J = 7.37 Hz), 144.86, 145.71, 146.17, 148.95, 162.10 (d, J = 2.34 Hz), 164.57 (d, J = 1.98 Hz); **^{19}F{^{1}H} NMR** (188 MHz, DMSO-d_6) δ -110.54, -110.49; **IR** (ATR) $\tilde{\nu}$ 3337 (m), 3048 (m), 1640 (m), 1601 (m), 1365 (s), 1277 (s), 1223 (s), 1154 (s), 526 (s); **Elemental analysis** calculated for $C_{24}H_{22}B_2Br_2F_2N_2O_4$: C = 46.35%, H = 3.57%, B = 3.48%, Br = 25.70%, F = 6.11%, N = 4.50%, O = 10.29%, found: C = 46.25%, H = 3.86%, N = 5.89%; **HRMS** ESI-TOF m/z calculated for $C_{24}H_{21}B_2F_2N_2O_4$ [M-H]+: 461.1670 found: 461.1651.

***N*,*N*'-4,4'-bis-(benzyl-5-(trifluoromethyl)-2-boronic acid)-bipyridinium dibromide; CF$_3$-4,4'-*o*-BBV (13)**

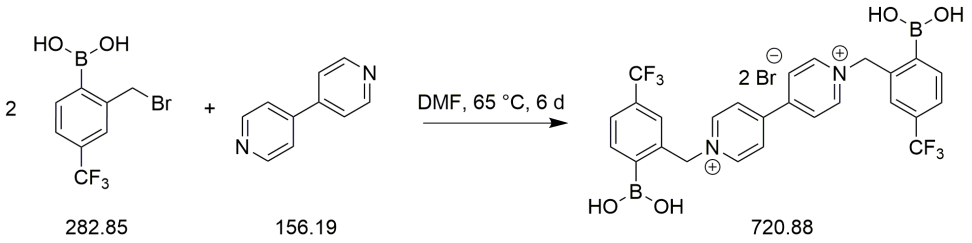

282.85 156.19 720.88

The title compound was isolated as a yellowish odorless solid: 133 mg total (41% yield).

^{1}H NMR (600 MHz, DMSO-d_6) δ 6.21 (s, 4H), 7.82 (d, J = 7.86 Hz, 2H), 7.87 (s, 2H), 8.01 (d, J = 7.86 Hz, 2H), 8.77 (d, J = 7.02 Hz, 8H), 9.35 (d, J = 6.96 Hz, 4H); **^{13}C{^{1}H}** NMR (150 MHz, DMSO-d_6) δ 62.80, 122.95, 124.76, 125.15 (d, J = 3.33 Hz), 126.59 (d, J = 3.40 Hz), 126.76, 136.24, 138.15, 145.86, 148.90; **^{19}F{^{1}H} NMR** (188 MHz, DMSO-d_6) δ -61.71; **Elemental analysis** calculated for $C_{26}H_{21}B_2Br_2F_6N_2O_4$: C = 43.32%, H = 2.94%, B = 3.00%, Br = 22.17%, F = 15.81%, N = 3.89%, O = 8.88%, found: C = 43.12%, H = 3.07%, N = 3.85%, Br = 21.26%.

_N_,_N_'-3,3'-bis-(benzyl-5-(trifluoromethyl)-2-boronic acid)-bipyridinium dibromide; CF_3-3,3'-_o_-BBV (14)

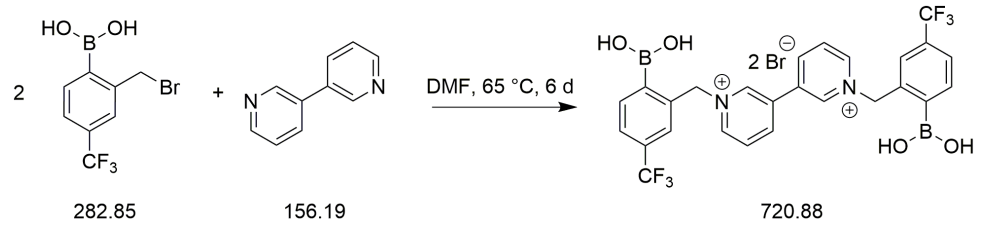

The title compound was isolated as a dirty white and odorless solid: 128 mg total (39% yield). **^{1}H NMR** (400 MHz, DMSO-d_6) δ 6.20 (s, 4H), 7.82 (t, J = 7.78 Hz, 4H), 8.01 (d, J = 7.76 Hz, 2H), 8.38 (q, J = 4.77 Hz, 2H), 8.80 (s, 4H), 9.07 (t, J = 8.10 Hz, 4H), 9.84 (s, 2H); **^{19}F{^{1}H} NMR** (188 MHz, DMSO-d_6) δ -61.65; **Elemental analysis** calculated for $C_{26}H_{21}B_2Br_2F_6N_2O_4$: C = 43.32%, H = 2.94%, B = 3.00%, Br = 22.17%, F = 15.81%, N = 3.89%, O = 8.88%, found: C = 42.96%, H = 3.11%, N = 3.70%, Br = 20.70%.

_N_,_N_'-3,4'-bis-(benzyl-5-(trifluoromethyl)-2-boronic acid)-bipyridinium dibromide; CF_3-3,4'-_o_-BBV (15)

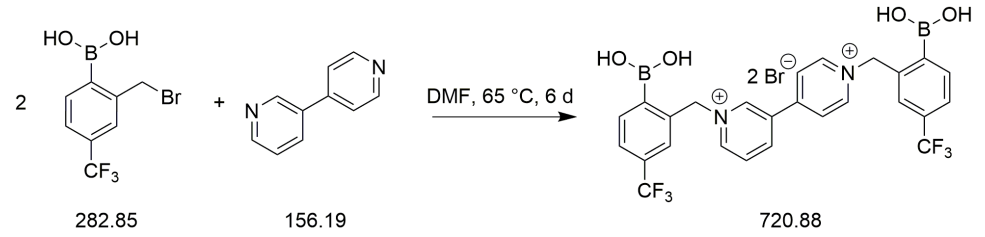

The title compound was isolated as a yellowish odorless solid: 143 mg total (44% yield).

^{1}H NMR (400 MHz, DMSO-d_6) δ 6.22 (s, 2H), 6.24 (s, 2H), 7.84 (m, 4H), 8.02 (m, 2H), 8.37 (q, J = 4.80 Hz, 1H), 8.73 (d, J = 6.96 Hz, 2H), 8.79 (d, J = 14.80 Hz, 4H), 9.10 (d, J = 6.16 Hz, 1H), 9.24 (d, J = 8.36 Hz, 1H), 9.36 (d, J = 6.96 Hz, 2H), 10.02 (s,1H); **^{13}C{^{1}H} NMR** (100 MHz, DMSO-d_6) δ 63.15, 63.83, 123.01, 125.61, 126.51, 128.85, 133.82, 136.68 (d, J = 17.14 Hz), 138.69 (d, J = 22.85 Hz), 145.42, 146.17, 149.36, 162.80; **^{19}F{^{1}H} NMR** (188 MHz, DMSO-d_6) δ -61.65, -61.70; **Elemental analysis** calculated for $C_{26}H_{21}B_2Br_2F_6N_2O_4$: C = 43.32%, H = 2.94%, B = 3.00%, Br = 22.17%, F = 15.81%, N = 3.89%, O = 8.88%, found: C = 42.28%, H = 3.35%, N = 4.03%, Br = 20.32%.

1-(2-borono-5-(trifluoromethyl)benzyl)-1'-(2-borono-5-fluorobenzyl)-[4,4'-bipyridine]-1,1'-diium dibromide; CF_3/F-4,4'-*o*-BBV (16)

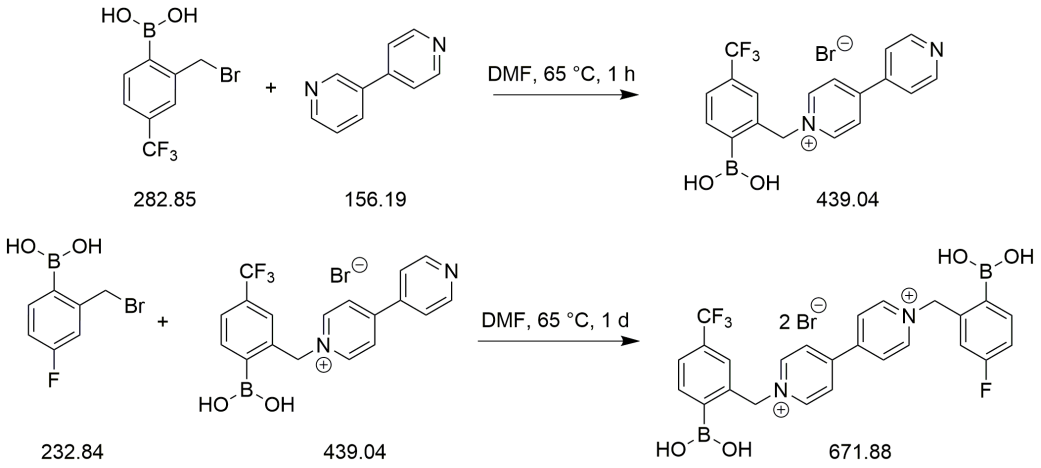

For the synthesis of unsymmetrical 1-(2-borono-5-(trifluoromethyl)benzyl)-1'-(2-borono-5-fluorobenzyl)-[4,4'-bipyridine]-1,1'-diium the following chemicals were purchased and used as described: 4,4'-bipyridine (Alfa Aesar), acetone (Roth) and diethyl ether (VWR) were used as received. Dimethylformamide (Roth) was purified and dried prior use. 2-bromomethyl-4-fluorophenylboronic acid and 2-bromomethyl-4-(trifluoromethyl)phenylboronic acid were synthesized as described before.

A mini vial with an attached syringe screw cap was loaded with 110mg (0.7 mmol) 4,4'-bipyridine dissolved in 0.5 mL dry DMF, a stirring bar and was then flushed with nitrogen via syringe for 15 minutes and was then heated and stirred at 65 °C. A degassed solution of 100 mg (0.35 mmol) 2-bromomethyl-4-(trifluoromethyl)phenylboronic acid in 1 mL dry DMF was added drop by drop to the vial within 10 minutes. After the addition the reaction was stirred and heated for one more hour. Next, the yellow mixture was dropped into a mixture of 20 mL acetone and diethyl ether, respectively, which induced precipitation of the mono alkylated product. After washing two-times with diethyl ether and drying in high vacuum, 90 mg (59% yield) of the precursor were obtained. For the next alkylation step, a mini vial with an attached syringe screw cap was loaded with 70 mg (0.16 mmol) of the mono-alkylated precursor, 57 mg (0.24 mmol) dissolved in 1 mL dry DMF and a stirring bar. The solution was flushed with nitrogen via syringe for 15 minutes and was then heated and stirred at 65 °C for three days. After cooling the mixture was transferred to a centrifuge vial and 10 mL acetone were added which induced precipitation of the crude dialkylated product and was consecutively centrifuged. The isolated product was then washed two-times in 20 mL acetone under vigorous

stirring at 30 °C. A final washing step was performed in 20 mL diethyl ether and the use of ultrasonic sound. The title bipyridinium salt was obtained after centrifugation and drying under a stream of nitrogen as a yellowish odorless solid: 85 mg (79% yield) with respect to mono-alkylated precursor).

^{1}H NMR (200 MHz, DMSO-d_6) δ 6.15 (s, 2H), 6.18 (s, 2H), 7.26 (m, 2H), 7.92 (m, 4H), 8.58 (s, 2H), 8.72 (d, J = 6.70 Hz, 4H) 8.81 (s, 2H), 9.32 (d, J = 6.64 Hz 4H); **^{19}F{^{1}H} NMR** (188 MHz, DMSO-d_6) δ -61.71, -110.46.

4,4'-(ethane-1,2-diyl)bis(1-(2-borono-5-fluorobenzyl)pyridin-1-ium) dibromide; F-4,4'-*o*-BBEpy (17)

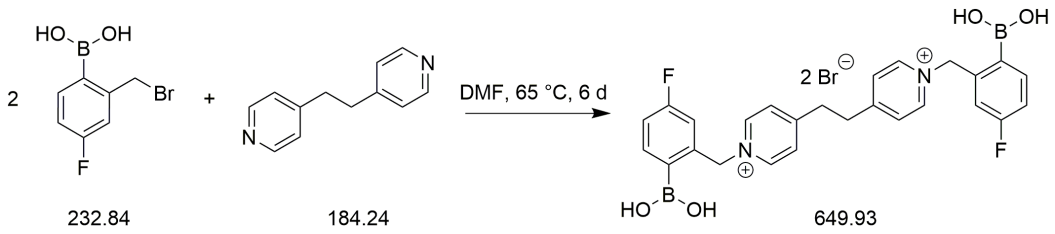

The title compound was isolated as a yellowish odorless solid: 256 mg total (90% yield).

^{1}H NMR (400 MHz, DMSO-d_6) δ 2.49 (m, J = 1.79 Hz, 4H), 6.00 (s, 4H), 7.18 (q, J = 4.25 Hz, 2H), 7.28 (m, J = 3.95 Hz,2H), 7.86 (q, J = 5.01 Hz, 2H), 8.10 (d, J = 6.84 Hz, 4H), 8.47 (s, 4H), 8.95 (s, 2H), 8.96 (s, 2H); **^{13}C{^{1}H} NMR** (100 MHz, DMSO-d_6) δ 33.78, 62.09, 115.25 (d, J = 19.32 Hz), 116.64 (d, J = 21.29 Hz), 127.79, 138.10 (d, J = 8.14 Hz), 140.80 (d, J = 7.29 Hz), 144.40, 160.48, 163.24 (d, J = 247.72 Hz); **^{19}F{^{1}H} NMR** (188 MHz, DMSO-d_6) δ -110.61.

4,4'-(diazene-1,2-diyl)bis(1-(2-borono-5-fluorobenzyl)pyridin-1-ium) dibromide; F-4,4'-*o*-BBazpy (18)

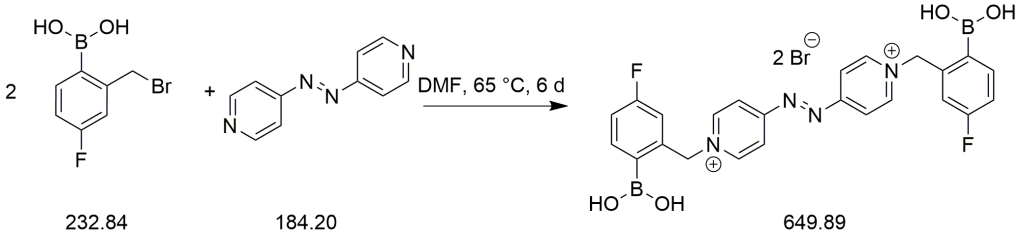

The title compound was isolated as a dark-brown odorless solid: 222 mg total (76% yield).

^{1}H NMR (400 MHz, DMSO-d_6) δ 5.72 (s), 7.07 (m), 7.21 (m), 7.85 (t, J = 7.52 Hz, 3H), 8.34 (s, 6H), 8.46 (d, J = 7.08 Hz, 4H); **^{13}C{^{1}H} NMR** (100 MHz, DMSO-d_6) δ 60.31, 115.25 (d, J = 19.49 Hz), 116.13 (d, J = 21.23 Hz), 38.37 (d, J = 8.14 Hz), 142.52 (d, J = 7.23 Hz), 157.85, 163.72 (d, J = 247.40 Hz); **^{19}F{^{1}H} NMR** (188 MHz, DMSO-d_6) δ -110.79.

ADVANCED RECEPTOR PROPERTIES

pH Titration Experiments for pK_a Determination of Boronic Acid Receptors

Potentiometric pH titration experiments were conducted using a Mettler Toledo-S20-SevenEasy pH-meter at 22-23 °C. At first, to solutions of **1-5** (8 mM each) in deionized water, a drop of conc. HCl was added with a resulting pH of ~ 2. Under stirring, 50 µL aliquots of aqueous base solution (100 mM NaOH and 150 mM NaCl) were added via a 1000 µL Eppendorf Research® pro pipette (50 µL dispensing mode) while the resulting pH of the solution was recorded at the equilibrium. The weak acid-strong base titration was conducted until a pH of ~ 12 was reached. The resulting pK_a value of each boronic acid-containing receptor molecule was taken from the halfway point of each graph.

Photostability Testing of Boronic Acid Receptors

All UV/vis absorption spectra were recorded on an Analytik Jena UV-vis Specord S600 spectrometer and the use of one single 10 mm Hellma QS® cuvette within a wavelength range of 200 to 800 nm (WinASPECT software, integration time = 75 ms, accumulation = 40). A fresh HEPES buffer solution (50 mM, pH 7.4) was used as the external reference before measurement.

A fresh solution of **1**, **2**, **3**, **4, 10, 11 and 12** (50 µM) was prepared by dissolving in aqueous. HEPES buffer solution (50 mM, pH 7.4). The solution was then divided into two aliquots (2.5 mL each), whereupon one of the two aliquots was stored in the dark at room temperature during the whole experiment duration. This was done to investigate the stability of the receptor solution under light-protected conditions. UV-vis absorption spectra of the second aliquot was recorded to determine a possible photo-degradation process under laboratory ambient light by measuring in the opened UV-vis spectrometer. Spectra of the aliquots were recorded at the start and after 24 hours, respectively. Resulting spectra are illustrated by Figure S 1 – 7 which indicate no significant change in absorption for compound **1** whereas the bipyridines are sensitive to light (upcoming absorption band at ~ 450 nm).

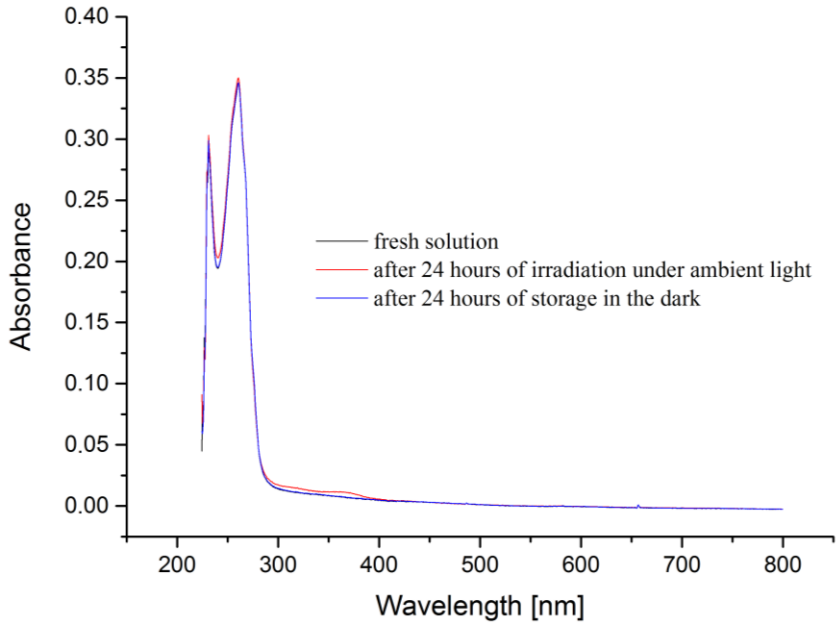

Figure S 1: UV/vis absorption spectra of 5-F-*o*-BBpy (1) for testing the robustness under ambient light and in the dark.

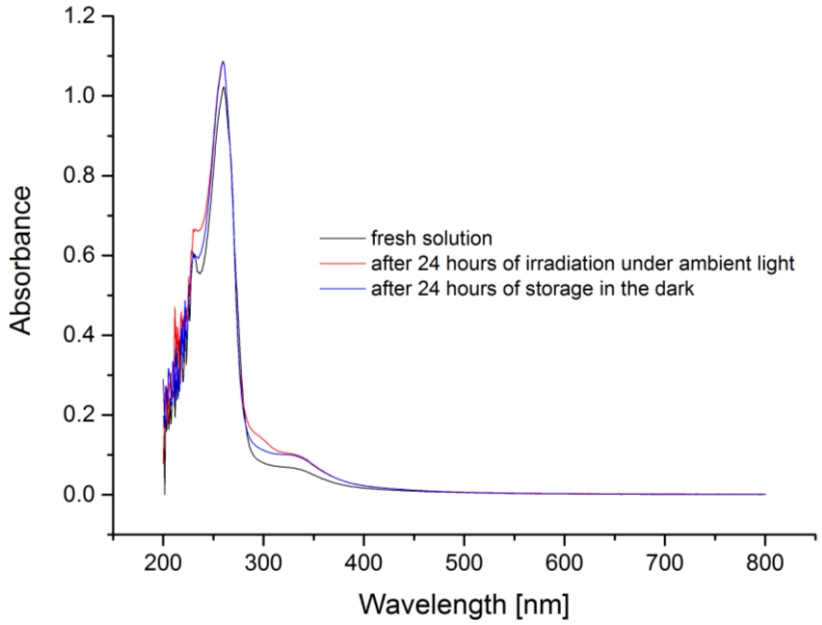

Figure S 2: UV/vis absorption spectra of 4-F-*o*-BBpy (2) for testing the robustness under ambient light and in the dark.

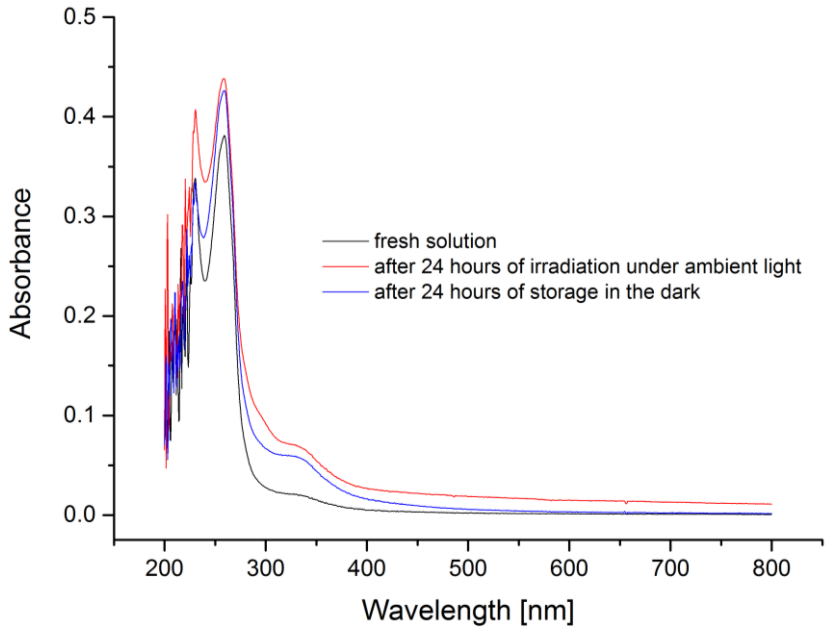

Figure S 3: UV/vis absorption spectra of 3-F-*o*-BBpy (3) for testing the robustness under ambient light and in the dark.

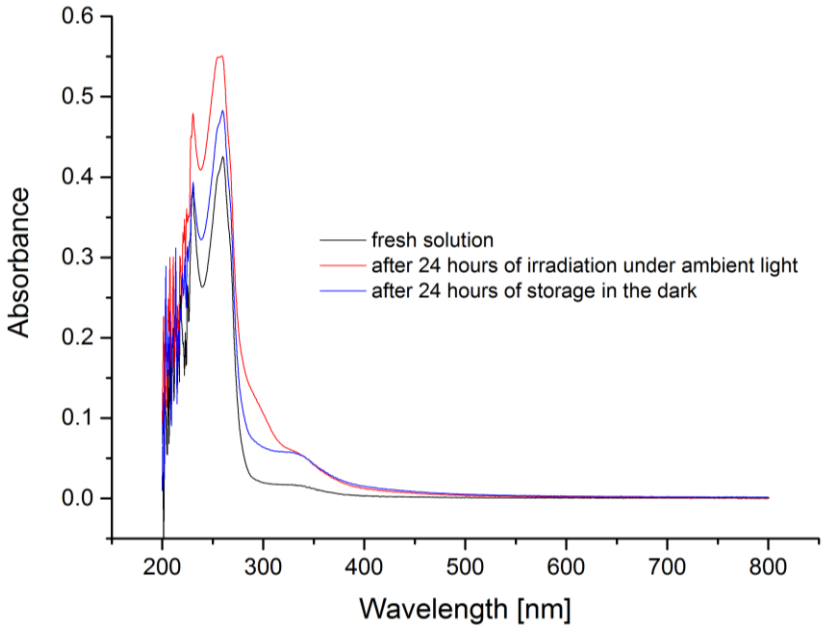

Figure S 4: UV/vis absorption spectra of 5-CF_3-*o*-BBpy (4) for testing the robustness under ambient light and in the dark.

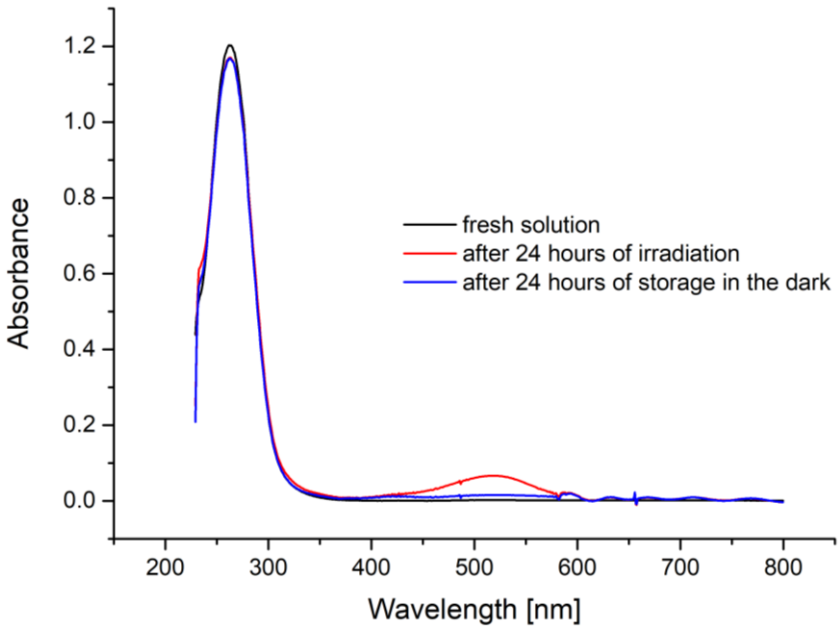

Figure S 5: UV/vis absorption spectra of F-4,4'-*o*-BBV (10) for testing the robustness under ambient light and in the dark.

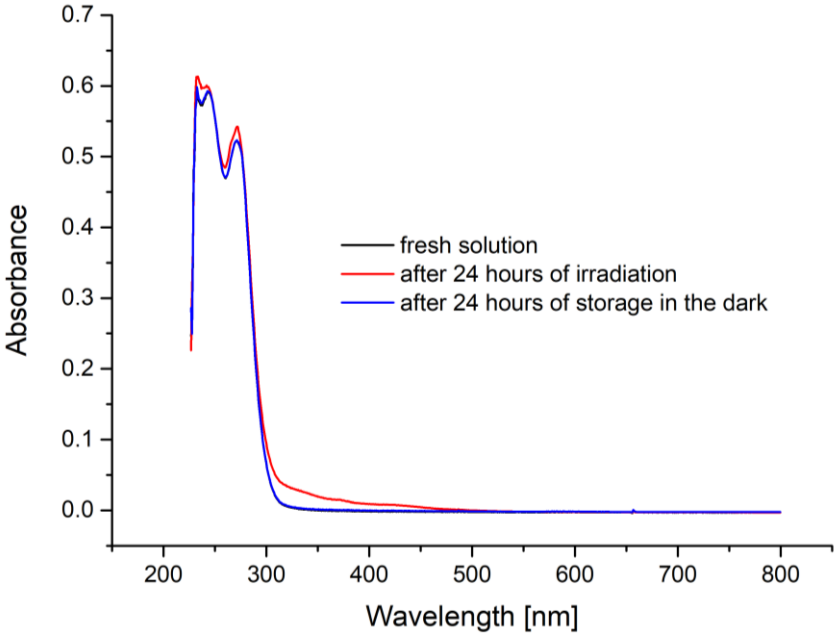

Figure S 6: UV/vis absorption spectra of F-3,3'-*o*-BBV (11) for testing the robustness under ambient light and in the dark.

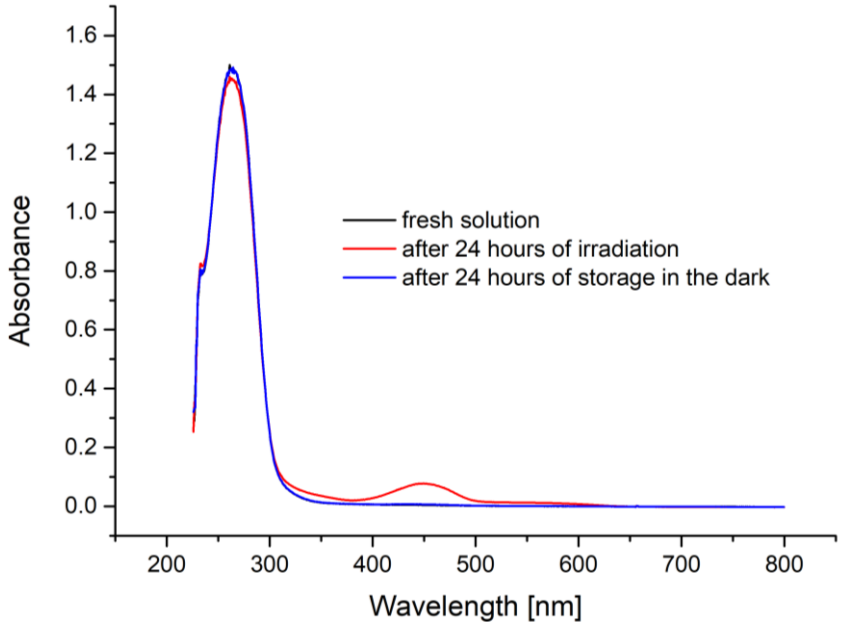

Figure S 7: UV/vis absorption spectra of F-3,4'-*o*-BBV (12) for testing the robustness under ambient light and in the dark.

^{19}F NMR SENSING EXPERIMENTS

All used receptor and analyte solutions were prepared freshly prior appropriate ^{19}F NMR measurements. All dispensing steps were performed using Eppendorf Research® pro pipettes (1000 µL and 100 µL). Norrel® high throughput and Wilmad® precision NMR tubes were used for all ^{19}F NMR experiments. 10vol% of deuterium oxide per sample was used for locking.

The following chemicals were purchased and used as received without further purification: 2-[4-(2-hydroxyethyl)piperazin-1-yl]ethanesulfonic acid, aniline, catechol, dopamine hydrochloride, D-talose, D-ribose, dihydroxyacetone, D-maltose monohydrate, D-cellobiose, *N*-acetyl-D-glucosamine, D-xylose, α-cyclodextrin, β-cyclodextrin, phenol, hydroquinone, resorcinol, D-lyxose, D-dulcitol (all Alfa Aesar), 1,3-propanediol, 3-aminopropanol, adenosine, adenosine 5´-monophosphate disodium salt, adenosine 5´-diphosphate sodium salt, adenosine 5´-triphosphate disodium salt hydrate, *N*-acetyl-D-mannosamine monohydrate, *o*-phenylendiamin, D-fructose, L-fructose, D-fructose-6-phosphate disodium salt hydrate, D-glucose, L-glucose, D-/L-glyceraldehyde, D-/L-lactic acid, D-glucose diethyl mercaptal, D-glucose-1-phosphate dipotassium salt, D-glucose-6-phosphate disodium salt hydrate, D-galactose, D-lactose monohydrate, D-mannitol, D-sorbitol, D-mannose, salicylhydroxamic acid, *N*-acetyl-D-galactosamine, D-ribose-5-phosphate disodium salt hydrate, cis/trans-1,3-cyclohexane, cis-1,2-cyclohexane, trans-1,2-cyclohexane, cis/trans-1,3-cyclopentane, cis-1,2-cyclopentane, trans-1,2-cyclopentane, trifluoroacetic acid, sucrose phosphorylase, potassium dihydrogen phosphate, Surine™ negative urine control (all Sigma Aldrich), D-/L-alanine, β-alanine, D_2O (all Roth), *N*-acetylneuraminic acid, 4,4'-*o*-BBV (all Carbosynth), L-ascorbic acid, glycine, γ-cyclodextrin, sucrose (all Merck), methanol, ethanol, ethylene glycol, and glycerol (all VWR).

The processing of the NMR data was performed using the Bruker Top Spin 3.2 software. The parameters of the used NMR machine and spectra acquisition of all performed ^{19}F NMR sensing experiments can be found in Table S 1.

Table S 1: **General acquisition parameters of the inverse gated ^{1}H-decoupled ^{19}F one-pulse experiments collected on a Bruker Avance I and Bruker Avance III spectrometer operating at 200.13 MHz (^{1}H) / 188.31 MHz (^{19}F) and 400.22 MHz (^{1}H) / 376.55 MHz (^{19}F) equipped with a 5mm QNP probe head.**

Parameter	Spectrometer	
	Bruker Avance I	Bruker Avance III
Temperature (T)	297 K	
Number of Scans (NS)	32 - 1024	
Interscan Delay (D1)	2 sec.	
Spectral Width (SW)	239 ppm	24 ppm
Acquisition Time (AQ)	0.73 sec	0.35 sec
^{19}F Transmitter Freq. Offset (O1P)	-79.8 ppm	-80 ppm
^{1}H Transmitter Freq. Offset (O1P)	4 ppm	8 ppm
^{1}H Decoupling Sequence (CPDPRG)	waltz16	waltz16
Pulse Sequence Name (PULPROG)	zgfhigqn	zgpg30

Preparation of HEPES Buffer Stock Solution (100 mM, 10% D_2O, pH = 7.4)

A 250 mL Erlenmeyer flask was loaded with 2.383 g (10 mmol) 2-[4-(2-hydroxyethyl)piperazin-1-yl]ethanesulfonic acid, approx. 80 mL of deionized water and 10 mL D_2O (NMR Lock) and the solution was made homogeneous. Subsequently, under vigorous stirring and the use of a Mettler Toledo Seven Easy pH meter a concentrated potassium hydroxide solution was added dropwise until the pH value was adjusted to exactly a physiological pH of 7.4. The buffer solution was then quantitatively transferred into a 100 mL graduated flask, filled up with deionized water and homogenized.

Cleaning of the NMR Tubes

Prior used NMR tubes were first exhausted by shaking and were then three-times flushed with a stream of deionized water and the use of an improved NMR tube cleaning device. A final wash was performed by flushing the tubes two-times with acetone. Afterwards, the tubes were dried over night at 120 °C in the glass oven.

Preparation of Receptor Stock Solutions

Fresh receptor solutions (in general 12 mM) were prepared by dissolving appropriate amount of receptor in HEPES buffer solution in a glass vial. A vortexer was used to accomplish complete dissolution. The solutions of the light-stable receptors were stored without any precaution at room temperature.

Preparation of Analyte Stock Solutions

Fresh analyte solutions (in general 600 mM) were prepared by dissolving of appropriate diol in HEPES buffer solution in a glass vials. A vortexer was used to accomplish complete dissolution. The solutions were stored without any precaution at room temperature.

Sample Preparation for qualitative Analyte Sensing assisted by ^{19}F NMR Spectroscopy

In general, 500 µL of receptor stock solutions were pipetted into 1.5 mL Eppendorf vials. Afterwards, 100 µL of receptor stock solution were added to achieve total concentrations of 10 mM receptor and 100 mM appropriate analyte, respectively. Each vial was then vortexed for five seconds to fulfill homogeneity of the samples. Next, NMR tubes were filled with 560 µL of each receptor/analyte solution, then capped and stored. After 5 hours of storage to ensure establishment of equilibrium the samples were then measured at the NMR laboratory.

Diol Sensing of binary D-fructose and D-glucose Mixtures using ^{19}F NMR Spectroscopy

^{19}F NMR measurements of binary D-fructose and D-glucose mixtures have been performed as described in the following. Stock solutions of receptor **1** (15 mM), D-fructose (30 mM) and D-glucose (30 mM) were prepared by dissolving in HEPES buffer solution (100 mM, pH 7.4, 10% D_2O). Eppendorf vials were then loaded with 400 µL receptor solution and 0-200/200-0 µL D-fructose/ D-glucose solution respectively to achieve total concentrations of 10 mM **1** and total 10 mM saccharide (ranging from 0-10 mM each). Finally, 560 µL of each Eppendorf vial was then transferred into an NMR tube for subsequent measurement at the NMR laboratory. The smallest detectable concentration of saccharide was then determined by using the LOD approach as described in the appropriate section. Thus, D-glucose could be positively detected in a mixture with D-fructose at a minimum of 1/9 mM respectively. Vice versa D-fructose could be positively detected at a minimum of 1/9 mM respectively and below.

Dependency of pH upon ^{19}F NMR Sensing Behavior of Receptor 1 and D-glucose

Stock solutions were prepared as stated above but this time with a total concentration of 12 mM for receptor **1** and 300 mM for D-glucose. The used HEPES buffer solutions were adjusted to appropriate pH using a few drops of concentrated NaOH or HCl solution. The pH values were exactly adjusted by a Mettler Toledo-S20-SevenEasy pH-meter at 23 °C. Then, 500 µL of receptor stock solutions were pipetted into 1.5 mL Eppendorf vials. Afterwards, 100 µL of receptor stock solution were added to achieve total concentrations of 10 mM receptor and 50 mM appropriate diol, respectively. Each vial was then vortexed for five seconds to fulfill homogeneity of the sample. Next, NMR tubes were filled with 560 µL of each receptor/analyte solution, then capped and stored. After 5 hours of storage to ensure establishment of equilibrium the samples were then measured at the NMR laboratory.

Determination of the Limit of Detection (LOD) and Quantification (LOQ)

The LOD for D-fructose, D-glucose and catechol detection via receptor **1** was exemplary calculated using the noise range of δ_F -118 to -120 ppm and the most intensive receptor-analyte signal of appropriate ^{19}F NMR spectrum by using the following equation: $LOD = y_{blind} + 3*s_{blind}$, whereas y_{blind} is the mean value and s_{blind} is the standard deviation of the absolute intensity of the noted ppm range (noise). The LOQ was calculated using equation: $LOQ = y_{blind} + 9*s_{blind}$. Graphic illustrations are given by Figure S 8 which contains the threshold of LOD and LOQ.

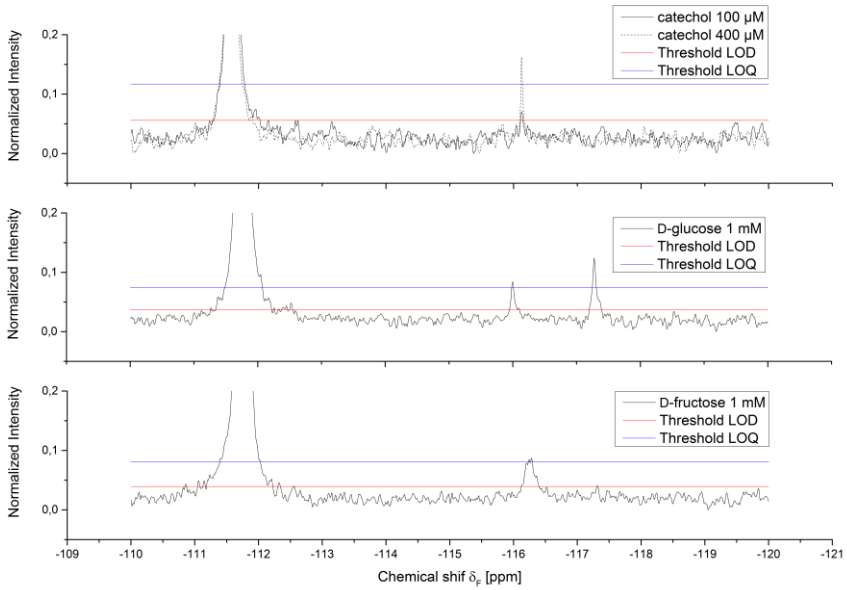

Figure S 8: $^{19}F[^{1}H]$ NMR spectra of receptor 1 in presence of D-fructose, D-glucose and catechol. The determined thresholds for LOD and LOQ are shown as well. Conditions: receptor 1 (10 mM), appropriate diol (0.1 – 1 mM) in aqueous HEPES buffer solution (100 mM, pH 7.4, 10% D_2O) at 188 MHz, 256 scans and 24 °C.

Binding Constant K_b Determination via ^{19}F NMR Spectroscopy

Binding constants K_b of **1** to a collection of diol-containing analytes containing D-fructose, -glucose, -glucose-6-phosphate, -galactose, -mannitol, -sorbitol, *N*-acetylneuraminic acid and catechol were conducted using the quantitative ^{19}F NMR spectroscopy technique. For each series of measurement single samples (560 µL each) containing a solution of **1** (10 mM) titrated with appropriate analyte (0 up to 100 mM) were prepared in aqueous HEPES buffer (100 mM, pH 7.4, 10% D_2O) and consecutively recorded at a 188 MHz, 256 scans and 24 °C. The FID of each spectrum was processed with the data processing guide (automatic mode) of the Bruker Top Spin 3.2 software containing Fourier transformation, phase and baseline correction. With the knowledge of a total fluorine concentration of 10 mM per sample and good ^{19}F signal separation the absolute concentrations of unbound receptor and receptor-analyte complex could be determined via signal integration, whereas the free analyte concentration could be calculated. Finally, the obtained data was plotted as $[HG]/[H_0]$ vs. [G], whereas [HG] is the concentration of the receptor-diol complex (overall value of all appearing receptor-diol signal), H_0 the initial concentration of receptor **1** (10 mM) and [G] is the concentration of unbound diol.[202] Fitting of the obtained data with equation 1 (1:1 binding model) resulted the binding constants K_b. The overall good quality of data fitting supports the existence of a 1:1 binding of **1** to the tested diols.

Binding Constant K_b Determination via Fluorescence Assay

Fluorescence measurements of the bipyridine receptors **10-12** and the reference compound 4,4'-*o*-BBV were conducted on a Perkin Elmer, Luminescence Spectrometer LS50B. At first, stock solutions of the receptors/quenchers (8 µM), HPTS (0.24 mM) and appropriate saccharide (1 M) were prepared in 50 mM HEPES buffer solution (pH 7.4). A Hellma QS cuvette (d = 10 x 10 mm) was loaded with 2 mL of a 1:1 quencher/dye solution and consecutively 0 to 100 µL saccharide solution was added by the use of an Eppendorf Research® pro pipette and the fluorescence emission spectra were recorded. The extracted fluorescence emission data (512 nm) was plotted in Origin 9.1G software as F/F_0 versus the saccharide concentration and then fitted with the following equation for obtaining the apparent binding constant K_b: $F/F_0 = (1 + (F_{max}/F_0)K_b[A])/(1 + K_b[A])$, whereas F_0 is the fluorescence intensity of the quenched HPTS dye, F_{max} is the fluorescence intensity of the unquenched dye at its maximum value, [A] is the concentration of saccharide present in solution (dissolution neglected) and K_b is the apparent binding constant.[89] Furthermore, all obtained data plots, the associated fittings and the resulting binding constant values are represented in the following.

Table 8: Apparent Binding constants K_b [M^{-1}] of bipyridine receptors/quenchers 10-12, 4,4'-*o*-BBV and HPTS dye to selected diols determined via the fluorescence assay at 24°C.[89]

	catechol	D-fructose	D-glucose	D-glucose-1-phosphate	D-glucose-6-phosphate	D-galactose	sucrose
4,4'-*o*-BBV	n/a	1107 ± 108	24 ± 3	26 ± 3	68 ± 3	101 ± 7	284 ± 114
10	n/a	1692 ± 208	45 ± 7	15 ± 1	115 ± 3	166 ± 7	2 ± 2
11	n/a	210 ± 14	16 ± 5	12 ± 8	1031 ± 92	435 ± 39	n/a
12	n/a	142 ± 14	n/a	58 ± 13	536 ± 33	183 ± 11	27 ± 8

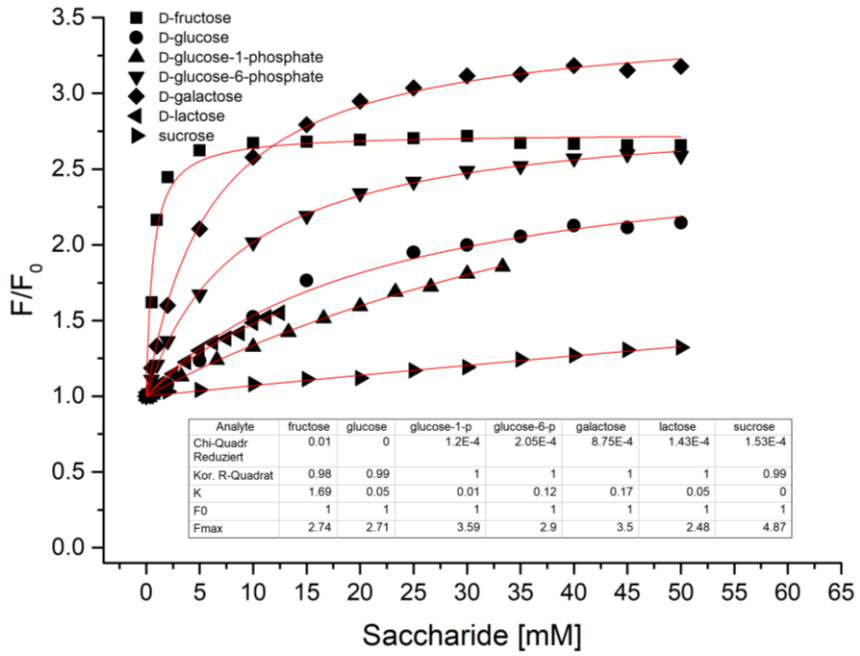

Analyte	fructose	glucose	glucose-1-p	glucose-6-p	galactose	lactose	sucrose
Chi-Quadr Reduziert	0.01	0	1.2E-4	2.05E-4	8.75E-4	1.43E-4	1.53E-4
Kor. R-Quadrat	0.98	0.99	1	1	1	1	0.99
K	1.69	0.05	0.01	0.12	0.17	0.05	0
F0	1	1	1	1	1	1	1
Fmax	2.74	2.71	3.59	2.9	3.5	2.48	4.87

Figure S 9: Fluorescence emission increase (at 512 nm) of receptor/quencher F-4,4'-*o*-BBV (10) and fluorescence dye upon saccharide addition for binding constant K_b determination. Conditions: receptor 10 (0.12 mM), HPTS dye (4 µM), appropriate saccharide (0 – 50 mM) measured in aqueous HEPES buffer solution (50 mM and pH 7.4) at 24 °C.

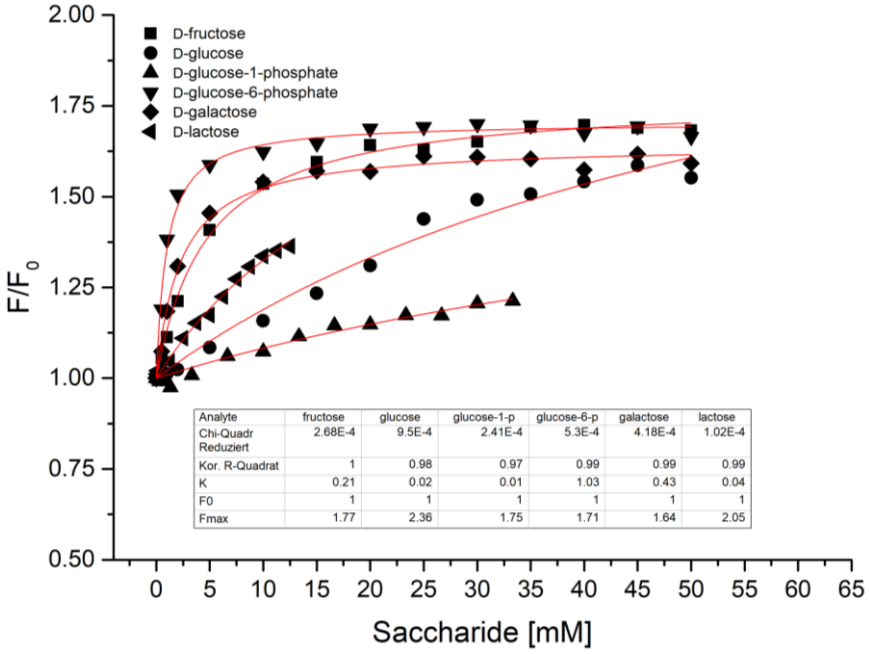

Analyte	fructose	glucose	glucose-1-p	glucose-6-p	galactose	lactose
Chi-Quadr Reduziert	2.68E-4	9.5E-4	2.41E-4	5.3E-4	4.18E-4	1.02E-4
Kor. R-Quadrat	1	0.98	0.97	0.99	0.99	0.99
K	0.21	0.02	0.01	1.03	0.43	0.04
F0	1	1	1	1	1	1
Fmax	1.77	2.36	1.75	1.71	1.64	2.05

Figure S 10: Fluorescence emission increase (at 512 nm) of receptor/quencher F-3,3'-*o*-BBV (11) and fluorescence dye upon saccharide addition for binding constant K_b determination. Conditions: receptor 11 (0.12 mM), HPTS dye (4 µM), appropriate saccharide (0 – 50 mM) measured in aqueous HEPES buffer solution (50 mM and pH 7.4) at 24 °C.

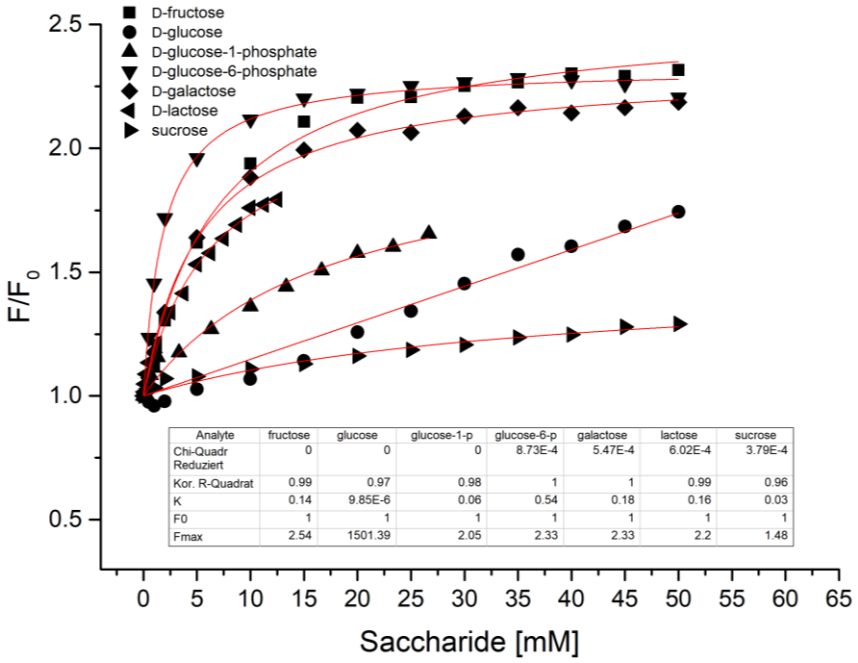

Analyte	fructose	glucose	glucose-1-p	glucose-6-p	galactose	lactose	sucrose
Chi-Quadr Reduziert	0	0	0	8.73E-4	5.47E-4	6.02E-4	3.79E-4
Kor. R-Quadrat	0.99	0.97	0.98	1	1	0.99	0.96
K	0.14	9.85E-6	0.06	0.54	0.18	0.16	0.03
F0	1	1	1	1	1	1	1
Fmax	2.54	1501.39	2.05	2.33	2.33	2.2	1.48

Figure S 11: Fluorescence emission increase (at 512 nm) of receptor/quencher F-3,4'-*o*-BBV (12) and fluorescence dye upon saccharide addition for binding constant K_b determination. Conditions: receptor 12 (0.12 mM), HPTS dye (4 µM), appropriate saccharide (0 – 50 mM) measured in aqueous HEPES buffer solution (50 mM and pH 7.4) at 24 °C.

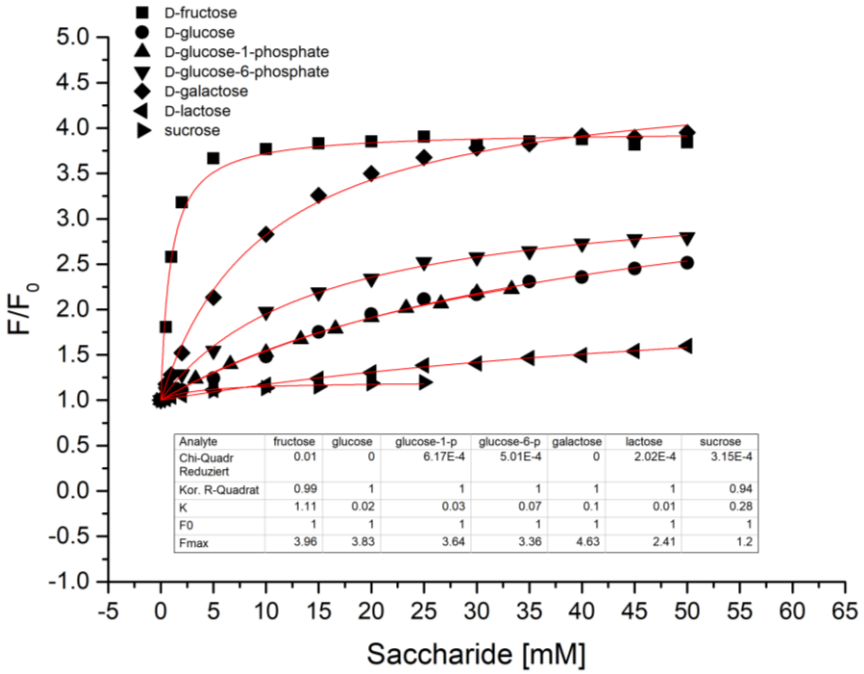

Analyte	fructose	glucose	glucose-1-p	glucose-6-p	galactose	lactose	sucrose
Chi-Quadr Reduziert	0.01	0	6.17E-4	5.01E-4	0	2.02E-4	3.15E-4
Kor. R-Quadrat	0.99	1	1	1	1	1	0.94
K	1.11	0.02	0.03	0.07	0.1	0.01	0.28
F0	1	1	1	1	1	1	1
Fmax	3.96	3.83	3.64	3.36	4.63	2.41	1.2

Figure S 12: Fluorescence emission increase (at 512 nm) of receptor/quencher 4,4'-*o*-BBV and fluorescence dye upon saccharide addition for binding constant K_b determination. Conditions: 4,4'-*o*-BBV (0.12 mM), HPTS dye (4 µM), appropriate saccharide (0 – 50 mM) measured in aqueous HEPES buffer solution (50 mM and pH 7.4) at 24 °C.

Monitoring of D-glucose in Synthetic Urine via ^{19}F NMR Spectroscopy

In a glass container, 7 mL synthetic urine (Surine™) was mixed with 3 mL HEPES buffer (100 mM, pH 7.4, 10% D_2O) and used as the medium for a stock solution of receptor **1** (15 mM) and D-glucose (15 mM). To Eppendorf vials containing 400 µL of receptor stock solution 0-200 µL of D-glucose stock solution and appropriate medium were added up to a total volume of 600 µL with resulting total concentrations of 10 mM for receptor **1** and 0-5 mM (effective concentration) for D-glucose. Next, 530µL of each vial were transferred to Wilmad® precision NMR tubes. A Wilmad® coaxial insert was loaded with 50 µL trifluoroacetic acid (100 mM dissolved in deionized water) and was used as an external reference. Each NMR tube with the coaxial insert containing was then measured at 188 MHz and 256 scans. The absolute concentrations of formed receptor-glucose complexes were determined by ^{19}F NMR signal integration. The external method uses the ratio of TFA reference integral versus the integral of the complex, whereas the internal method uses the total amount of overall appearing ^{19}F signals (10 mM total fluorine content with respect to receptor **1**) versus the integral of the complex.

Monitoring of D-fructose in an Enzyme Catalyzed Reaction via ^{19}F NMR Spectroscopy

The formation of D-fructose was followed up in an exemplary enzyme reaction. The enzyme sucrose phosphorylase (SPO) transferred the substrate sucrose to α-D-glucose-1-phosphate and D-fructose whereas the latter can be tracked by receptor **1** and ^{19}F NMR spectroscopy. In detail, stock solutions of receptor **1** (25 mM), sucrose (15-120 mM), KH_2PO_4 (240 mM) and SPO, (7.58 U/mL) were prepared using HEPES buffer (100 mM, pH 7.4, 10% D_2O). A Wilmad® coaxial insert containing 100 mM trifluoroacetic acid (50 µL) dissolved in deionized water was freshly prepared to be used as an external reference. To an Eppendorf vial 240 µL receptor **1**, 200 µL sucrose, 100 µL KH_2PO_4 and 60 µL HEPES buffer were added to achieve total concentrations of 10 mM for receptor **1**, 5-40 mM for sucrose and 40 mM for KH_2PO_4. The mixture was then vortexed and 530 µL transferred to an Wilmad® precision NMR tube and the TFA coaxial insert was inserted and subsequently measured as the reference sample without SPO (t = 0 min) at 24 °C. Consequently, a fresh SPO containing sample was prepared using the same procedure but this time adding 60 µL of SPO stock solution instead of buffer to yield total concentrations of 10 mM for receptor **1**, 5-40 mM for sucrose, 40 mM for KH_2PO_4 and 1.89 U/mL for SPO. 530 µL of the mixture (SPO = 1 U) was immediately transferred to a Wilmad® precision NMR tube. The coaxial TFA reference was inserted and measured with an acquisition

time of 6 minutes each spectrum (188 MHz, 128 scans at 24 °C). The complex/TFA ratio was directly determined using the integrals of the upcoming complex (δ_F -116.23 ppm) and the TFA reference signal (δ_F -75.91 ppm). By the use of a calibration curve with increasing amount of D-fructose, the absolute concentrations of D-fructose could be determined at each point of the NMR acquisition and thus the reaction rates of SPO could be obtained.

Procedure for the Generation of ^{19}F NMR-based Bar codes using the Receptors 10-12

To overcome the need of multivariate analysis for confident analyte discrimination two-dimensional barcodes were generated to simplify this task. Thus, the recorded ^{19}F NMR data of the bipyridine receptors **10-12** and in presence of diol-containing analytes was first extracted out of the spectra and then interpreted as two-dimensional barcodes. This procedure will be described as follows.

The FID of each spectrum was processed with the data processing guide (automatic mode) of Bruker Top Spin 3.2 software containing Fourier transformation, phase and baseline correction. ^{19}F NMR peaks with an S/N ratio of at least 5 (S/N tool of Bruker Top Spin 3.2) were assigned via the peak picking tool to cut off diminutive and noise signals. The relative intensity of the most intensive peak was set to 100% relative intensity. Hence, the exact chemical shift and the relative intensity (rounded value) were then collected (see Table S 2). With these data in hand unique barcodes representing each receptor-analyte combination were generated. Colored squares corresponding to appropriate receptor (**10** = blue, **11** = red and **12** = green) at precise chemical shifts and in their size equal to the ^{19}F signals relative intensity were used to transfer the characteristic ^{19}F NMR signals to 2D bar codes. Four square sizes represent the relative peak intensities with thresholds at 25, 50 and 75% relative intensity, respectively. Consequently, a two-dimensional bar code was simply obtained by stacking the single barcodes of the receptors **10-12** together.

Table S 2: ^{19}F NMR data of receptor 10-12 and in presence of diol-containing analytes extracted of the corresponding spectra used for the generation of 2D bar codes. The ^{19}F data of unbound 11 and 12 have been simplified by removing the observed side signals resulting in one peak for 11 (δ_F –111.86 removed) and two peaks for 12 (δ_F –111.89 removed).[a]

	F-4,4'-*o*-BBV (10)		F-3,3'-*o*-BBV (11)		F-3,4'-*o*-BBV (12)	
	δ_F [ppm]	rel. Int. [%]	δ_F [ppm]	rel. Int. [%]	δ_F [ppm]	rel. Int. [%]
pure receptor	–111.76	100	–112.21[a]	100	–112.24[a]	100
					–112.33[a]	71
catechol	–116.05	100	–115.81	100	–115.92	85
					–116.09	100
dopamine	–115.93	100	–115.60	100	–112.11	19
					–115.76	94
					–115.95	100
D-fructose	–116.10	100	–112.21	19	–112.23	70
			–115.97	100	–112.32	45
					–116.00	82
					–116.11	100
D-glucose	–115.72	100	–112.21	25	–112.23	100
	–117.04	72	–116.04	60	–112.32	69
			–116.65	100	–116.68	62
					–117.07	32
D-glucose-1-phosphate	–111.78	100	–112.21	100	–112.24	100
					–112.33	78
D-glucose-6-phosphate	–110.66	24	–112.20	39	–112.23	100
	–116.37	100	–116.56	100	–112.33	67
	–117.07	48	–116.76	83	–116.22	22
					–116.66	36
					–117.00	30
					–117.23	39
					–117.56	22
D-galactose	–115.90	100	–112.21	74	–112.24	100
			–115.74	100	–112.33	74
			–116.48	18	–115.77	42
			–116.65	17	–115.91	55
D-lactose	–111.67	100	–112.19	100	–112.23	100
	–117.07	72	–116.82	27	–112.32	84
					–117.01	13
sucrose	–111.79	100	–112.20	100	–112.23	100
					–112.32	77

CRYSTALLOGRAPHIC DATA

Structure Determination

The intensity data for the compounds were collected on a Nonius KappaCCD diffractometer using graphite-monochromated Mo-K_α radiation. Data were corrected for Lorentz and polarization effects; absorption was taken into account on a semi-empirical basis using multiple-scans.[203-205]

The structures were solved by direct methods (SHELXS[206]) and refined by full-matrix least squares techniques against Fo^2 (SHELXL-97[206]). The hydrogen atoms bounded to the compounds **1**, **2**, and to both hydroxy-groups O1 and O2 of **4** were located by difference Fourier synthesis and refined isotropically. All other hydrogen atoms of **4** were included at calculated positions with fixed thermal parameters. The crystal of **4** was a non-merohedral twin. The twin law was determined by PLATON[207] to (-1.0 0.0 0.0) (0.0 -1.0 0.0) (0.693 0.0 1.0). The contribution of the main component was refined to 0.505(1). All non-hydrogen atoms were refined anisotropically.[206] Crystallographic data as well as structure solution and refinement details are summarized in Table S 3. MERCURY[208] was used for structure representations.

Supporting Information available: Crystallographic data (excluding structure factors) has been deposited with the Cambridge Crystallographic Data Centre as supplementary publication CCDC-1426757 for **a**, CCDC-991571 for **1**, CCDC-1526342 for **2**, CCDC-1526343 for **4** and CCDC-991570 for **10**. Copies of the data can be obtained free of charge on application to CCDC, 12 Union Road, Cambridge CB2 1EZ, UK [E- mail: deposit@ccdc.cam.ac.uk]

Table S 3: Crystal data and refinement details for the X-ray structure determinations of the compounds a, 1, 2, 4 and 10.

Compound	a	1	2	4	10
formula	$C_{21}H_{15}B_3Br_3F_3O_3$	$C_{12}H_{12}BBrFNO_2$	$C_{12}H_{12}BBrFNO_2$	$C_{13}H_{12}BBrF_3NO_2$	$C_{28}H_{34}B_2Br_2F_2N_2O_6$
fw (g·mol^{-1})	644.49	311.95	311.95	361.96	714.01
T/°C	-140	-140	-140	-140	-140
crystal system	monoclinic	monoclinic	monoclinic	triclinic	triclinic
space group	C 2/c	P 2_1/c	P 2_1/c	P $\bar{1}$	P $\bar{1}$
a/ Å	14.6558(2)	7.5296(1)	7.5193(2)	6.5845(3)	8.1548(3)
b/ Å	13.8575(3)	17.7540(4)	18.3049(5)	7.2237(3)	9.0537(2)
c/ Å	22.2655(4)	9.5971(2)	9.5705(3)	15.3914(6)	10.7095(3)
α/°	90	90	90	82.136(2)	89.663(2)
β/°	95.266(1)	103.537(1)	107.611(1)	79.133(2)	89.756(1)
γ/°	90	90	90	89.205(3)	72.525(2)
V/Å^3	4502.88(14)	1247.30(4)	1255.55(6)	712.14(5)	754.19(4)
Z	8	4	4	2	1
ρ (g·cm^{-3})	1.901	1.661	1.650	1.688	1.572
μ (cm^{-1})	54.23	32.99	32.78	29.22	27.44
measured data	17476	7585	9496	8752	4663
data with I > 2σ(I)	4542	2507	2645	2819	3280
unique data (R_{int})	5130/0.0282	2843/0.0259	2860/0.0223	2930/0.0403	3414/0.0160
wR_2 (all data, on F^2)[a)]	0.0644	0.0514	0.0498	0.0723	0.0602
R_1 ($I > 2\sigma(I)$) [a)]	0.0282	0.0246	0.0202	0.0290	0.0247
S [b)]	1.079	1.087	1.053	1.056	1.061
Res. dens./e·Å^{-3}	0.378/-0.612	0.374/-0.331	0.383/-0.267	0.595/-0.473	0.374/-0.379
absorpt method	multi-scan	multi-scan	multi-scan	multi-scan	multi-scan
absorpt corr $T_{min/max}$	0.5417/ 0.7456	0.6954/0.7456	0.6435/0.7456	0.4129/0.7454	0.5432/ 0.7456
CCDC No.	1426757	991571	1526342	1526343	991570

[a)] Definition of the *R* indices: $R_1 = (\Sigma \| |F_o| - |F_c| \|)/\Sigma |F_o|$;
$wR_2 = \{\Sigma[w(F_o^2-F_c^2)^2]/\Sigma[w(F_o^2)^2]\}^{1/2}$ with $w^{-1} = \sigma^2(F_o^2) + (aP)^2+bP$; $P = [2F_c^2 + \mathrm{Max}(F_O^2]/3$; [b)] $s = \{\Sigma[w(F_o^2-F_c^2)^2]/(N_o-N_p)\}^{1/2}$.

SPECTROSCOPIC AND SPECTROMETRIC DATA

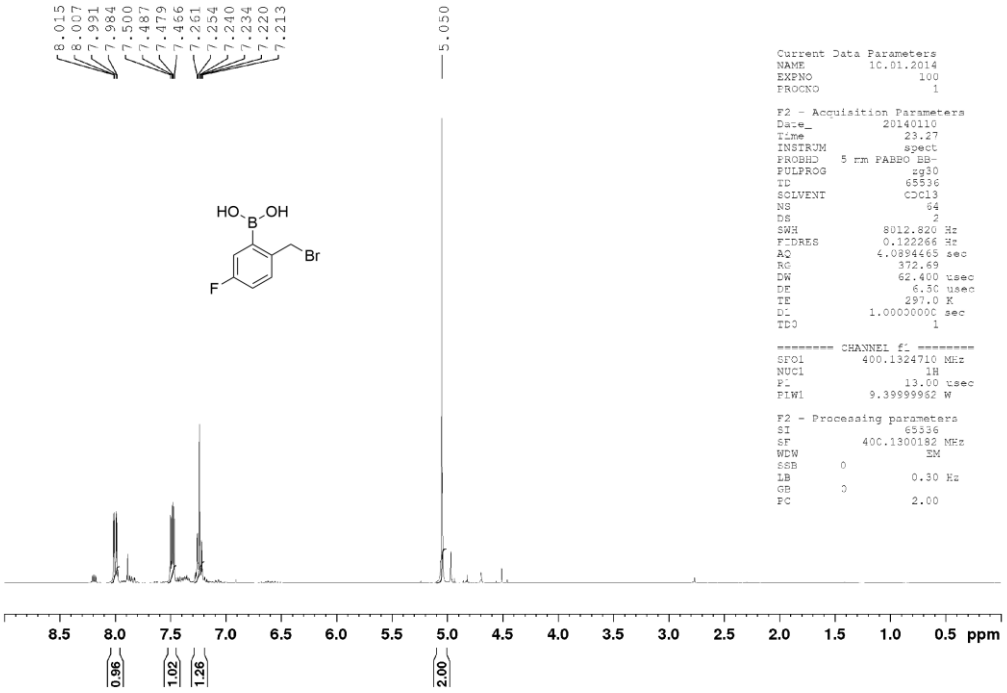

Figure S 13: ^{1}H NMR (400 MHz, $CDCl_3$) spectrum of 2-bromomethyl-5-fluorophenylboronic acid.

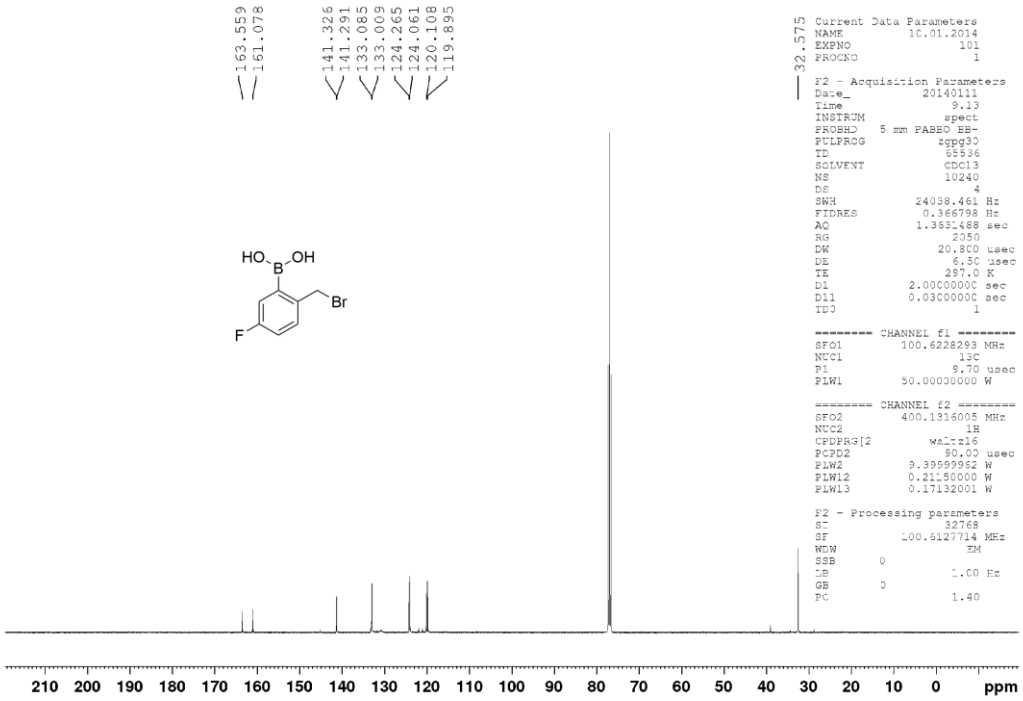

Figure S 14: $^{13}C\{^{1}H\}$ NMR (100 MHz, $CDCl_3$) spectrum of 2-bromomethyl-5-fluorophenylboronic acid.

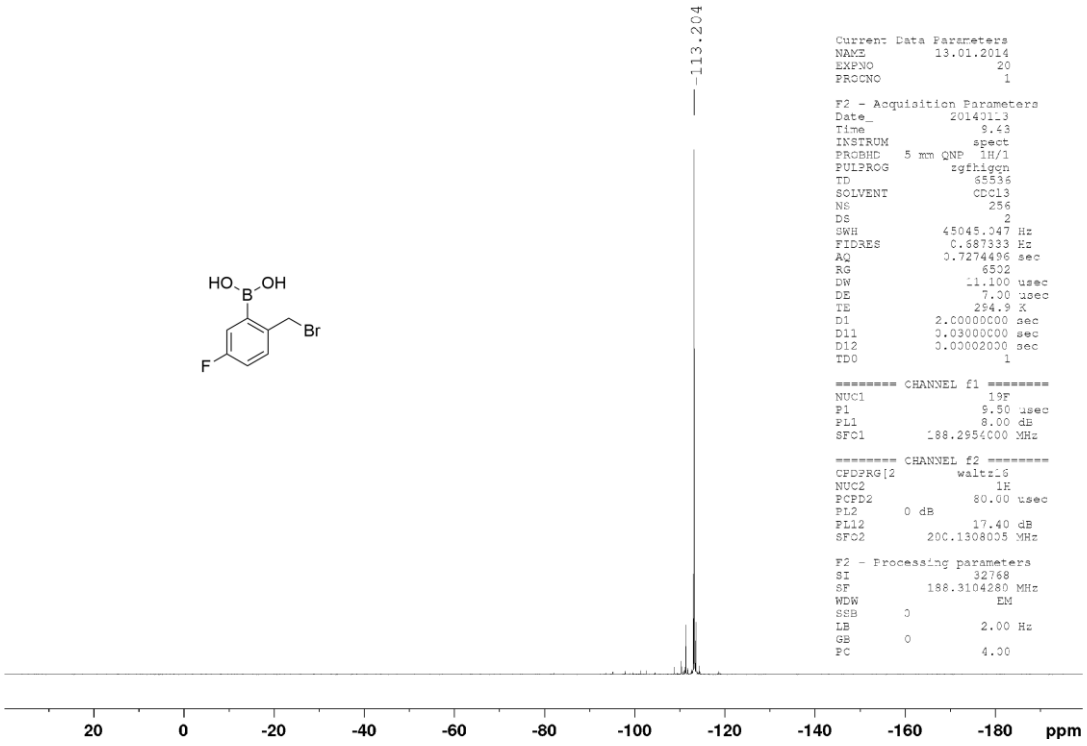

Figure S 15: $^{19}F\{^{1}H\}$ NMR (188 MHz, $CDCl_3$) spectrum of 2-bromomethyl-5-fluorophenylboronic acid.

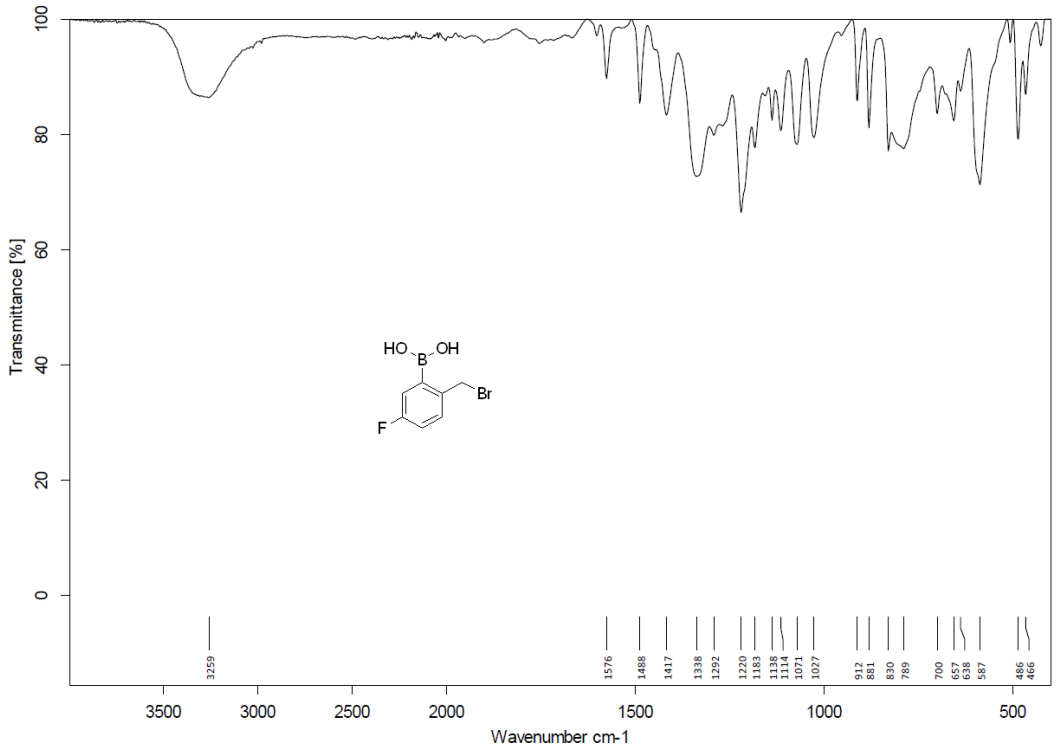

Figure S 16: FT-IR (ATR) spectrum of 2-bromomethyl-5-fluorophenylboronic acid.

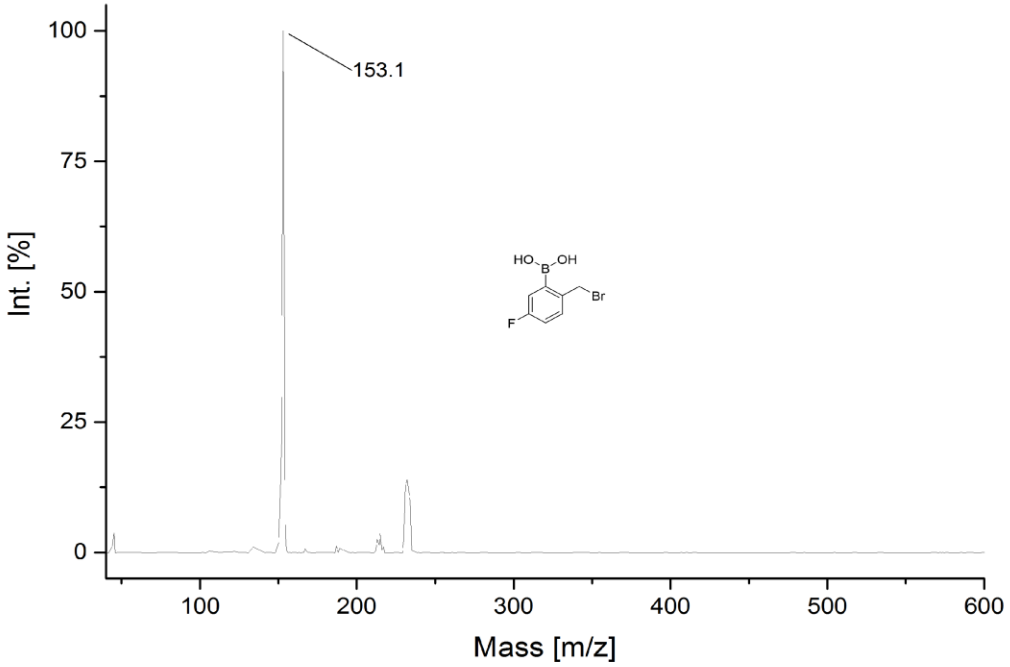

Figure S 17: MS (EI+) spectrum of 2-bromomethyl-5-fluorophenylboronic acid.

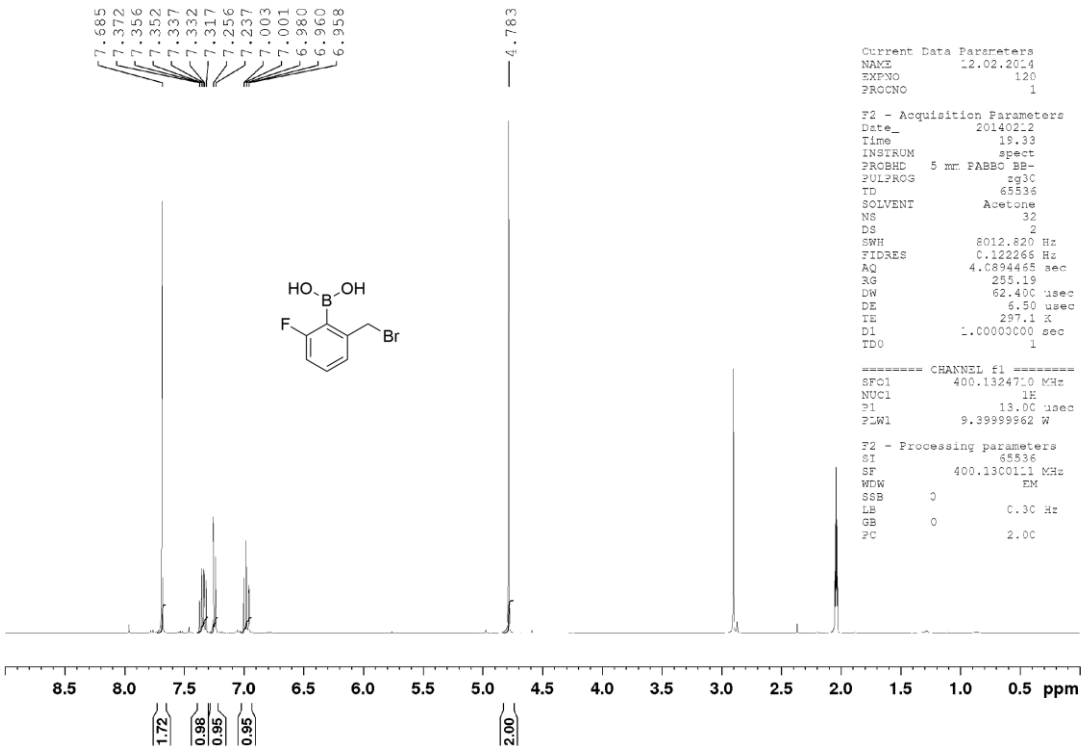

Figure S 18: ^{1}H NMR (400 MHz, acetone-d$_6$) spectrum of 2-bromomethyl-6-fluorophenylboronic acid.

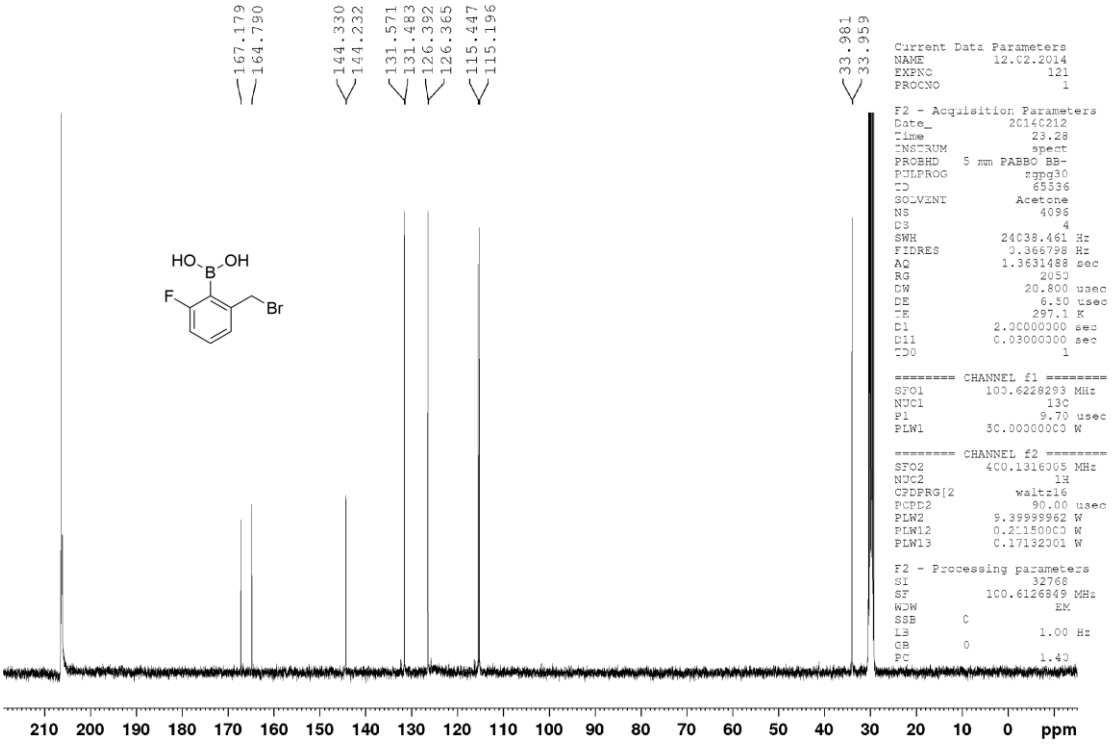

Figure S 19: $^{13}C\{^{1}H\}$ NMR (100 MHz, acetone-d_6) spectrum of 2-bromomethyl-6-fluorophenylboronic acid.

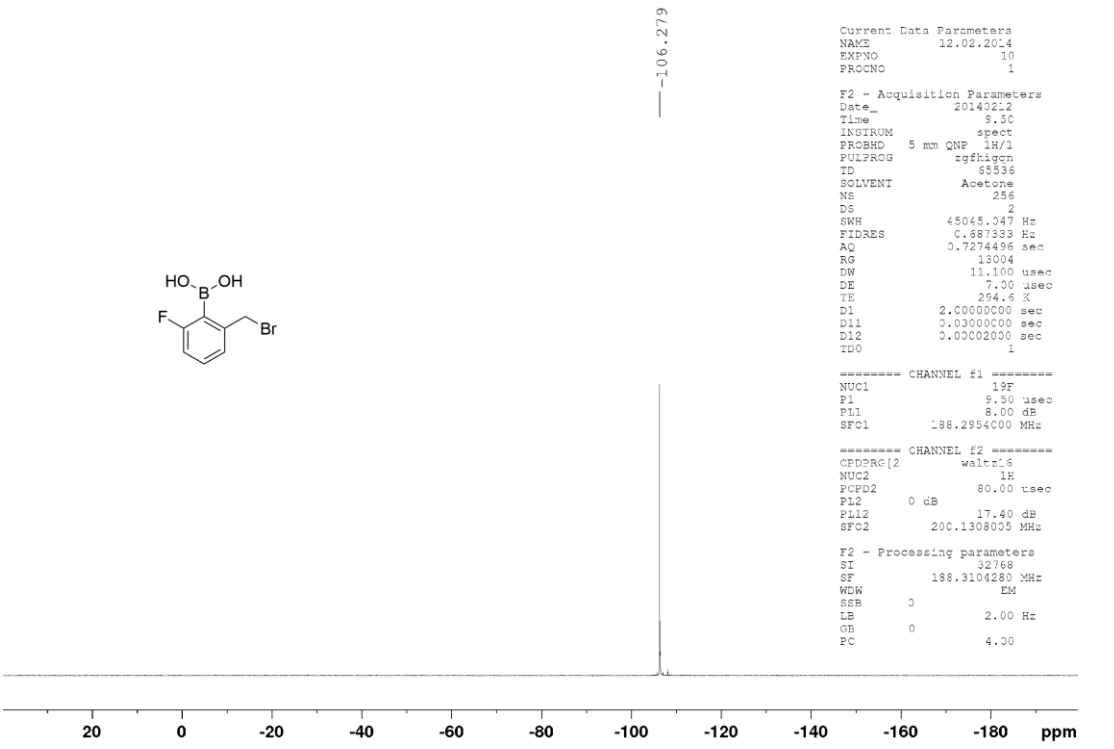

Figure S 20: $^{19}F\{^{1}H\}$ NMR (188 MHz, acetone-d_6) spectrum of 2-bromomethyl-6-fluorophenylboronic acid.

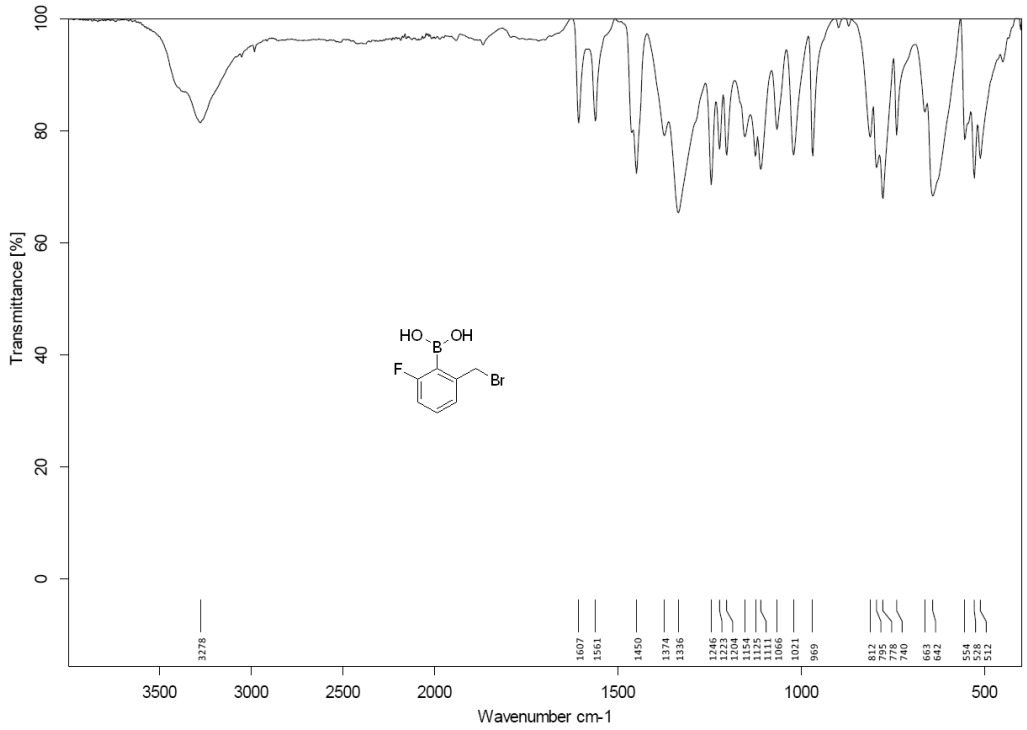

Figure S 21: FT-IR (ATR) spectrum of 2-bromomethyl-6-fluorophenylboronic acid.

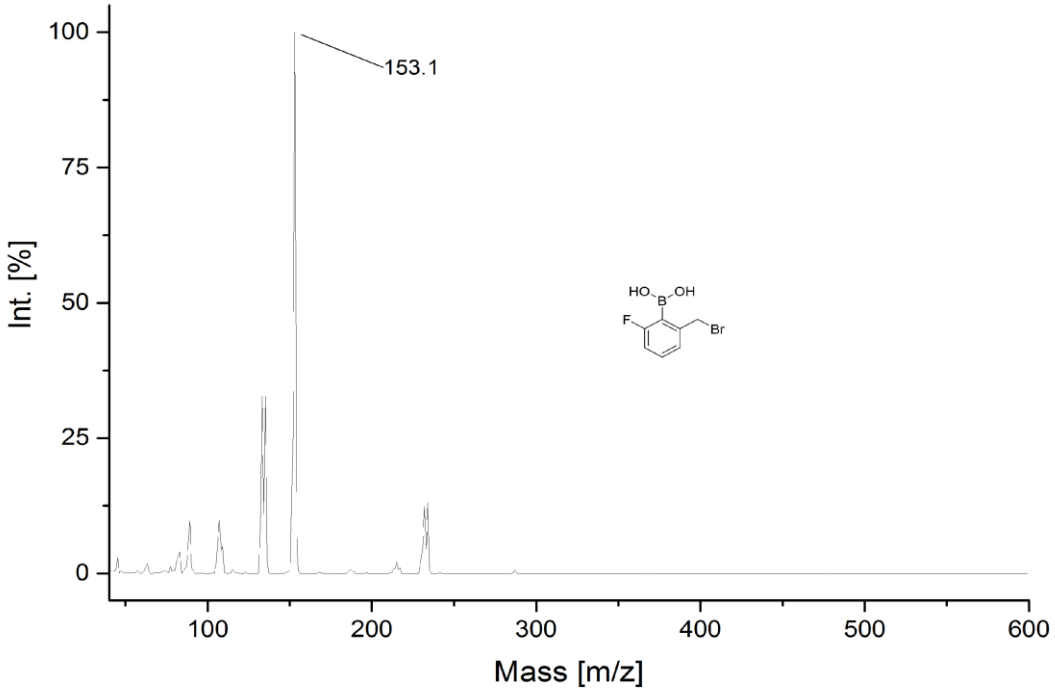

Figure S 22: MS (EI+) spectrum of 2-bromomethyl-6-fluorophenylboronic acid.

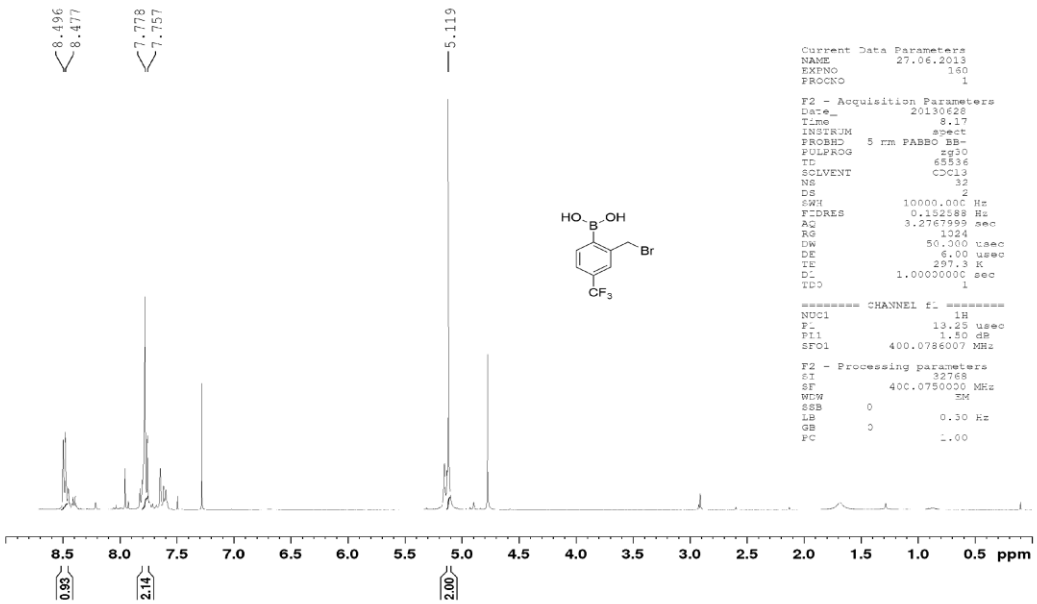

Figure S 23: ^{1}H NMR (400 MHz, $CDCl_3$) spectrum of 2-bromomethyl-4-trifluoromethylphenylboronic acid. Sideband signals indicate anhydrides of the compound.

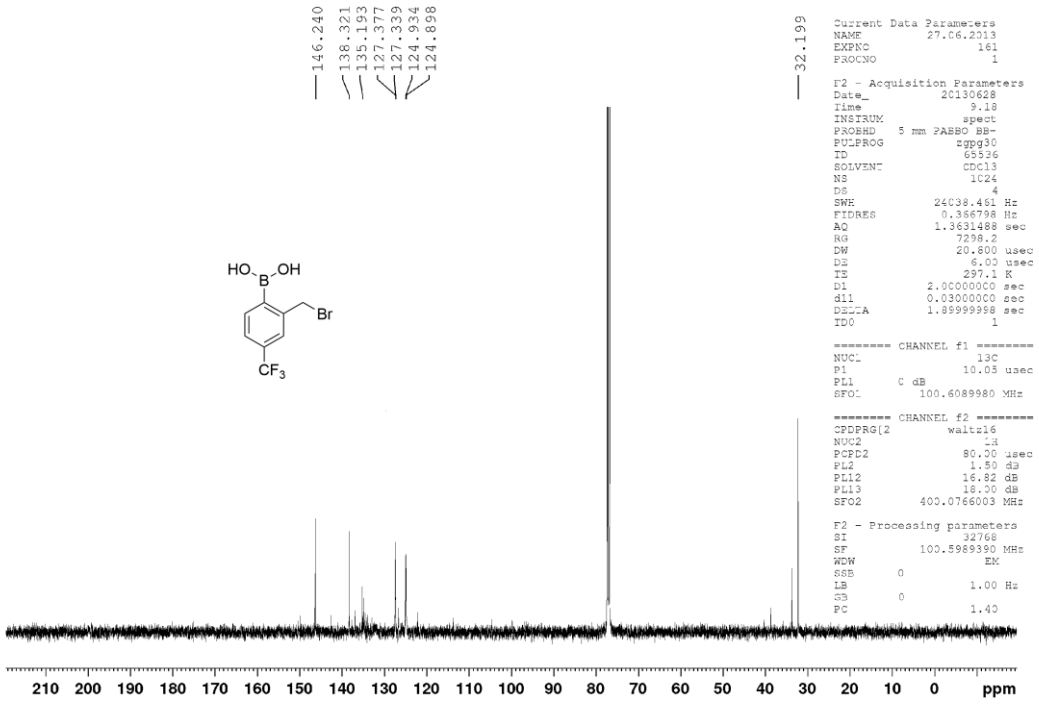

Figure S 24: $^{13}C\{^{1}H\}$ NMR (100 MHz, $CDCl_3$) spectrum of 2-bromomethyl-4-trifluoromethylphenylboronic acid. Sideband signals indicate anhydrides of the compound.

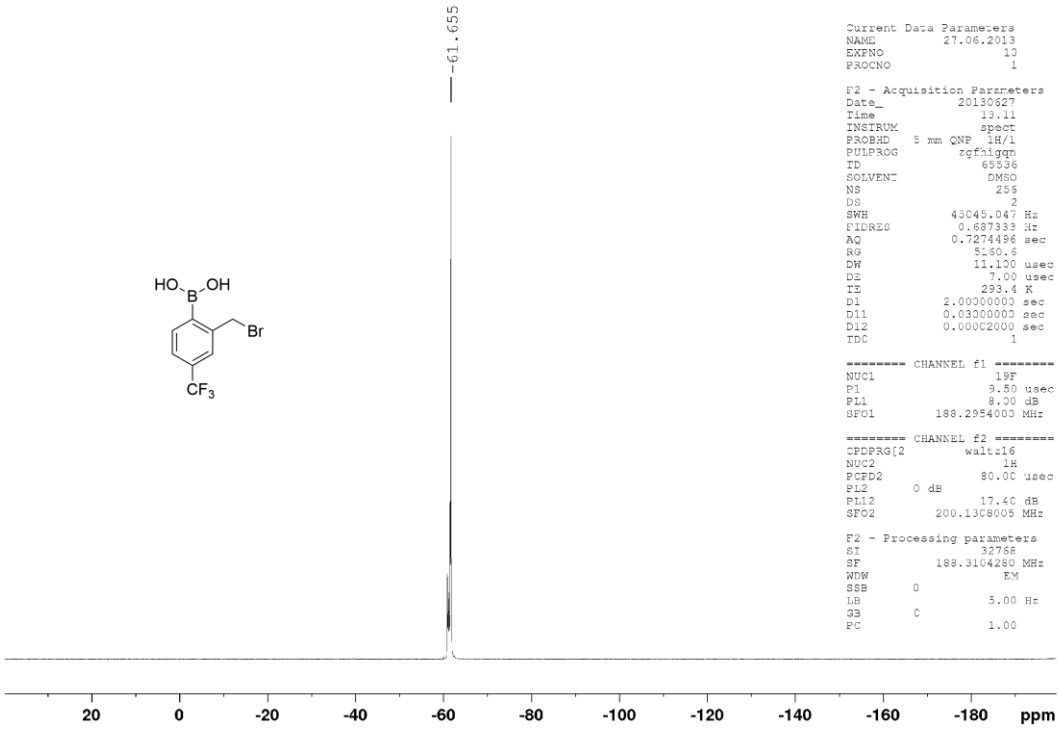

Figure S 25: $^{19}F\{^{1}H\}$ NMR (188 MHz, $CDCl_3$) spectrum of 2-bromomethyl-4-trifluoromethylphenylboronic acid. Sideband signals indicate anhydrides of the compound.

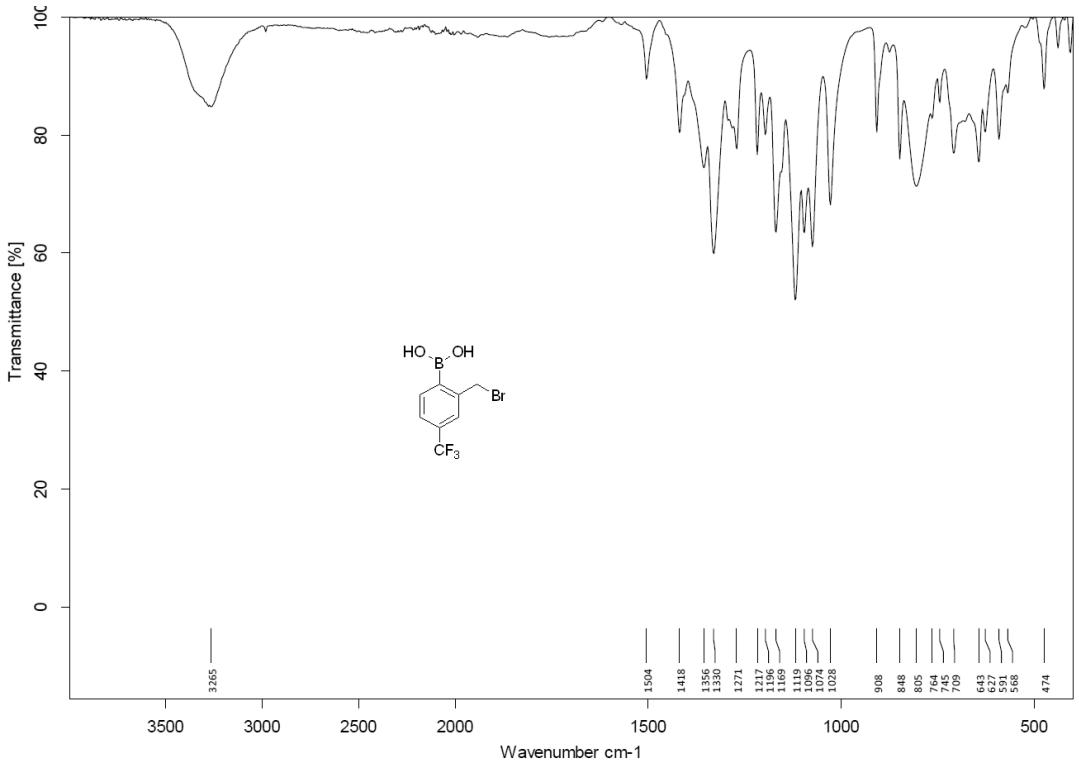

Figure S 26: FT-IR (ATR) spectrum of 2-bromomethyl-4-trifluoromethylphenylboronic acid.

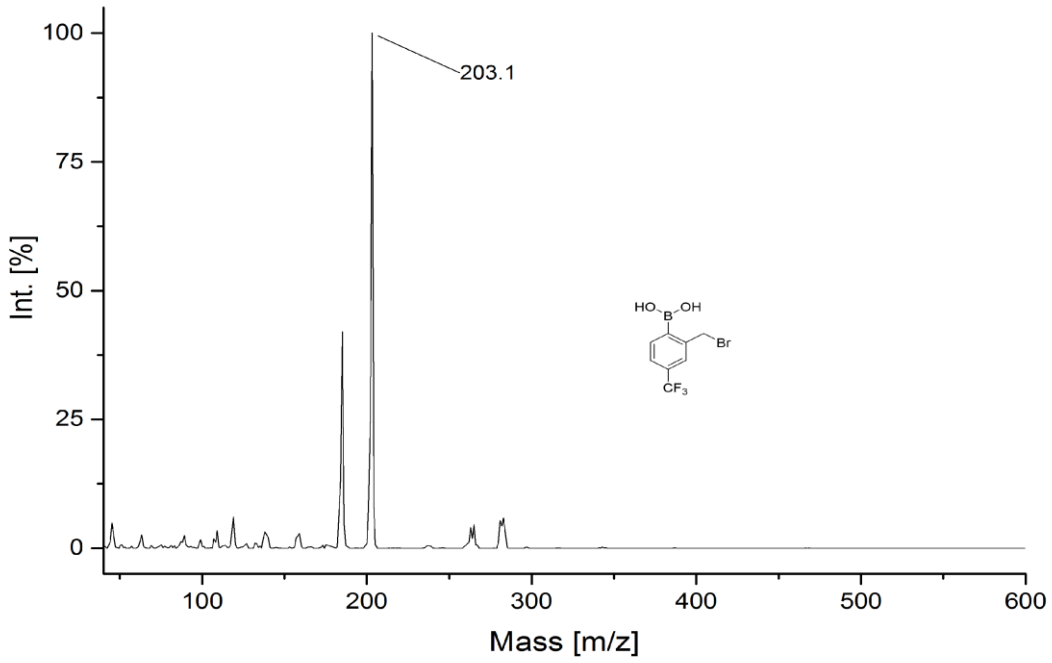

Figure S 27: MS (EI+) spectrum of 2-bromomethyl-4-trifluoromethylphenylboronic acid.

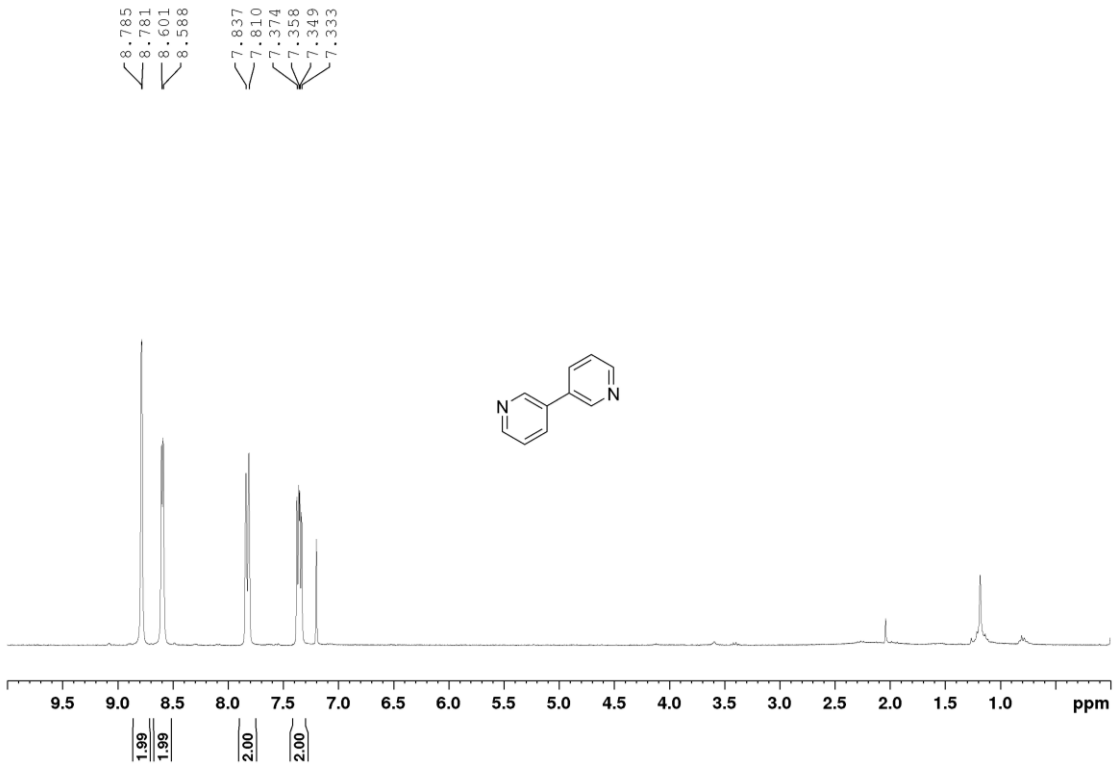

Figure S 28: ^{1}H NMR (300 MHz, $CDCl_3$) spectrum of 3,3'-bipyridine.

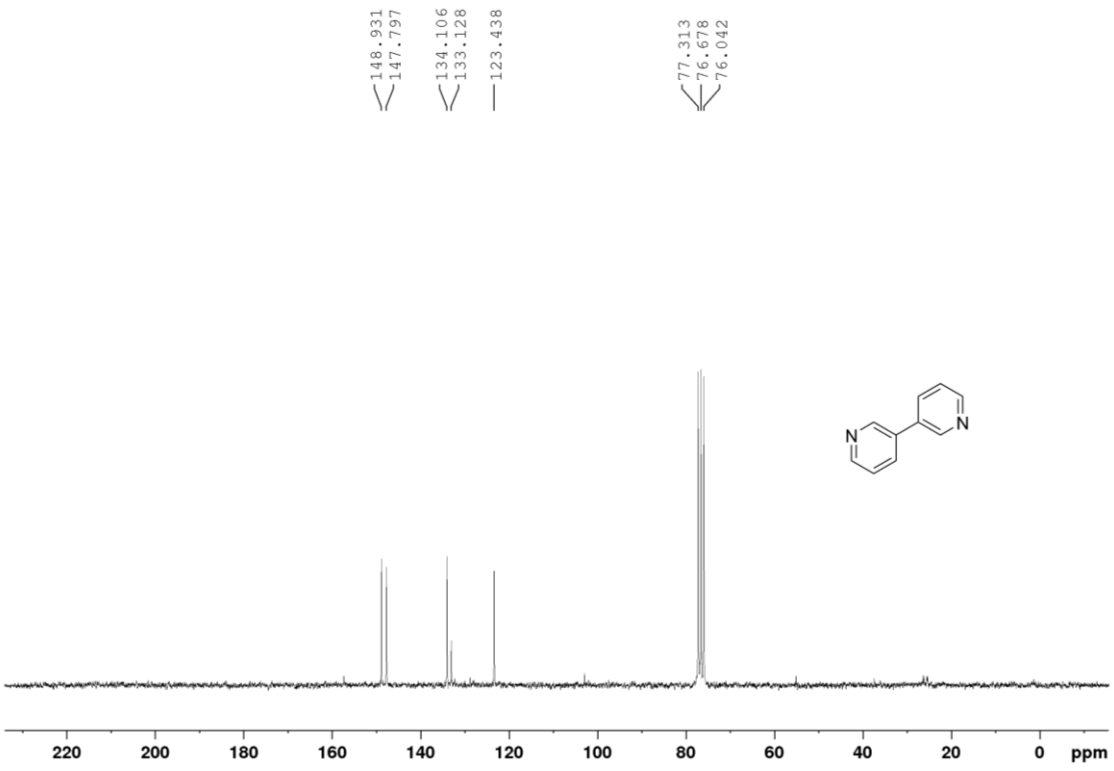

Figure S 29: $^{13}C\{^{1}H\}$ NMR (50 MHz, $CDCl_3$) spectrum of 3,3'-bipyridine.

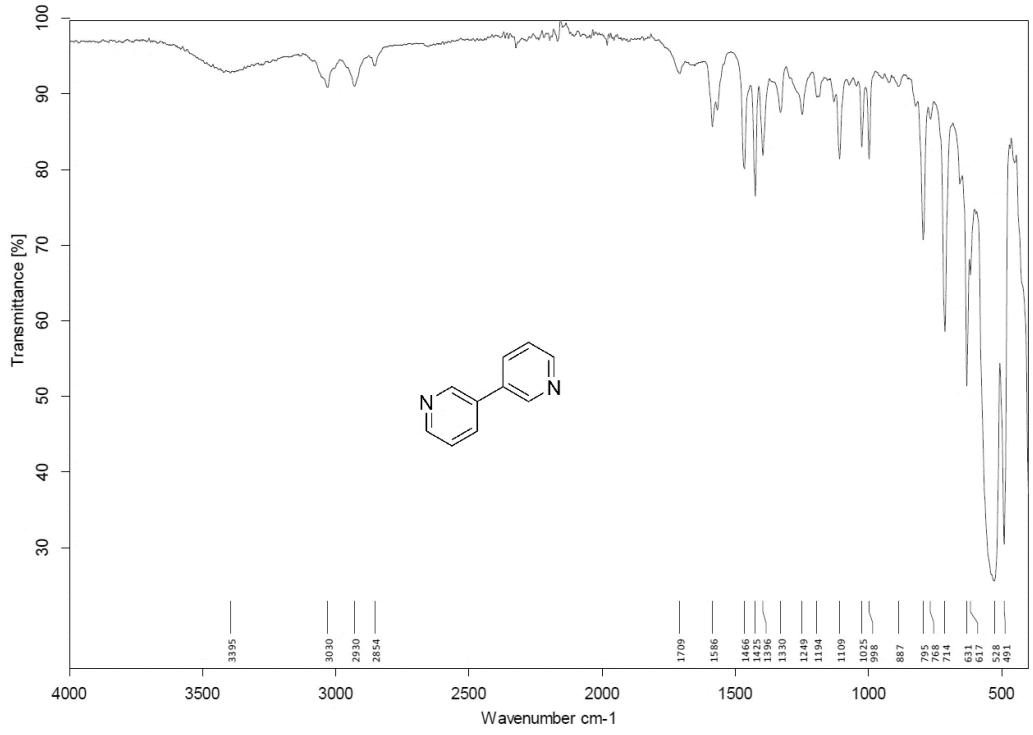

Figure S 30: FT-IR (ATR) spectrum of 3,3'-bipyridine.

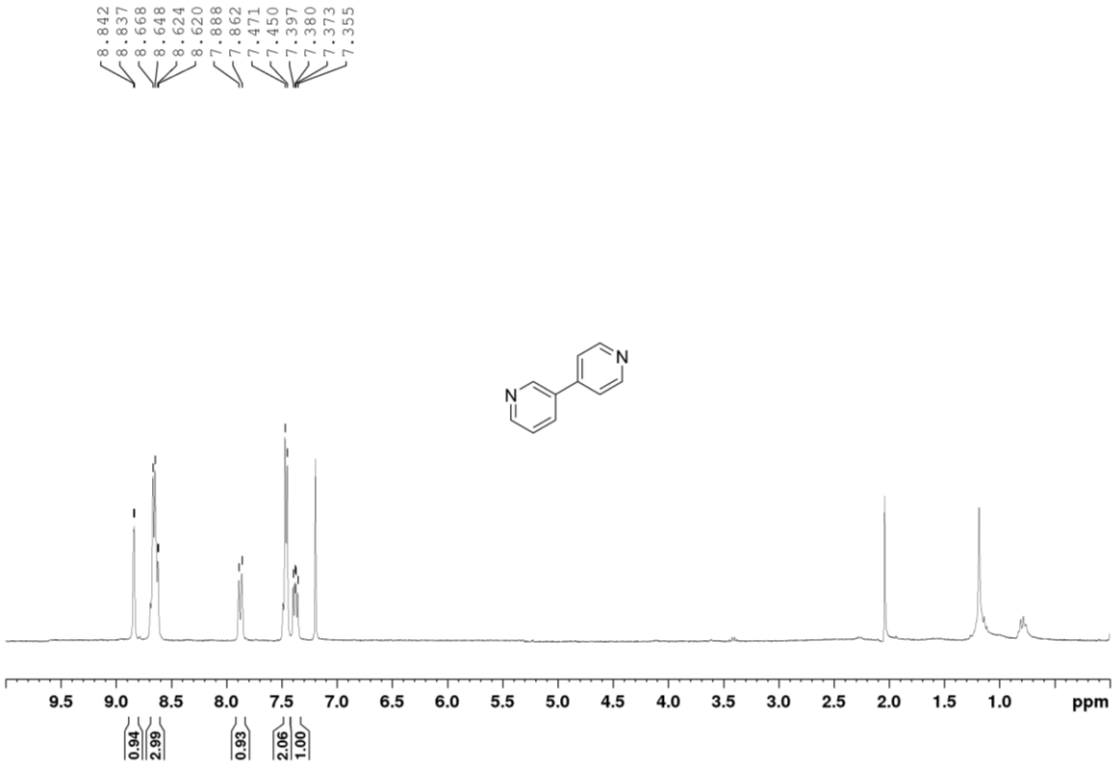

Figure S 31: ^{1}H NMR (300 MHz, $CDCl_3$) spectrum of 3,4'-bipyridine.

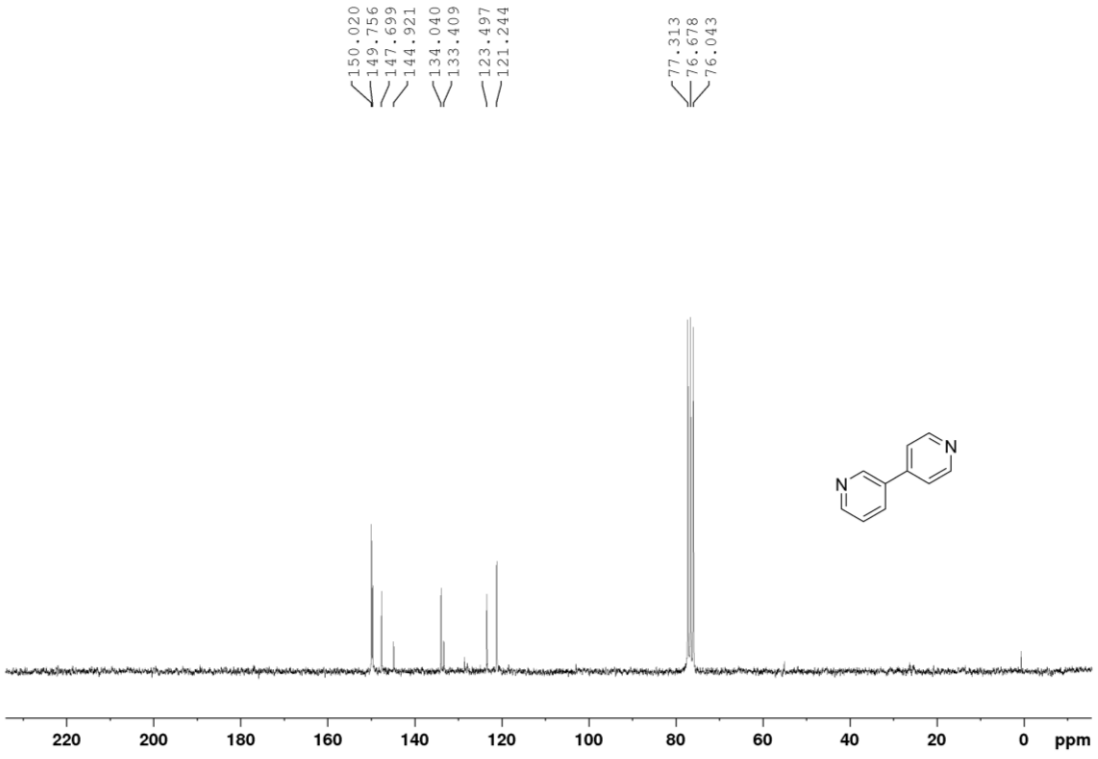

Figure S 32: $^{13}C\{^{1}H\}$ NMR (50 MHz, $CDCl_3$) spectrum of 3,4'-bipyridine.

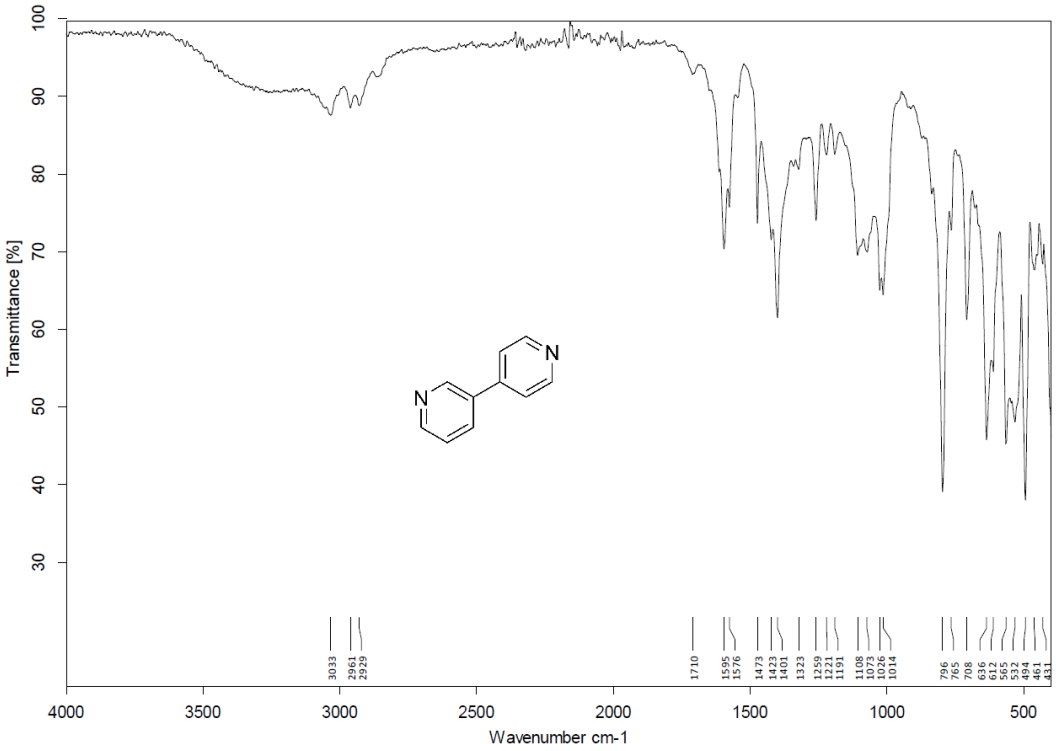

Figure S 33: FT-IR (ATR) spectrum of 3,4'-bipyridine.

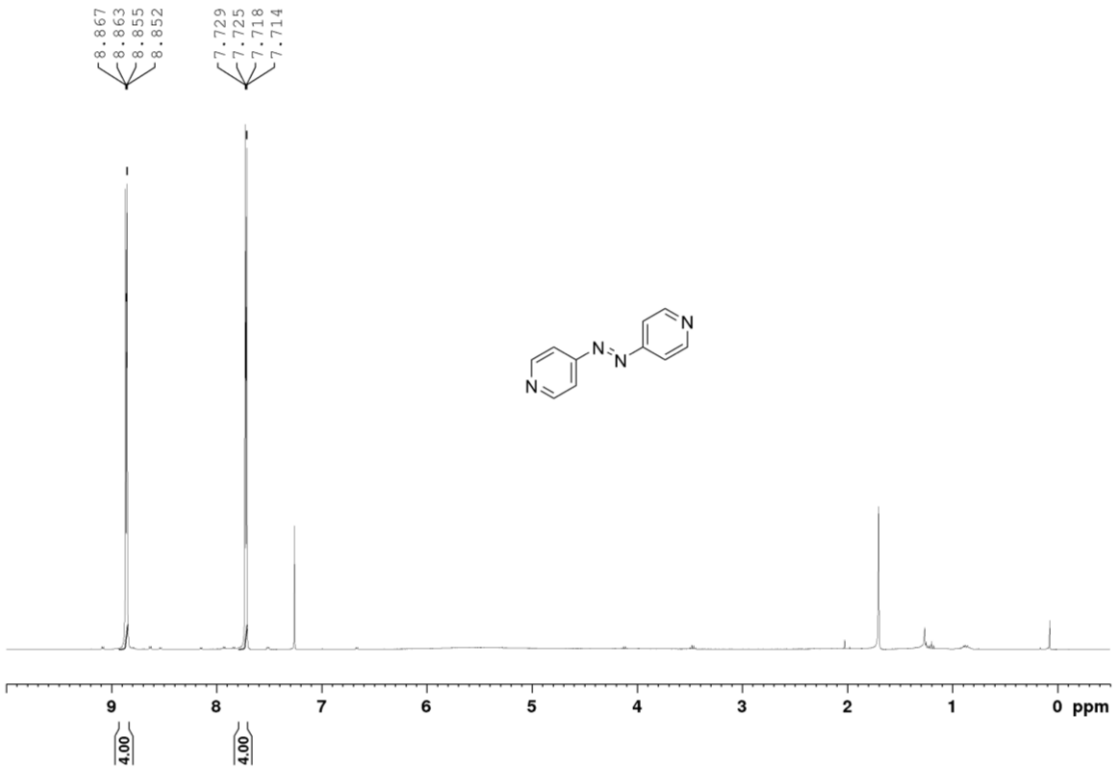

Figure S 34: ^{1}H NMR (400 MHz, $CDCl_3$) spectrum of 4,4′-azopyridine.

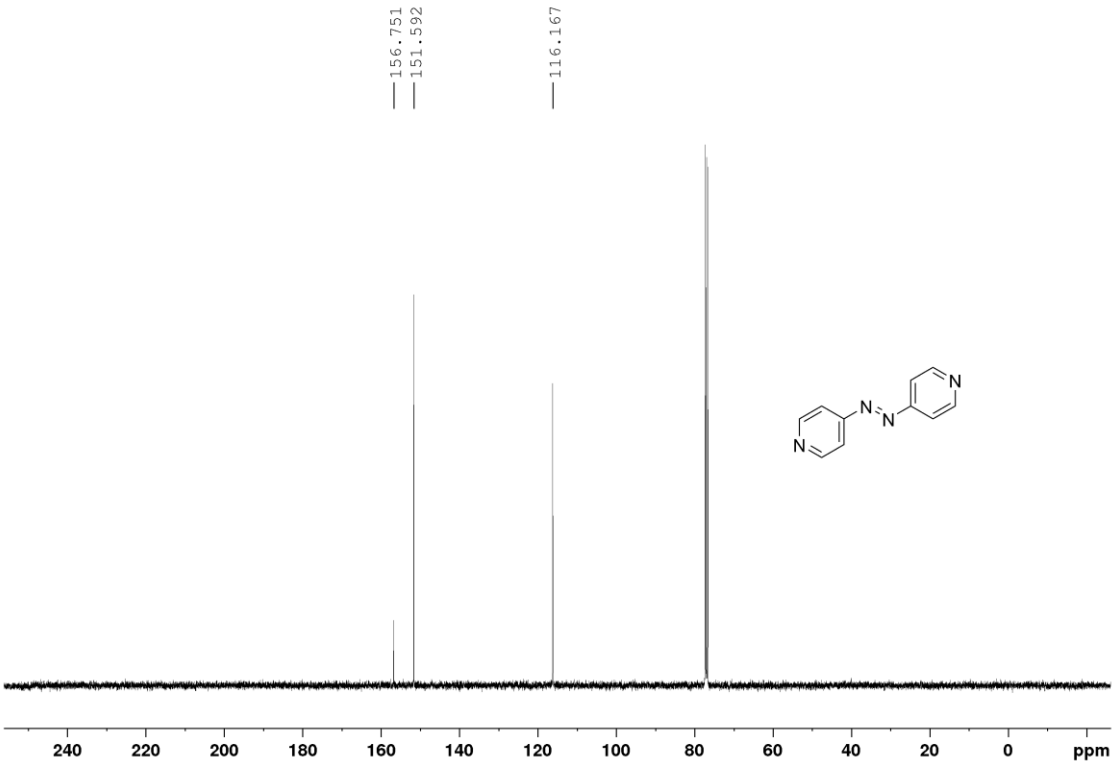

Figure S 35: $^{13}C\{^{1}H\}$ NMR (100 MHz, $CDCl_3$) spectrum of 4,4′-azopyridine.

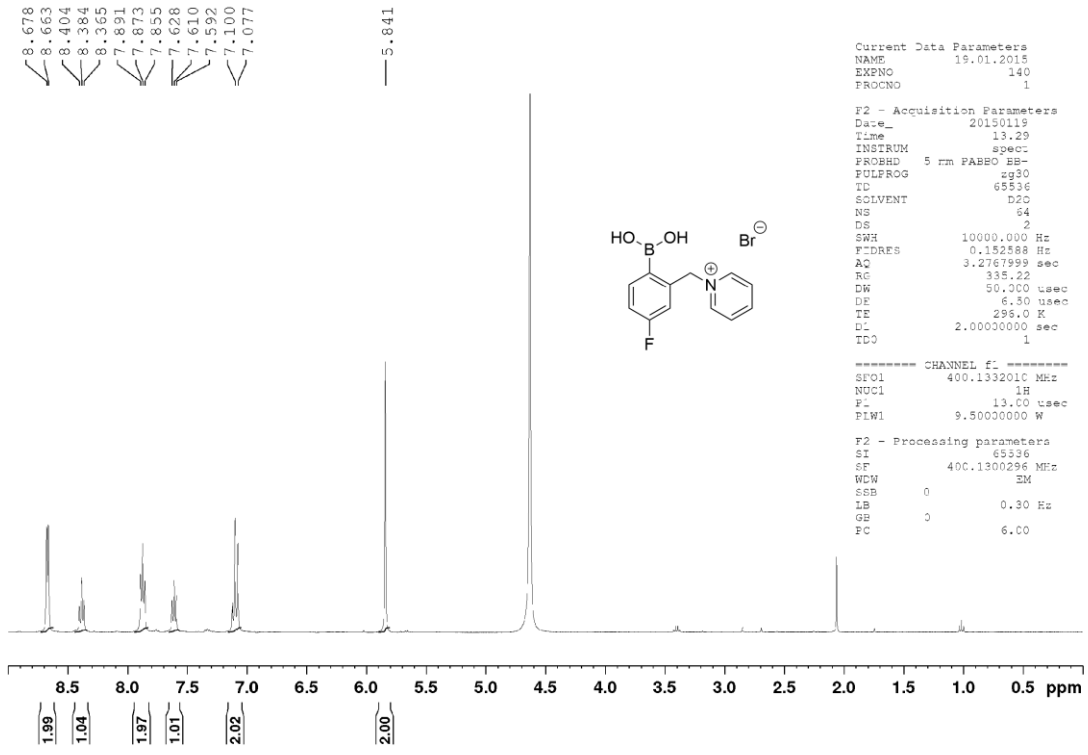

Figure S 36: ^{1}H NMR (400 MHz, D_2O) spectrum of 5-F-*o*-BBpy (1).

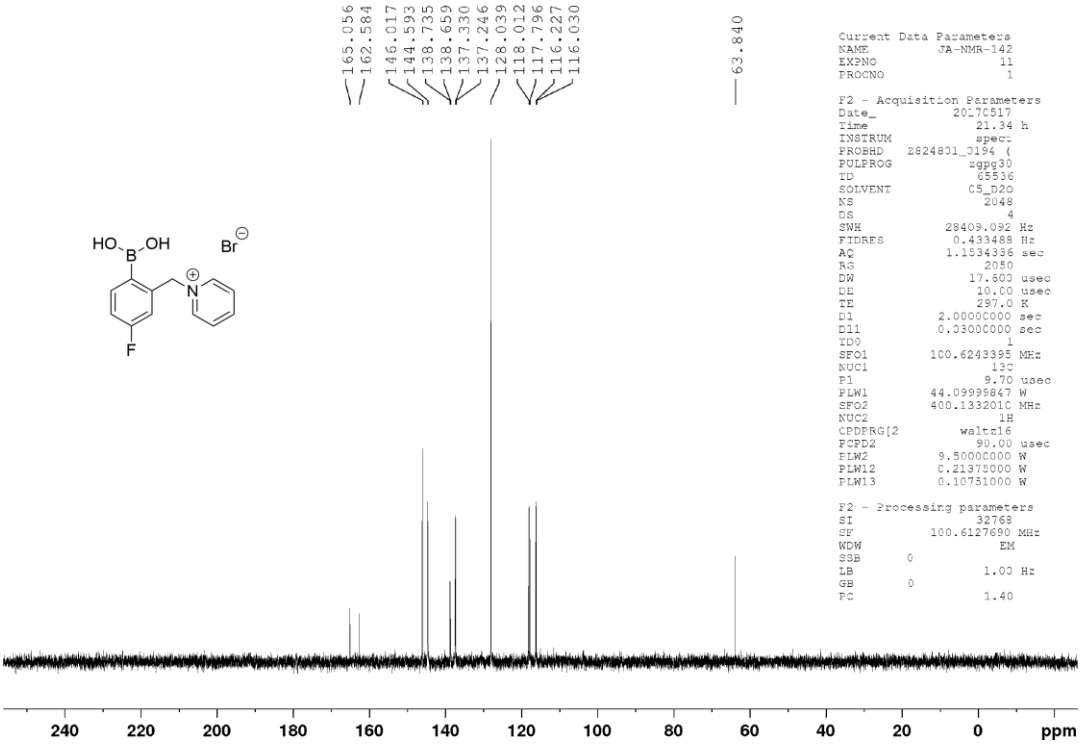

Figure S 37: $^{13}C\{^{1}H\}$ NMR (100 MHz, D_2O) spectrum of 5-F-*o*-BBpy (1).

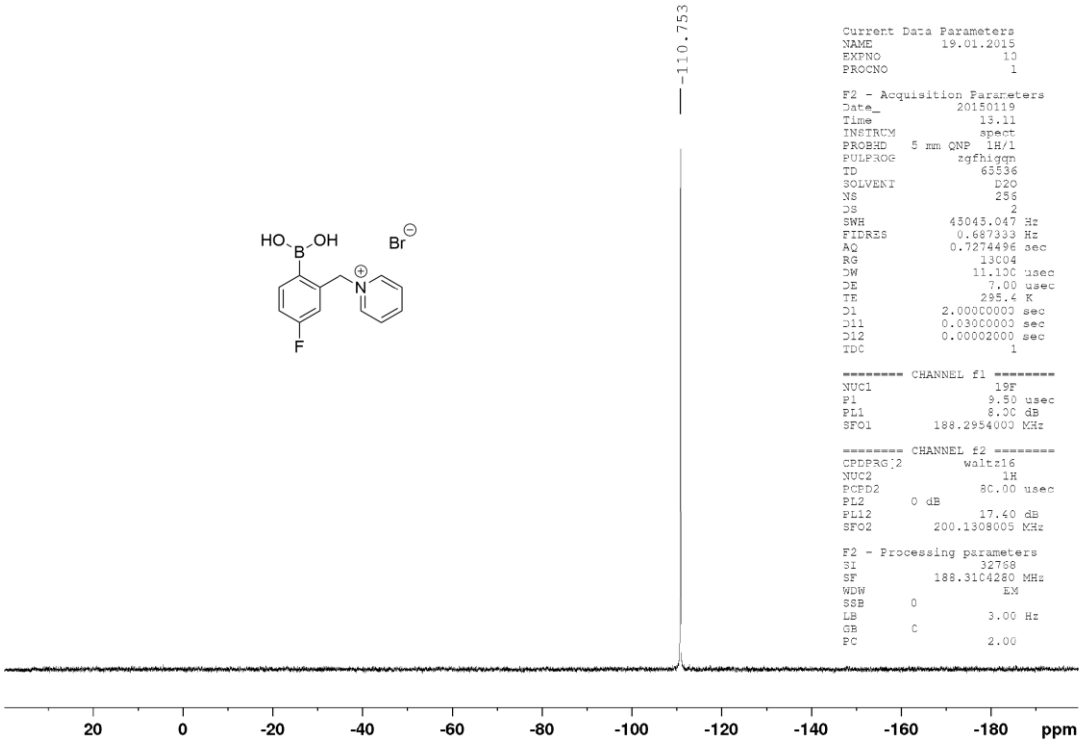

Figure S 38: $^{19}F\{^{1}H\}$ NMR (188 MHz, D_2O) spectrum of 5-F-*o*-BBpy (1).

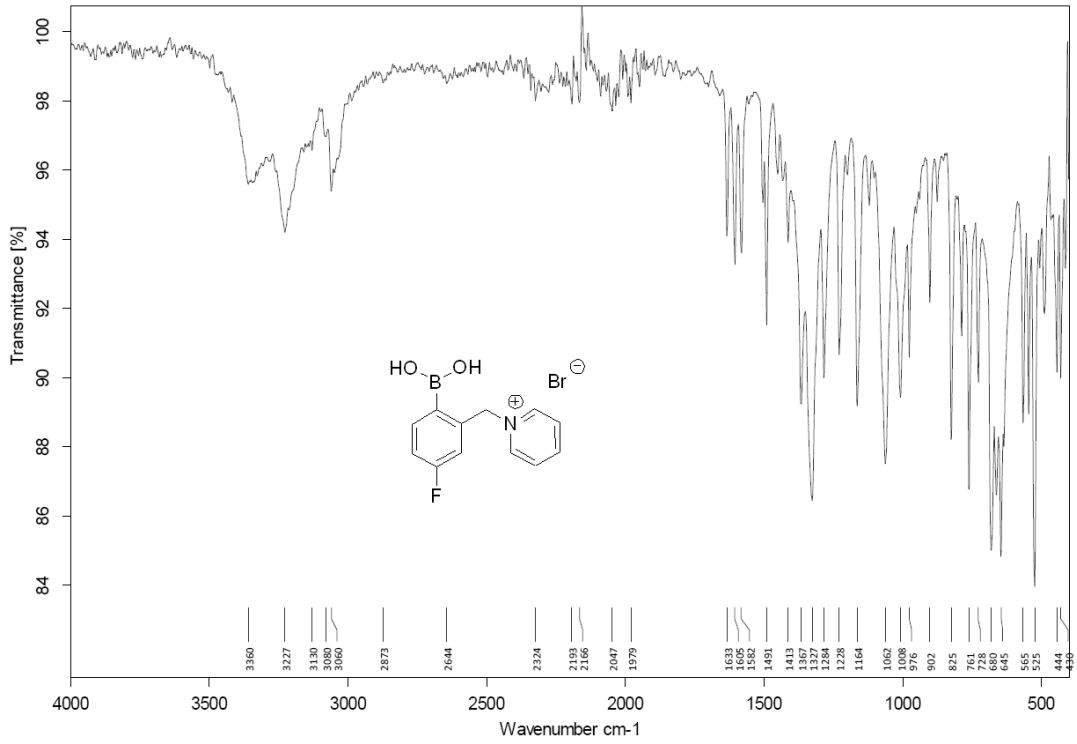

Figure S 39: FT-IR (ATR) spectrum of 5-F-*o*-BBpy (1).

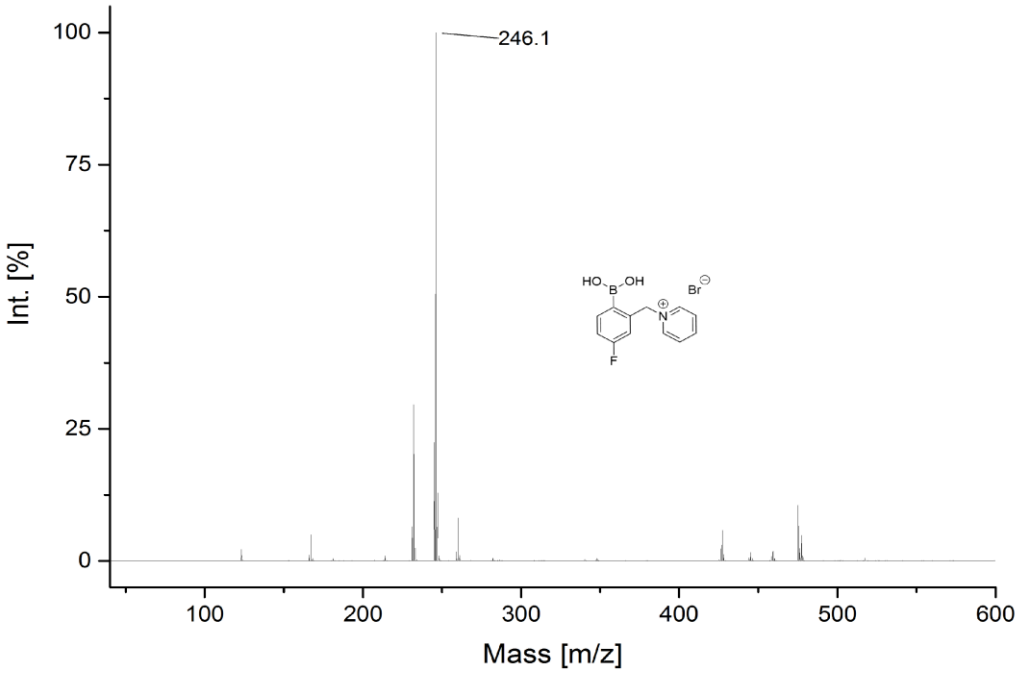

Figure S 40: MS (ESI+) spectrum of 5-F-*o*-BBpy (1).

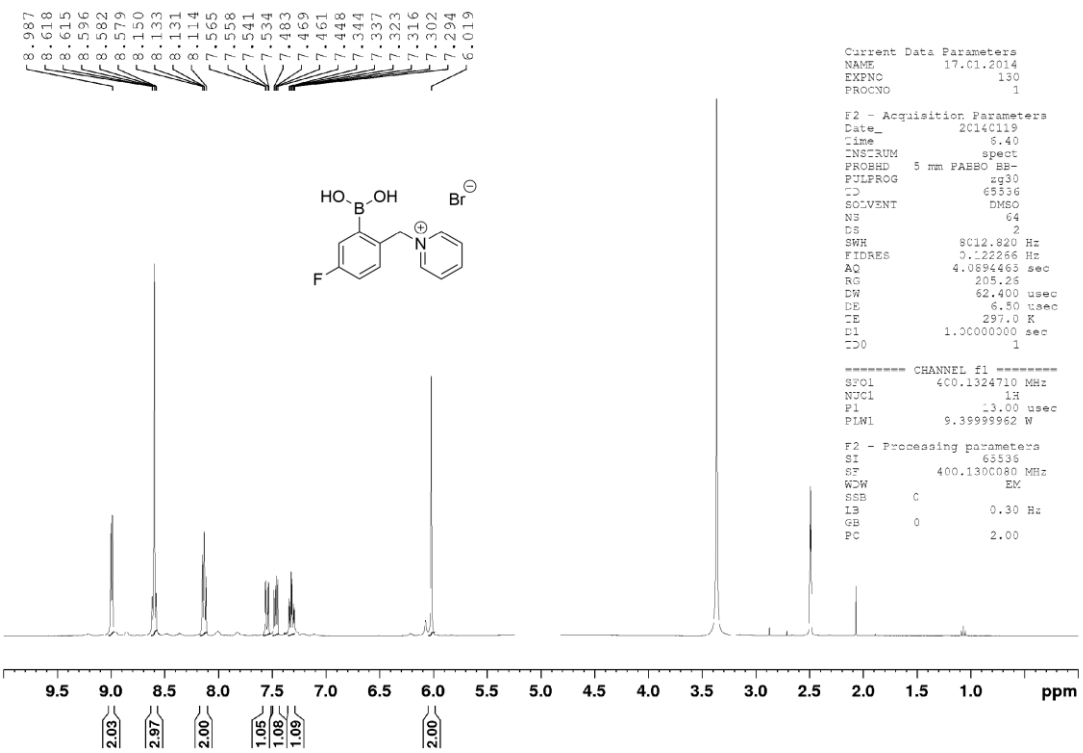

Figure S 41: ^{1}H NMR (400 MHz, DMSO-d$_6$) spectrum of 4-F-*o*-BBpy (2).

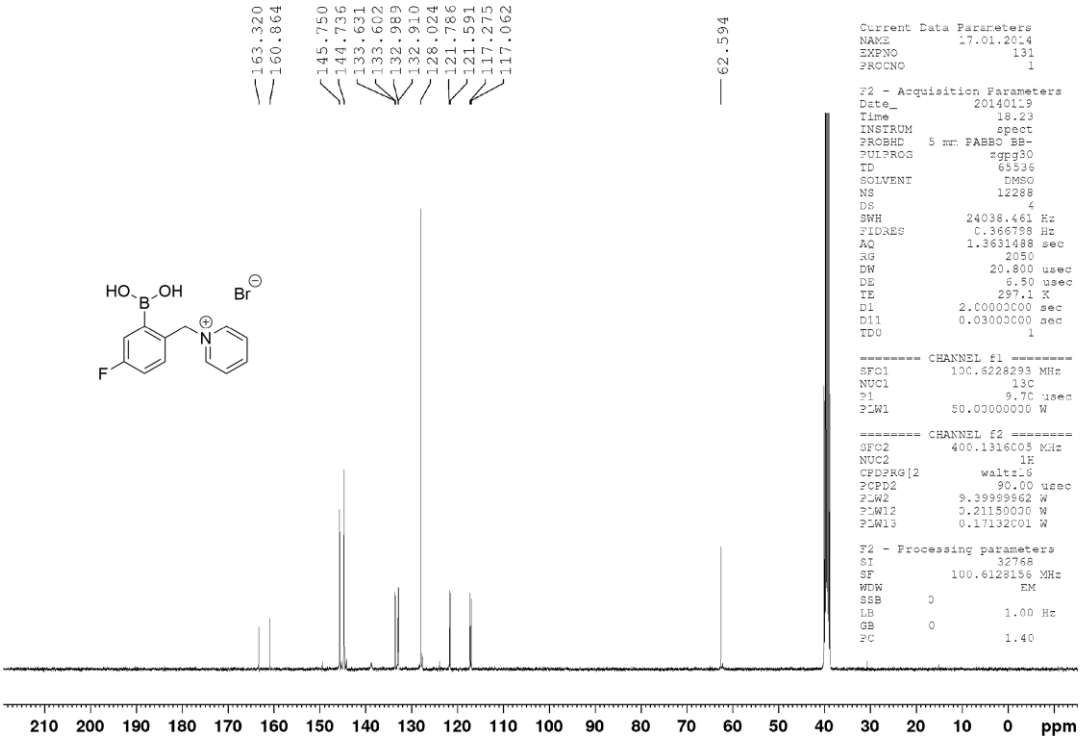

Figure S 42: ^{13}C{^{1}H} NMR (100 MHz, DMSO-d$_6$) spectrum of 4-F-*o*-BBpy (2).

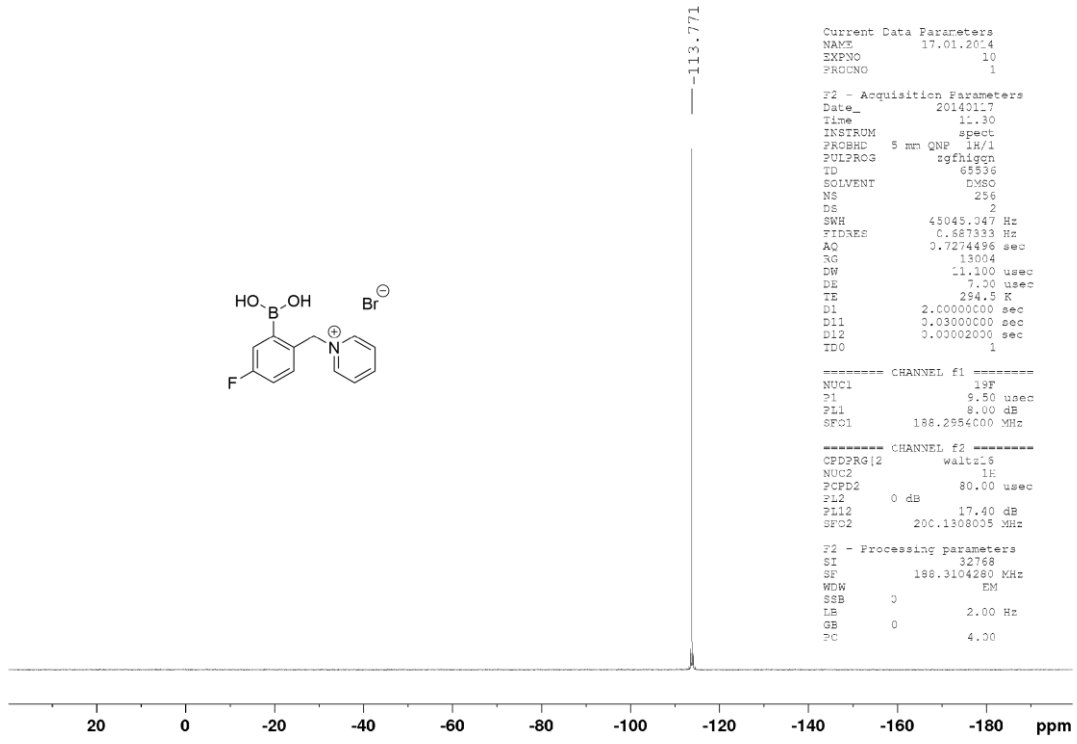

Figure S 43: $^{19}F\{^{1}H\}$ NMR (188 MHz, DMSO-d_6) spectrum of 4-F-*o*-BBpy (2).

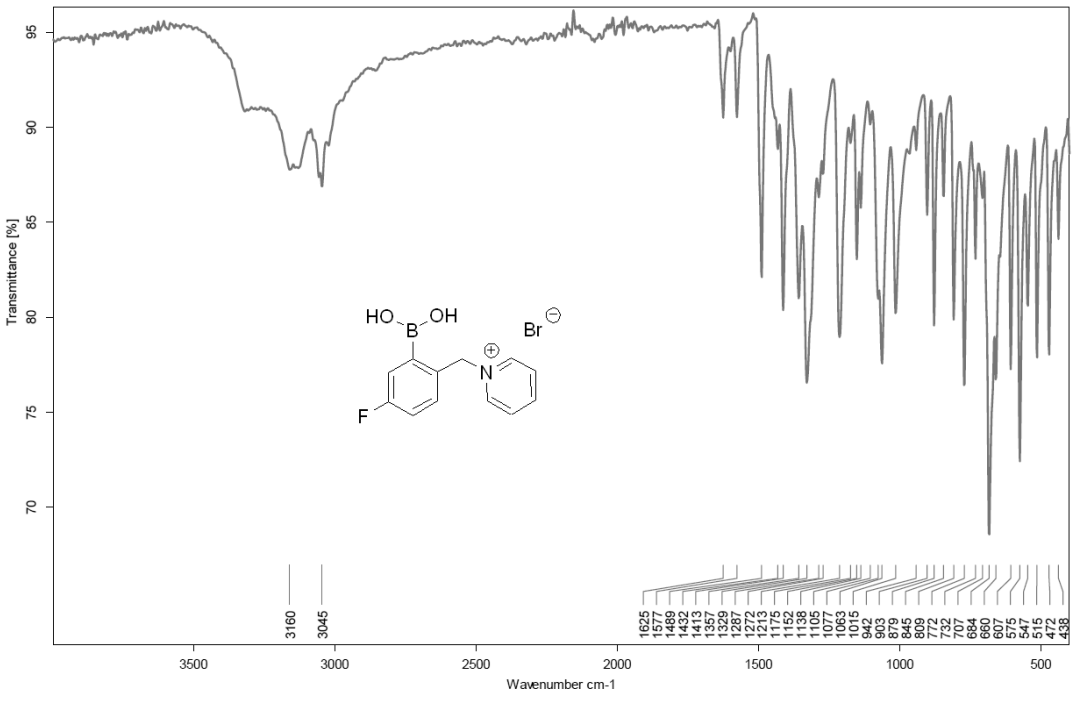

Figure S 44: FT-IR (ATR) spectrum of 4-F-*o*-BBpy (2).

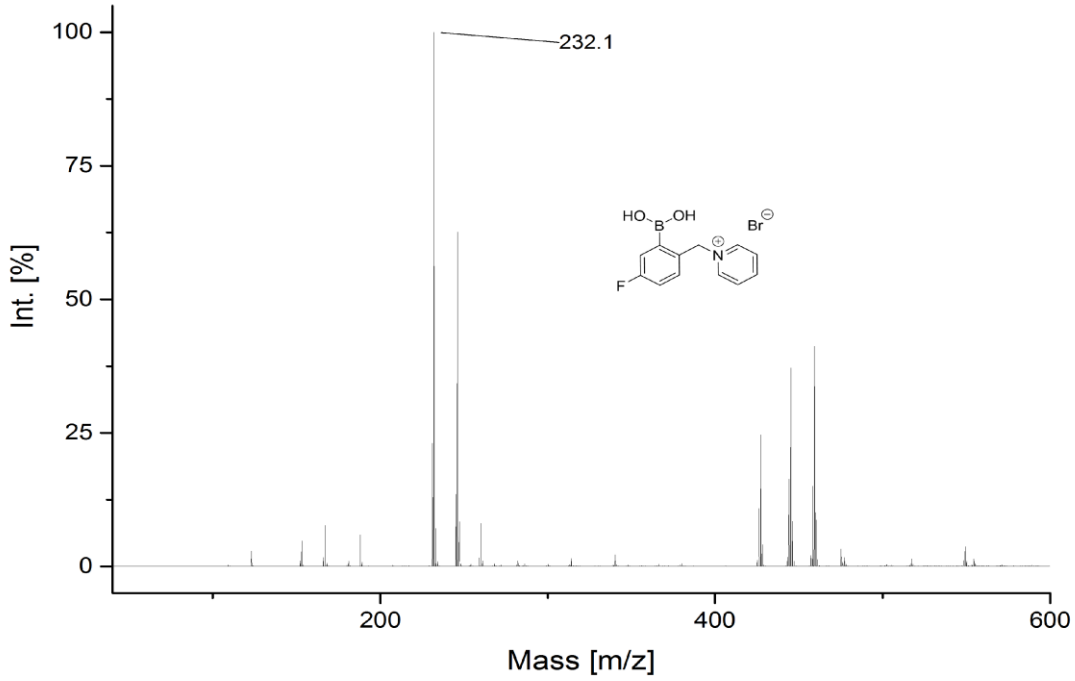

Figure S 45: MS (ESI+) of 4-F-*o*-BBpy (2).

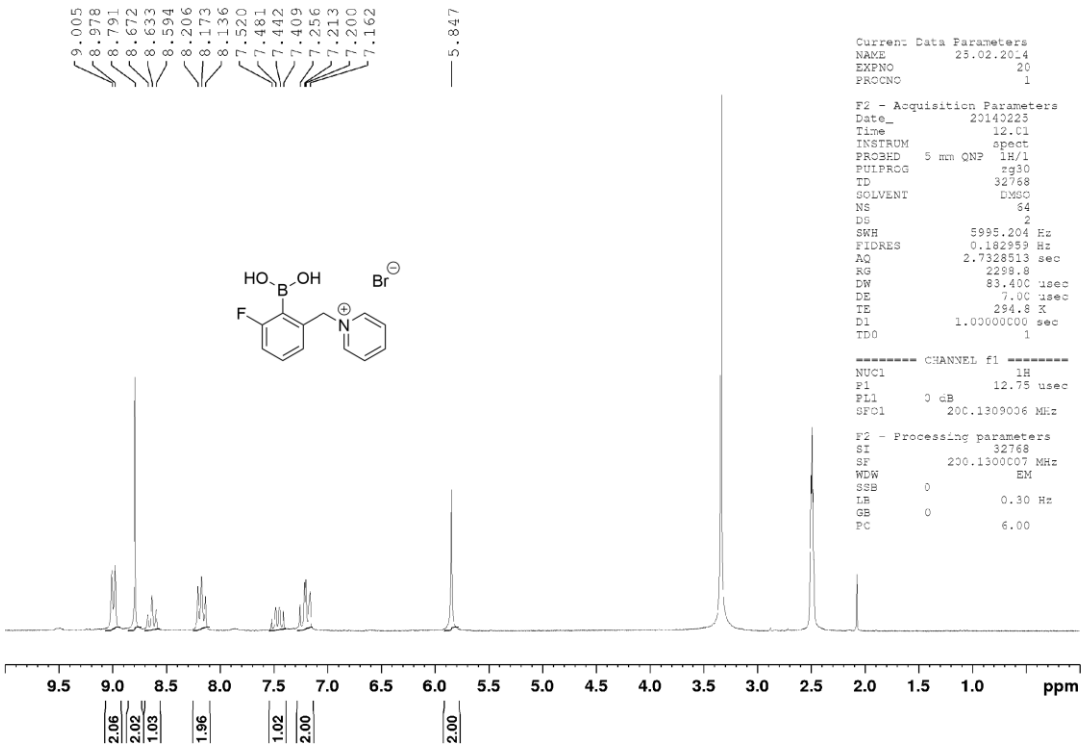

Figure S 46: ^{1}H NMR (200 MHz, DMSO-d$_6$) spectrum of 3-F-*o*-BBpy (3).

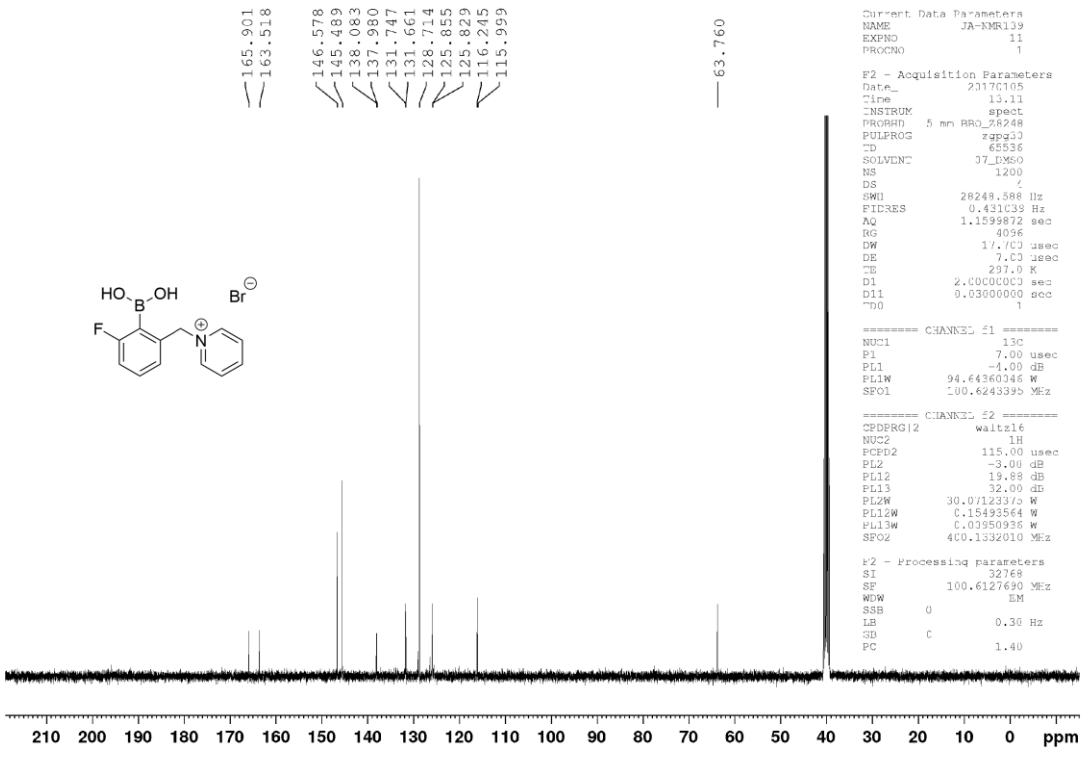

Figure S 47: $^{13}C\{^{1}H\}$ NMR (100 MHz, DMSO-d_6) spectrum of 3-F-*o*-BBpy (3).

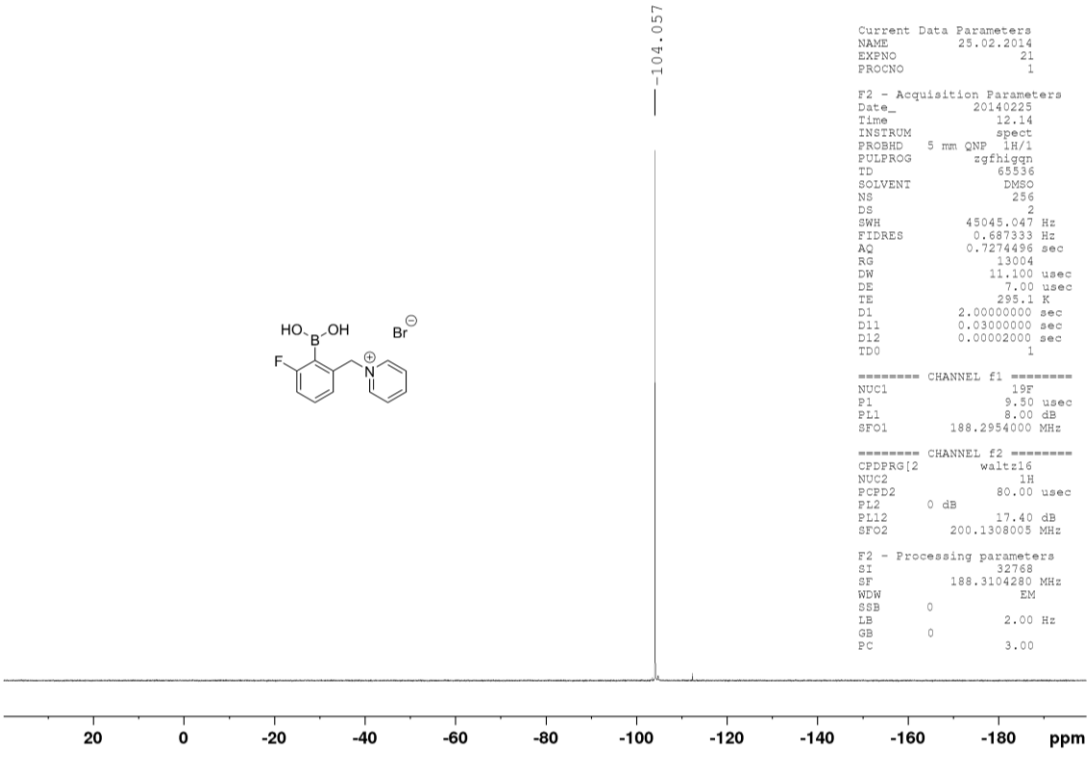

Figure S 48: $^{19}F\{^{1}H\}$ NMR (188 MHz, DMSO-d_6) spectrum of 3-F-*o*-BBpy (3).

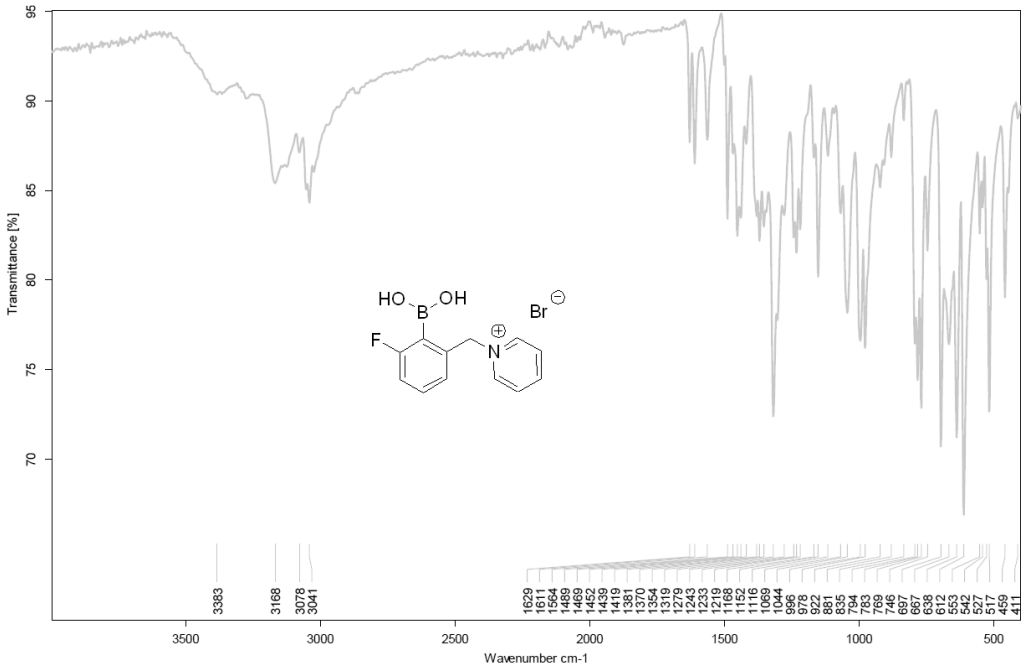

Figure S 49: FT-IR (ATR) spectrum of 3-F-*o*-BBpy (3).

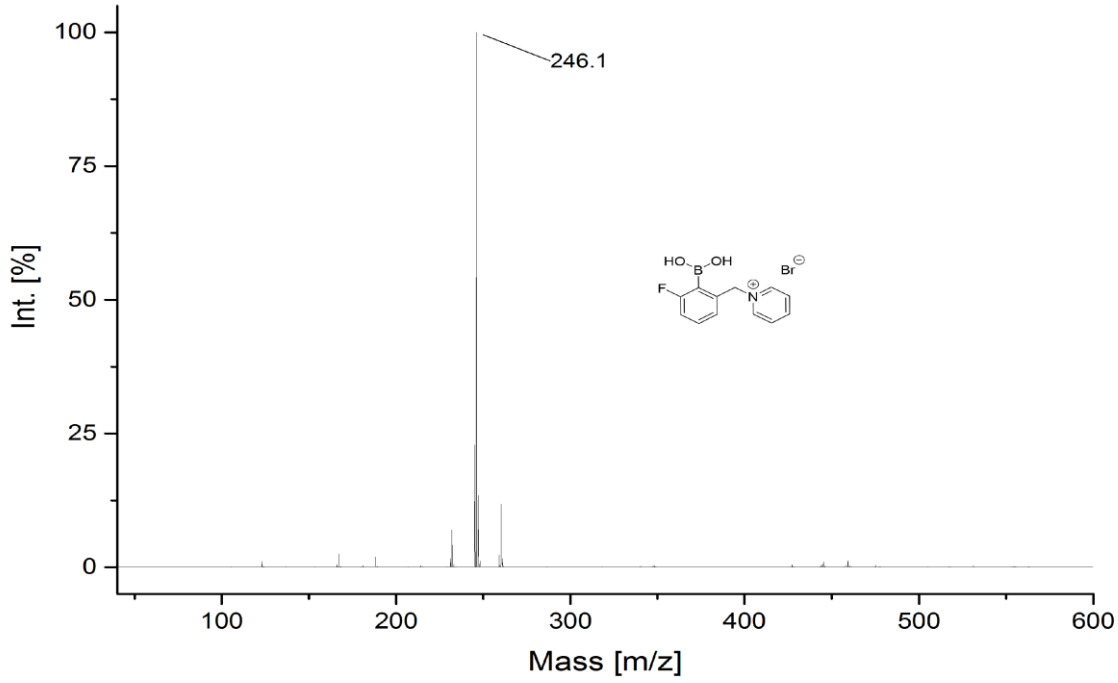

Figure S 50: MS (ESI+) spectrum of 3-F-*o*-BBpy (3).

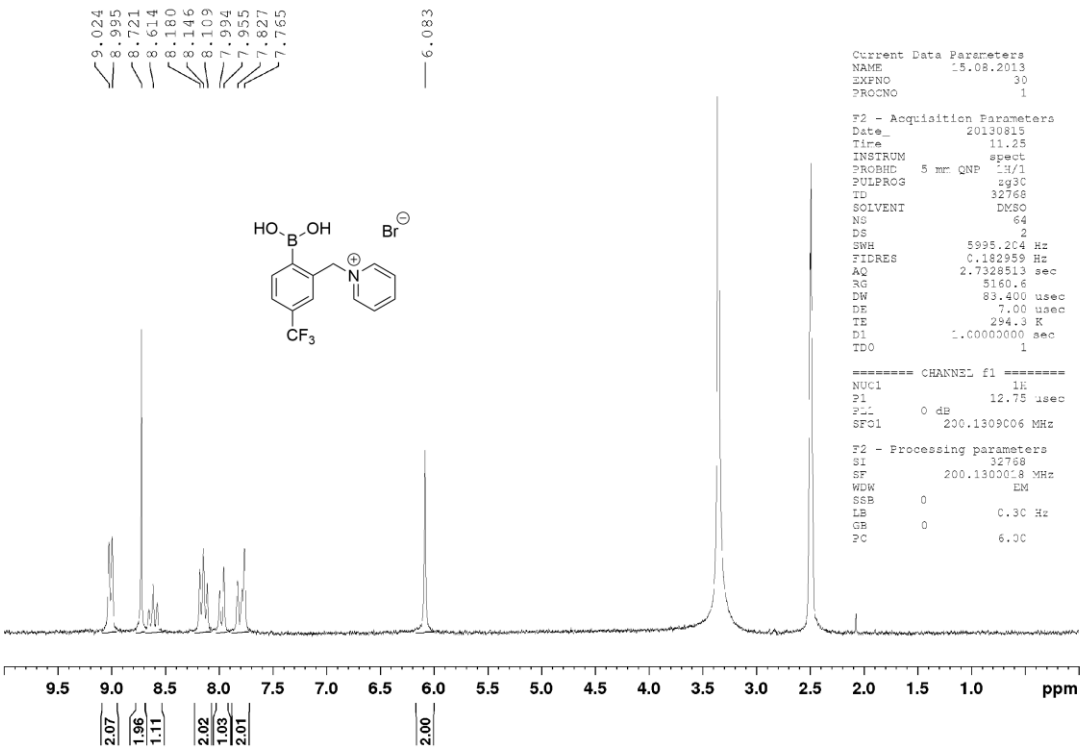

Figure S 51: ^{1}H NMR (200 MHz, DMSO-d$_6$) spectrum of 5-CF$_3$-*o*-BBpy (4).

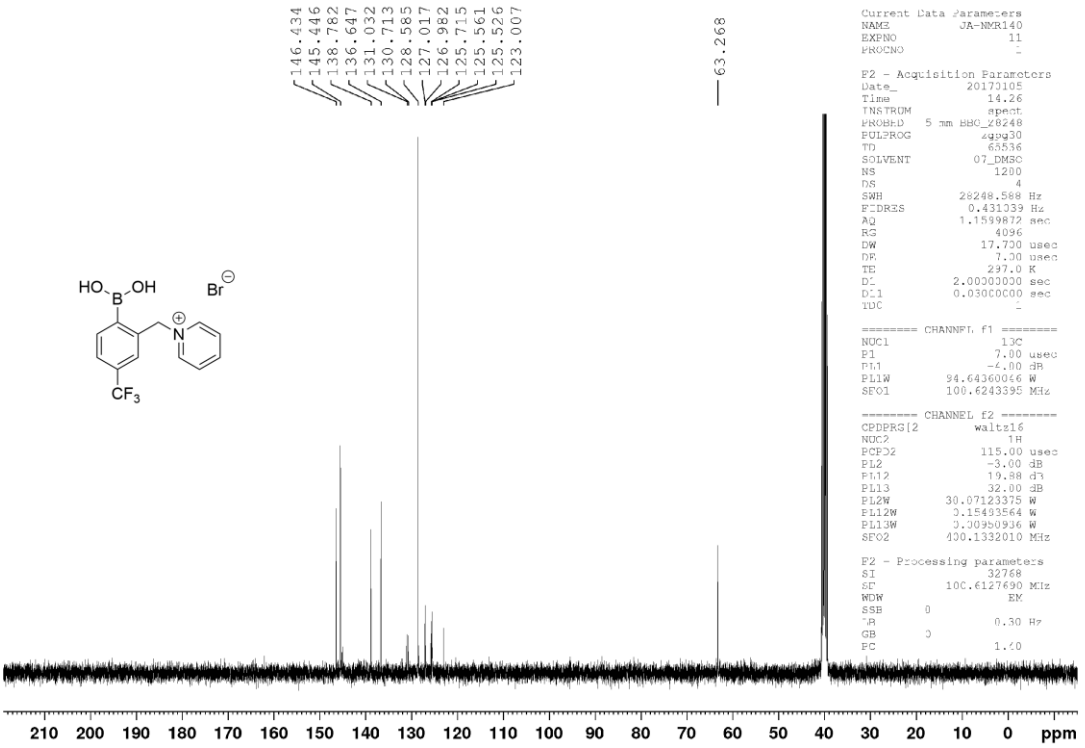

Figure S 52: ^{13}C{^{1}H} NMR (100 MHz, DMSO-d$_6$) spectrum of 5-CF$_3$-*o*-BBpy (4).

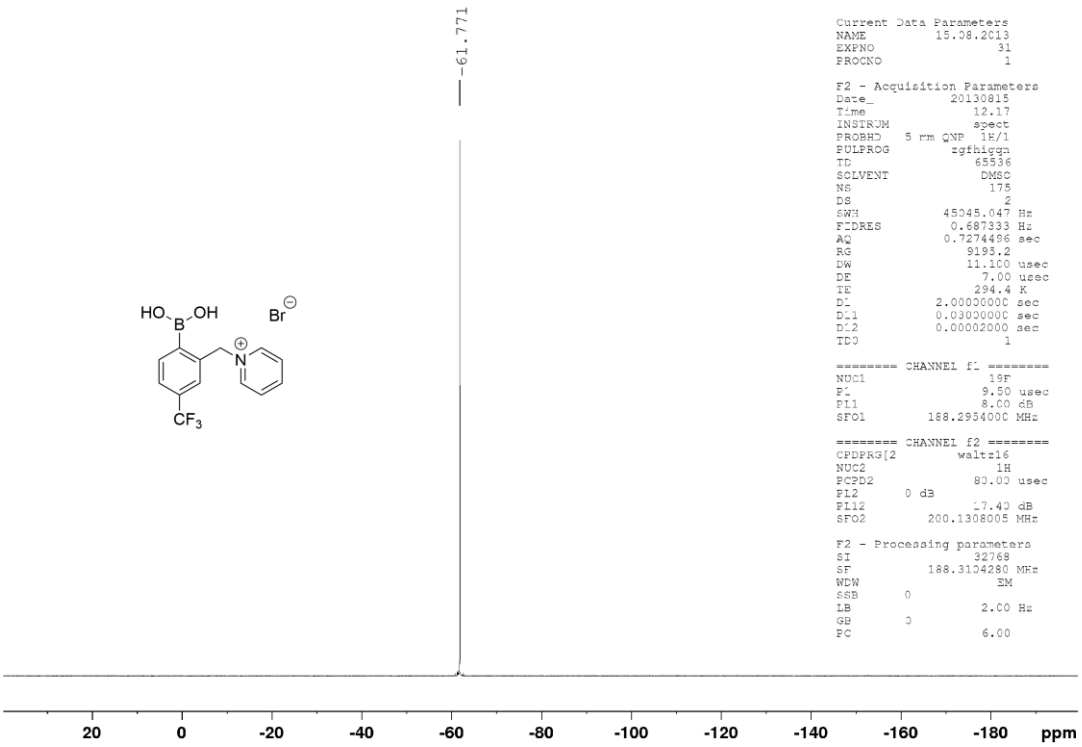

Figure S 53: $^{19}F\{^{1}H\}$ NMR (188 MHz, DMSO-d_6) spectrum of 5-CF_3-*o*-BBpy (4).

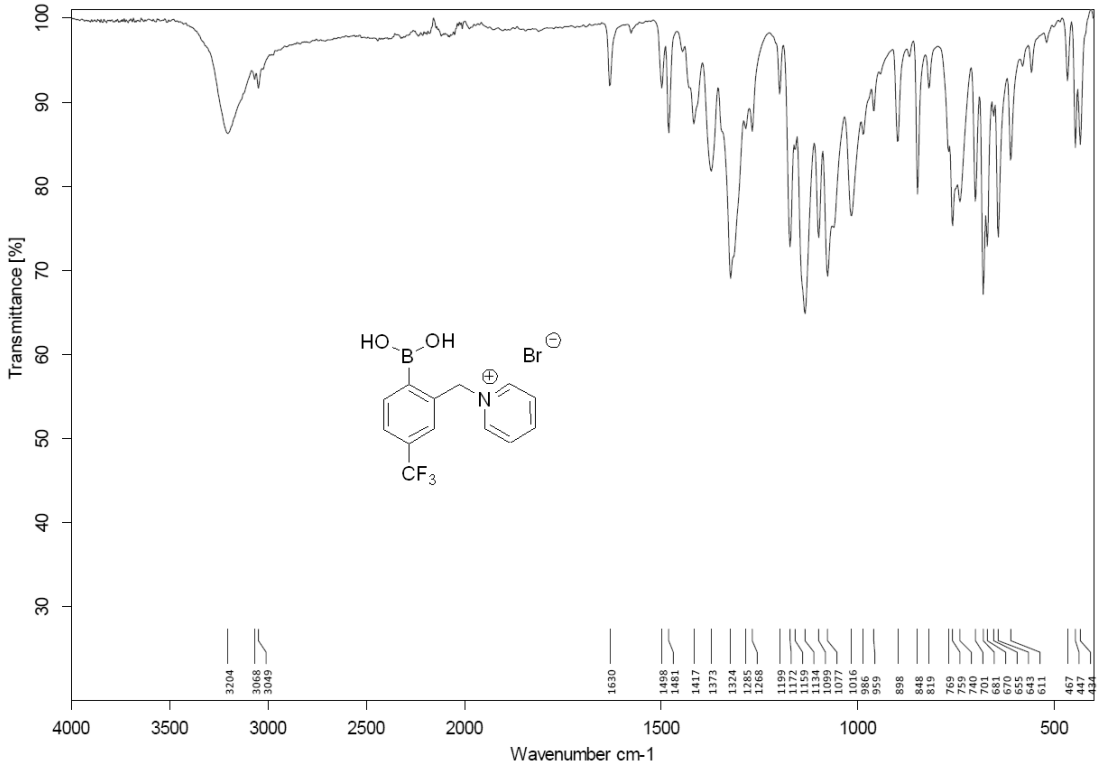

Figure S 54: FT-IR (ATR) spectrum of 5-CF_3-*o*-BBpy (4).

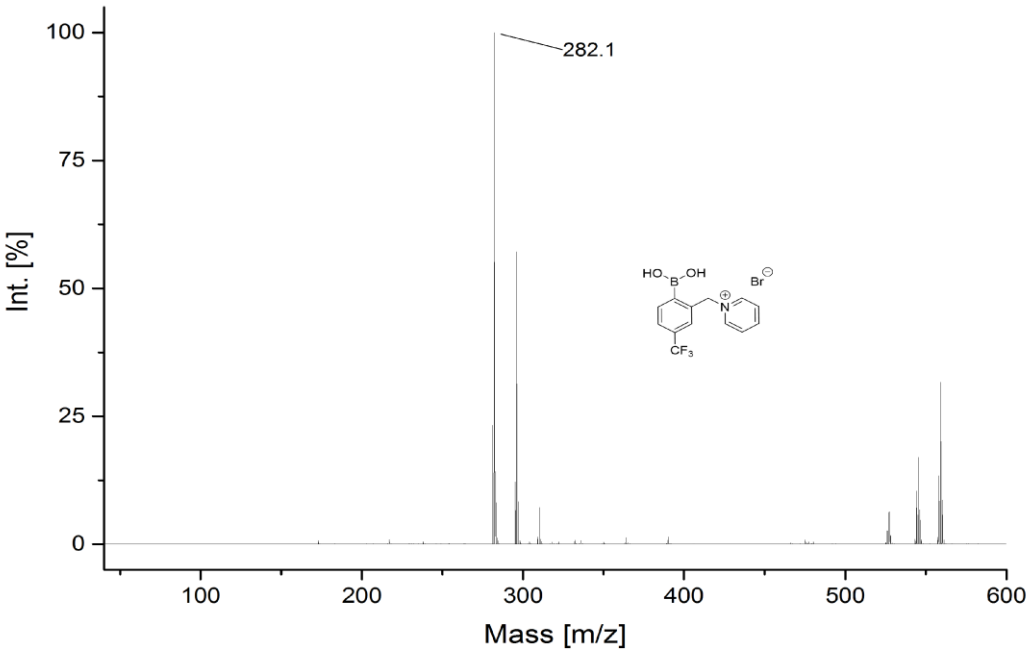

Figure S 55: MS (ESI+) spectrum of 5-CF_3-*o*-BBpy (4).

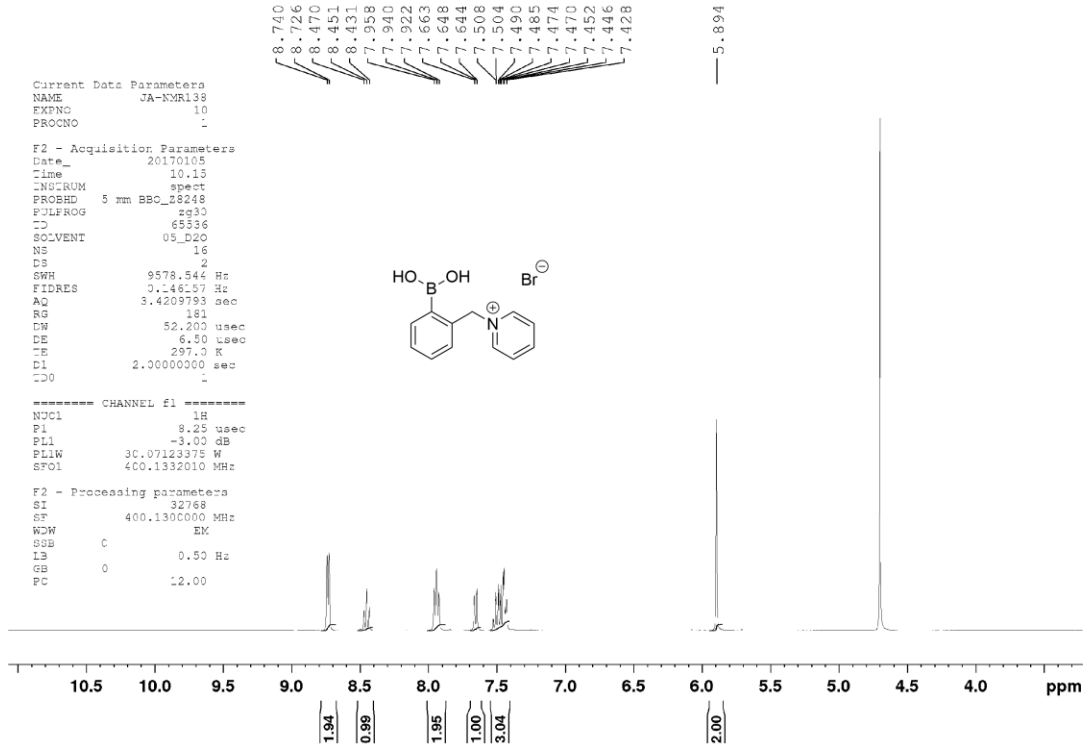

Figure S 56: ^{1}H NMR (400 MHz, D_2O) spectrum of *o*-BBpy (5).

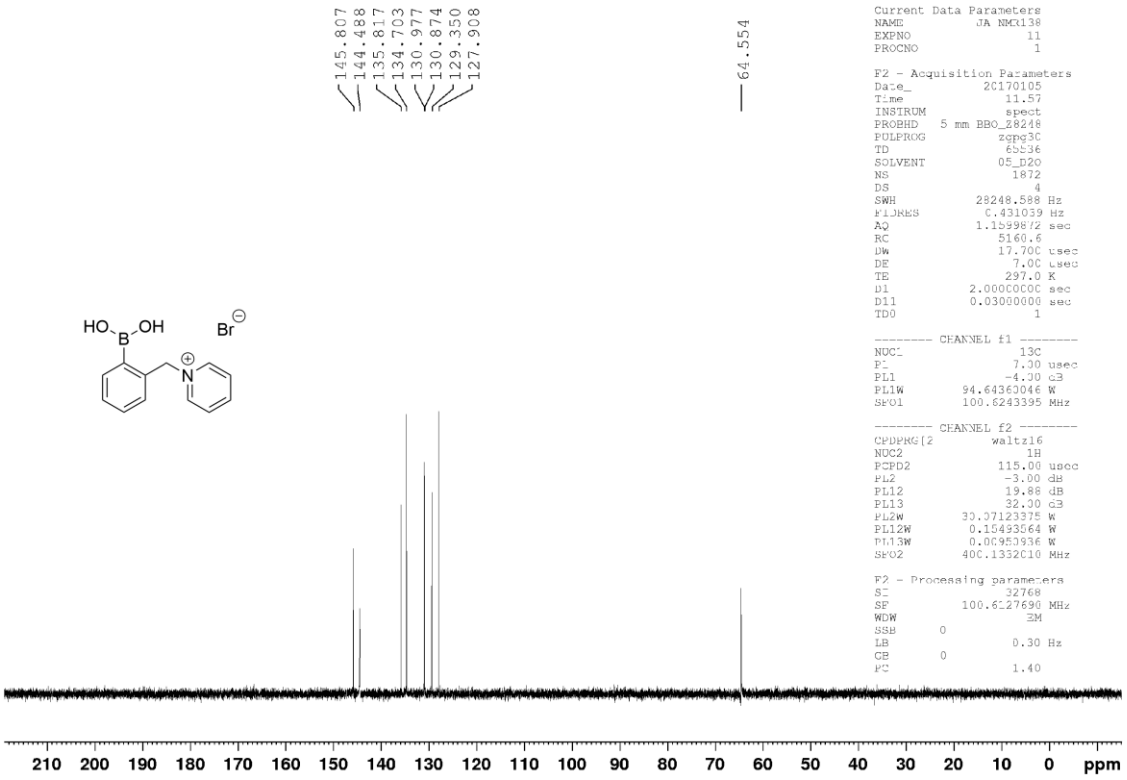

Figure S 57: $^{13}C\{^{1}H\}$ NMR (100 MHz, D_2O) spectrum of *o*-BBpy (5).

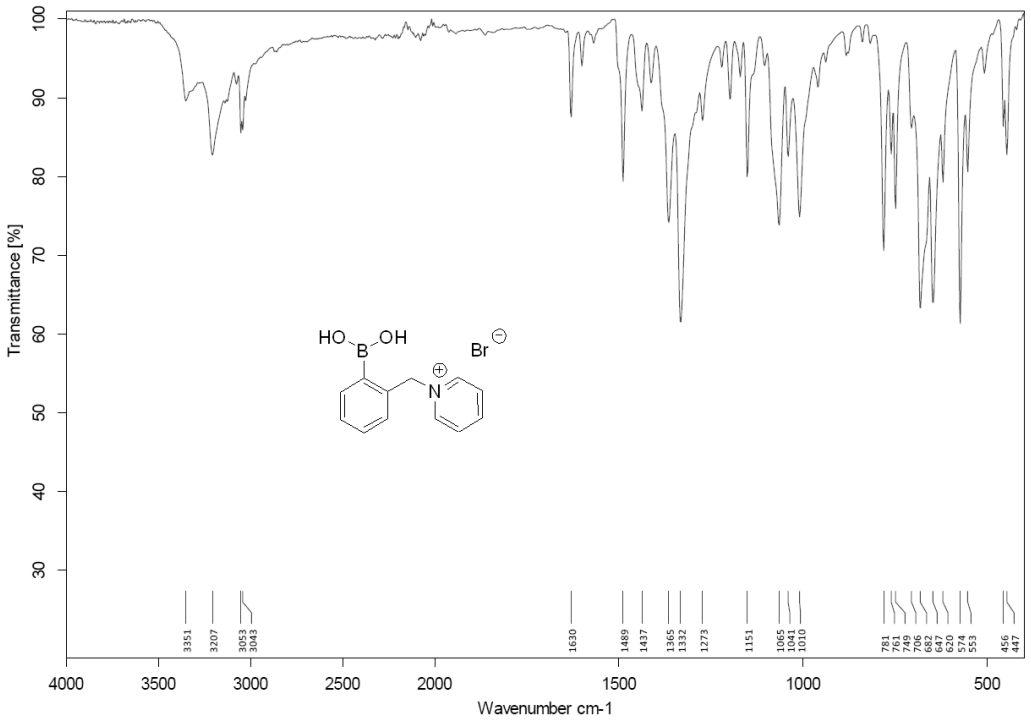

Figure S 58: FT-IR (ATR) spectrum of *o*-BBpy (5).

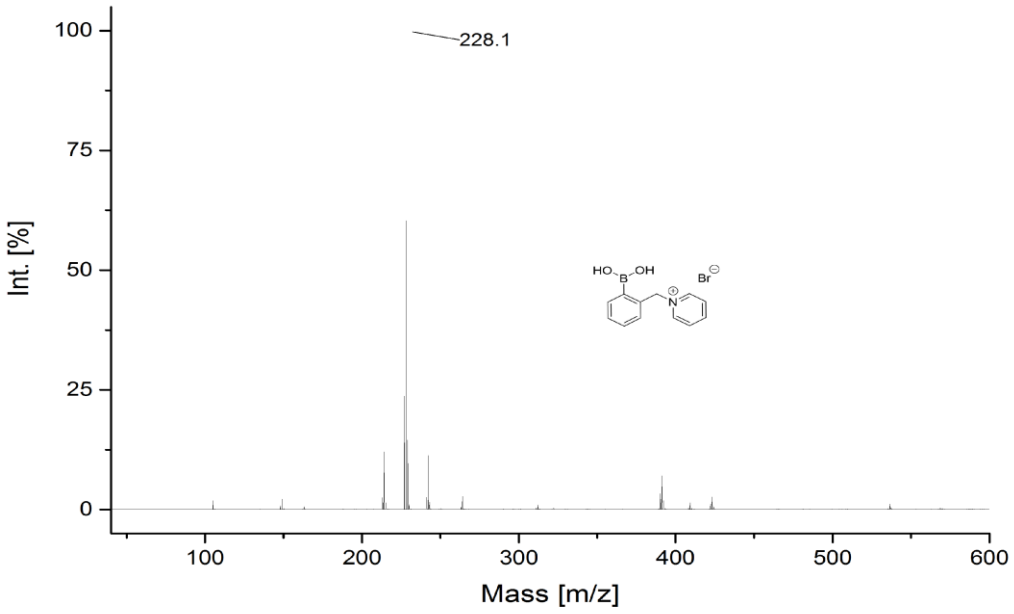

Figure S 59: MS (ESI+) spectrum of *o*-BBpy (5).

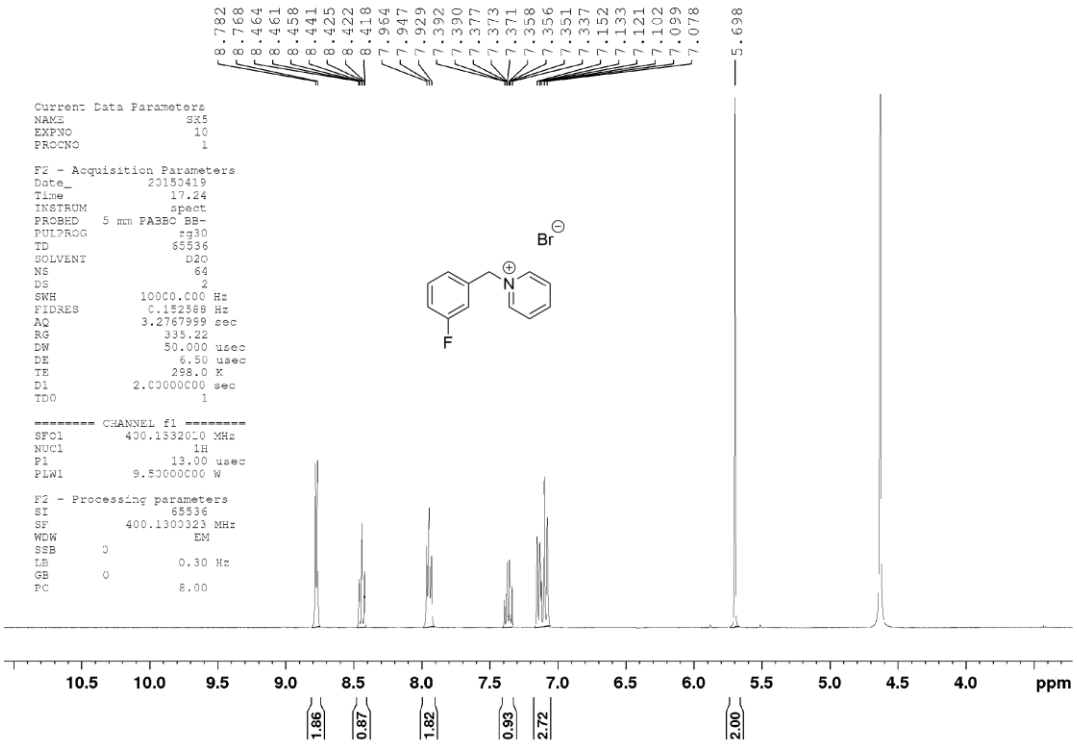

Figure S 60: ^{1}H NMR (400 MHz, D_2O) spectrum of 3-F-Bpy (6).

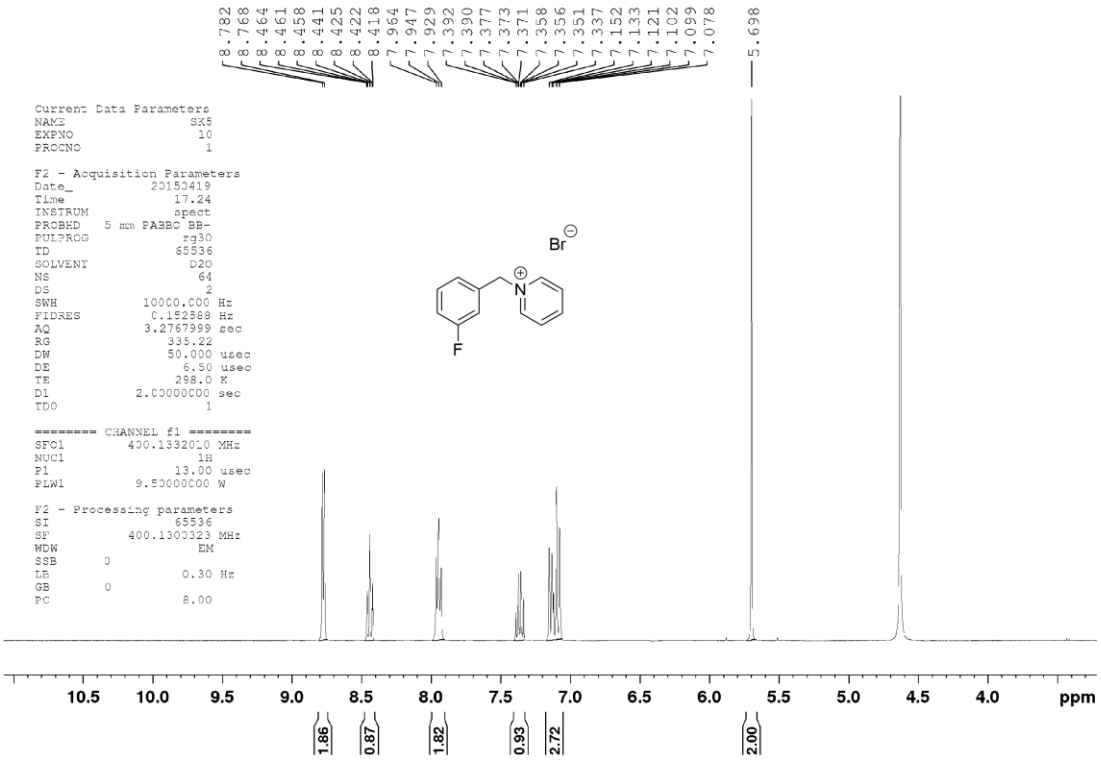

Figure S 61: $^{13}C\{^{1}H\}$ NMR (100 MHz, D_2O) spectrum of 3-F-Bpy (6).

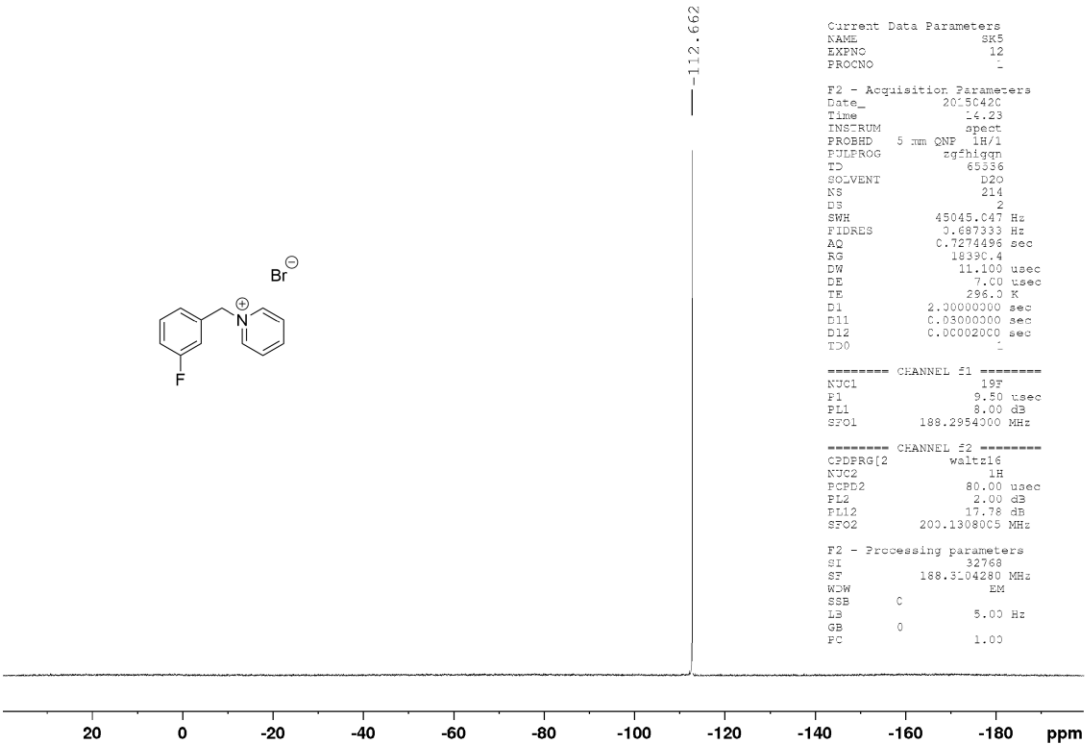

Figure S 62: $^{19}F\{^{1}H\}$ NMR (188 MHz, D_2O) spectrum of 3-F-Bpy (6).

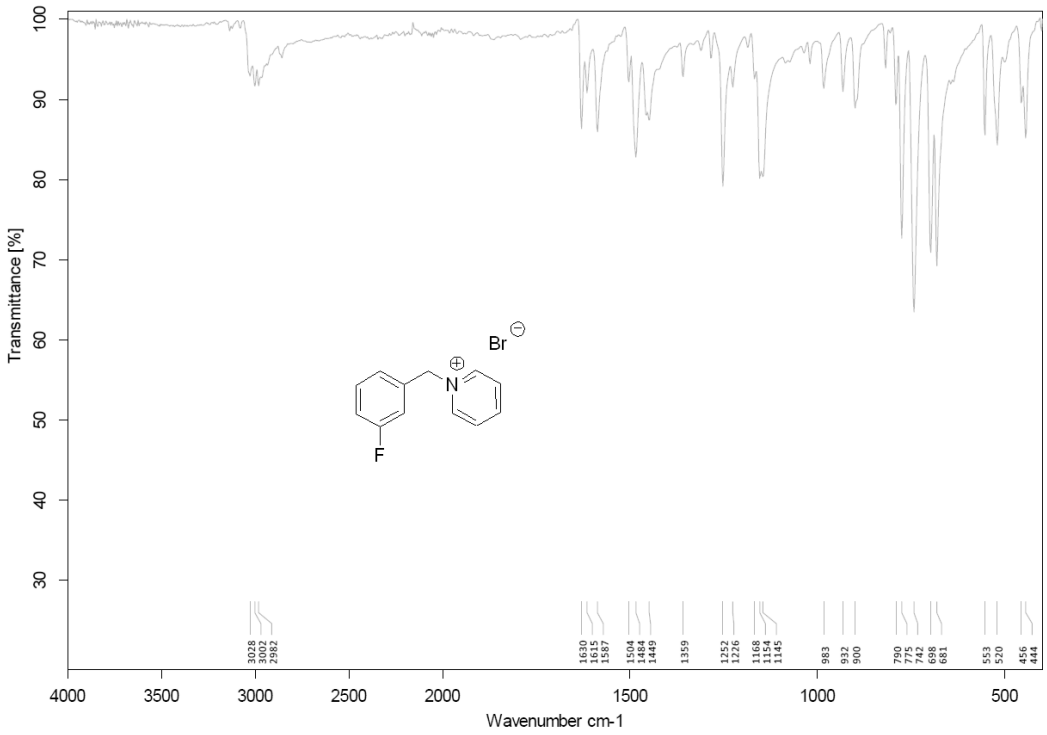

Figure S 63: FT-IR (ATR) spectrum of 3-F-Bpy (6).

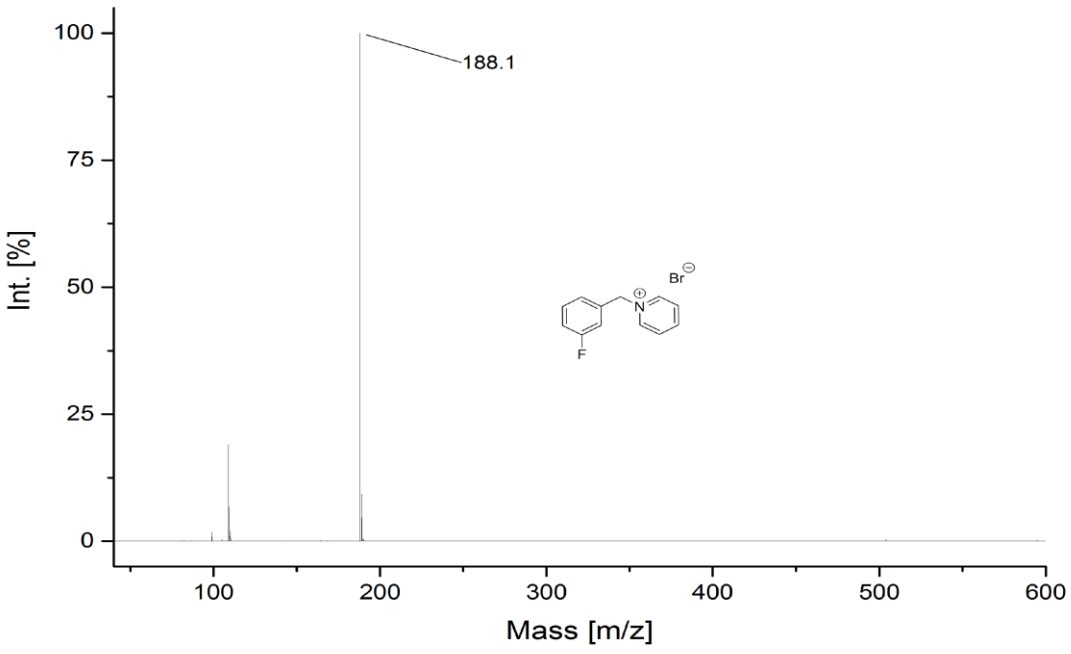

Figure S 64: MS (ESI+) spectrum of 3-F-Bpy (6).

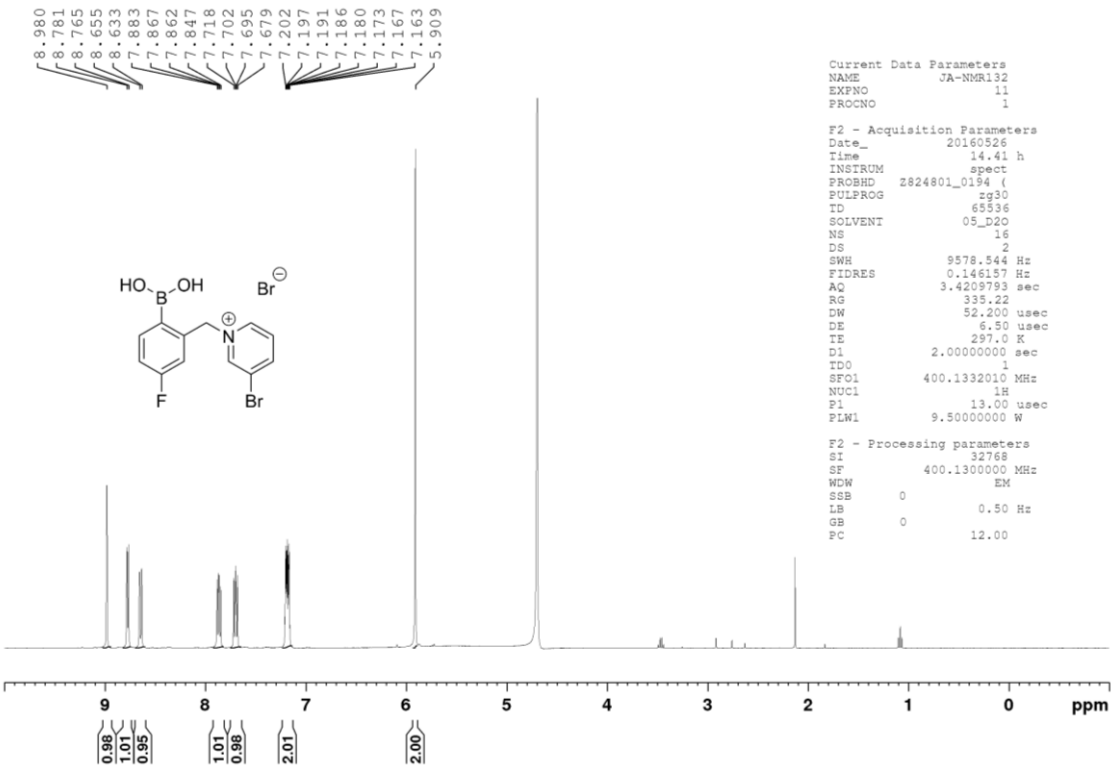

Figure S 56: ^{1}H NMR (400 MHz, D_2O) spectrum of 5-F-*o*-BBBrpy (7).

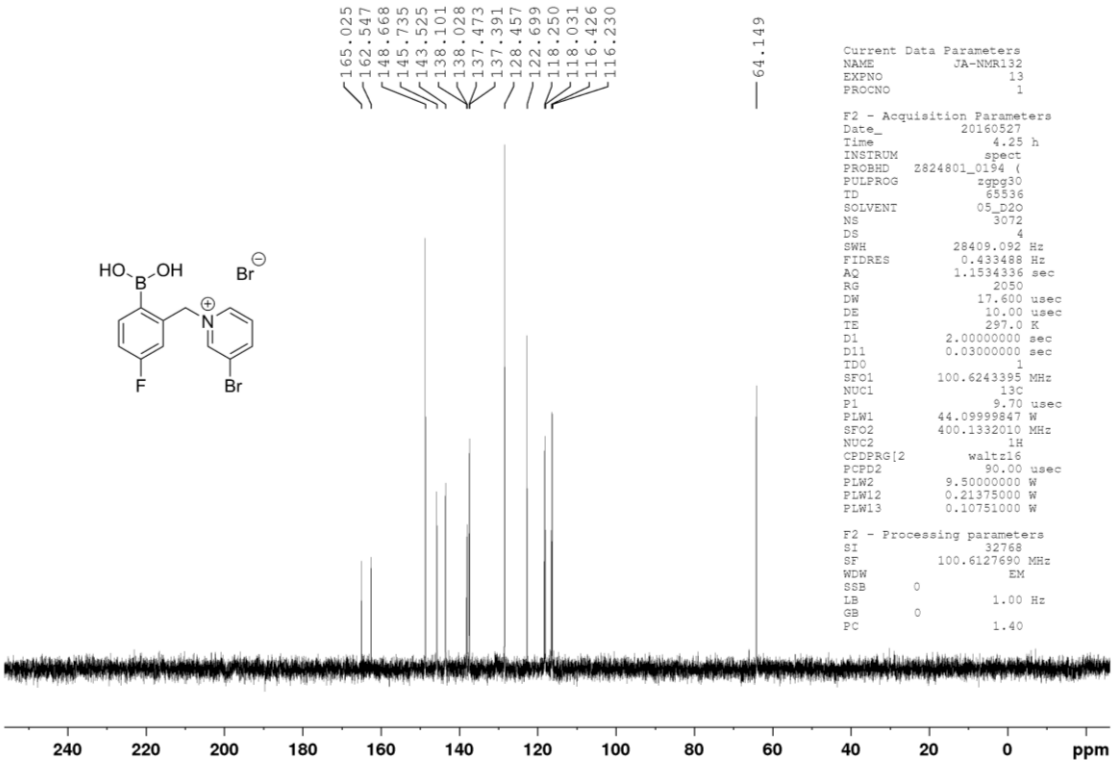

Figure S 57: $^{13}C\{^{1}H\}$ NMR (100 MHz, D_2O) spectrum of 5-F-*o*-BBBrpy (7).

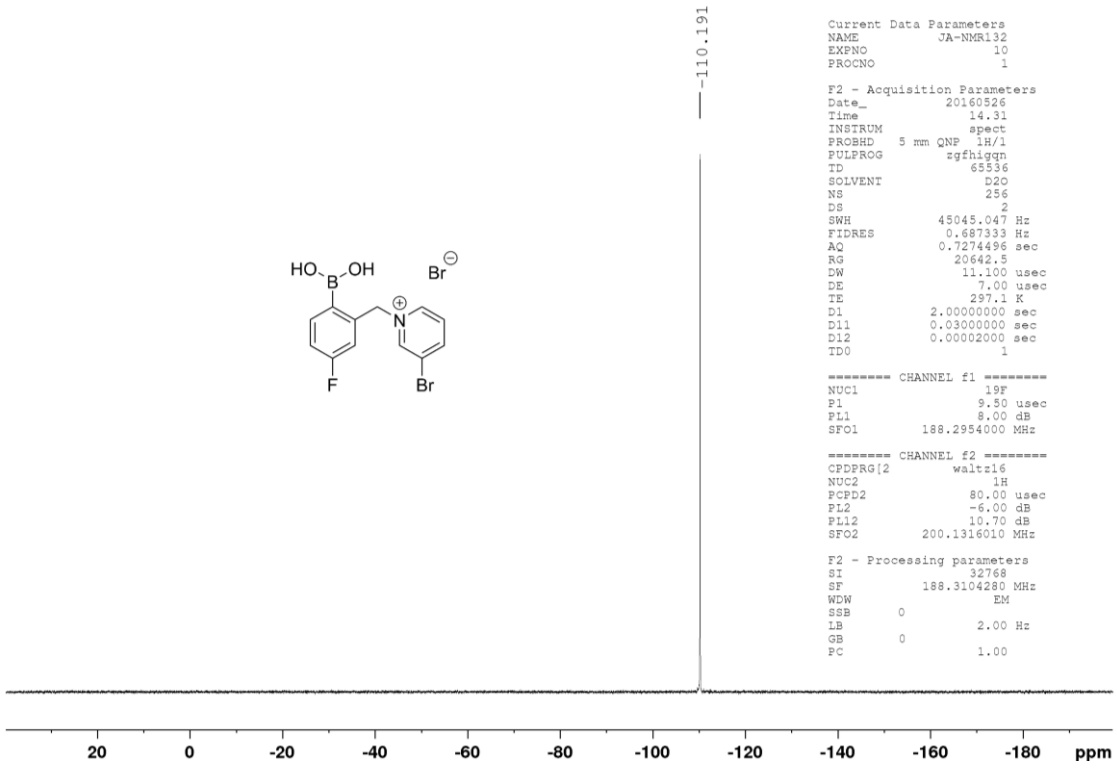

Figure S 58: $^{19}F\{^{1}H\}$ NMR (188 MHz, D_2O) spectrum of 5-F-*o*-BBBrpy (7).

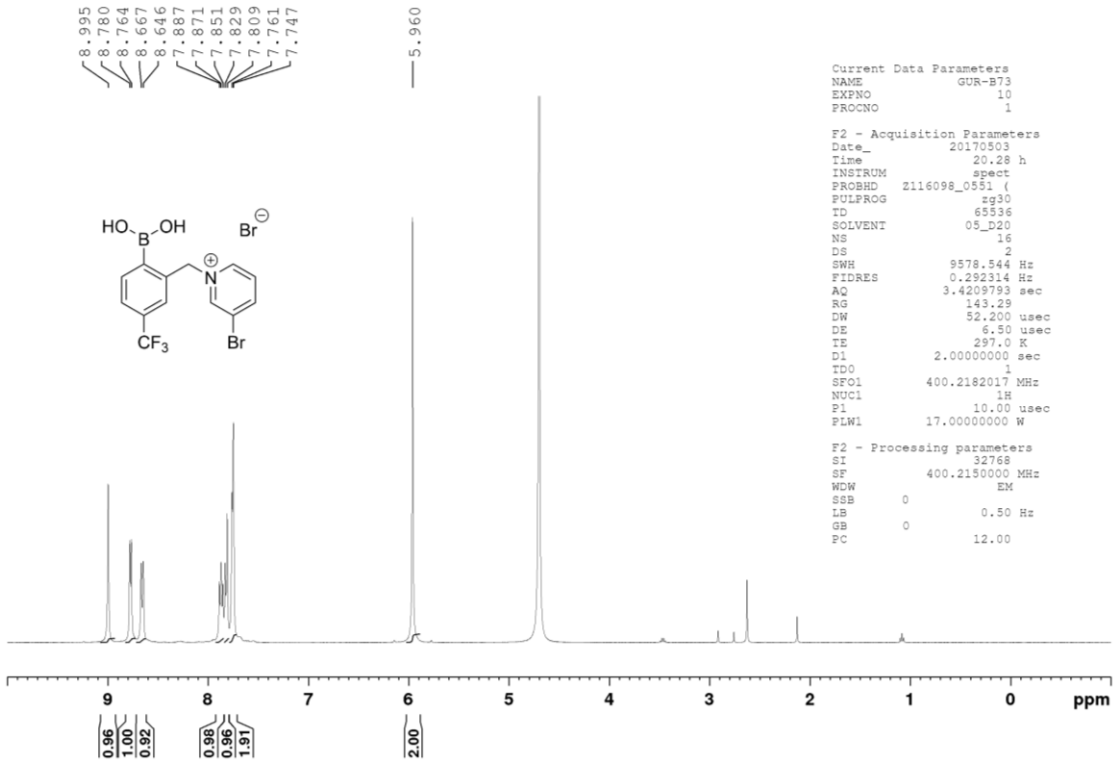

Figure S 59: ^{1}H NMR (400 MHz, D_2O) spectrum of 5-CF_3-*o*-BBBrpy (8).

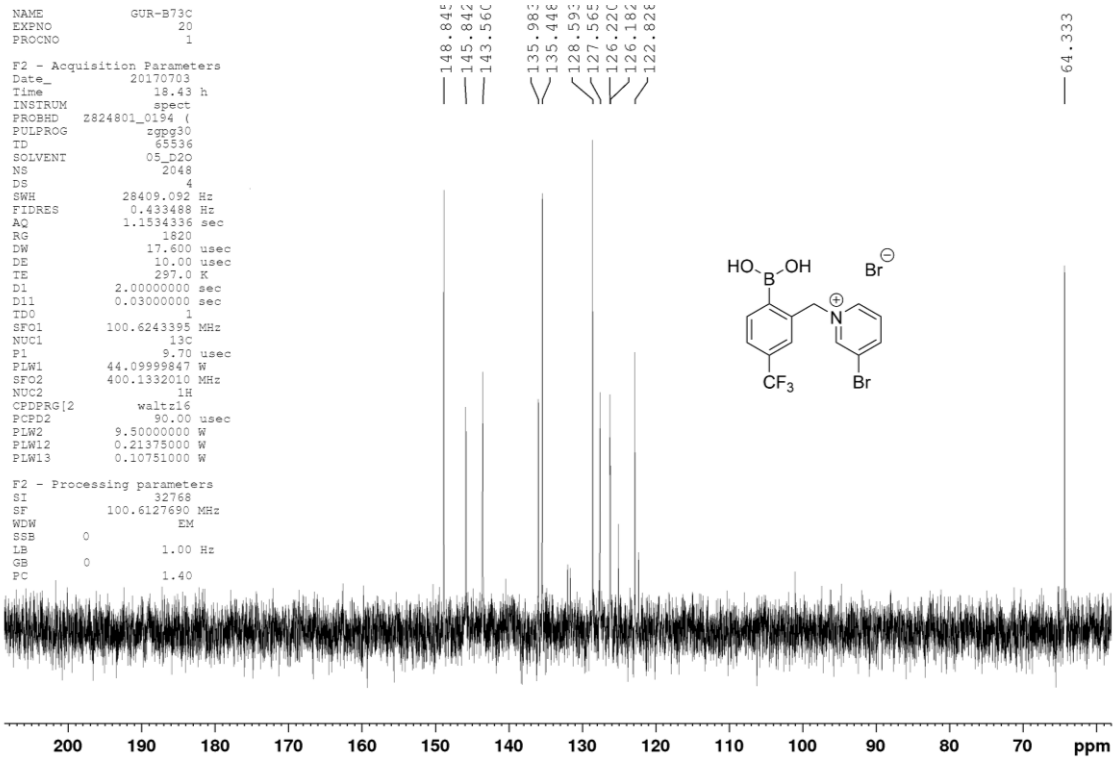

Figure S 60: $^{13}C\{^{1}H\}$ NMR (100 MHz, D_2O) spectrum of 5-CF_3-*o*-BBBrpy (8).

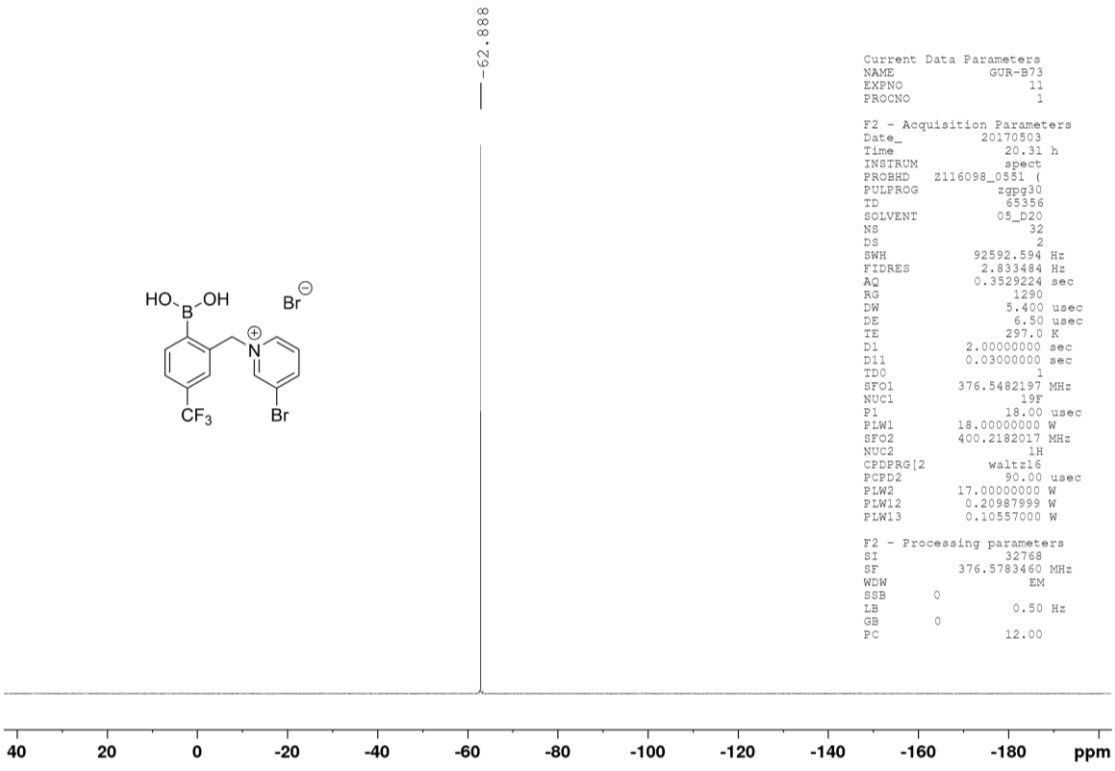

Figure S 61: $^{19}F\{^{1}H\}$ NMR (377 MHz, D_2O) spectrum of 5-CF_3-*o*-BBBrpy (8).

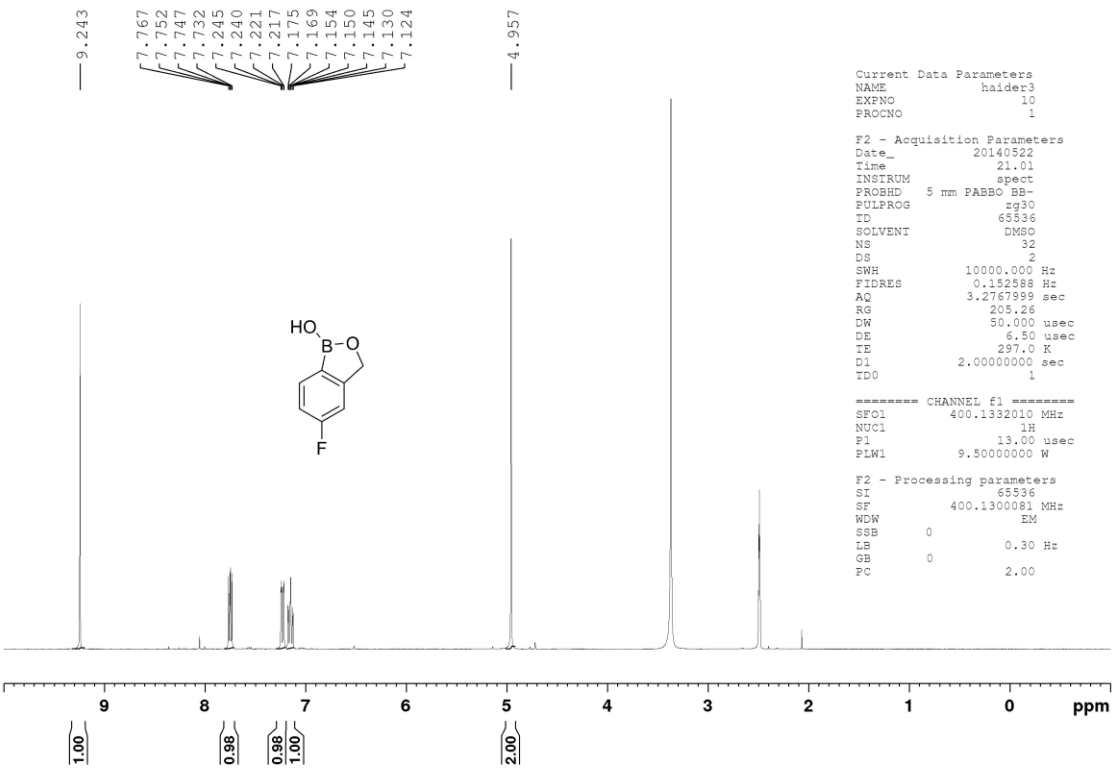

Figure S 62: ^{1}H NMR (400 MHz, DMSO-d$_6$) spectrum of 5-F-*o*-Boxab (9).

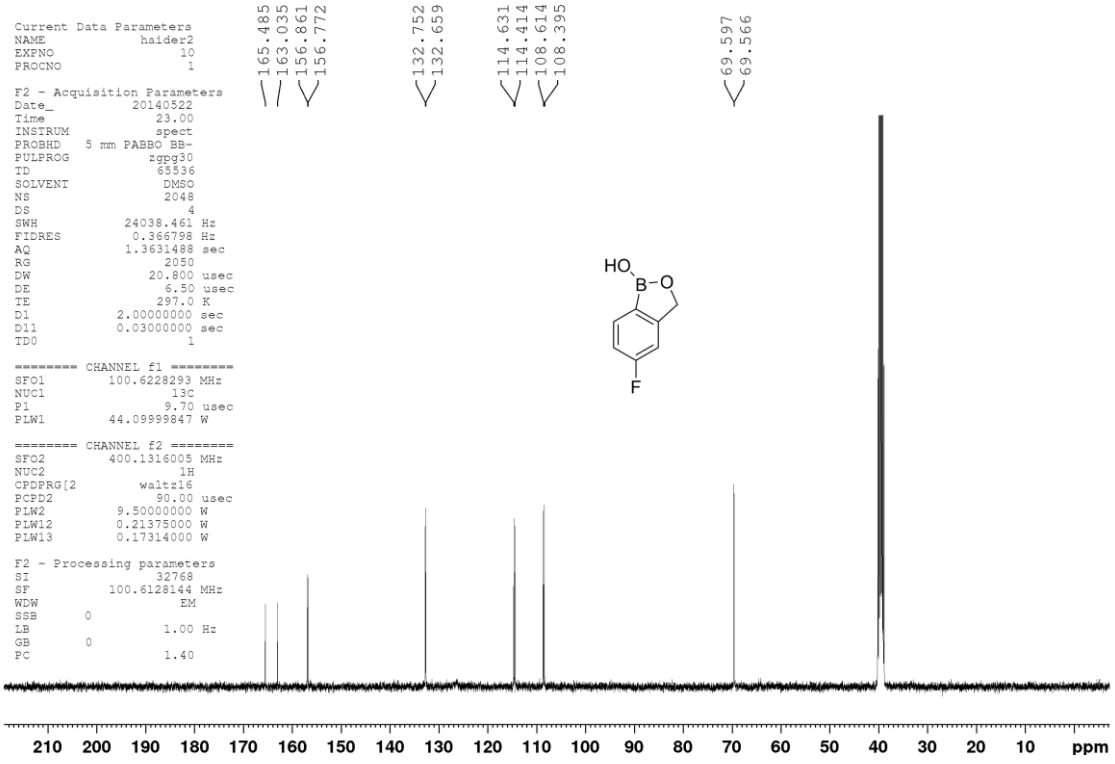

Figure S 63: ^{13}C{^{1}H} NMR (100 MHz, DMSO-d$_6$) spectrum of 5-F-*o*-Boxab (9).

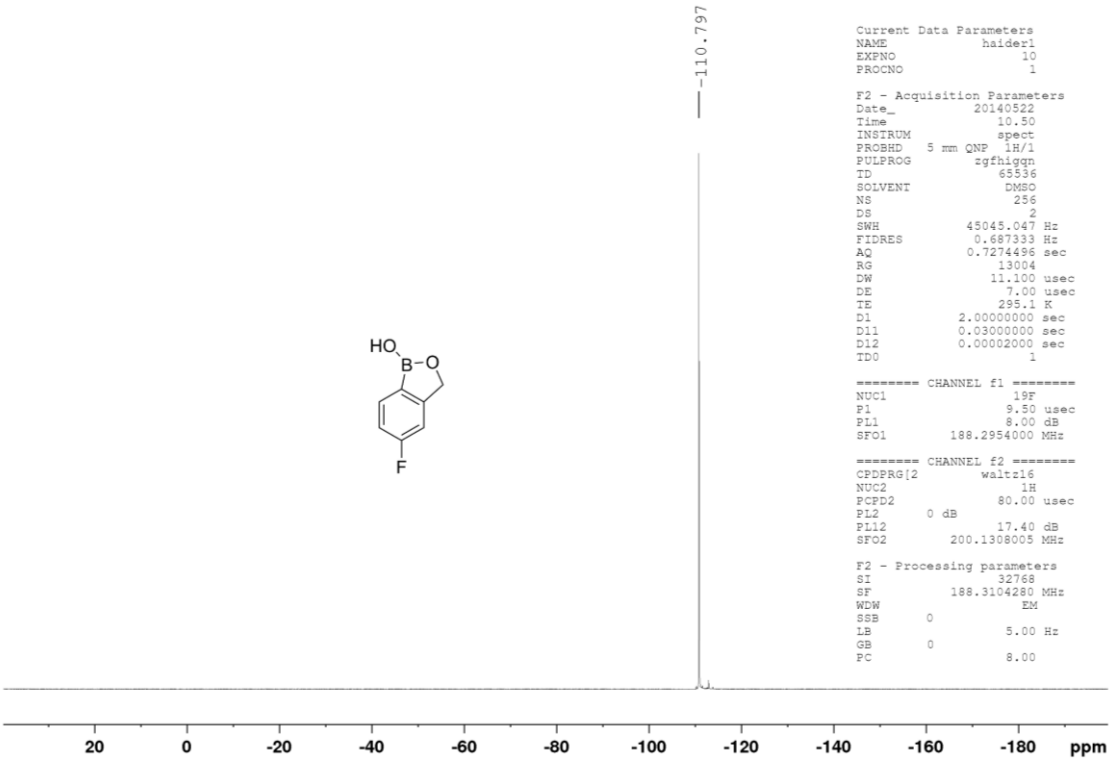

Figure S 64: $^{19}F\{^{1}H\}$ NMR (188 MHz, DMSO-d_6) spectrum of 5-F-*o*-Boxab (9).

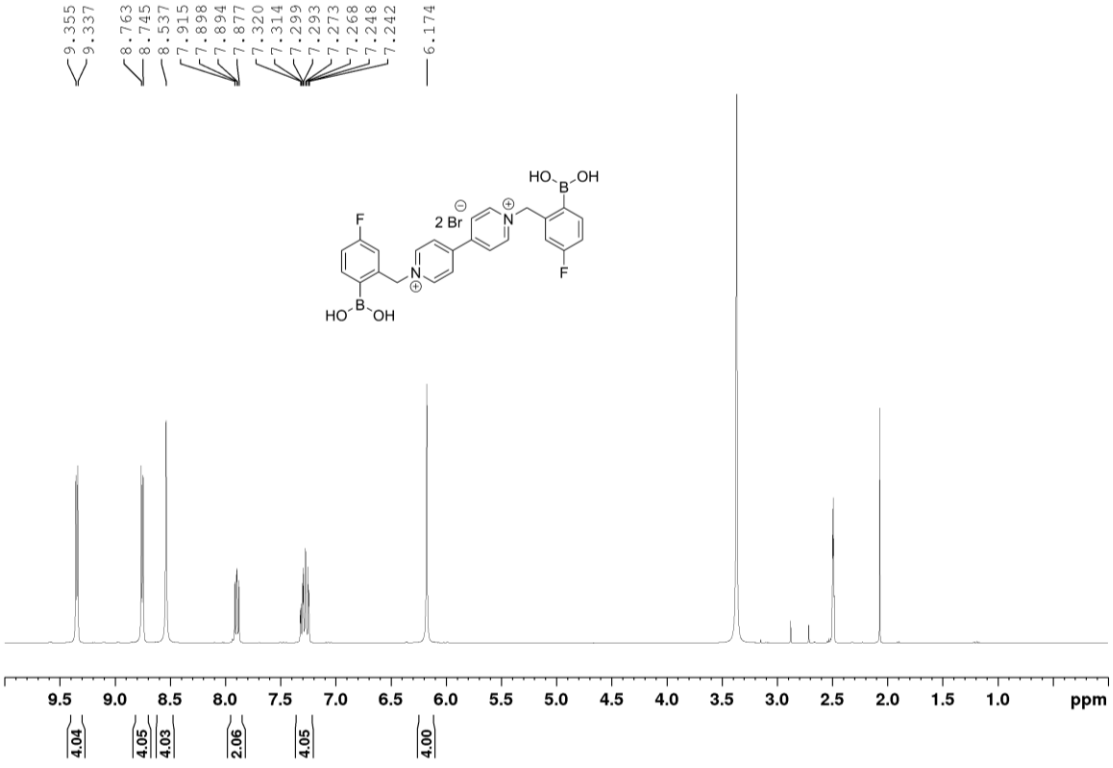

Figure S 65: ^{1}H NMR (400 MHz, DMSO-d_6) spectrum of F-4,4'-*o*-BBV (10).

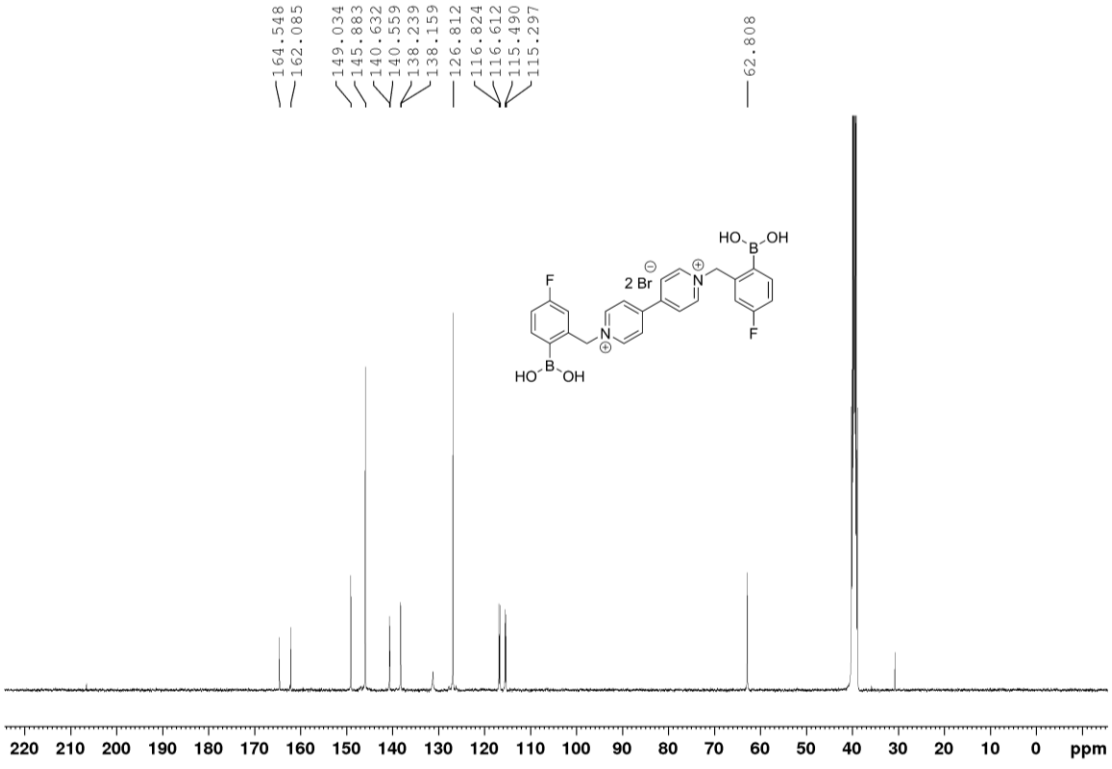

Figure S 66: $^{13}C\{^{1}H\}$ NMR (100 MHz, DMSO-d_6) spectrum of F-4,4'-*o*-BBV (10).

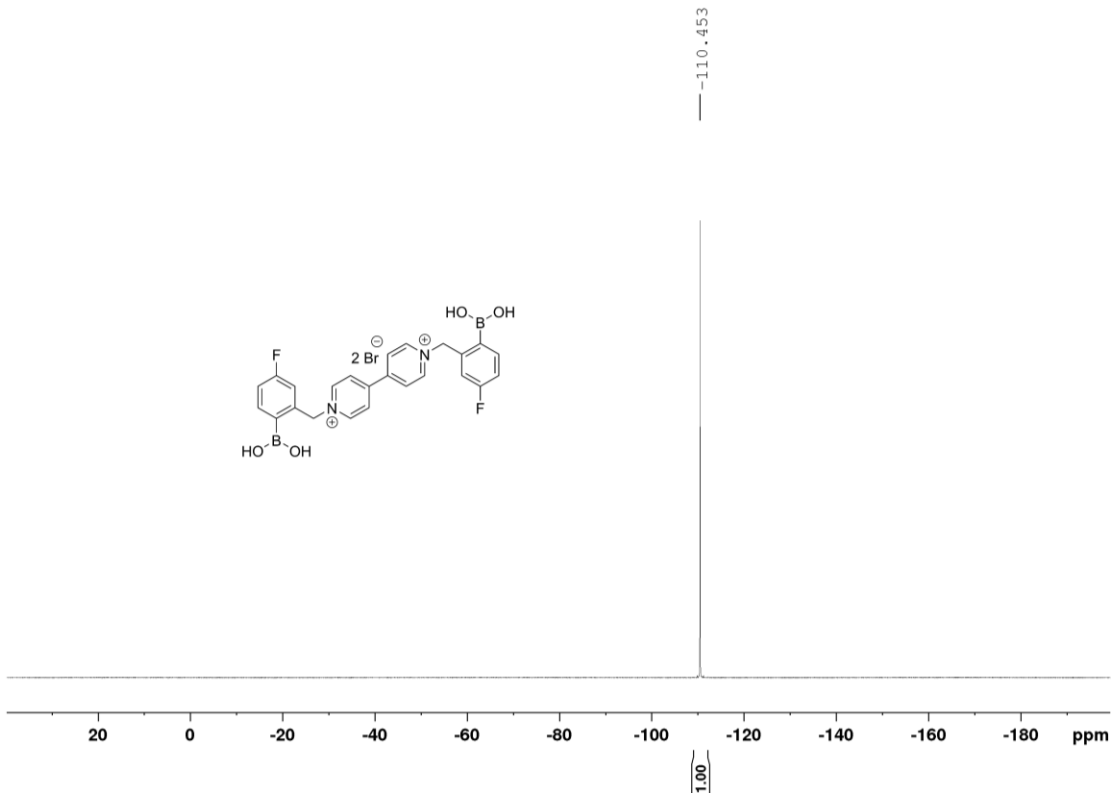

Figure S 67: $^{19}F\{^{1}H\}$ NMR (188 MHz, DMSO-d_6) spectrum of F-4,4'-*o*-BBV (10).

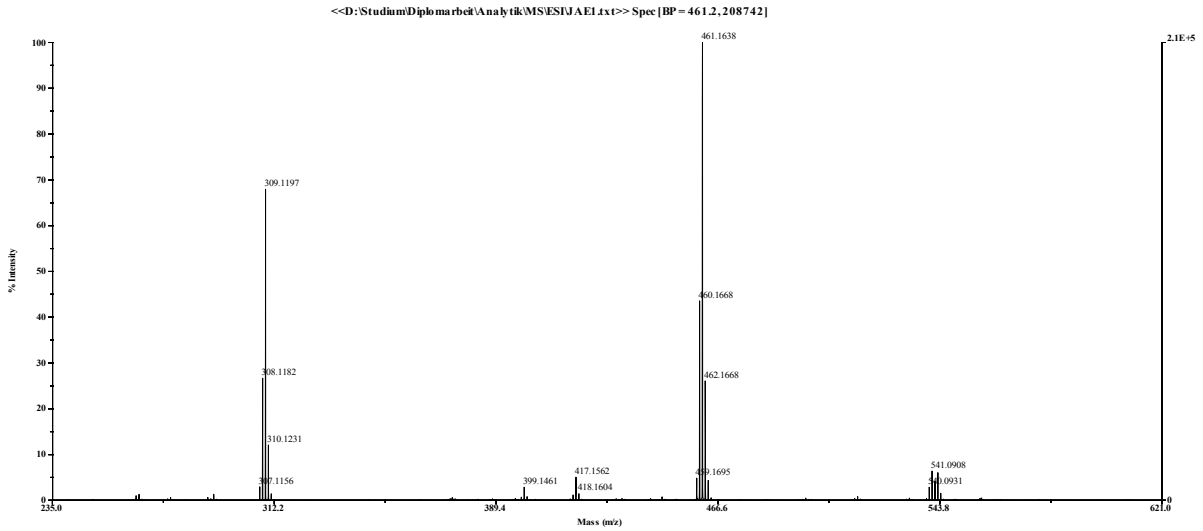

Figure S 68: High resolution ESI-TOF MS spectrum of F-4,4'-*o*-BBV (10).

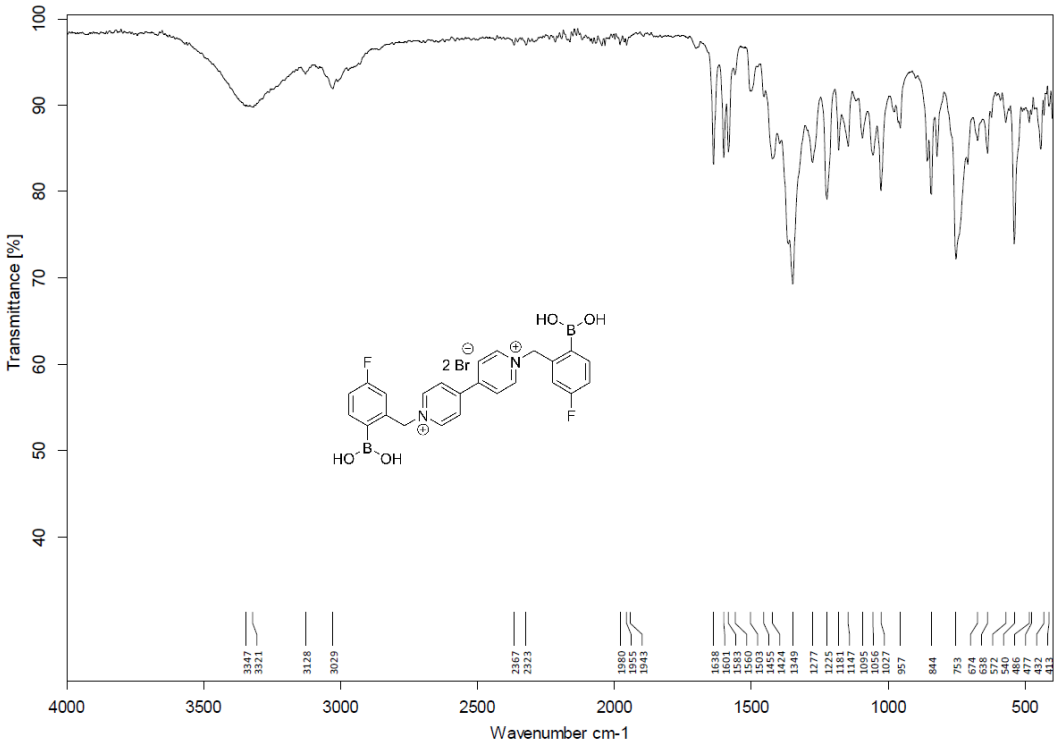

Figure S 69: IR (ATR) spectrum of F-4,4'-*o*-BBV (10).

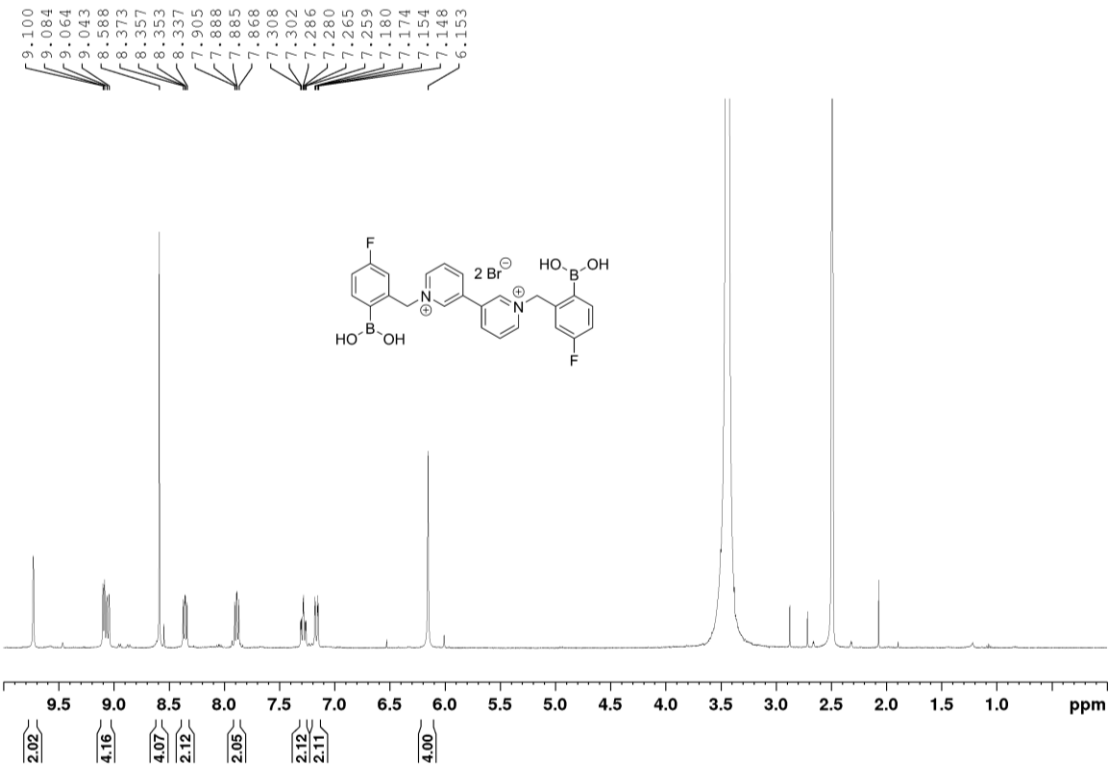

Figure S 70: ^{1}H NMR (400 MHz, DMSO-d$_6$) spectrum of F-3,3'-*o*-BBV (11).

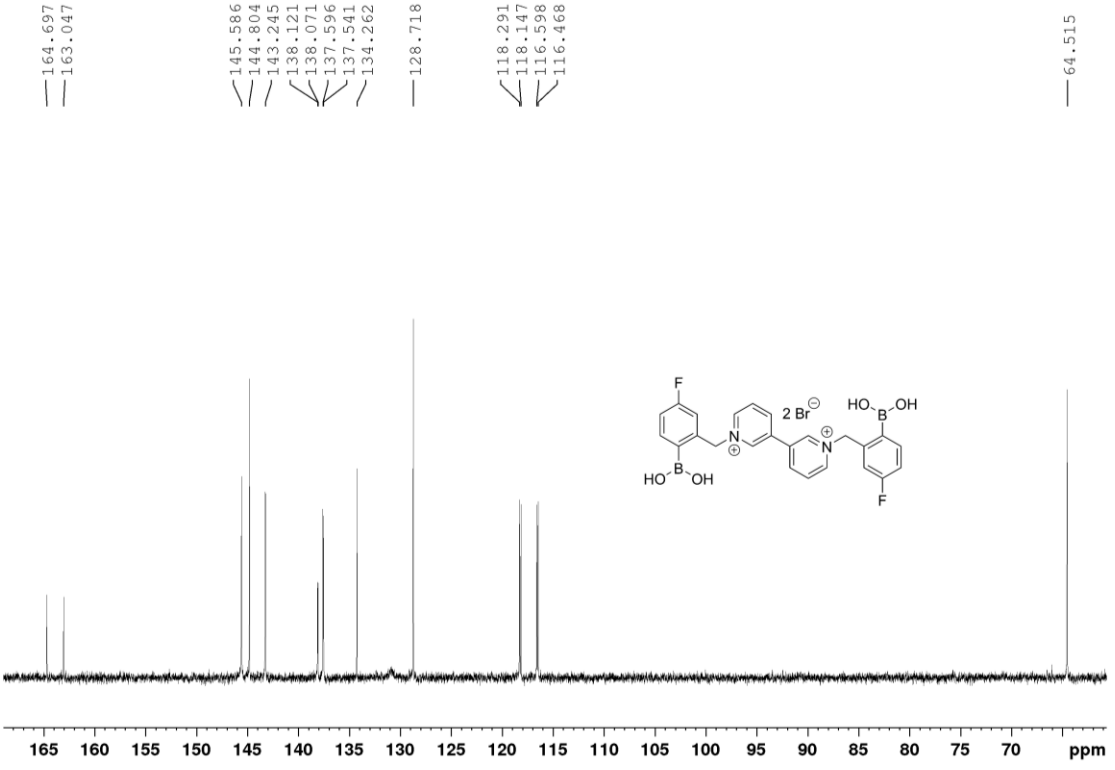

Figure S 71: ^{13}C{^{1}H} NMR (150 MHz, D$_2$O) spectrum of F-3,3'-*o*-BBV (11).

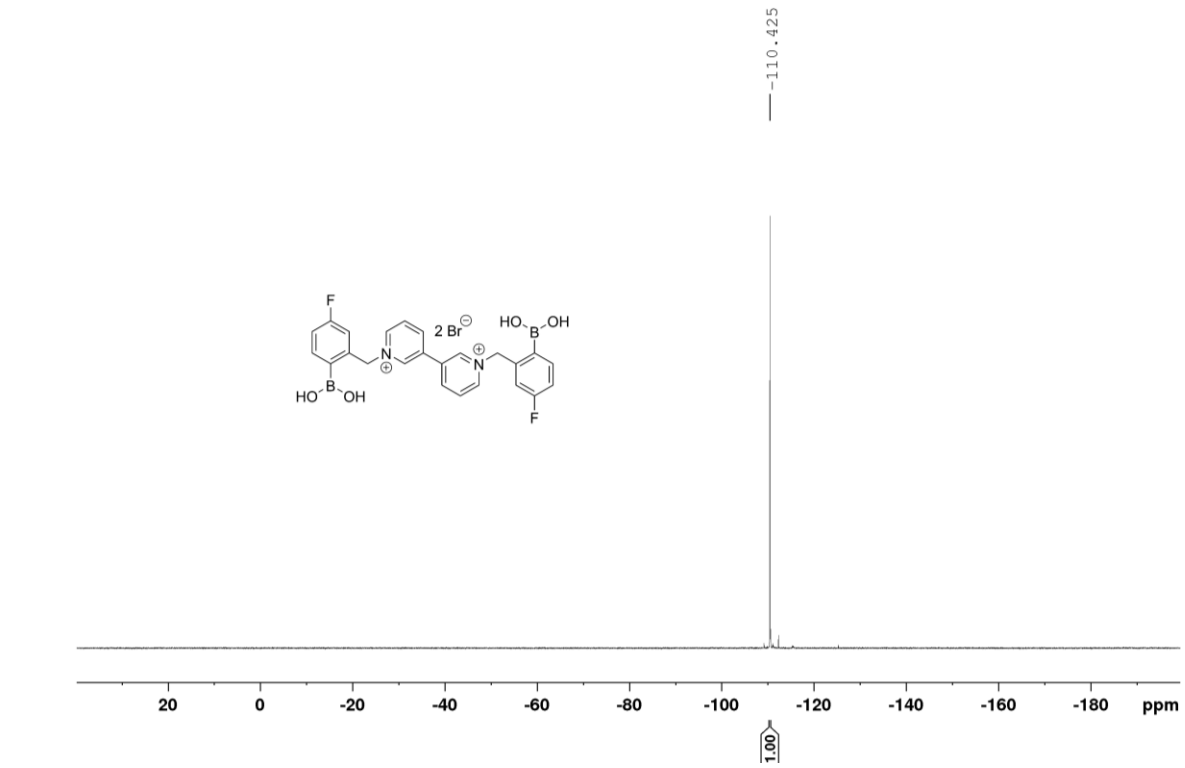

Figure S 72: $^{19}F\{^{1}H\}$ NMR (180MHz, DMSO-d_6) spectrum of F-3,3'-*o*-BBV (11).

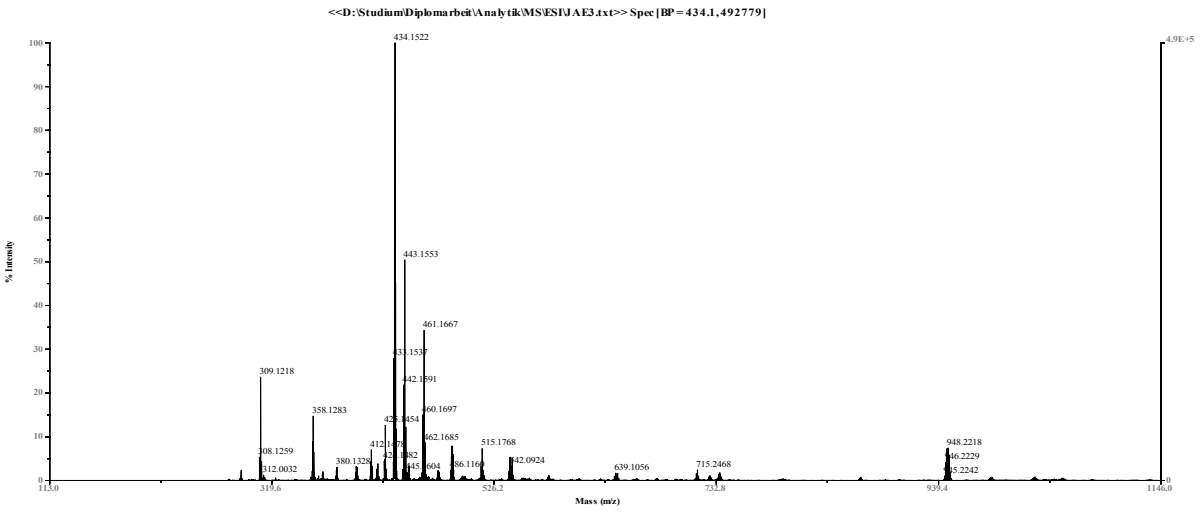

Figure S 73: High resolution ESI-TOF MS spectrum of F-3,3'-*o*-BBV (11).

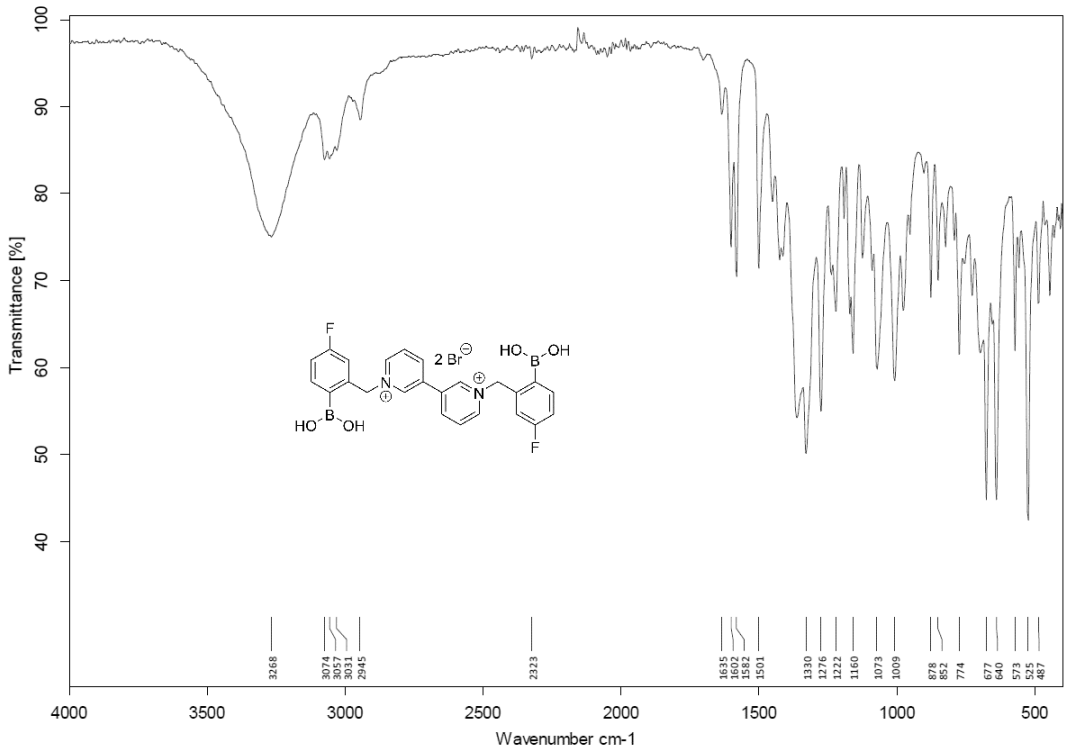

Figure S 74: IR (ATR) spectrum of F-3,3'-*o*-BBV (11).

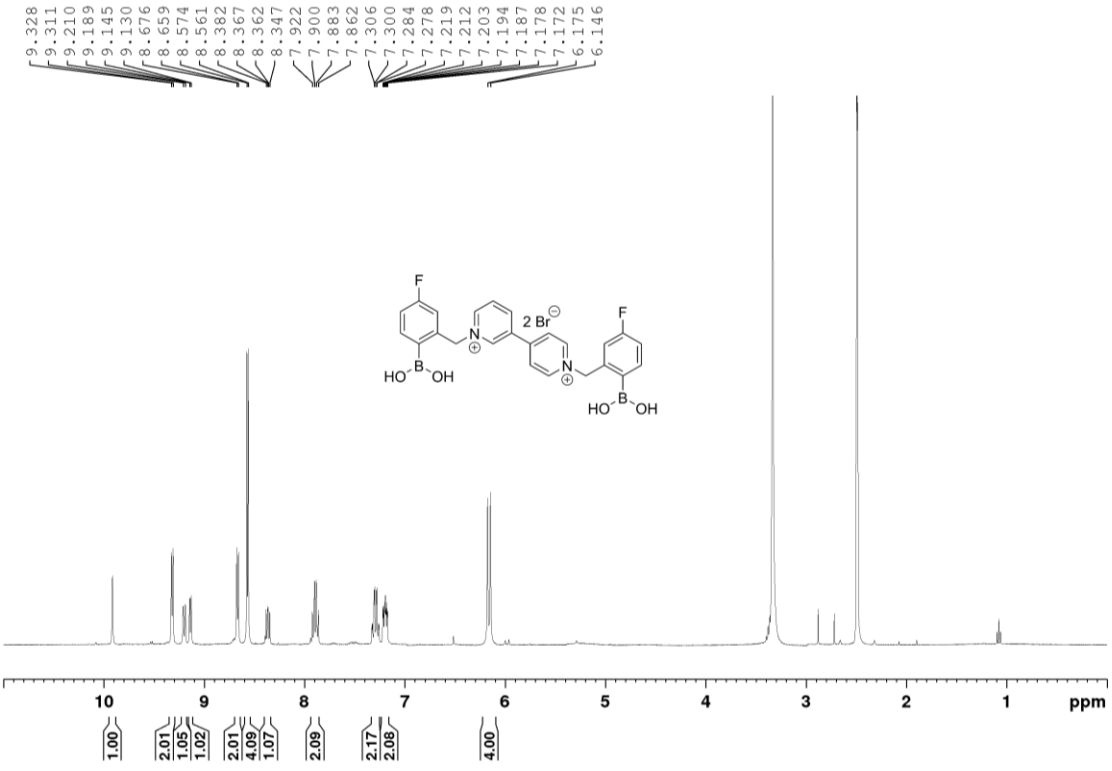

Figure S 75: ^{1}H NMR (400 MHz, DMSO-d$_6$) spectrum of F-3,4'-*o*-BBV (12).

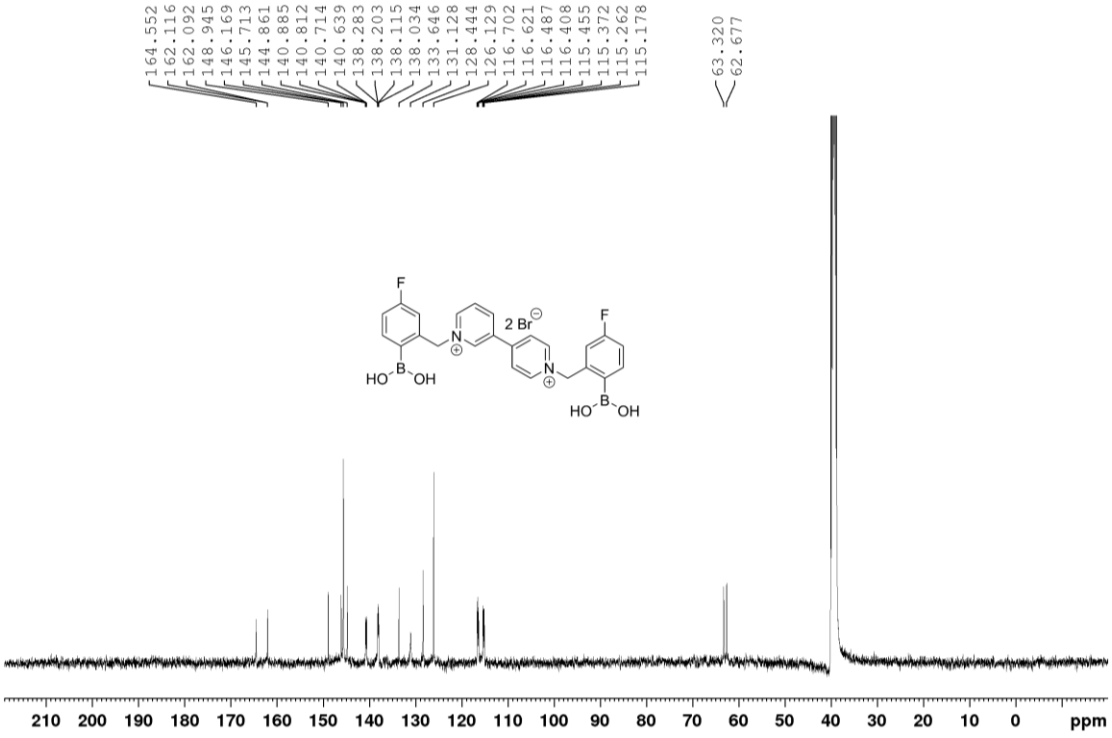

Figure S 76: $^{13}C\{^{1}H\}$ NMR (100 MHz, DMSO-d_6) spectrum of F-3,4'-*o*-BBV (12).

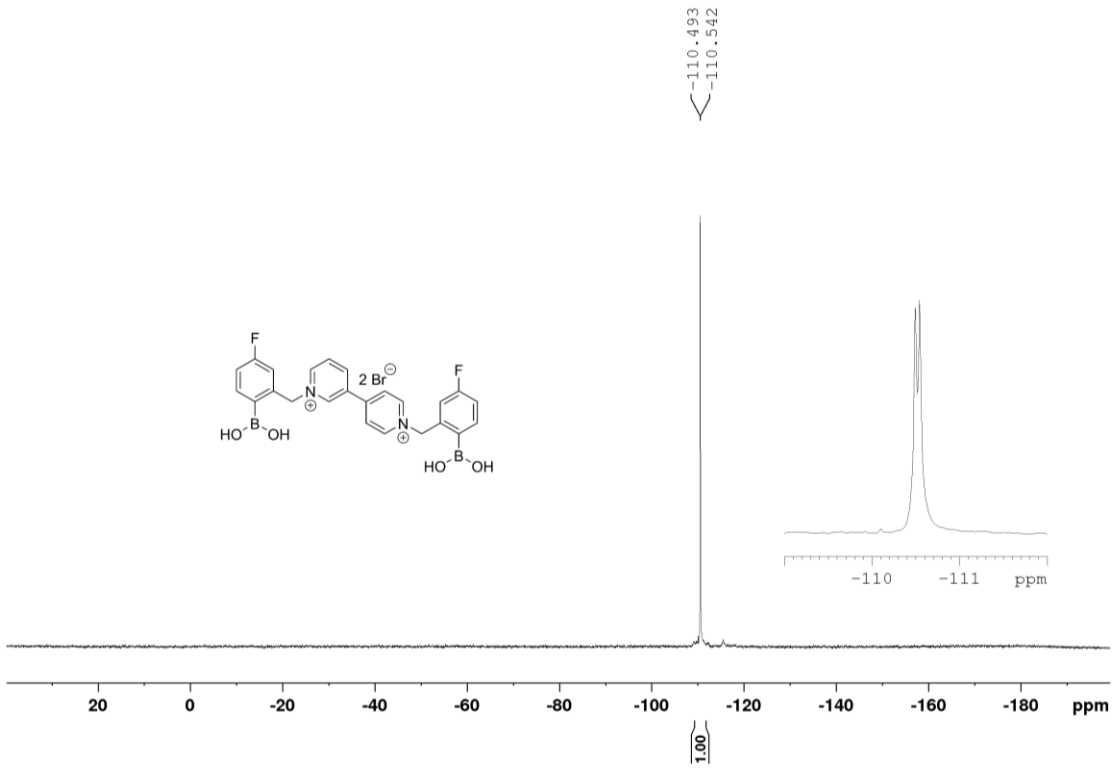

Figure S 77: $^{19}F\{^{1}H\}$ NMR (188 MHz, DMSO-d_6) spectrum of F-3,4'-*o*-BBV (12).

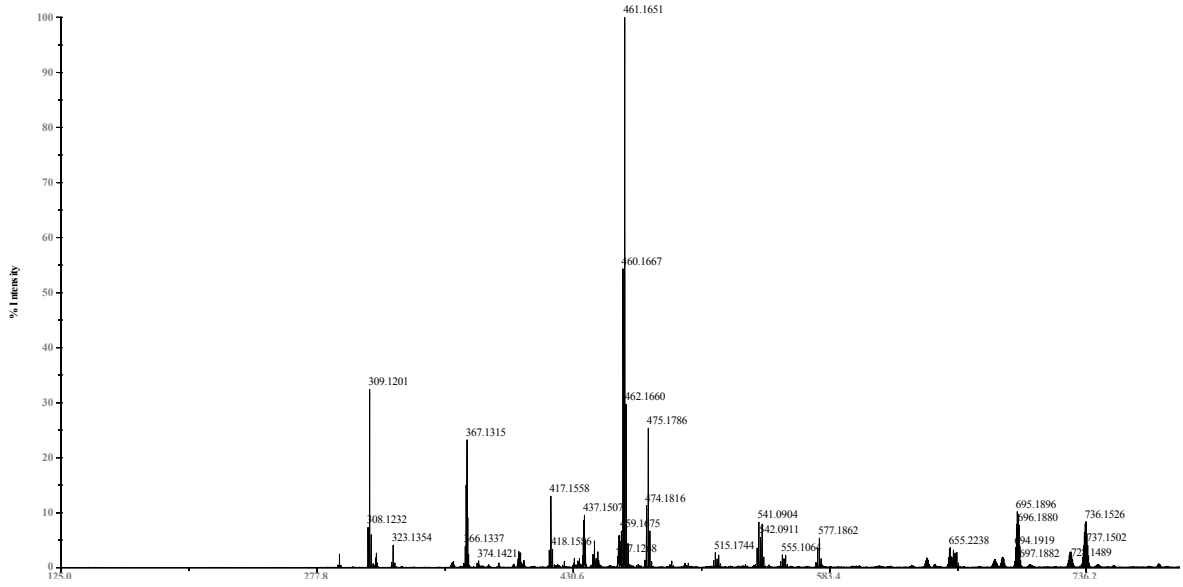

Figure S 78: High resolution ESI-TOF MS spectrum of F-3,4'-*o*-BBV (12).

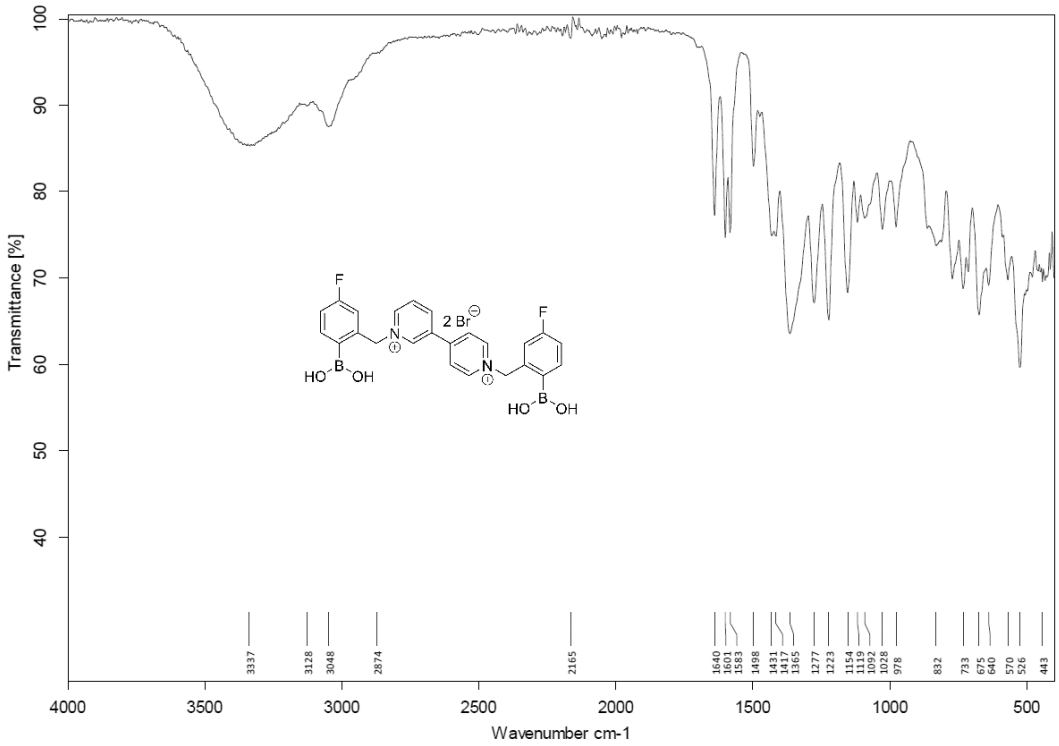

Figure S 79: IR (ATR) spectrum of F-3,4'-*o*-BBV (12).

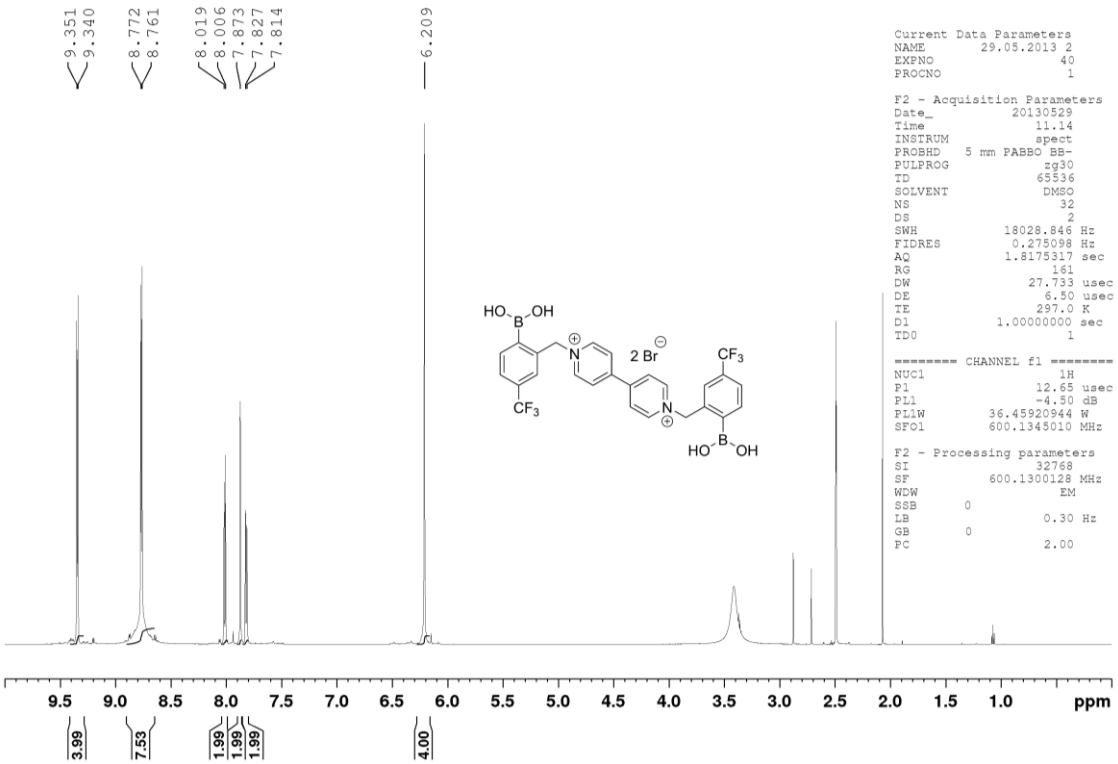

Figure S 80: ^{1}H NMR (600 MHz, DMSO-d$_6$) spectrum of CF$_3$-4,4'-*o*-BBV (13).

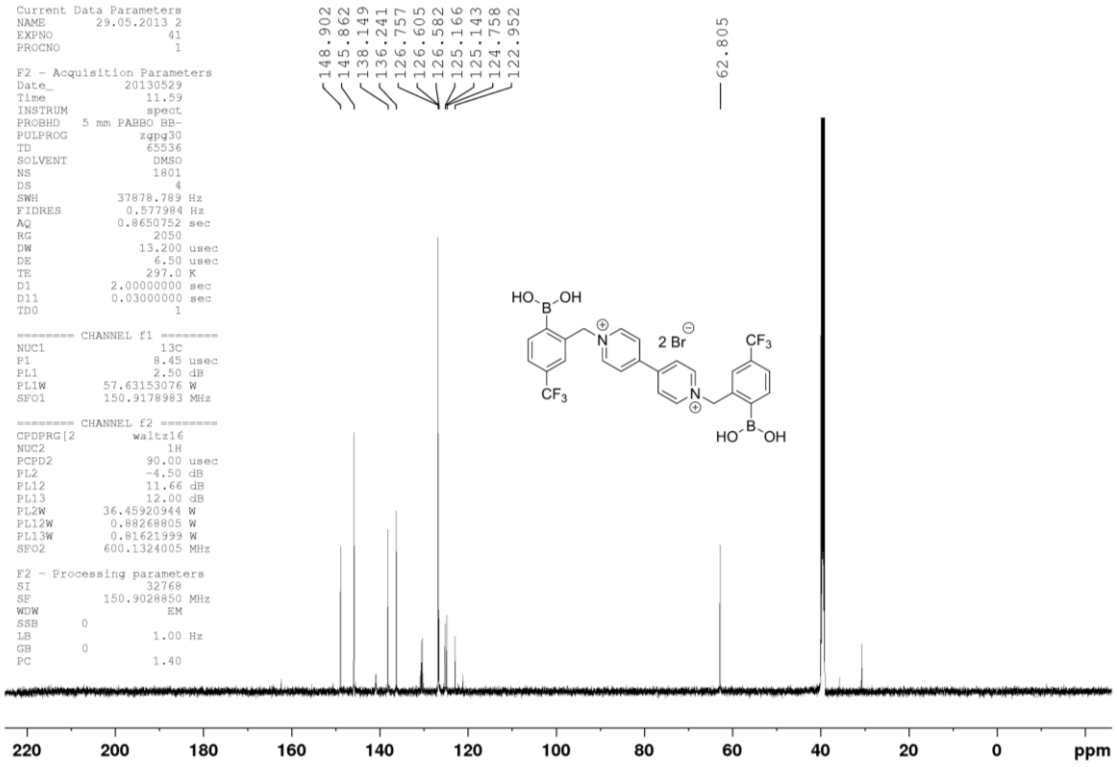

Figure S 81: ^{13}C{^{1}H} NMR (150 MHz, DMSO-d$_6$) spectrum of CF$_3$-4,4'-*o*-BBV (13).

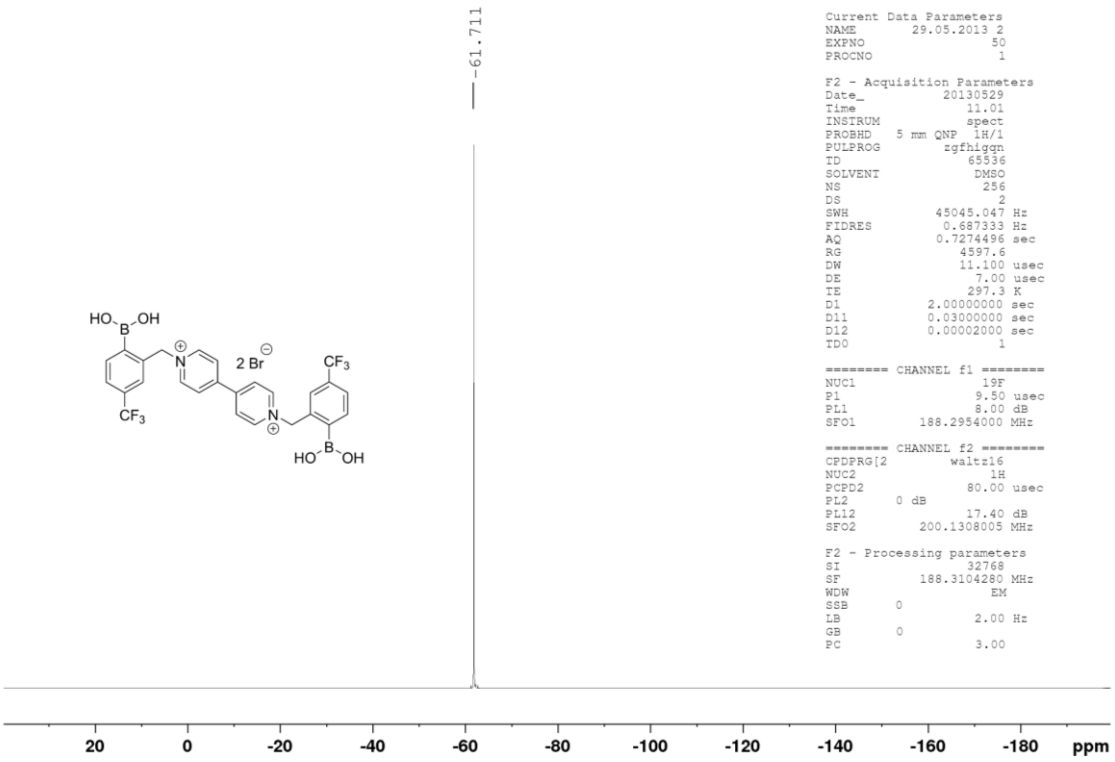

Figure S 82: $^{19}F\{^{1}H\}$ NMR (188 MHz, DMSO-d_6) spectrum of CF_3-4,4'-*o*-BBV (13).

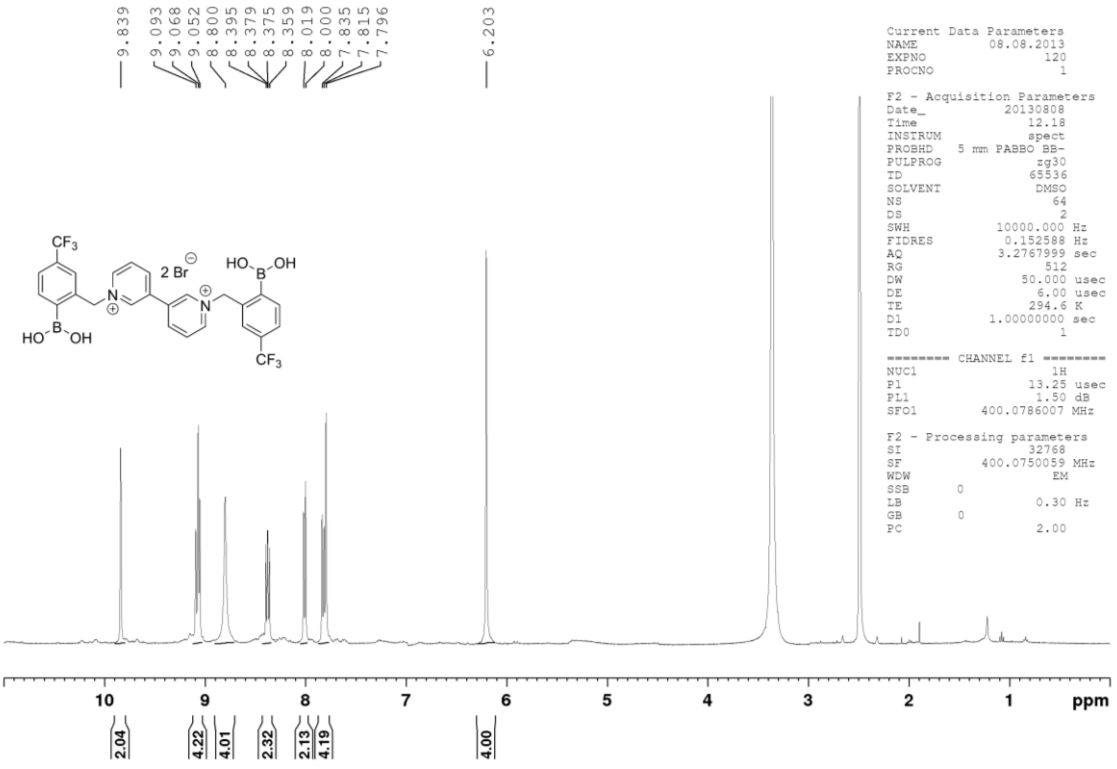

Figure S 83: ^{1}H NMR (400 MHz, DMSO-d_6) spectrum of CF_3-3,3'-*o*-BBV (14).

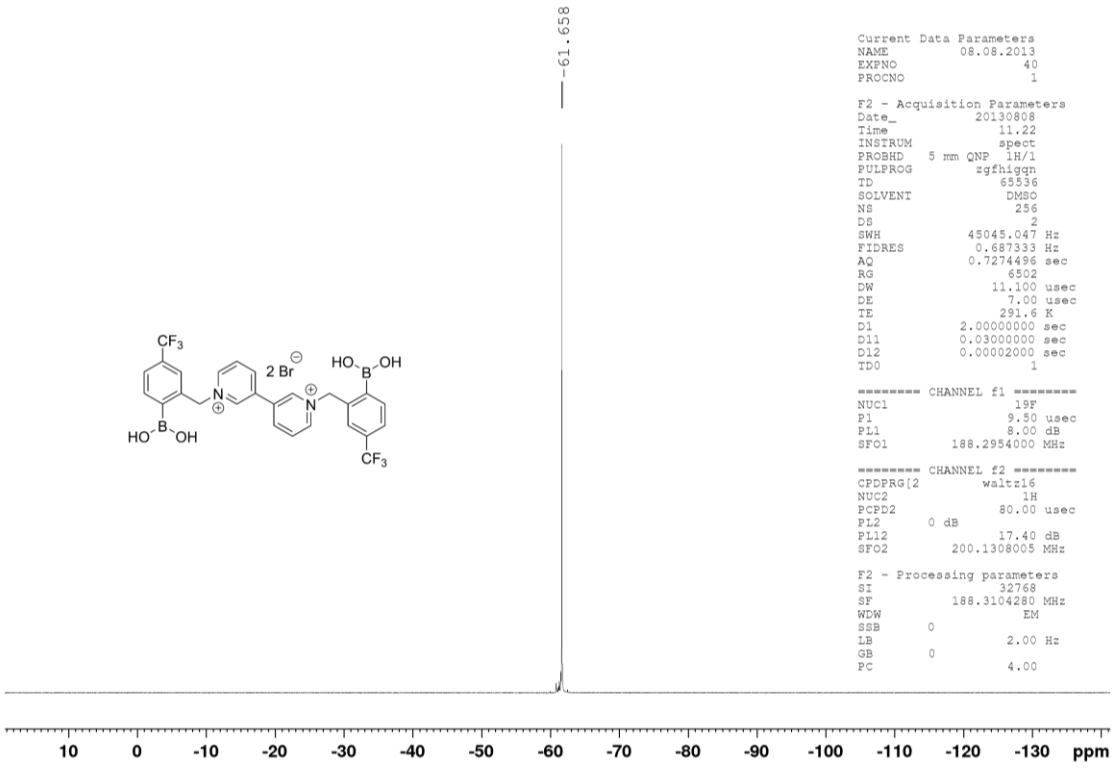

Figure S 84: $^{19}F\{^{1}H\}$ NMR (188 MHz, DMSO-d_6) spectrum of CF_3-3,3'-*o*-BBV (14).

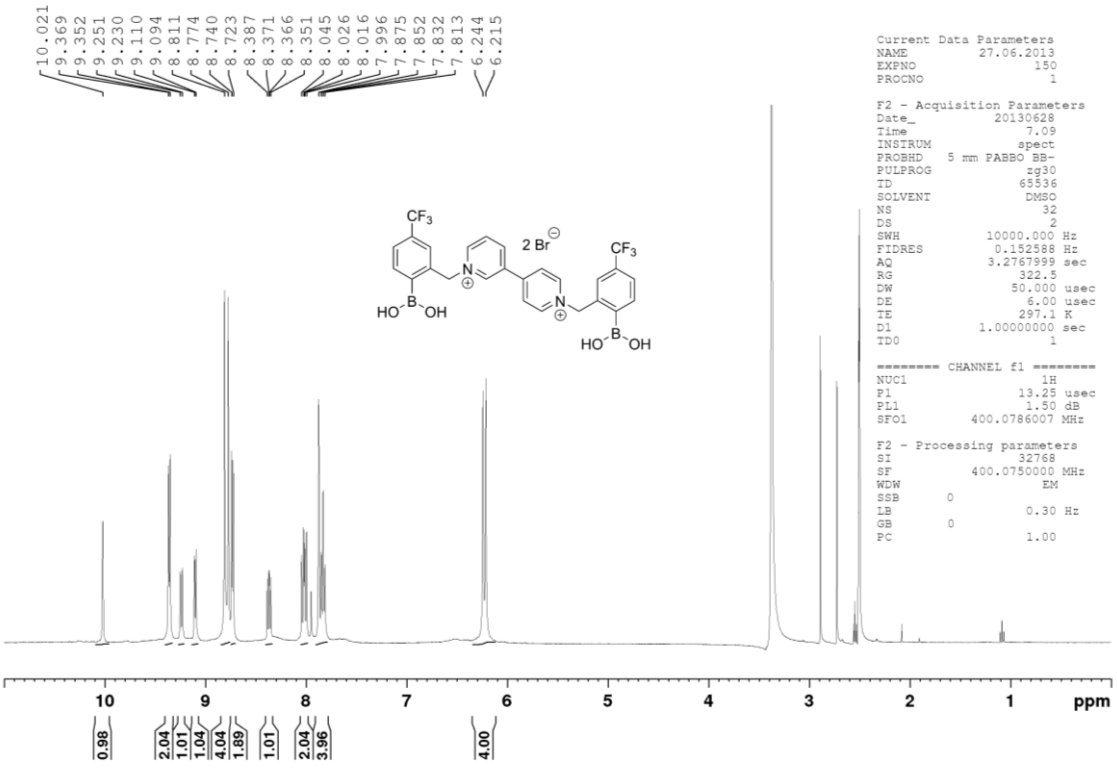

Figure S 85: ^{1}H NMR (400 MHz, DMSO-d_6) spectrum of CF_3-3,4'-*o*-BBV (15).

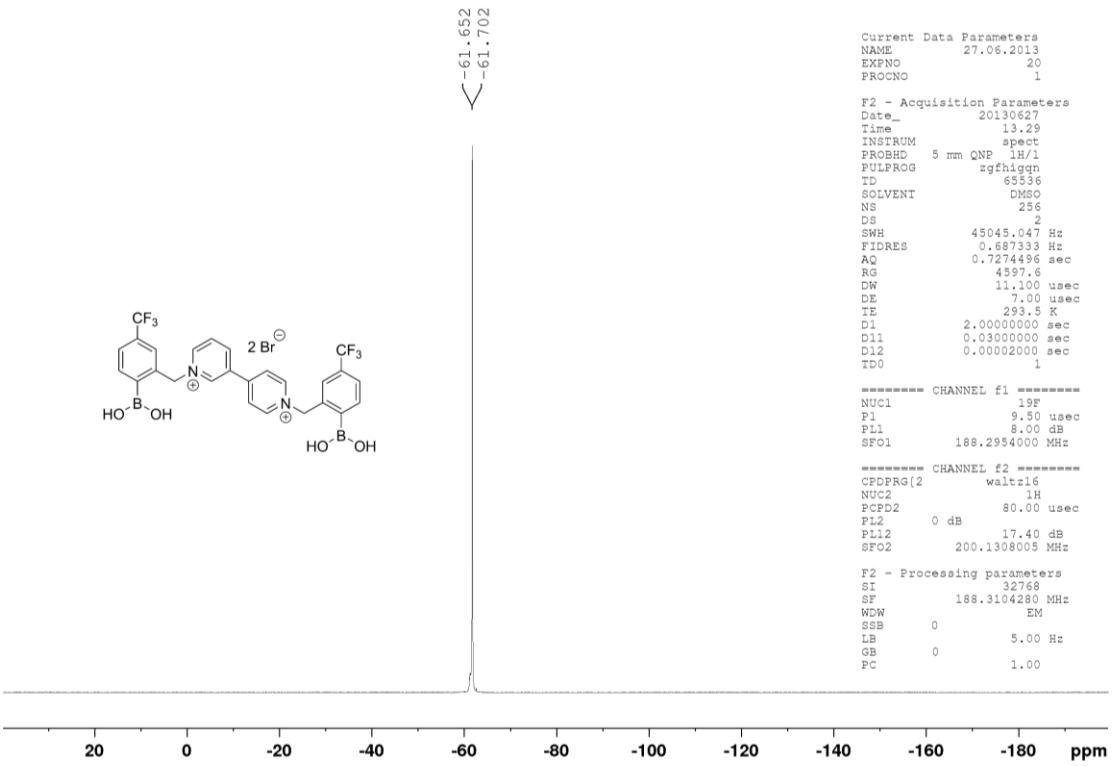

Figure S 86: $^{19}F\{^{1}H\}$ NMR (188 MHz, DMSO-d_6) spectrum of CF_3-3,4'-*o*-BBV (15).

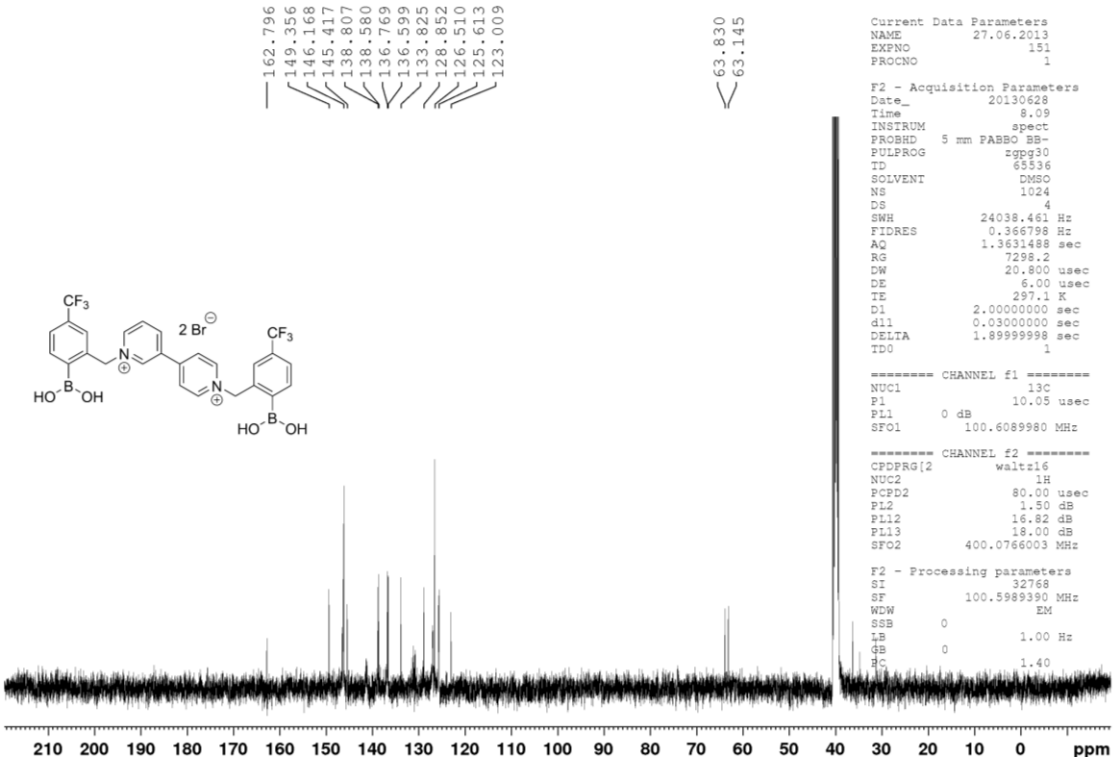

Figure S 87: $^{13}C\{^{1}H\}$ NMR (100 MHz, DMSO-d_6) spectrum of CF_3-3,4'-*o*-BBV (15).

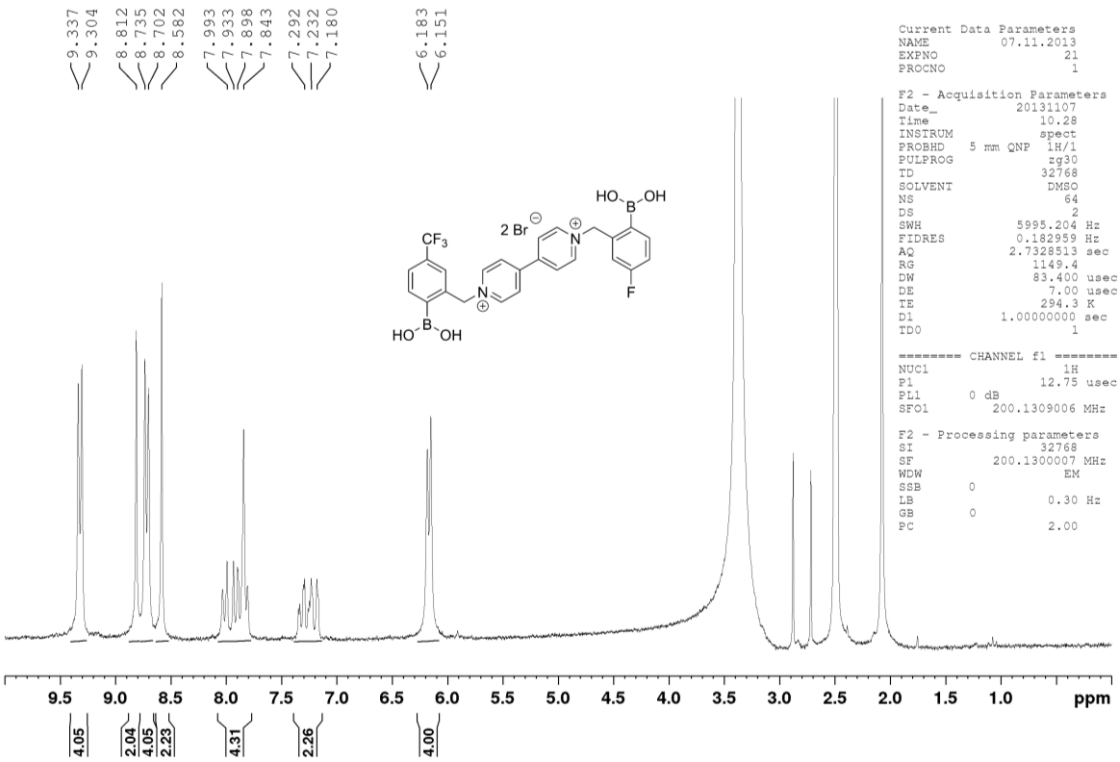

Figure S 88: ^{1}H NMR (200 MHz, DMSO-d$_6$) spectrum of CF$_3$/F-4,4'-*o*-BBV (16).

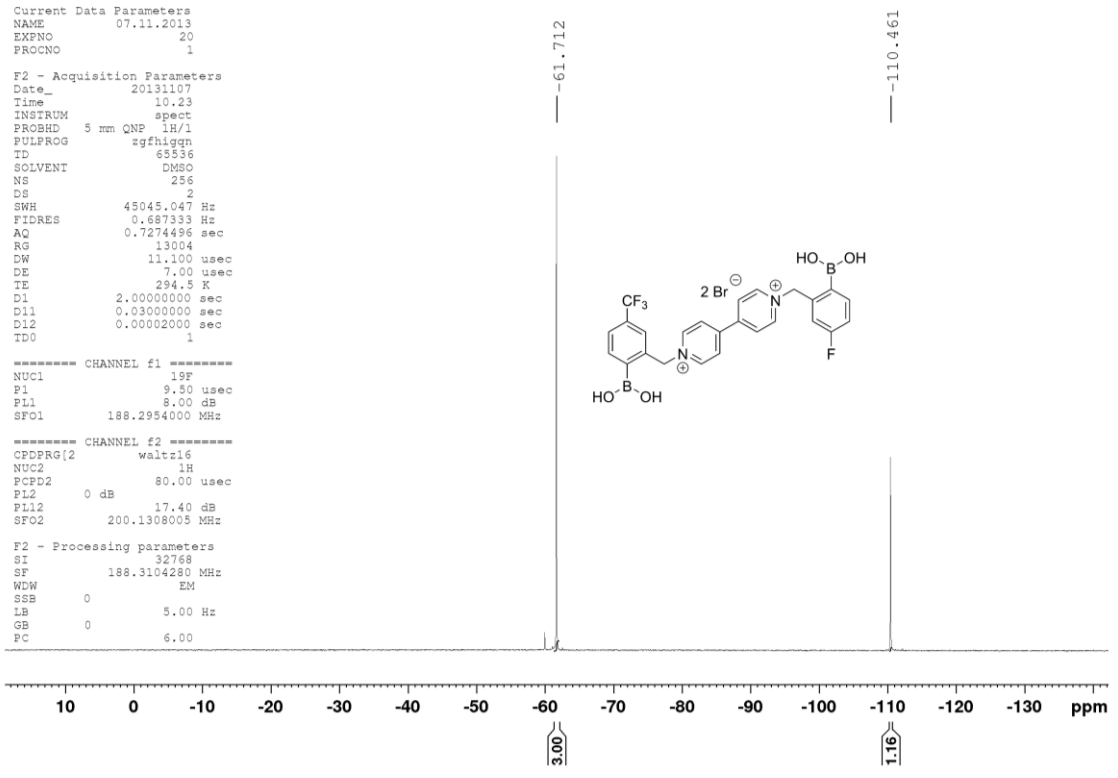

Figure S 89: ^{19}F{^{1}H} NMR (188 MHz, DMSO-d$_6$) spectrum of CF$_3$/F-4,4'-*o*-BBV (16).

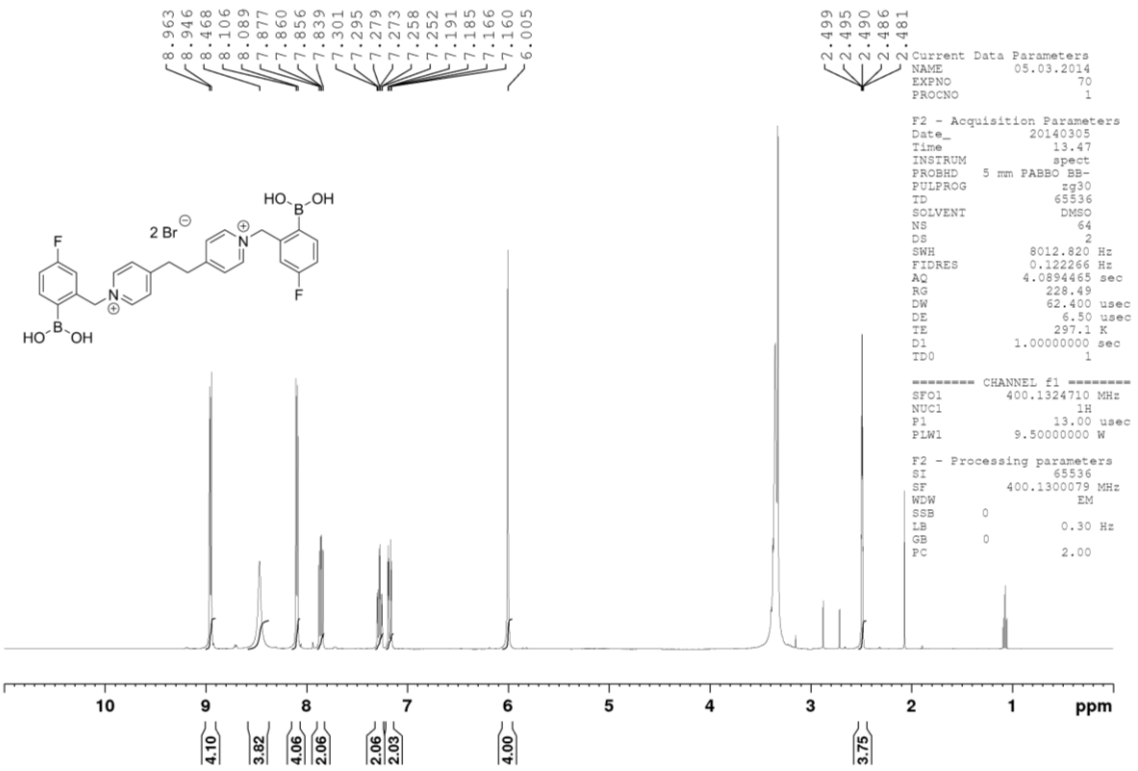

Figure S 90: ^{1}H NMR (400 MHz, DMSO-d$_6$) spectrum of F-4,4'-*o*-BBEpy (17).

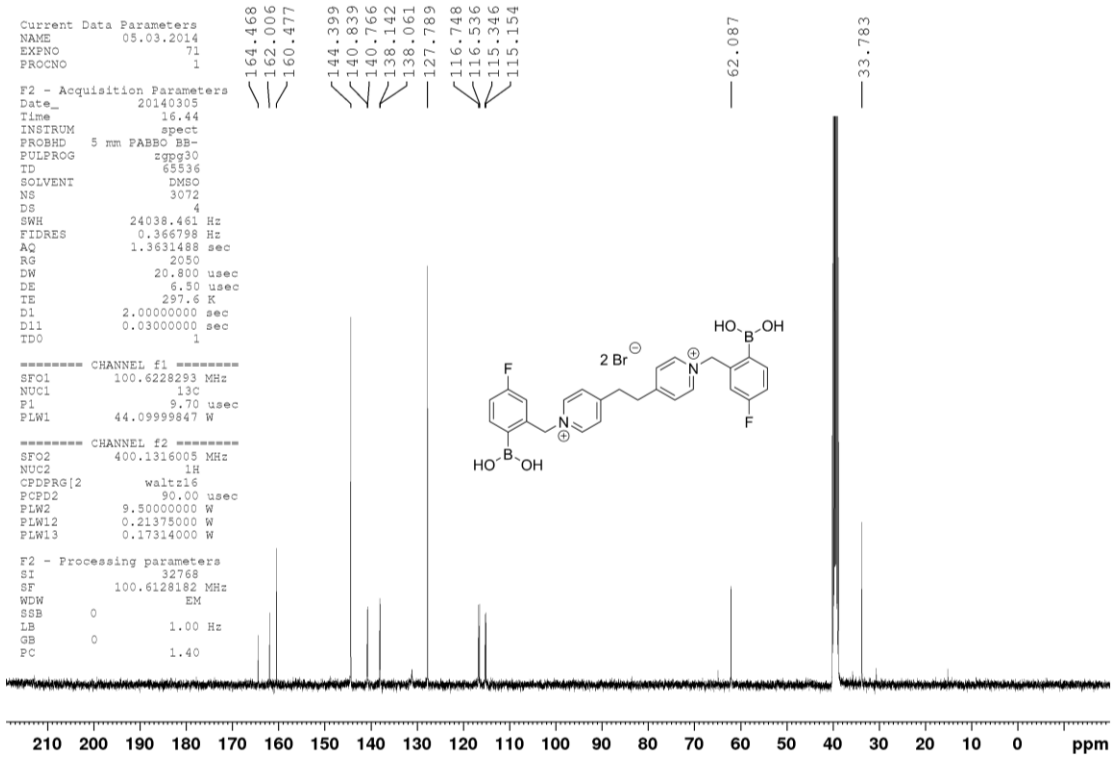

Figure S 91: ^{13}C{^{1}H} NMR (100 MHz, DMSO-d$_6$) spectrum of F-4,4'-*o*-BBEpy (17).

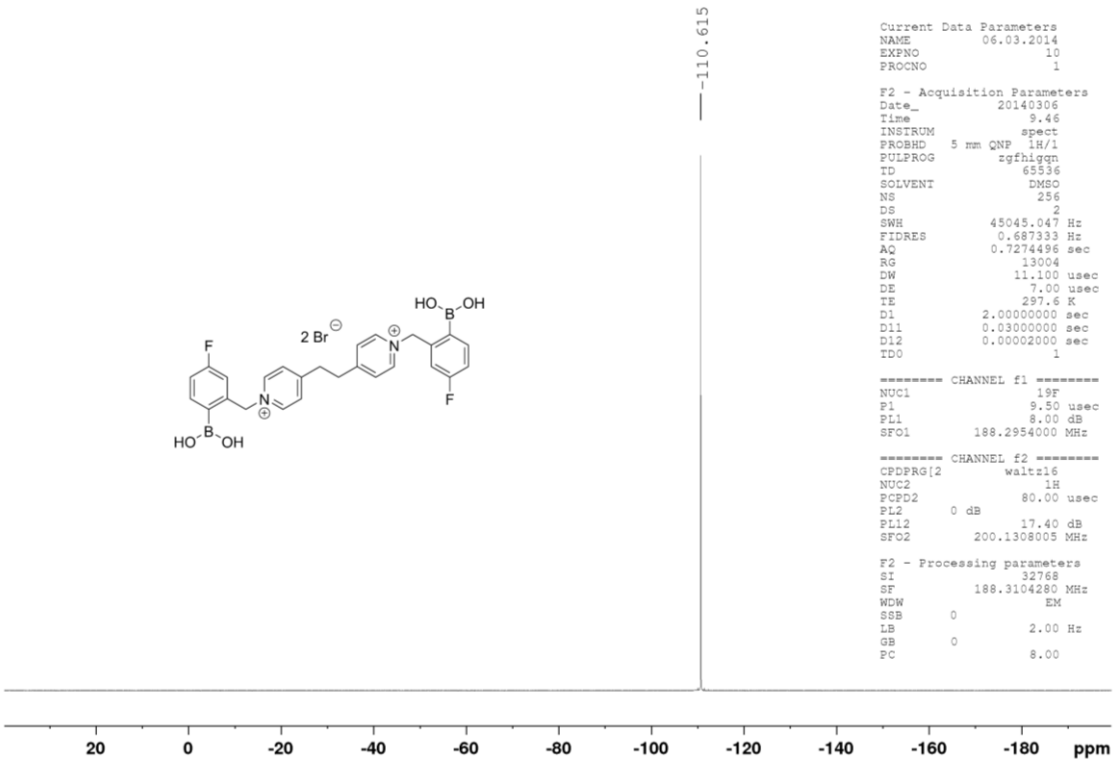

Figure S 92: $^{19}F\{^{1}H\}$ NMR (188 MHz, DMSO-d_6) spectrum of F-4,4'-*o*-BBEpy (17).

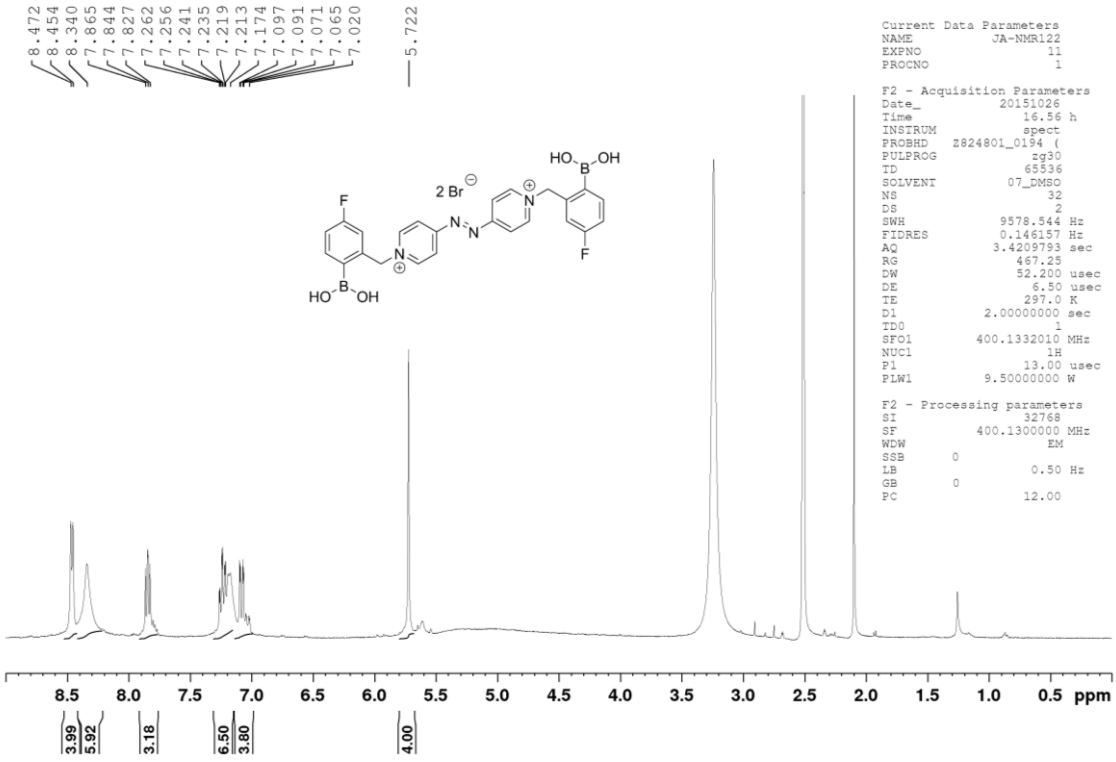

Figure S 93: ^{1}H NMR (400 MHz, DMSO-d_6) spectrum of F-4,4'-*o*-BBazpy (18).

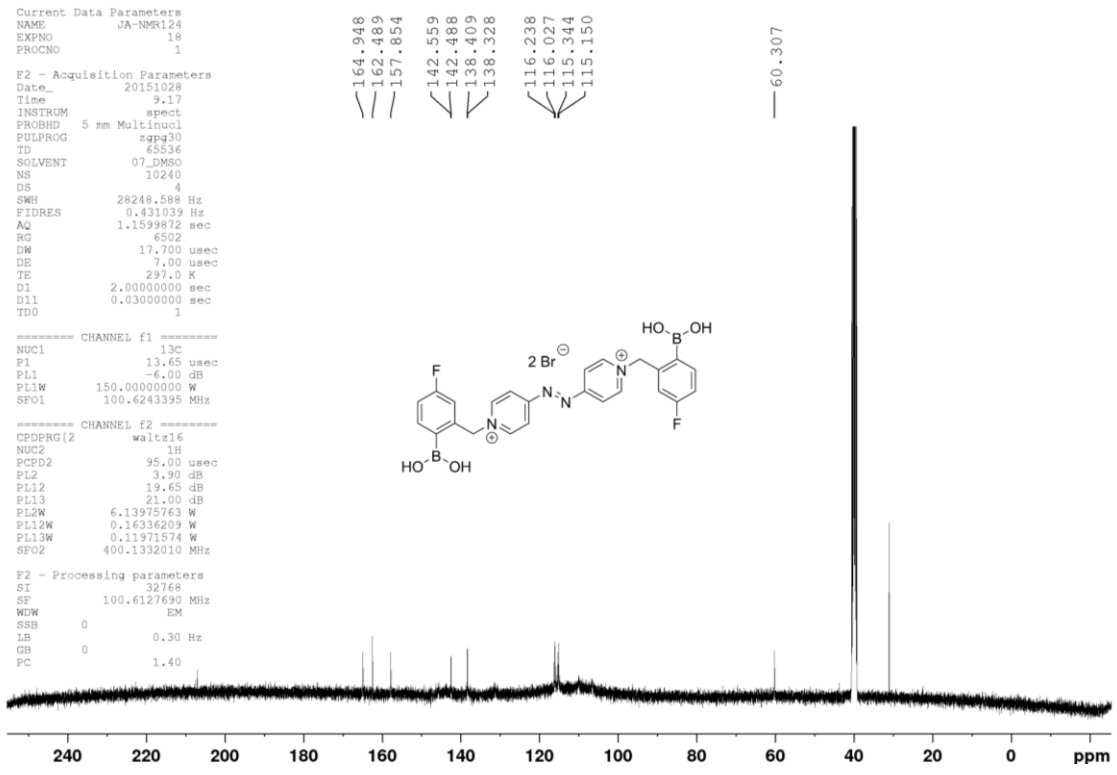

Figure S 94: $^{13}C\{^{1}H\}$ NMR (100 MHz, DMSO-d_6) spectrum of F-4,4'-*o*-BBazpy (18).

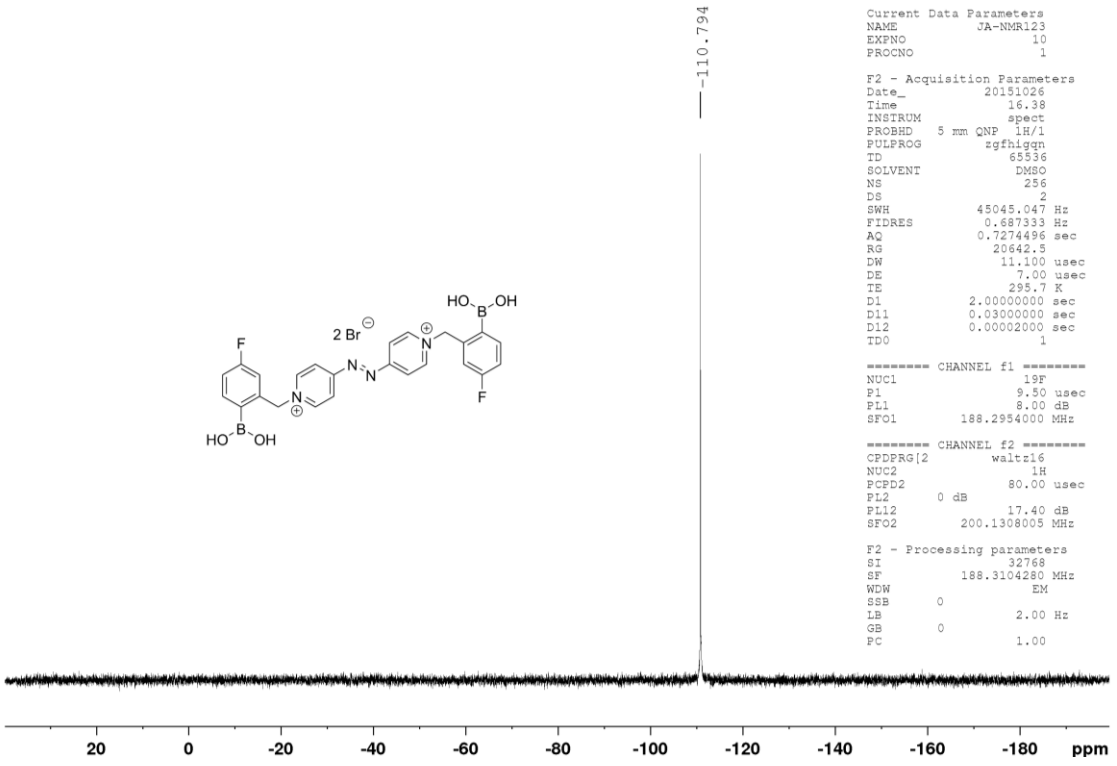

Figure S 95: $^{19}F\{^{1}H\}$ NMR (188 MHz, DMSO-d_6) spectrum of F-4,4'-*o*-BBazpy (18).

APPENDIX

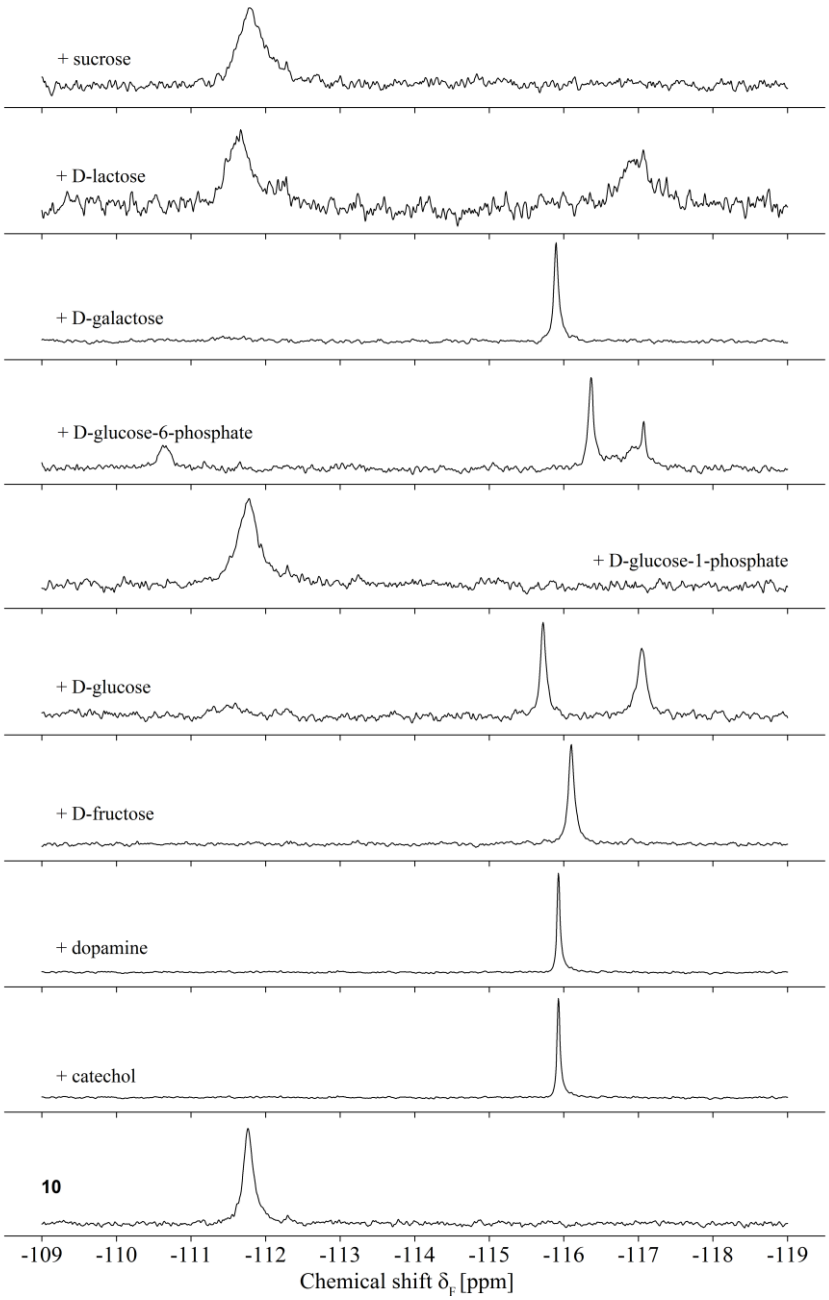

Appendix I: ^{19}F {^{1}H} NMR spectra of F-4,4'-*o*-BBV (10) and 10 in presence of diol-containing analytes. Condition: Receptor 10 (4 mM) and appropriate diol (40 mM) measured in aqueous phosphate buffer (50 mM, 10% D_2O, pH 7.4) at 188 MHz, 256 scans and 25°C.

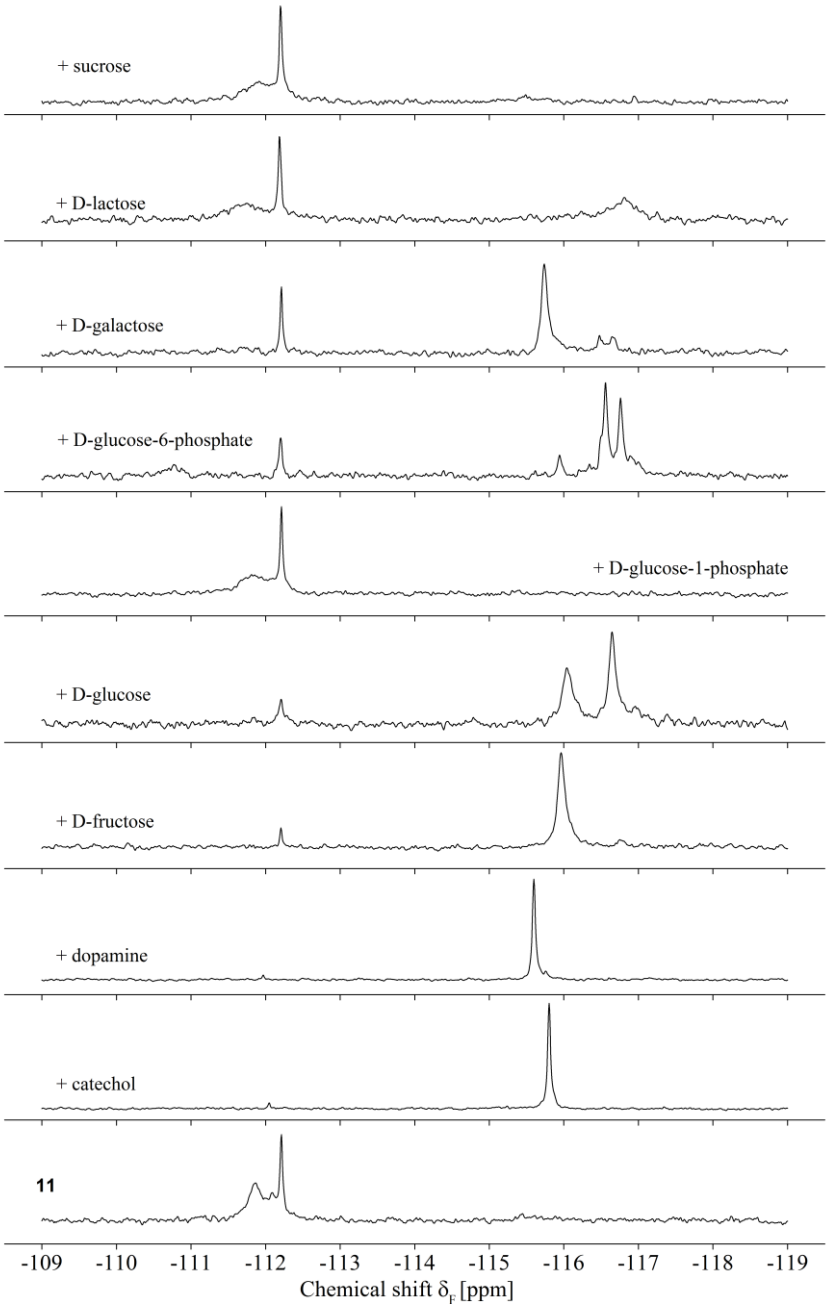

Appendix II: ^{19}F {^{1}H} NMR spectra of F-3,3'-*o*-BBV (11) and 11 in presence of diol-containing analytes. Condition: Receptor 11 (4 mM) and appropriate diol (40 mM) measured in aqueous phosphate buffer (50 mM, 10% D_2O, pH 7.4) at 188 MHz, 256 scans and 25°C.

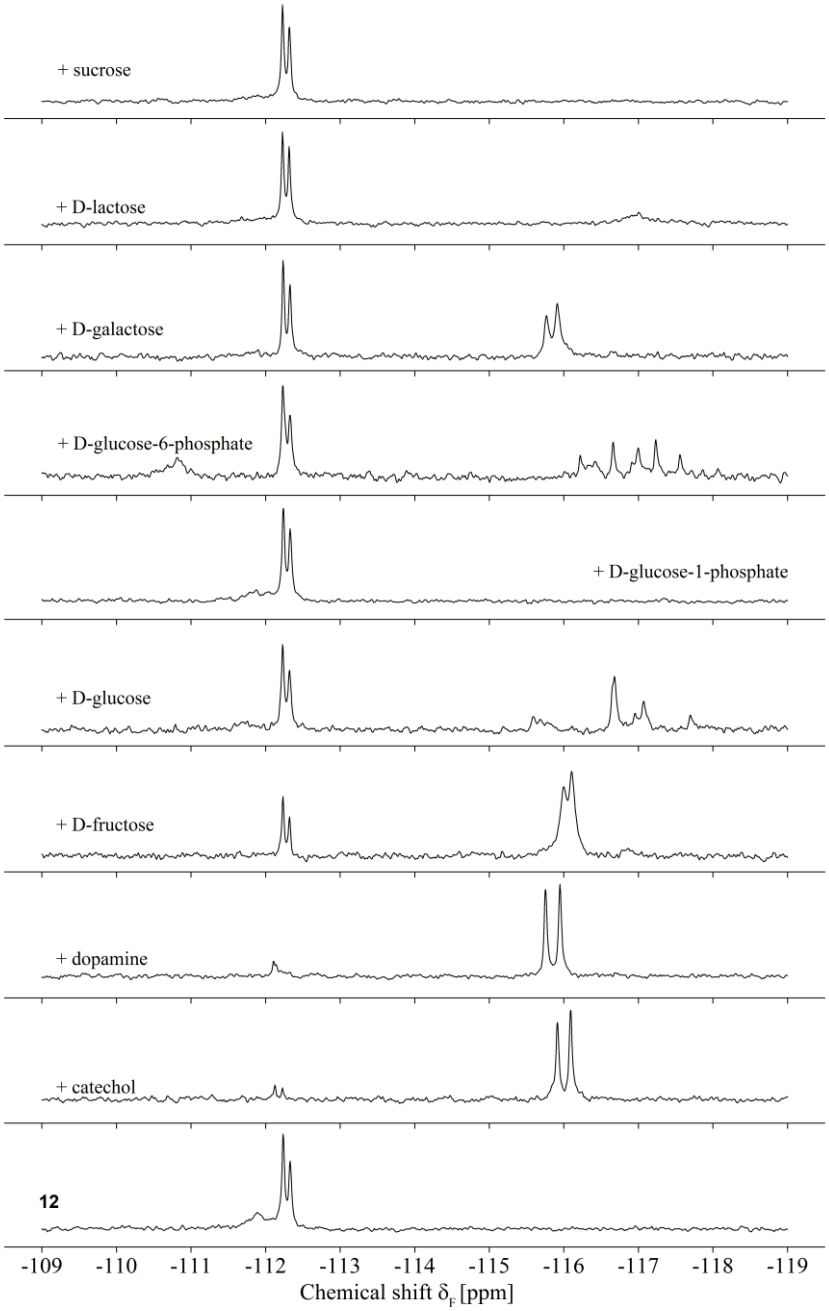

Appendix III: ^{19}F {^{1}H} NMR spectra of F-3,4'-*o*-BBV (12) and 12 in presence of diol-containing analytes. Condition: Receptor 12 (4 mM) and appropriate diol (40 mM) measured in aqueous phosphate buffer (50 mM, 10% D_2O, pH 7.4) at 188 MHz, 256 scans and 25°C.

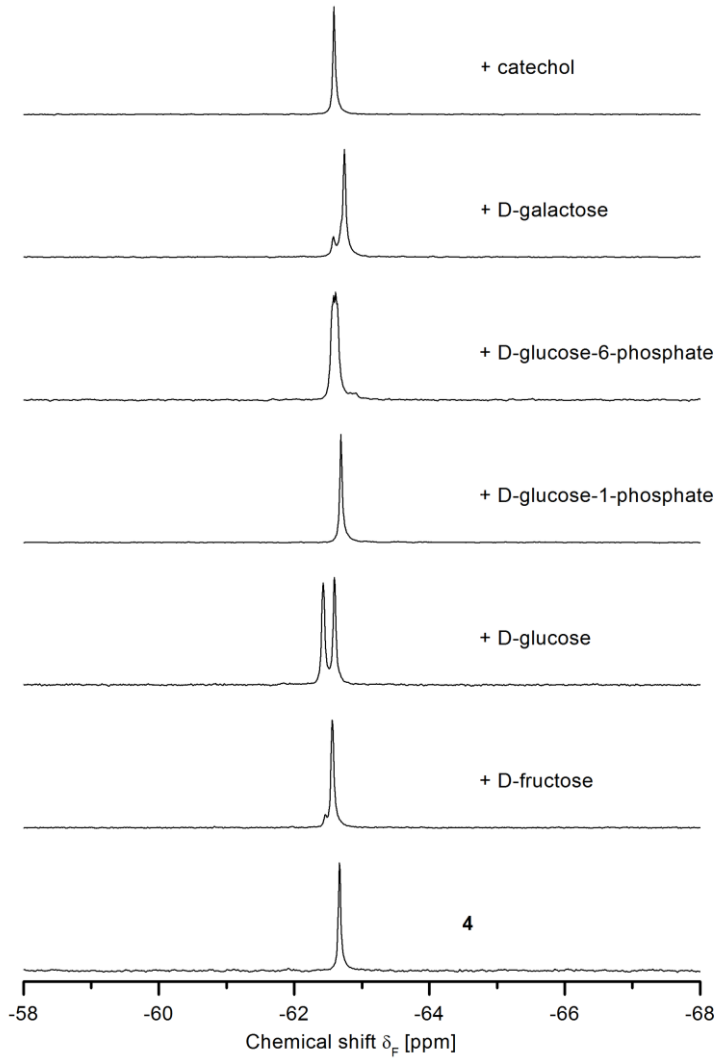

Appendix IV: ^{19}F {^{1}H} NMR spectra of 5-CF_3-*o*-BBpy (4) and 4 in presence of diol-containing analytes. Condition: Receptor 4 (1 mM) and appropriate diol (10 mM) measured in aqueous HEPES buffer (100 mM, 10% D_2O, pH 7.4) at 188 MHz, 256 scans and 25°C.

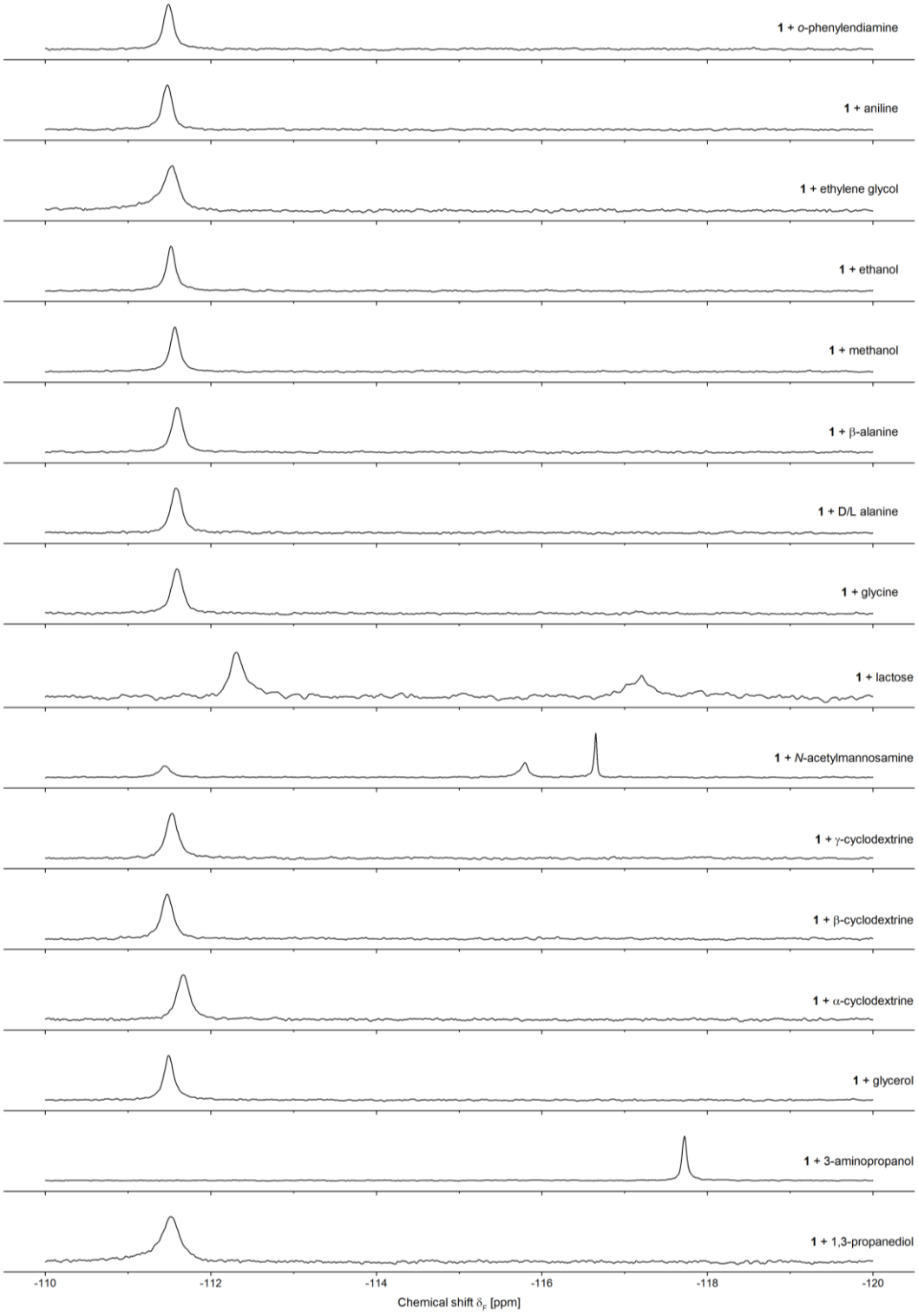

Appendix V: ^{19}F {^{1}H} NMR spectra of 5-F-*o*-BBpy (1) and 1 in presence of (di)ol-containing analytes. Condition: Receptor 1 (10 mM) and appropriate (di)ol (100 mM) measured in aqueous HEPES buffer (100 mM, 10% D_2O, pH 7.4) at 188 MHz, 256 scans and 25°C.

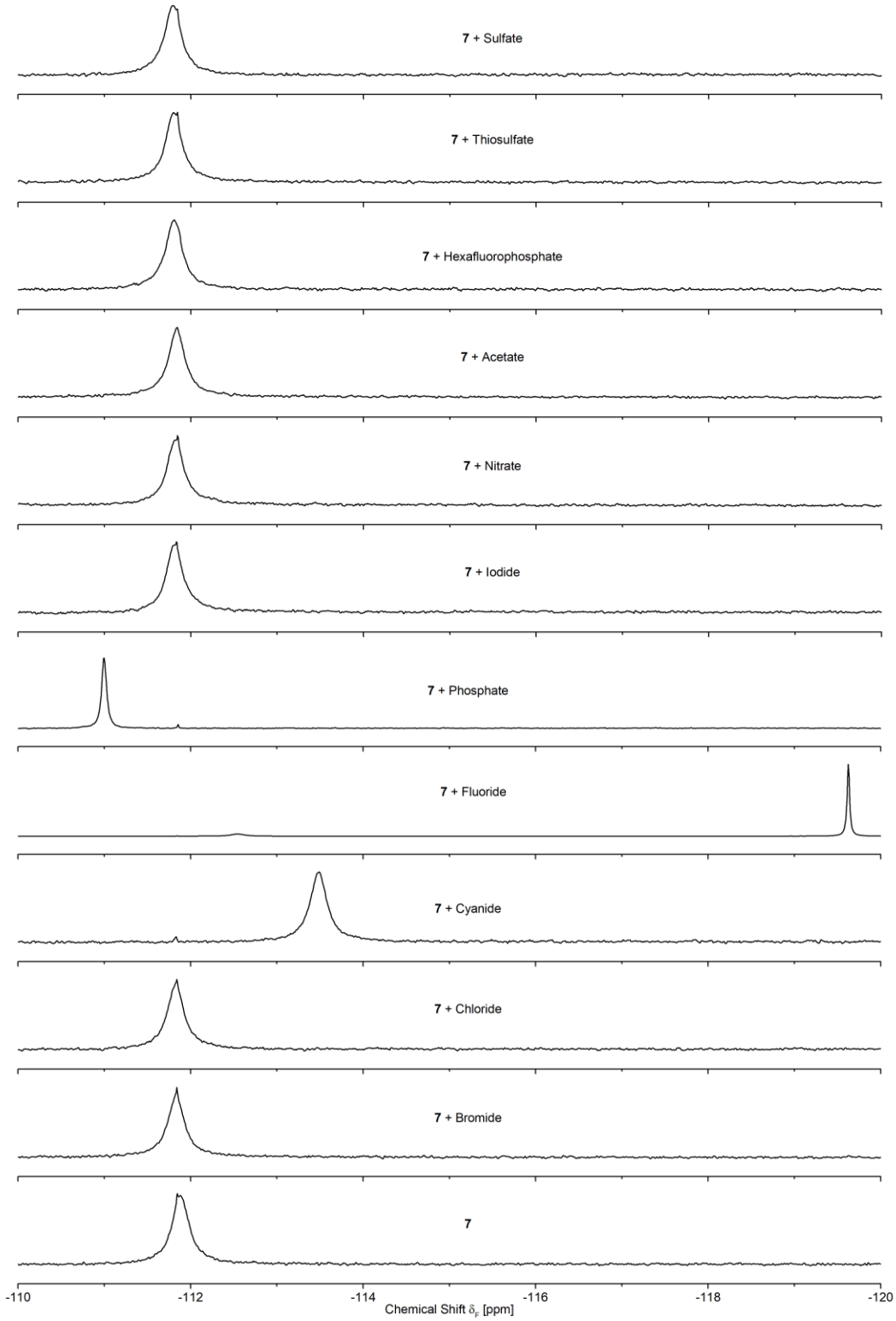

Appendix VI: ^{19}F {^{1}H} NMR spectra of 5-F-*o*-BBBrpy (7) and 7 in presence of inorganic anions. Condition: Receptor 7 (5 mM) and appropriate anion (25 mM) measured in aqueous HEPES buffer (100 mM, 10% D_2O, pH 7.4) at 377 MHz, 256 scans and 25°C.

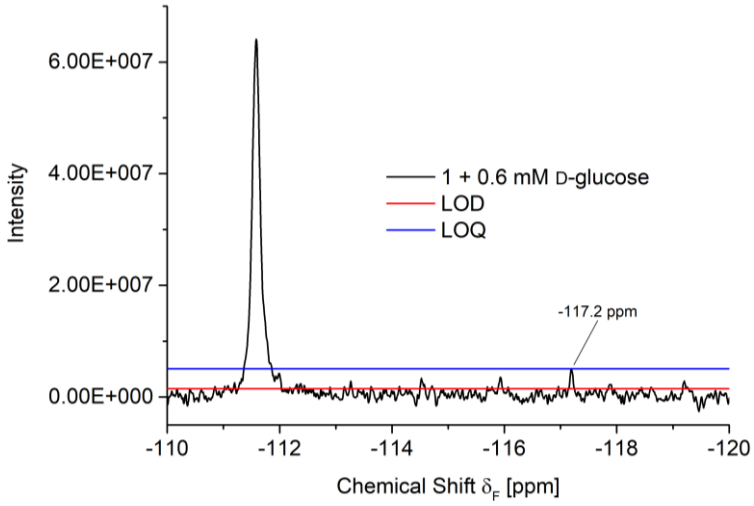

Appendix VII: ^{19}F {^{1}H} NMR spectra of 5-F-*o*-BBV and D-fructose for LOD and LOQ determination. Conditions: Receptor 1 (10 mM) and D-glucose (0.6 mM) measured in HEPES buffer (30 mM 10% D_2O, pH 7.4) at 188 MHz, 256 scans and 25°C.

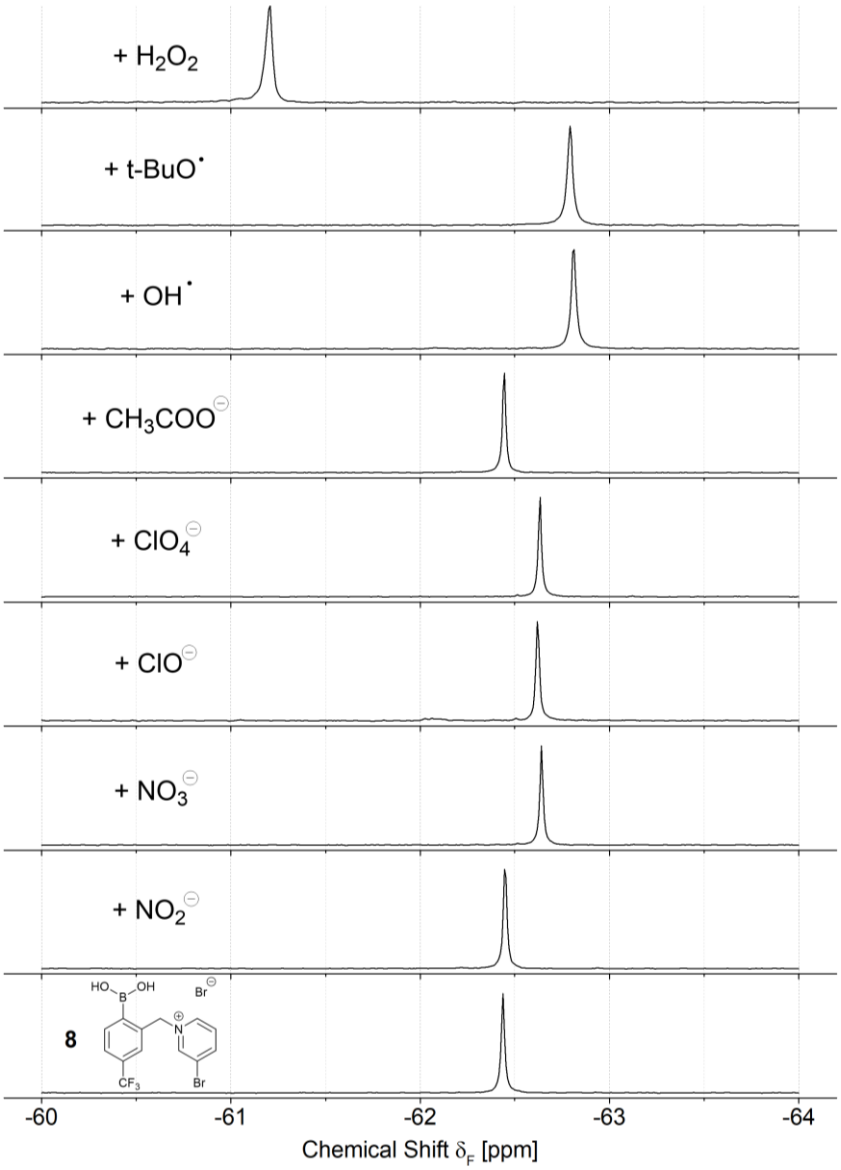

Appendix VIII: ^{19}F {^1H} NMR spectra of 5-CF_3-*o*-BBBrpy (8) and 8 in presence of ROS. Condition: Receptor 8 (3 mM) and appropriate ROS (16.66 mM) measured in aqueous HEPES buffer (50 mM, 10% D_2O, pH 7.0) at 377 MHz, 32 scans and 25°C.

ACKNOWLEDGEMENT

First of all, many thanks to my doctoral adviser, PD Dr. ès sc. habil. Alexander Schiller, for providing me the interesting and very fruitful research topic, for giving me the opportunity to work always independently, for the funding of the project, and for giving me the possibility to present my work to a broad audience on national and international conferences. Furthermore, I thank you for the helpful discussions and the scientific support that guided me through the whole process.

Many thanks to Prof. Dr. Winfried Plass for reviewing this dissertation.

I like to thank the NMR laboratory staff Dr. Peter Bellstedt, Friederike Pielenz, Bärbel Rambach and Gabriele Sentis for measuring over 1500 ^{19}F NMR samples, which were essential for the project. I also would like to thank the MS laboratory staff members Dr. Wolfgang Poppitz, Dr. Nico Ueberschaar, Monika Heineck and Sigrid Schönau for MS analysis and Dr. Helmar Görls for determining the X-ray crystal structures. Furthermore, I would like to thank all other staff members at the Institute of Inorganic and Analytical Chemistry, who helped me directly or indirectly to write this work.

Especially, I would like to say thank you to my co-workers Dr. Gandra Upendar Reddy, Dr. Sven Askes, Dr. Vadde Ramu, Dr. Carmen Bohlender, Dr. Amilan Jose Devadoss, DC Steve Gläser, DC Tobias Otto, DC Martin Elstner, MSc Jingjing Liu for the pleasant working atmosphere inside and outside the laboratory and the many interesting and helpful discussions concerning not only chemistry. Thanks to the undergraduate students Zuzanna Kowalczyk, Magdalena Janota, Magdalena Kusideł, Kinga Lindner, Kerjosse Steven, Sebastian Bold, Tobias Haider, Philipp Traber, Philipp Borchers, Florian Nöller, Fabian Dröge, André Schumann and Martin Klein for their support in synthesis and the sensing experiments.

A very big thank you to my bro Chrissi, Tobi, Stevi, Ali and Felix of the “Philosophen Mensa” group, you guys turned every terrible day into something good! Markus, thanks for the glorious time in Jena and the hard workouts we had! Thanks to my West German friend Christian for not doing stupid things – not. You are the craziest guy I ever met, nevertheless, we spent some breakneck and awesome time together! Robert, Franz and Bianca thank you for all the “petrol talks” and the car projects we managed together, always a good compensation for the mental work!

I would like to say thank you to my whole family, my friends and especially to my mother Petra who have supported me as much as they could and who gave me every time the encouragement to go on.

Thank you, Anne, for the strong support in every life situation, you give me everything that I could ever desire. Thank you for giving birth to our little daughter Mira Sophie. You are our little sunshine. I love you two!

WISSENSCHAFTLICHE PUBLIKATIONEN

- Elstner, M., Axthelm, J. & Schiller, A. Sugar-based molecular computing via material implication. *Angew. Chem. Int. Ed*., **53**, 7339-7343 (2014).
- Elstner, M., Axthelm, J. & Schiller, A. Zuckerbasierter molekularer Rechner mit Implikationslogik. *Angew. Chem*., **126**, 7467-7471 (2014).
- Axthelm, J.; Görls, H.; Schubert, U. S. & Schiller, A. Fluorinated Boronic Acid-Appended Bipyridinium Salts for Diol Recognition & Discrimination via 19F NMR Barcodes. *J. Am. Chem. Soc*. **137**, 15402-15405 (2015).
- Reddy, G. U.; Axthelm, J.; Hoffmann, P.; Taye, N.; Gläser, S.; Görls, H.; Hopkins, S. L.; Plass, W.; Neugebauer, U.; Bonnet, S. & Schiller, A. Co-registered molecular logic gate with a CO-releasing molecule triggered by light and peroxide. *J. Am. Chem. Soc*. **139**, 4991–4994 (2017).
- Axthelm, J.; Elstner, M.; Reddy, G. U.; Görls, H.; Bellstedt, P. & Schiller, A. Fluorinated Boronic Acid-Appended Pyridinium Salts and 19F NMR Spectroscopy for Diol Sensing. *J. Am. Chem. Soc*. **139**, 11413–11420 (2017).

REFERENCES

(1) Wang, B.; Anslyn, E. V., *Chemosensors: Principles, Strategies, and Applications*. Wiley: 2011.

(2) American Diabetes, A., *Diabetes Care* **2017**, *40,* S11.

(3) Vashist, S. K.; Zheng, D.; Al-Rubeaan, K.; Luong, J. H.; Sheu, F. S., *Anal. Chim. Acta* **2011**, *703,* 124.

(4) Liu, L.; Li, Q.; Li, N.; Ling, J.; Liu, R.; Wang, Y.; Sun, L.; Chen, X. H.; Bi, K., *J. Sep. Sci.* **2011**, *34,* 1198.

(5) Ponz de Antonio, I.; Ruiz Cantador, J.; Gonzalez Garcia, A. E.; Oliver Ruiz, J. M.; Sanchez-Recalde, A.; Lopez-Sendon, J. L., *Rev. Esp. Cardiol. (Engl Ed)* **2017**, *70,* 673.

(6) Verly, I. R.; van Kuilenburg, A. B.; Abeling, N. G.; Goorden, S. M.; Fiocco, M.; Vaz, F. M.; van Noesel, M. M.; Zwaan, C. M.; Kaspers, G. L.; Merks, J. H.; Caron, H. N.; Tytgat, G. A., *Eur. J. Cancer.* **2017**, *72,* 235.

(7) Camargo, J. A.; Alonso, A., *Environ Int* **2006**, *32,* 831.

(8) Correll, D. L., *J. Environ. Qual.* **1998**, *27,* 261.

(9) Bull, S. D.; Davidson, M. G.; van den Elsen, J. M.; Fossey, J. S.; Jenkins, A. T.; Jiang, Y. B.; Kubo, Y.; Marken, F.; Sakurai, K.; Zhao, J.; James, T. D., *Acc. Chem. Res.* **2013**, *46,* 312.

(10) Nishiyabu, R.; Kubo, Y.; James, T. D.; Fossey, J. S., *Chem. Commun. (Camb)* **2011**, *47,* 1124.

(11) Frankland, E.; Duppa, B. F., *Annalen der Chemie und Pharmacie* **1860**, *115,* 319.

(12) Springsteen, G.; Wang, B., *Tetrahedron* **2002**, *58,* 5291.

(13) Yan, J.; Springsteen, G.; Deeter, S.; Wang, B., *Tetrahedron* **2004**, *60,* 11205.

(14) Lorand, J. P.; Edwards, J. O., *J. Org. Chem.* **1958**, *24,* 769.

(15) Petasis, N. A., *Aust. J. Chem.* **2007**, *60,* 795.

(16) Miyaura, N., *Bull. Chem. Soc. Jpn.* **2008**, *81,* 1535.

(17) Ishihara, K.; Yamamoto, H., *Eur. J. Org. Chem.* **1999**, *1999,* 527.

(18) Stefani, H. A.; Cella, R.; Vieira, A. S., *Tetrahedron* **2007**, *63,* 3623.

(19) Brown, H. C.; Ramachandran, P. V., *Acc. Chem. Res.* **2002**, *25,* 16.

(20) Brown, H. C.; Singaram, B., *Acc. Chem. Res.* **2002**, *21,* 287.

(21) Marqués-López, E.; Herrera, R. P., Multicomponent Reactions with Organoboron Compounds. In *Multicomponent Reactions*, John Wiley & Sons, Inc: 2015; pp 127.

(22) Christinat, N.; Scopelliti, R.; Severin, K., *J. Org. Chem.* **2007**, *72,* 2192.

(23) Petasis, N. A., **2005**, 199.

(24) Miyaura, N.; Suzuki, A., *Chem. Rev.* **1995**, *95,* 2457.

(25) Suzuki, A., The Suzuki Reaction with Arylboron Compounds in Arene Chemistry. In *Modern Arene Chemistry*, Wiley-VCH Verlag GmbH & Co. KGaA: 2002; pp 53.

(26) Suzuki, A., *Angew. Chem. Int. Ed. Engl.* **2011**, *50,* 6722.

(27) Yang, W.; Gao, X.; Wang, B., *Med. Res. Rev.* **2003**, *23,* 346.

(28) Trippier, P. C.; McGuigan, C., *Med. Chem. Comm.* **2010**, *1,* 183.

(29) Hall, D. G.; Ni, N.; Wang, B., *Boronic Acids: Preparation and Applications in Organic Synthesis, Medicine and Materials (Volume 1 and 2), Second Edition*. Wiley-VCH Verlag GmbH & Co. KGaA: 2011.

(30) Hall, D. G., Structure, Properties, and Preparation of Boronic Acid Derivatives. Overview of Their Reactions and Applications. In *Boronic Acids*, Wiley-VCH Verlag GmbH & Co. KGaA: 2006; pp 1.

(31) Richardson, P. G.; Mitsiades, C.; Hideshima, T.; Anderson, K. C., *Annu. Rev. Med.* **2006**, *57,* 33.

(32) Matteson, D. S., *Med.Res. Rev.***2008**, *28,* 233.

(33) Baker, S. J.; Zhang, Y. K.; Akama, T.; Lau, A.; Zhou, H.; Hernandez, V.; Mao, W.; Alley, M. R.; Sanders, V.; Plattner, J. J., *J. Med. Chem.* **2006**, *49,* 4447.

(34) Clerici, M.; Shearer, G. M., *Immunology Today* **1994**, *15,* 575.

(35) Jay, J. I.; Shukair, S.; Langheinrich, K.; Hanson, M. C.; Cianci, G. C.; Johnson, T. J.; Clark, M. R.; Hope, T. J.; Kiser, P. F., *Adv. Funct. Mater.* **2009**, *19,* 2969.

(36) Hutin, M.; Bernardinelli, G.; Nitschke, J. R., *Chemistry* **2008**, *14,* 4585.

(37) Höpfl, H.; Farfán, N., *J. Organomet. Chem.* **1997**, *547,* 71.

(38) Nishimura, N.; Yoza, K.; Kobayashi, K., *J. Am. Chem. Soc.* **2010**, *132,* 777.

(39) Kataoka, K.; Okuyama, S.; Minami, T.; James, T. D.; Kubo, Y., *Chem. Commun. (Camb)* **2009**, 1682.

(40) Mikami, M.; Shinkai, S., *Chem. Lett.* **1995**, *24,* 603.

(41) Nakazawa, I.; Suda, S.; Masuda, M.; Asai, M.; Shimizu, T., *Chem. Commun.* **2000**, 881.

(42) Spitler, E. L.; Dichtel, W. R., *Nat. Chem.* **2010**, *2,* 672.

(43) Brooks, W. L.; Sumerlin, B. S., *Chem. Rev.* **2016**, *116,* 1375.

(44) Davis, A. P.; Wareham, R. S., *Angew. Chem. Int. Ed.* **1999**, *38,* 2978.

(45) Lavigne, J. J.; Anslyn, E. V., *Angew. Chem. Int. Ed. Engl.* **2001**, *40,* 3118.

(46) Anslyn, E. V., *J. Org. Chem.* **2007**, *72,* 687.

(47) Wright, A. T.; Anslyn, E. V., *Chem. Soc. Rev.* **2006**, *35,* 14.

(48) Wise, B. M.; Gallagher, N. B., *Journal of Process Control* **1996**, *6,* 329.

(49) Kumar, N.; Bansal, A.; Sarma, G. S.; Rawal, R. K., *Talanta* **2014**, *123,* 186.

(50) Sun, X.; James, T. D., *Chem. Rev.* **2015**, *115,* 8001.

(51) James, T. D.; Shinkai, S., Artificial Receptors as Chemosensors for Carbohydrates. In *Host-Guest Chemistry*, Penadés, S., Ed. Springer Berlin Heidelberg: Berlin, Heidelberg, 2002; pp 159.

(52) Wu, X.; Chen, X. X.; Jiang, Y. B., *Analyst* **2017**, *142,* 1403.

(53) Li, M.; Zhu, W.; Marken, F.; James, T. D., *Chem. Commun. (Camb)* **2015**, *51,* 14562.

(54) Kikuchi, A.; Suzuki, K.; Okabayashi, O.; Hoshino, H.; Kataoka, K.; Sakurai, Y.; Okano, T., *Anal. Chem.* **1996**, *68,* 823.

(55) Anzai, J. I., *Mater. Sci. Eng. C. Mater. Biol. Appl.* **2016**, *67,* 737.

(56) Lakowicz, J. R., *Principles of Fluorescence Spectroscopy*. 2006.

(57) He, X. P.; Zang, Y.; James, T. D.; Li, J.; Chen, G. R., *Chem. Soc. Rev.* **2015**, *44,* 4239.

(58) Que, E. L.; Domaille, D. W.; Chang, C. J., *Chem. Rev.* **2008**, *108,* 1517.

(59) Wang, W.; Gao, X.; Wang, B., *Curr. Org. Chem.* **2002**, *6,* 1285.

(60) Lacina, K.; Skladal, P.; James, T. D., *Chem. Cent. J.* **2014**, *8,* 60.

(61) Fossey, J. S.; James, T. D., Boronic Acid-Based Receptors. In *Supramol. Chem.*, John Wiley & Sons, Ltd: 2012.

(62) Tsien, R. Y., *Biochemistry* **1980**, *19,* 2396.

(63) Russell, A., P. Photometric method and means involving dyes for detecting vicinal polyhydroxyl compounds. US 5,137,833, 1992.

(64) Wu, J.; Liu, W.; Ge, J.; Zhang, H.; Wang, P., *Chem. Soc. Rev.* **2011**, *40,* 3483.

(65) de Silva, A. P.; Gunaratne, H. Q.; Gunnlaugsson, T.; Huxley, A. J.; McCoy, C. P.; Rademacher, J. T.; Rice, T. E., *Chem. Rev.* **1997**, *97,* 1515.

(66) Yoon, J.; Czarnik, A. W., *Bioorg. Med. Chem.* **1993**, *1,* 267.

(67) Arimori, S.; Bosch, L. I.; Ward, C. J.; James, T. D., *Tetrahedron Lett.* **2001**, *42,* 4553.

(68) Bosch, L. I.; Mahon, M. F.; James, T. D., *Tetrahedron Lett.* **2004**, *45,* 2859.

(69) Arimori, S.; Bosch, L. I.; Ward, C. J.; James, T. D., *Tetrahedron Lett.* **2002**, *43,* 911.

(70) DiCesare, N.; Lakowicz, J. R., *J. Phys. Chem. A* **2001**, *105,* 6834.

(71) Callan, J. F.; de Silva, A. P.; Magri, D. C., *Tetrahedron* **2005**, *61,* 8551.

(72) Daly, B.; Ling, J.; de Silva, A. P., *Chem. Soc. Rev.* **2015**, *44,* 4203.

(73) James, T. D., Saccharide-Selective Boronic Acid Based Photoinduced Electron Transfer (PET) Fluorescent Sensors. In *Creative Chemical Sensor Systems*, Springer, 2007, pp 107.

(74) James, T. D.; Sandanayake, K. R. A. S.; Shinkai, S., *J. Chem. Soc., Chem. Commun.* **1994**, 477.

(75) James, T. D.; Sandanayake, K. R. A. S.; Iguchi, R.; Shinkai, S., *J. Am. Chem. Soc.* **1995**, *117,* 8982.

(76) Bielecki, M.; Eggert, H.; Norrild, J. C., *J. Chem. Soc., Perkin Trans. 2,* **1999**, 449.

(77) Eggert, H.; Frederiksen, J.; Morin, C.; Norrild, J. C., *The Journal of Organic Chemistry* **1999**, *64,* 3846.

(78) Phillips, M. D.; Fyles, T. M.; Barwell, N. P.; James, T. D., *Chem. Commun. (Camb)* **2009**, 6557.

(79) Kumai, M.; Kozuka, S.; Samizo, M.; Hashimoto, T.; Suzuki, I.; Hayashita, T., *Anal. Sci.* **2012**, *28,* 121.

(80) Xing, Z.; Wang, H.-C.; Cheng, Y.; Zhu, C.; James, T. D.; Zhao, J., *Eur. J. Org. Chem.* **2012**, *2012,* 1223.

(81) Shabbir, S. H.; Joyce, L. A.; da Cruz, G. M.; Lynch, V. M.; Sorey, S.; Anslyn, E. V., *J. Am. Chem. Soc.* **2009**, *131,* 13125.

(82) Zhao, J.; James, T. D., *Chem. Commun. (Camb)* **2005**, 1889.

(83) Wiskur, S. L.; Ait-Haddou, H.; Lavigne, J. J.; Anslyn, E. V., *Acc. Chem. Res.* **2001**, *34,* 963.

(84) Springsteen, G.; Wang, B., *Chem. Commun. (Camb)* **2001**, 1608.

(85) Zhu, L.; Anslyn, E. V., *J. Am. Chem. Soc.* **2004**, *126,* 3676.

(86) Zhong, Z.; Anslyn, E. V., *J. Am. Chem. Soc.* **2002**, *124,* 9014.

(87) Arimori, S.; Ward, C. J.; James, T. D., *Tetrahedron Lett.* **2002**, *43,* 303.

(88) Cordes, D. B.; Singaram, B., *Pure Appl. Chem.* **2012**, *84,* 2183.

(89) Gamsey, S.; Miller, A.; Olmstead, M. M.; Beavers, C. M.; Hirayama, L. C.; Pradhan, S.; Wessling, R. A.; Singaram, B., *J. Am. Chem. Soc.* **2007**, *129,* 1278.

(90) Cordes, D. B.; Gamsey, S.; Sharrett, Z.; Miller, A.; Thoniyot, P.; Wessling, R. A.; Singaram, B., *Langmuir* **2005**, *21,* 6540.

(91) Camara, J. N.; Suri, J. T.; Cappuccio, F. E.; Wessling, R. A.; Singaram, B., *Tetrahedron Lett.* **2002**, *43,* 1139.

(92) de Borba, E. B.; Amaral, C. L. C.; Politi, M. J.; Villalobos, R.; Baptista, M. S., *Langmuir* **2000**, *16,* 5900.

(93) Cordes, D. B.; Miller, A.; Gamsey, S.; Sharrett, Z.; Thoniyot, P.; Wessling, R.; Singaram, B., *Org. Biomol. Chem.* **2005**, *3,* 1708.

(94) Cordes, D. B.; Gamsey, S.; Singaram, B., *Angew. Chem. Int. Ed. Engl.* **2006**, *45,* 3829.

(95) Gamsey, S.; Baxter, N. A.; Sharrett, Z.; Cordes, D. B.; Olmstead, M. M.; Wessling, R. A.; Singaram, B., *Tetrahedron* **2006**, *62,* 6321.

(96) Sharrett, Z.; Gamsey, S.; Fat, J.; Cunningham-Bryant, D.; Wessling, R. A.; Singaram, B., *Tetrahedron Lett.* **2007**, *48,* 5125.

(97) Sharrett, Z.; Gamsey, S.; Levine, P.; Cunningham-Bryant, D.; Vilozny, B.; Schiller, A.; Wessling, R. A.; Singaram, B., *Tetrahedron Lett.* **2008**, *49,* 300.

(98) Schiller, A.; Wessling, R. A.; Singaram, B., *Angew. Chem. Int. Ed. Engl.* **2007**, *46,* 6457.

(99) Desmet, T.; Soetaert, W.; Bojarova, P.; Kren, V.; Dijkhuizen, L.; Eastwick-Field, V.; Schiller, A., *Chemistry* **2012**, *18,* 10786.

(100) Gamsey, S.; Suri, J. T.; Wessling, R. A.; Singaram, B., *Langmuir* **2006**, *22,* 9067.

(101) Jose, D. A.; Elstner, M.; Schiller, A., *Chemistry* **2013**, *19,* 14451.

(102) Schiller, A., *Molecules at Work*. Wiley-VCH: Weinheim, 2012.

(103) Vilozny, B.; Schiller, A.; Wessling, R. A.; Singaram, B., *Anal. Chim. Acta* **2009**, *649,* 246.

(104) de Silva, A. P., *Nature* **2008**, *454,* 417.

(105) Silva, A. P. d., *Molecular Logic-based Computation*. 2012.

(106) Elstner, M.; Weisshart, K.; Mullen, K.; Schiller, A., *J. Am. Chem. Soc.* **2012**, *134,* 8098.

(107) Andreasson, J.; Pischel, U., *Chem. Soc. Rev.* **2010**, *39,* 174.

(108) Elstner, M.; Schiller, A., *J. Chem. Inf. Model* **2015**, *55,* 1547.

(109) Sun, X.; Zhai, W.; Fossey, J. S.; James, T. D., *Chem. Commun. (Camb)* **2016**, *52,* 3456.

(110) Zhang, X. T.; Liu, G. J.; Ning, Z. W.; Xing, G. W., *Carbohydr. Res.* **2017**, *452,* 129.

(111) O'Hagan, D., *Chem. Soc. Rev.* **2008**, *37,* 308.

(112) Harper, D. B.; O'Hagan, D., *Nat. Prod. Rep.* **1994**, *11,* 123.

(113) Pauling, L., *The nature of the chemical bond and the structure of molecules and crystals; an introduction to modern structural chemistry*. Cornell University Press; H. Milford, Oxford University Press: Ithaca, N.Y.; London, 1939.

(114) Bondi, A., *The Journal of Physical Chemistry* **1964**, *68,* 441.

(115) Carcenac, Y.; Tordeux, M.; Wakselman, C.; Diter, P., *New J. Chem.* **2006**, *30,* 447.

(116) Avdeef, A., *Curr. Top. Med. Chem.* **2001**, *1,* 277.

(117) Purser, S.; Moore, P. R.; Swallow, S.; Gouverneur, V., *Chem. Soc. Rev.* **2008**, *37,* 320.

(118) Isanbor, C.; O'Hagan, D., *J. Fluorine Chem.* **2006**, *127,* 303.

(119) Smart, B. E., *J. Fluorine Chem.* **2001**, *109,* 3.

(120) Curtis-Marof, R.; Doko, D.; Rowe, M. L.; Richards, K. L.; Williamson, R. A.; Howard, M. J., *Org. Biomol. Chem.* **2014**, *12,* 3808.

(121) Martino, R.; Gilard, V.; Desmoulin, F.; Malet-Martino, M., *Chemotherapy* **2006**, *52,* 215.

(122) Gakh, Y. G.; Gakh, A. A.; Gronenborn, A. M., *Magn. Reson. Chem.* **2000**, *38,* 551.

(123) Gerig, J. T., *Prog. Nucl. Magn. Reson. Spectrosc.* **1993**, *26,* 293.

(124) Meyer, B.; Peters, T., *Angew. Chem. Int. Ed. Engl.* **2003**, *42,* 864.

(125) Agrawal, P. K., *Phytochemistry* **1992**, *31,* 3307.

(126) Lacey, M. E.; Subramanian, R.; Olson, D. L.; Webb, A. G.; Sweedler, J. V., *Chem. Rev.* **1999**, *99,* 3133.

(127) Harris, R. K., *Nuclear magnetic resonance: A physicochemical view*. Pitman: London, 1983.

(128) Dolbier, W. R., *Guide to fluorine NMR for organic chemists*. John Wiley & Sons, Inc.: 2009.

(129) Martino, R.; Gilard, V.; Desmoulin, F.; Malet-Martino, M., *J. Pharm. Biomed. Anal.* **2005**, *38,* 871.

(130) Gerig, J. T., *SelfPublished* **2001**, *21,* 1.

(131) Bloch, F., *Physical Review* **1946**, *70,* 460.

(132) Czeslik, C.; Seemann, H.; Winter, R., *Molekülspektroskopie*. 2010; p 309.

(133) Günther, H., *NMR Spectroscopy: Basic Principles, Concepts and Applications in Chemistry*. Wiley: 2013.

(134) Hentschel, K., *Physik Journal* **1996**, *52,* 1232.

(135) Chen, H.; Viel, S.; Ziarelli, F.; Peng, L., *Chem. Soc. Rev.* **2013**, *42,* 7971.

(136) Ruiz-Cabello, J.; Barnett, B. P.; Bottomley, P. A.; Bulte, J. W., *NMR Biomed.* **2011**, *24,* 114.

(137) Yu, J. X.; Kodibagkar, V. D.; Cui, W.; Mason, R. P., *Curr Med Chem* **2005**, *12,* 819.

(138) Cobb, S. L.; Murphy, C. D., *J. Fluorine Chem.* **2009**, *130,* 132.

(139) Marsh, E. N.; Suzuki, Y., *ACS Chem. Biol.* **2014**, *9,* 1242.

(140) Xu, Z.; Liu, C.; Zhao, S.; Chen, S.; Zhao, Y., *Chem. Rev.* **2019**, *119,* 195.

(141) Wang, W.; Xia, X.; Bian, G.; Song, L., *Chem. Commun. (Camb)* **2019**, *55,* 6098.

(142) Yu, W.; Yang, Y.; Bo, S.; Li, Y.; Chen, S.; Yang, Z.; Zheng, X.; Jiang, Z. X.; Zhou, X., *J. Org. Chem.* **2015**, *80,* 4443.

(143) Tirotta, I.; Dichiarante, V.; Pigliacelli, C.; Cavallo, G.; Terraneo, G.; Bombelli, F. B.; Metrangolo, P.; Resnati, G., *Chem. Rev.* **2015**, *115,* 1106.

(144) Nakamura, T.; Matsushita, H.; Sugihara, F.; Yoshioka, Y.; Mizukami, S.; Kikuchi, K., *Angew. Chem. Int. Ed. Engl.* **2015**, *54,* 1007.

(145) Amiri, H.; Srinivas, M.; Veltien, A.; van Uden, M. J.; de Vries, I. J.; Heerschap, A., *Eur. Radiol.* **2015**, *25,* 726.

(146) Tirotta, I.; Mastropietro, A.; Cordiglieri, C.; Gazzera, L.; Baggi, F.; Baselli, G.; Bruzzone, M. G.; Zucca, I.; Cavallo, G.; Terraneo, G.; Baldelli Bombelli, F.; Metrangolo, P.; Resnati, G., *J. Am. Chem. Soc.* **2014**, *136,* 8524.

(147) Muraro, P. I. R.; de Freitas, A. G. O.; Trindade, S. G.; Giacomelli, F. C.; Bonvent, J.-J.; Schmidt, V.; dos Santos, F. P.; Giacomelli, C., *J. Fluorine Chem.* **2014**, *168,* 251.

(148) Jacoby, C.; Temme, S.; Mayenfels, F.; Benoit, N.; Krafft, M. P.; Schubert, R.; Schrader, J.; Flogel, U., *NMR Biomed.* **2014**, *27,* 261.

(149) Jacoby, C.; Borg, N.; Heusch, P.; Sauter, M.; Bonner, F.; Kandolf, R.; Klingel, K.; Schrader, J.; Flogel, U., *MAGMA* **2014**, *27,* 101.

(150) Zhao, Y.; Chen, L.; Swager, T. M., *Angew. Chem. Int. Ed. Engl.* **2016**, *55,* 917.

(151) Zhao, Y.; Swager, T. M., *J. Am. Chem. Soc.* **2015**, *137,* 3221.

(152) Zhao, Y.; Markopoulos, G.; Swager, T. M., *J. Am. Chem. Soc.* **2014**, *136,* 10683.

(153) Zhao, Y.; Swager, T. M., *J. Am. Chem. Soc.* **2013**, *135,* 18770.

(154) Plaunt, A. J.; Clear, K. J.; Smith, B. D., *Chem. Commun. (Camb)* **2014**, *50,* 10499.

(155) Gan, H.; Oliver, A. G.; Smith, B. D., *Chem. Commun. (Camb)* **2013**, *49,* 5070.

(156) Moulton, C. J.; Shaw, B. L., *J. Chem. Soc., Dalton Trans.* **1976**, 1020.

(157) Holland, G. N.; Bottomley, P. A.; Hinshaw, W. S., *Journal of Magnetic Resonance (1969)* **1977**, *28,* 133.

(158) Yuan, Y.; Sun, H.; Ge, S.; Wang, M.; Zhao, H.; Wang, L.; An, L.; Zhang, J.; Zhang, H.; Hu, B.; Wang, J.; Liang, G., *ACS Nano* **2015**, *9,* 761.

(159) Vivian, D.; Cheng, K.; Khurana, S.; Xu, S.; Kriel, E. H.; Dawson, P. A.; Raufman, J. P.; Polli, J. E., *Mol. Pharm.* **2014**, *11,* 1575.

(160) London, R. E.; Gabel, S. A., *J. Am. Chem. Soc.* **1994**, *116,* 2570.

(161) London, R. E.; Gabel, S. A., *J. Am. Chem. Soc.* **1994**, *116,* 2562.

(162) Yeste, S. L.; Powell, M. E.; Bull, S. D.; James, T. D., *J. Org. Chem.* **2009**, *74,* 427.

(163) Iannazzo, L.; Benedetti, E.; Catala, M.; Etheve-Quelquejeu, M.; Tisne, C.; Micouin, L., *Org. Biomol. Chem.* **2015**, *13,* 8817.

(164) Reddy, G. U.; Axthelm, J.; Bellstedt, P.; Schiller, A., *In Preparation* **2019**.

(165) Axthelm, J.; Reddy, G. U.; Bellstedt, P.; Schiller, A., *In Preparation* **2019**.

(166) Axthelm, J.; Askes, S. H. C.; Elstner, M.; Reddy, G. U.; Gorls, H.; Bellstedt, P.; Schiller, A., *J. Am. Chem. Soc.* **2017**, *139,* 11413.

(167) Axthelm, J.; Gorls, H.; Schubert, U. S.; Schiller, A., *J. Am. Chem. Soc.* **2015**, *137,* 15402.

(168) Teichert, J. F.; Mazunin, D.; Bode, J. W., *J. Am. Chem. Soc.* **2013**, *135,* 11314.

(169) Yang, M.; Liu, Y.; Jiang, X., *Chem. Soc. Rev.* **2019**, *48,* 850.

(170) bar code generator. https://www.gs1.org/barcodes/ean-upc.

(171) Ramsay, W. J.; Bayley, H., *Angew. Chem. Int. Ed. Engl.* **2018**, *57,* 2841.

(172) Bubb, W. A., *Concepts in Magnetic Resonance* **2003**, *19A,* 1.

(173) Norrild, J. C.; Eggert, H., *Journal of the Chemical Society, Perkin Transactions 2* **1996**, 2583.

(174) Barclay, T.; Ginic-Markovic, M.; Johnston, M. R.; Cooper, P.; Petrovsky, N., *Carbohydr. Res.* **2012**, *347,* 136.

(175) Angyal, S. J., *Adv. Carbohydr. Chem. Biochem.* **1991**, *49,* 19.

(176) Angyal, S. J., *Adv. Carbohydr. Chem. Biochem.* **1984**, *42,* 15.

(177) Heller, A.; Feldman, B., *Chem. Rev.* **2008**, *108,* 2482.

(178) Adams, J.; Palombella, V. J.; Sausville, E. A.; Johnson, J.; Destree, A.; Lazarus, D. D.; Maas, J.; Pien, C. S.; Prakash, S.; Elliott, P. J., *Cancer Res* **1999**, *59,* 2615.

(179) Goddard, J. P.; Reymond, J. L., *Trends Biotechnol.* **2004**, *22,* 363.

(180) Reymond, J. L.; Fluxa, V. S.; Maillard, N., *Chem. Commun. (Camb)* **2009**, 34.

(181) Goedl, C.; Schwarz, A.; Minani, A.; Nidetzky, B., *J. Biotechnol.* **2007**, *129,* 77.

(182) Aerts, D.; Verhaeghe, T.; Joosten, H. J.; Vriend, G.; Soetaert, W.; Desmet, T., *Biotechnol. Bioeng.* **2013**, *110,* 2563.

(183) Beer, P. D.; Gale, P. A., *Angew. Chem. Int. Ed. Engl.* **2001**, *40,* 486.

(184) Ayoob, S.; Gupta, A. K., *Critical Reviews in Environmental Science and Technology* **2006**, *36,* 433.

(185) Eisler, R.; Wiemeyer, S. N., *Rev. Environ. Contam. Toxicol.* **2004**, *183,* 21.

(186) Kelly, C. P.; Cramer, C. J.; Truhlar, D. G., *J. Phys. Chem. B* **2006**, *110,* 16066.

(187) Galbraith, E.; James, T. D., *Chem. Soc. Rev.* **2010**, *39,* 3831.

(188) Connors, K. C., *Binding constants. In: The Measurement of Molecular Complex Stability*. Wiley-Interscience: 1987.

(189) Alberti, K. G.; Zimmet, P. Z., *Diabet. Med.* **1998**, *15,* 539.

(190) Heo, Y. J.; Takeuchi, S., *Adv. Healthc. Mater.* **2013**, *2,* 43.

(191) Newman, J. D.; Turner, A. P., *Biosens. Bioelectron.* **2005**, *20,* 2435.

(192) Bankar, S. B.; Bule, M. V.; Singhal, R. S.; Ananthanarayan, L., *Biotechnol. Adv.* **2009**, *27,* 489.

(193) Farandos, N. M.; Yetisen, A. K.; Monteiro, M. J.; Lowe, C. R.; Yun, S. H., *Adv. Healthc. Mater.* **2015**, *4,* 792.

(194) Badugu, R.; Lakowicz, J. R.; Geddes, C. D., *Curr. Opin. Biotechnol.* **2005**, *16,* 100.

(195) Ipe, D. S.; Ulett, G. C., *J. Microbiol. Methods* **2016**, *127,* 164.

(196) Yang, Y.; Zhao, Q.; Feng, W.; Li, F., *Chem. Rev.* **2013**, *113,* 192.

(197) Lippert, A. R.; Van de Bittner, G. C.; Chang, C. J., *Acc. Chem. Res.* **2011**, *44,* 793.

(198) Apel, K.; Hirt, H., *Annu. Rev. Plant. Biol.* **2004**, *55,* 373.

(199) Veal, E. A.; Day, A. M.; Morgan, B. A., *Mol. Cell.* **2007**, *26,* 1.

(200) van der Vliet, A.; Janssen-Heininger, Y. M., *J. Cell. Biochem.* **2014**, *115,* 427.

(201) Chen, X.; Wang, F.; Hyun, J. Y.; Wei, T.; Qiang, J.; Ren, X.; Shin, I.; Yoon, J., *Chem. Soc. Rev.* **2016**, *45,* 2976.

(202) Thordarson, P., *Chem. Soc. Rev.* **2011**, *40,* 1305.

(203) Hooft, R., Collect. Nonius BV, Delft, The Netherlands: 1998.

(204) Otwinowski, Z.; Minor, W., *Macromolecular Crystallography, Pt A* **1997**, *276,* 307.

(205) Sheldrick, G., *Bruker AXS Inc., Madison, Wisconsin, USA* **2003**.

(206) Sheldrick, G. M., *Acta. Crystallogr. A* **2008**, *64,* 112.

(207) Spek, A. L., *Acta. Crystallogr. D Biol. Crystallogr.* **2009**, *65,* 148.

(208) Macrae, C. F.; Edgington, P. R.; McCabe, P.; Pidcock, E.; Shields, G. P.; Taylor, R.; Towler, M.; van de Streek, J., *J. Appl. Crystallogr.* **2006**, *39,* 453.

SELBSTSTÄNDIGKEITSERKLÄRUNG

Ich, Jörg Harald Axthelm, erkläre hiermit, dass ich die vorliegende Arbeit selbstständig und unter Verwendung der angegebenen Hilfsmittel, persönlichen Mitteilungen und Quellen angefertigt habe.

Rudolstadt, 13.07.2020